

Department of Civil Engineering
University of Strathclyde

**Investigation of Desiccation Cracks in
Drying Soil**

A Thesis presented for the Degree of Doctor of Philosophy

Alvis Atique

2013

To my mom.....

“মধুর আমার মায়ের হাসি, চাঁদের মুখে ঝরে
মা'কে মনে পড়ে আমার, মা'কে মনে পড়ে”

This thesis is the result of the author's original research. It has been composed by the author and has not been previously submitted for examination which has led to the award of a degree.

The copyright of this thesis belongs to the author under the terms of the United Kingdom Copyright Acts as qualified by University of Strathclyde Regulation 3.50.

Due acknowledgement must always be made of the use of any material contained in, or derived from, this thesis.

Signed:

Date:

ABSTRACT

This research investigates desiccation cracking behaviour of a fill material from a flood embankment along the Bengawan Solo River in East Java, Indonesia, an area that is prone to extremes in flooding and drying. A detailed study of the previous works on this topic showed the absence of fully-monitored laboratory tests dedicated to desiccation cracking behaviour. This study combined traditional and new techniques to characterise desiccation cracking behaviour in this material in a suite of laboratory tests.

Desiccation plate tests were conducted to gain basic knowledge of the cracking behaviour of Bengawan Solo soil and identify the influences of plate shape on test results. Crack initiation, evolution, and final pattern were studied in detail. Results of the experiments showed that plate geometry had minimal effect on cracking behaviour except for the final cracking pattern.

Crack initiation and evolution was characterised with a 2D/3D profile laser sensor coupled to a motion controller that allowed scanning of the overall surface of the drying soil. The system developed for this work was used to track the three most relevant variables associated with the behavior of soils during desiccation: volume change, water loss, and evolving crack network morphology. With this new method, the evolution of crack aperture, crack depth, surface contour levels (settlements) and evolution of global volume change were captured in real time, significantly improving upon previous methods for crack monitoring.

Finally, the effects of moisture content and dry density on tensile strength during cracking was investigated at two states: reconstituted and compacted. Microstructural investigation illustrated the fabric changes during drying at two states to complement the experimental results for tensile strength. The comparison of tensile strength between reconstituted and compacted state has been found promising and believed to be useful in earthwork construction projects.

PUBLICATIONS

- Sanchez, M., **Atique, A.**, Kim, S., Romero, E., and Zielinski, M., ‘Exploring desiccation cracks in soils using a 2D profile laser device’, ACTA Geotechnica, Accepted on 7 June 2013.
- Sanchez, **M.**, **Atique, A.**, Kim, S., et al., ‘Desiccation Cracks in Soils: Recent Advances in Experimental and Numerical Techniques’, The 18th International Conference on Soil Mechanics and Geotechnical Engineering (18th ICSMGE), Paris, France, 2-6 September, 2013.
- **Atique, A.**, Sanchez, M., Romero, E., and Zielinski, M., ‘Compact 2D/3D profile laser sensor to study the behavior of drying soils’, Geotechnical Testing Journal, Under review, Submitted.
- **Atique, A.**, Sanchez, M. & Romero, E., ‘*The effect of desiccation on tensile strength of drying soil: Reconstituted versus compacted state*’, **Journal under preparation.**
- **Atique, A.**, Sanchez, M., ‘*Analysis of Cracking Behaviour of Drying Soil*’, Proceedings of 2nd International Conference on Environmental Science and Technology-ICEST 2011, 26-28, February 2011, Singapore.
- Zielinski, M., Sentenac, P., **Atique, A.**, Sanchez, M., & Romero, E., ‘*Comparison of four methods for determining the soil water retention curve*’. Unsaturated Soils - Alonso, E. & Gens, A. (eds), Proceedings of the fifth international conference on unsaturated soils, Barcelona, Spain, 6-8 September 2010, vol. 1, pp.113-136.
- **Atique, A.**, Sanchez, M., ‘*Investigation of crack desiccation in soil from a flood protection embankment*’, Proceedings of 4th Asia-Pacific Conference on Unsaturated Soils, 23-25 November 2009, Newcastle, Australia, vol. 1, pp.413-418, CRC Press, Taylor & Francis Group, London, UK.

ACKNOWLEDGEMENT

At first I would like to thank my supervisor Dr Marcelo Sanchez for encouraging me to pick such an interesting topic for research, for his inspiration throughout the research as well as his mental support during some of my difficult time at Strathclyde. I am thankful to Prof. Minna Karstunen who took on a supervisory after Marcelo moved to Texas, USA and helped me in the final completion stage. I am also grateful to Prof Rebecca J Lunn for her involvement in my research by her significant contribution for my experimental equipment from the departmental fund.

The microstructural studies presented in this research was carried out at Unversitat Politecnica de Catalunya (UPC), Barcelona. I am very grateful to Dr Enrique Romero, my co-supervisor for his support during my stay there. Throughout my research he provided valuable discussion on relevant tests I performed at UPC lab. I am thankful to the past PhD students at UPC Analice, Manuel, Rodrigo, Lab technician Hosse for their kind help during my visit.

I would specially like to thank Mr Gerry Carr, for his technical support at the lab in the department of Civil Engineering at University of Strathclyde. Also special thanks to Mr Alex Brown and the rest of the technical staff in the department for their support whenever I needed.

I am grateful to my past and present PhD student colleagues at University of Strathclyde- Grainne, Marti, Edriyana, Shiva, Neung, O, Rahman, Marchin, David, Money, Panos, Matt, whose various support always helped me to cheer up and start again. I am particularly grateful to Grainne for many discussions we had throughout my research and during my writing up. She always comforted me whenever I needed; she was always there for me as a friend. I also appreciate technical help of Marchin Zielinski during my research and for preparing the digital model of the soil from the scanner data (X, Y, Z) file in chapter 5.

I am very grateful to the faculty of engineering at University of Strathclyde for providing me with Ronald Miller Scholarship throughout my PhD studies. I am

grateful for the Mac Robertson travel grant which allowed me to travel Barcelona UPC to carry out the microstructural investigations.

I would like to thank my mom Rahima Khatun who recently passed away, for her endless support and prayer thorough out my study period, my dad Mohammad Ali Ashraf Bhuiyan, sisters Bilkis, Nargis, Parvis, Iris and Jhumur and brothers Humayun, Alamgir, Jahangir and Shahjahan, my husband Sumon, my son Advi and my newborn Rutvi; your countless support and patience helped me towards this achievement.

Table of Contents

ABSTRACT	i
PUBLICATIONS	ii
ACKNOWLEDGEMENT	iii
Chapter 1: Introduction	1
1.1 BACKGROUND	1
1.2 OBJECTIVES	4
1.3 OUTLINE AND PUBLICATIONS	5
Chapter 2: State of the art	8
2.1 INTRODUCTION.....	8
2.2 DESICCATION CRACKS	9
2.3 CLASSIFICATION OF SOIL CRACKING	10
2.3.1 <i>Classification after Fookes and Denness</i>	10
2.3.2 <i>Classification after Fang</i>	12
2.3.2.1 Shrinkage cracking	13
2.3.2.2 Thermal cracking.....	14
2.3.2.3 Tensile cracking.....	14
2.3.2.4 Fracture cracking	14
2.3.3 <i>Other forms of cracks</i>	15
2.4 COMMON CAUSES FOR DESICCATION CRACKS IN SOIL.....	15
2.4.1 <i>Soil composition and structure</i>	16
2.4.2 <i>Tensile strength</i>	20
2.4.3 <i>Soil suction</i>	21
2.4.4 <i>Vegetation</i>	22
2.5 EXPERIMENTAL STUDIES INVESTIGATING SOIL DESICCATION AND CRACKING	22
2.5.1 <i>Laboratory Experiments</i>	22
2.5.2 <i>Field Experiments</i>	29
2.6 SOIL SHRINKAGE	34
2.7 WATER RETENTION BEHAVIOUR	37
2.7.1 <i>Testing techniques</i>	37
2.7.2 <i>Variation of retention behaviour</i>	38

2.8 METHODS TO MEASURE VOLUME CHANGE IN SOIL TESTING	41
2.8.1 Contact methods.....	42
2.8.2 Non-contact methods	42
2.9 FABRIC STUDY	45
2.9.1 Classification in soil fabric.....	46
2.9.2 Microstructural study: compacted versus reconstituted states.....	50
2.10 CONCLUSION	55
Chapter 3: Soil characterisation	56
3.1 INTRODUCTION	56
3.2 BENGAWAN SOLO EMBANKMENT	57
3.2.1 Geological Origin	57
3.2.2 Site Description	58
3.2.3 Geotechnical Failures along Bengawan solo embankment	61
3.2.4 Evidence of Desiccation Cracks	62
3.3 BASIC SOIL PROPERTIES	64
3.3.1 Soil mineralogy	65
3.3.2 Shrinkage, shrinkage limit and shrinkage characteristics of Bengawan solo soil	68
3.3.2.1 Linear shrinkage test	70
3.3.2.2 Volumetric Shrinkage.....	72
3.4 COMPACTION CURVES.....	74
3.5 SAMPLE PREPARATION.....	75
3.5.1 Soil Mixing.....	76
3.5.2 Preparing Reconstituted Soil.....	77
3.5.3 Preparing Compacted Soil.....	78
3.6 CONCLUSION	79
Chapter 4: Desiccation plate tests	80
4.1 INTRODUCTION	80
4.2 CHARACTERISTICS OF SOIL CRACKING	81
4.3 DESICCATION PLATE TESTS	84
4.3.1 Objectives	84
4.3.2 Experimental Methodology	84
4.3.2.1 Desiccation test methodology	85
4.3.3 Quantitative analysis of cracks by digital image analysis technique	90
4.4 OBSERVATIONS OF EXPERIMENTAL RESULTS	92

4.4.1 Square desiccation plate.....	93
4.4.1.1 Cracking Pattern.....	93
4.4.1.2 Effect of wetting and drying on the crack pattern	94
4.4.2 Rectangular desiccation plate	96
4.4.2.1 Cracking Pattern.....	96
4.4.3 Circular desiccation plate.....	98
4.4.3.1 Cracking Pattern for different soil thickness	98
4.4.3.2 Influence of the base pattern and thickness on cracking.....	99
4.4.3.3 Cracking moisture content.....	101
4.4.4 Effect of different Plate Shape	102
4.4.5 Summary of Desiccation plate test results.....	105
4.5 CONCLUSION	108
Chapter 5: Desiccation Tests using 2D/3D compact Laser Scanner.....	109
5.1 INTRODUCTION	109
5.2 BACKGROUND.....	110
5.2.1 Why new technique?	110
5.3 OBJECTIVES AND EXPERIMENTAL CAMPAIGN.....	113
5.4 EXPERIMENTAL SET-UP.....	114
5.4.1 Scan CONTROL 2700-100: Compact 2D/3D profile sensor with integrated controller	117
5.4.2 Laser 2D/3D Resolution	118
5.5 EXPERIMENTAL METHODOLOGY	119
5.6 GENERAL SET-UP AND ANALYSIS PROCEDURES.....	121
5.6.1 Setting up the scanner and Motion Controller.....	121
5.6.2 Data acquisition system for scanCONTROL 2700 and Software operation.....	124
5.7 CALIBRATION OF THE LASER SCANNER	125
5.7.1 Calibration of laser scanner for volume change estimation with an alternative method	129
5.8 RESULTS AND DISCUSSION	131
5.8.1 Digital model.....	131
5.8.2 Cracking mechanism observed from scanner result	134
5.8.3 Estimation of volume change of the drying soil specimen.....	135
5.8.4 Evolution of the drying desiccated soil specimen	137
5.8.5 Analysis of crack network propagation from 3D scanner	139
5.8.6 Cracking parameter: 3D scanner vs. image analysis	142
5.8.7 Measuring volumetric shrinkage form laser scanner data	147
5.9 CONCLUSION	149

Chapter 6: Tensile strength and micromechanical state.....	150
6.1 INTRODUCTION	150
6.2 BACKGROUND.....	151
6.3 OBJECTIVES AND EXPERIMENTAL CAMPAIGN.....	153
6.4 EXPERIMENTAL METHODOLOGY	154
6.4.1 Specimen preparation.....	154
6.4.2 Selection of the initial condition for tensile test specimen	159
6.4.3 Preparing reconstituted specimen	161
6.4.4 Preparing compacted specimen.....	162
6.4.4 Tensile strength testing device	165
6.4.5 Mounting of specimen within the device and testing procedure.....	168
6.5 RESULTS	173
6.5.1 Tensile strength for reconstituted and compacted specimen	173
6.6 PROBLEM ASSOCIATED WITH DIRECT TENSILE TESTING DEVICE	175
6.7 FABRIC STUDY.....	177
6.7.1 Mercury Intrusion Porosimetry (MIP) tests.....	178
6.7.1.1 Principle	178
6.7.1.2 MIP Equipment	179
6.7.1.3 Specimen Preparation.....	180
6.7.1.4 Experimental methodology.....	181
6.7.1.5 Calculations.....	182
6.7.1.6 Results.....	183
6.7.2 The Field Emission Scanning Electron Microscope (FESEM) tests	186
6.7.2.1 Experimental equipment	186
6.7.2.2 Specimen preparation.....	187
6.7.2.3 Chamber condition	188
6.7.2.4 FESEM results.....	189
6.8 WATER RETENTION BEHAVIOUR	192
6.9 SUMMARY.....	197
6.10 CONCLUSION	199
Chapter 7: Conclusions and recommendations for future work.....	201
7.1 CONCLUSIONS.....	201
7.2 RECOMMENDED FURTHER WORK	204
REFERENCE	206

List of Figures

Figure 2.1: Cracking patterns comparison between oven and air dried samples of Illite and Muscovite clay (Fang, 1997b).	13
Figure 2.2: Volumetric shrinkage strain versus soil properties; (a) Clay content, (b) Plastic index (Albrecht and Benson, 2001).....	17
Figure 2.3: Volumetric shrinkage strain and dry density (Albrecht and Benson, 2001).	18
Figure 2.4: Influence of thickness of soil on crack initiation (Corte and Higashi, 1960).	18
Figure 2.5: effect of soil structures on cracking patterns; (a) Flocculated structure, and (b) Dispersed structure (Fang, 1997b).....	19
Figure 2.6: Tensile strength variation with degree of saturation (Towner, 1987a). ..	21
Figure 2.7: (a) Image of vertical section of the sample at N=83. White bar represents 5 mm length. Arrows with S and B denote the position of the surface and bottom, representatively. The symbols (c), (d), and (e) represent the position of horizontal slices, which is indicated by the same symbol; (b) Snapshots of signal intensity along vertical direction. The vertical axis corresponds to the depth from the surface and the horizontal axis represents the intensity; Horizontal images (c), (d), and (e) are averaged snapshots around N=83 at the position indicated by the symbol in (a) (Mizuguchi et al., 2005).....	24
Figure 2.8: A sequence of images of a crack-portion pattern forming in a layer of final depth at 1.51 ± 0.06 mm with a <i>Teflon coated</i> substrate and with field of view 5.1 cm x 4.8 cm. Image (a) is 33 hours after the start of the run and the elapsed time between (a) and (f) is 6 hours. This sequence illustrates the <i>arching</i> process (Shorlin et al., 2000).....	25

Figure 2.9: A sequence of images of a crack-portion pattern forming in a layer of final depth at 1.88 ± 0.10 mm with an uncoated substrate and with field of view 7.1 cm^2 . Image (a) is 67 hours after the start of the run and the elapsed time between (a) and (f) is 17 hours. This sequence illustrates the <i>laddering</i> process (Shorlin et al., 2000).	26
Figure 2.10: <i>Left</i> : Cracking pattern of compacted clay at the end of test (desiccation time: 144 hours); <i>Right</i> : Development of number of cracks with drying time for compacted clay (Kodikara and Choi 2006).....	27
Figure 2.11: Characteristics of test sections.....	31
Figure 2.12: (a) Oblique view of two adjacent mud cracks, (b) Their surface morphology interpretation. Crack origins (solid dots) are located at the bottom (Weinberger, 1999).	32
Figure 2.13: (a) Oblique view of a recovered polygon, (b) Surface morphology interpretation of an associated bounded crack. A single vertical plume axis branches in to separate sub-horizontal axes (along which cracks are propagated at opposite direction) that are obliquely oriented with respect to bedding (Weinberger, 1999)..	32
Figure 2.14: (a) Oblique view of a polygon, (b) Interpretation of surface morphology of an associated mud crack. The crack nucleates at depth, ruptures the desiccated layers and subsequently propagates bi-laterally away from the origin along curved paths (Weinberger, 1999).....	33
Figure 2.15: Interpretation of shrinkage behaviour (Haines, 1923a).	35
Figure 2.16: Behaviour of soils during drying and wetting process presented originally (Poulovas.A, 1970).....	36
Figure 2.17: Influence of soil type on water retention behaviour (Barbour, 1998, Vanapalli et al., 1999).	39
Figure 2.18 : Influence of void ratio and structure on soil water retention behaviour of Boom clay (Romero, 1999, Nuth and Laloui, 2008).	40

Figure 2.19: Soil–water characteristics for specimen compacted at different initial water content (Vanapalli et al., 1999).	41
Figure 2.20: Suction controlled triaxial apparatus (Bishop and Donald, 1961).....	43
Figure 2.21: Double wall triaxial cell (Wheeler, 1988).	44
Figure 2.22: Different types of particle assemblages (Collins and McGown, 1974a).	46
Figure 2.23: Schematic representation of types of pore space (Collins and McGown, 1974a).....	47
Figure 2.24: Types of microfabric; a) Clay matrix predominantly integrated by elementary particles of clay platelets and a few grains of slit or sand, b) Microfabric of a clay predominantly integrated by aggregations of elementary particle arrangements, c) Sand or slit matrix with clay connectors between individual grains, and d) Elementary particle arrangement in a parallel configuration (Alonso et al., 1987).	49
Figure 2.25: Comparison of PSD of compacted and reconstituted samples of Speswhite kaolin at similar suction (Tarantino, 2010).....	52
Figure 2.26: Comparison of PSD of compacted and reconstituted Barcelona red clayey silt (Tarantino, 2010).	53
Figure 2.27: Comparison of PSD of compacted (PS) and reconstituted (PR) samples of Bioley silt at zero suction (PR2 and PS3) and a suction of 500 kPa and a vertical stress of 500 kPa (PR1 and PS1b) (Koliiji et al., 2010).....	54
Figure 3.1: Geological map of Bengawan Solo River Basin, East Java, Indonesia (Takeuchi et al., 1995).	57
Figure 3.2: Site location within the Bengawan Solo River Basin (Sudarsono, 2009).	58

Figure 3.3: (a) Embankment; (b) Concrete slabs used as a surface protection to prevent erosion of the outward slope; (c) Man-made embankment; (d) River meandering (El Mountassir, 2011).....	60
Figure 3.4: Widespread desiccation cracking across the stepped surface (images (a), (b), and (c)), longitudinal cracking (images (d), (e) and (f)) and interfaces with the receding flood water (images (g) and (h)) (El Mountassir, 2011).	63
Figure 3.5: Particle size distribution for Bengawan Solo soil (El Mountassir, 2011).	64
Figure 3.6: XRD-patterns of random powder samples (total fraction) (Sm: montmorillonite, K: kaolinite; Phyll: total phyllosilicates; Qz: quartz; Plag: plagioclases; Cc: Calcite). D1=0.5-1.0 m and D2=1.0-1.5 m.....	66
Figure 3.7: X-Ray diffractograms of oriented samples (< 2 μm fraction) (Sm:montmorillonite; K: kaolinite).....	67
Figure 3.8: Correlation of soil volume change and consistency (Haines, 1923b, Hogentogler, 1937).	69
Figure 3.9: (a) Samples on linear shrinkage mould at initial state, air dried; (b) Samples on linear shrinkage mould started to shrink, air dried; (c) Samples on linear shrinkage mould at initial state, oven dried; (d) Samples on linear shrinkage mould shrunk after oven drying.	71
Figure 3.10: Shrinkage curve for Bengawan Solo soil.	73
Figure 3.11: Compaction curves at three different compactive efforts (El Mountassir, 2011); (i) Extreme Light,132 kJ/m ³ , (ii) BS Light, 596 kJ/m ³ and (iii) BS Heavy, 2682 kJ/m ³	75
Figure 3.12: Different stages of soil preparation before sampling; (a) Air dried hand broken large soil particle; (b) Crushed soil in a crushing machine; (c) 2 mm sieved soil ready to use for sampling.	76

Figure 4.1: Theoretical cracking pattern as suggested by Kodikara et al. (2000a); (a) is 2D cracking pattern, (b), (c) and (d) are essentially 3D cracking pattern.	83
Figure 4.2: Different desiccation plates used for the tests; (a) Grooved and smooth plates with different shapes, (b) Groove pattern in circular plate, and (c) Groove pattern in square and rectangular plate.....	86
Figure 4.3: Example of measuring cracking water content during desiccation test and how it effects the natural cracking propagation.	88
Figure 4.4: Temperature and relative humidity measurements during experiment. ..	89
Figure 4.5: Desiccation plate test setup.....	90
Figure 4.6: Flow chart showing the image processing and analysis.....	91
Figure 4.7: Image processing of crack network; (a) Greyscale image, (b) Binary image, (c) Skeleton of crack network (Atique and Sanchez, 2009).....	92
Figure 4.8: Orthogonal cracking Sequence in square plate.....	93
Figure 4.9: Experimental set-up.....	94
Figure 4.10: (a) Cracking pattern not affected by wetting cycle, (b) Ceramic plate sinking is soft soil failing to measure vertical deformation of soil layer.	95
Figure 4.11: (a) Primary crack in rectangular plate dividing the soil sample into two large blocks, 10 mm soil layer thickness, (b) Rectangular 10 mm final cracking pattern, (c) Final crack in rectangular plate dividing the soil sample into three large blocks, 20 mm soil layer thickness.	97
Figure 4.12: Final cracking pattern for circular plate in different base; <i>Left</i> : Smooth base, <i>Right</i> : Grooved base; (a) 5 mm plate, (b) 10 mm plate and (c) 20 mm.	100
Figure 4.13: Variation of water content over time (circular plate).	101
Figure 4.14: Effect of soil layer thickness on cracking water content (circular plate).	102

Figure 4.15: Final crack network pattern in 10 mm thickness sample; (a) Square plate; (b) Rectangular plate; (c) Circular plate.....	103
Figure 4.16: Water content variation curve for three different shaped desiccation plates with 10 mm thickness.	103
Figure 5.1: Schematic of set up of Desiccation plate tests using 3D compact Laser Scanner.....	115
Figure 5.2: Photo of desiccation test set-up using 3D compact Laser Scanner.	116
Figure 5.3: Measuring principle of the laser.	118
Figure 5.4: Glass desiccation plate used for laser scanner.....	120
Figure 5.5: Laser resolution measurement region (Microepsilon-Website, 2011). .	121
Figure 5.6: Positioning the desiccation plate within the laser resolution region.	122
Figure 5.7: Motion controller lab software screen.	122
Figure 5.8: Set up flow chart of laser scanner desiccation test.	123
Figure 5.9: Schematic of dummy sample.....	125
Figure 5.10: Aluminium Dummy sample.	126
Figure 5.11: Aluminium dummy sample with positioning place.....	126
Figure 5.12: 3D image of scanned dummy sample with lots of noise.	127
Figure 5.13: Surfer view of the dummy with measuring error at all direction.	127
Figure 5.14: <i>Left</i> : Scanned output of grove of the dummy sample; <i>Right</i> : Zoomed version.....	128
Figure 5.15: (a) Image of the children’s lego-type brick used for the volume calibration, (b) 3D image of the lego-type brick from surfer using scan data.	129

Figure 5.16: 2D visualisation of the Lego in scanCONTROL software screen.....	130
Figure 5.17: 3D images of the soil sample at two different time of drying, generated by Surfer after scanning (left) and digital images taken by camera (right) : (a) 6 hours and (b) 23 hours of drying.....	132
Figure 5.18: Evolution of typical cross section during drying showing the section profiles at different times (a) Cross-sectional profile along Y axis (model and experiment after 6h of drying), (b) Cross-sectional profile along X axis (model after 6h of drying).....	133
Figure 5.19: Evolution of the central cross-section along Y axis during drying, showing the section profiles at different times.	135
Figure 5.20: Time evolution of (a) volume change, (b) water content.	136
Figure 5.21: Contour levels at different times.	138
Figure 5.22: Crack propagation over time; <i>Left</i> Z-inverted, <i>Right</i> non-inverted.	141
Figure 5.23: (a) Region of interest which has been analysed for crack information by image analysis technique; (b) Region of interest which has been analysed for crack information by laser scanning technique.	143
Figure 5.24: Crack identification for the comparison analysis.	144
Figure 5.25: Volumetric shrinkage curve for Bengawan Solo Soil found using two methods, from laser scanner measurements and vernier calliper measurements.....	148
Figure 6.1: Photograph of the accessories used for tensile strength test specimen..	154
Figure 6.2: Difficulties in specimen preparation; (a) Crumbly compacted specimen at lower water content, (b) Specimen broke during cutting into shape to fit into complex shaped tensile mould, (c) The cut specimen does not fit properly inside the mould for test requirement, (d) Evidence of air-bubbles within specimen during drying in preparation of reconstituted specimen.	156

Figure 6.3: Schematic of sample preparation; (a) Reconstituted specimen preparation, (b) Compacted specimen preparation.....	158
Figure 6.4: Selection of points for tensile test specimens from compaction curve of Bengawan Solo soil.....	161
Figure 6.5: Points at compaction curve outside the zero air void line due to mistake in volume calculation of the tensile mould.	163
Figure 6.6: Image showing preparation of compacted specimen by tensile mould; (a) Compaction by tensile compaction tool in three layers, (b) Finished compacted specimen, (c) Specimen prepared for cutting into shape, (d) Cut compacted specimen placed inside the tensile testing device.	164
Figure 6.7: BS light compaction mould to prepare compacted specimen at higher dry density.	165
Figure 6.8: Schematic of direct tensile strength equipment; (a) Top view, (b) Front view.	167
Figure 6.9: Laboratory set-up for tensile test.	168
Figure 6.10: Assembling different parts of the tensile device and mounting the specimen step by step.....	170
Figure 6.11: Tensile test specimen during test: Starting of a crack in the failure zone (left); Front view of a test specimen (right)	171
Figure 6.12: Tensile test after failure; (a) Reconstituted specimen at lower water content, (b) Reconstituted specimen at higher water content, (c) Compacted specimen at lower water content, (d) Compacted specimen at higher water content.	172
Figure 6.13: Load deformation curve for reconstituted and compacted specimen during drying from higher water content towards lower water content.....	174

Figure 6.14: Evolution of tensile strength of Bengawan Solo soil during drying at reconstituted and compacted states.	175
Figure 6.15: MIP equipment used for the tests.	180
Figure 6.16: (a) MIP specimen wet, (b) MIP specimen freeze dried, (c) MIP specimen just before test, (d) MIP specimen after test, (e) MIP specimen broken after test in order to check proper mercury penetration during test.	181
Figure 6.17: MIP results for all reconstituted specimen at four different initial conditions to capture the evolution of soil microstructure during drying.	184
Figure 6.18: MIP results for all compacted specimen at four different initial conditions to capture the evolution of soil microstructure during drying.	184
Figure 6.19: MIP results for all reconstituted vs. compacted specimens.	185
Figure 6.20: FESEM (Field Emission SEM) equipment: JSM-7001F used for the tests.	187
Figure 6.21: Specimen holder with samples TTC01, TTR01, TTC03 and TTR03. Samples were freeze-dried and coated with 2 nm platinum and palladium.	188
Figure 6.22: Sample inside the high-vacuum FESEM chamber (absolute pressure of 9.6×10^{-5} Pa).	188
Figure 6.23: ESEM micrograph of inter-aggregate pore present in compacted specimen ($\approx 2.86 \mu\text{m}$ and $3.57 \mu\text{m}$); TTC01 (36.119%, 1.32 mg/m^3).	189
Figure 6.24: ESEM micrograph for reconstituted specimen TTR 01 (37.929%, 1.32 mg/m^3), soil aggregate not well defined.	190
Figure 6.25a: ESEM micrograph for compacted specimen TTC03 (23.600 w%, 1.56 mg/m^3).	191
Figure 6.25b: ESEM micrograph for reconstituted specimen TTR03 (24.005 w%, 1.57 mg/m^3); soil aggregate not well defined.	191

Figure 6.26: The main retention wetting/drying path for reconstituted specimen of Bengawan Solo soil.....	192
Figure 6.27: Water retention curve for Bengawan Solo soil compacted at different dry densities and water content.	193
Figure 6.28: Retention curve for reconstituted specimen and compacted specimen at two dry densities and water content.	194
Figure 6.29: Water retention curve for Bengawan Solo soil at compacted condition estimated from MIP.....	195
Figure 6.30: Water retention curve for Bengawan Solo soil at compacted and reconstituted condition for higher dry density estimated from MIP; compared with the test results of El Mountassir (2011).	196
Figure 6.31: Summary of tensile test campaign for Reconstituted and Compacted specimen; (a) Tensile strength, (b) MIP results at different dry densities, (c) FESEM micrograph at different dry densities.	198

List of Tables

Table 2.1. Size classification of fissure.....	11
Table 2.2. Surface geometry classification of fissures.....	11
Table 2.3: Fissure surface roughness classification.	12
Table 2.4: Intensity classification of fissure.	12
Table 2.5: Spacing classification of fissure.....	12
Table 2.6: Variation of tensile strength with test method by Harison et al. (1994) and after Lakshmikantha (2009).	20
Table 3.1: Summary of soil properties (some data after (El Mountassir, 2011)).....	65
Table 3.2: Methods used for determining soil property of Bengawan Solo soil.	65
Table 3.3: Soil mineralogy - Total fraction mineralogical semi-quantification by means of X-ray diffraction (% weight).	67
Table 3.4: Clay fraction (<2 μ m fraction) mineralogical semi-quantification by means of X-ray diffraction (% weight).	68
Table 4.1: Test reference for desiccation plate test.....	87
Table 4.2: Summary of the desiccation test for circular plate in grooved based at three different soil layer thicknesses.	98
Table 4.3: Summary of the desiccation test for different plate geometry.....	104
Table 4.4: Crack network parameters for three different plate geometries at similar soil layer thickness.	104

Table 4.5: Crack network parameters for three different thickness circular plate grooved base (D = 125 mm).	105
Table 5.1: Desiccation Test details using 3D compact Laser Scanner.	114
Table 5.2: Scan CONTROL 2700-100 scanner specification.....	117
Table 5.3a: Crack network analysis by Image analysis from LDT02.....	145
Table 5.3b: Crack network analysis by Laser scanner 3D image from test LDT02.	145
Table 5.4a: Crack network analysis by Image analysis from LDT03.....	146
Table 5.4b: Crack network analysis by Laser scanner 3D image from LDT03.....	146
Table 5.5: Comparison table: image analysis vs laser scanner results.....	147
Table 6.1: Initial condition of specimens used for tensile strength test campaign. .	160
Table 6.2: Details of tensile strength tests.	173

Chapter 1: Introduction

1.1 BACKGROUND

Desiccation is the process a material undergoes partially whilst experiencing drying. Naturally forming desiccation cracks start as wet, muddy sediments desiccate, and are caused contraction created by volumetric shrinkage. As soon as the crack is initiated, individual cracks join up to form an interconnected network. Cracking is a complex phenomenon in general, and especially for materials like soils. Soils are inherently heterogeneous, multiphase materials with history, time, temperature, and water content dependent behaviour. The rate, quantity and extent of desiccation cracking are dependent on various physical properties. These include moisture condition, suction effects, temperature and wet as well as drying cycles.

Desiccation cracks pose challenges to civil, geotechnical and environmental engineering works as they significantly affect soil performance and have the potential to cause significant damage to the surrounding environment. Cracks can develop due to various processes such as desiccation and shrinkage, tensile stress of the soil, freezing, penetration by plant roots etc. Shrinkage cracking is significant in earth embankments, slopes, foundations and roads. Tensile cracks influences the

stability of natural slopes and cuts (Baker, 1981, Bagge, 1985). Cracks create zones of weakness in a soil mass, reducing its overall strength and stability.

Other examples of desiccation cracks can be found in various geotechnical, agricultural and environmental applications e.g. irrigated land, tailing ponds for mining waste, landfill liners, earth embankments, reservoir beds etc. (Colina and Roux, 2000). In agricultural engineering, water and solute flow through cracked soil can enter in irrigated land. The presence of desiccation cracks can render a low conductivity barrier, constructed of clay soil, ineffective (Kodikara et al., 2000b). Drying of earth dams may leads to the formation of shrinkage cracks which might cause piping failures (Sherard, 1973). Cracks are also a possible prediction of failure surface at the top of the dams and embankments (Cooling and Marsland, 1953). Hydraulic conductivity of clay liner material in presence of cracks can increase from 1×10^{-9} m/s for wet and intact soil to 1×10^{-6} m/s in cracked soil (Albrecht and Benson, 2001). Compressibility increases and the rate of consolidation decreases with crack initiations (Morris et al., 1992b). Complex crack networks may create pathways for rapidly transporting pollutants to the subsoil, and this is a problem for accurately modelling flow and contaminant transport in clay soil (Vogel et al., 2005a, Vogel et al., 2005b).

Accurate measurement of parameters for soil shrinkage cracks is not easy by direct measurement. Large measurement errors are likely due to irregular shapes and complex cracks patterns. Despite this limitation, characterisation of crack patterns is useful in many different fields of science and engineering. Crack in soils has proven to be an important subject to study to improve the soil management, and treatment in agricultural science as well.

Considerable work has been done to study experimentally the physical phenomenon behind the crack formation. Desiccation cracks have been investigated for many years, e.g. Corte and Higashi (1960), Abu-hejleh and Znidarcic (1995), Konrad and Ayad (1997a), Abu-hejleh and Znidarcic (1995), Konrad and Ayad (1997b), Corte and Higashi (1960) . To explain the development and extent of desiccation cracking, several factors have been considered including clay content and mineralogy, particle

shape and size, soil thickness, surface configuration, rate of drying, total drying time etc. (Aitchinson and Holmes, 1953).

As the structure of a soil is an important property that affects water storage and movement, it is necessary to measure crack size and pattern precisely. Examples of basic crack measurements are reported in several works (Lima and Grismer, 1992, Abedine et al., 1971, Logsdon et al., 1990). With the advancement of computer hardware and software analysing tools, digital imaging techniques have grown in prominence in this research area. Guidi et al. (1978) executed electro-optical determination to estimate size distribution of crack. Lima and Grismer (1992) used photographic image analysis to determine soil surface cracking. Photographic image analysis techniques appeared to be a useful tool to distinguish differences in crack patterns (Vogel et al., 2005b, Costa and Kodikara, 2007, Lakshmikantha et al., 2009, Tang et al., 2008a).

Despite decades of research, the essential mechanisms of desiccation are not fully understood. Existing observations are limited by visibility from the soil surface. There is a need for development of device to study the formation and propagation of desiccation cracks in three dimensions. The new and advanced knowledge of unsaturated soil can sure make a significant contribution for explaining cracking mechanism from different angle.

This research has been conducted on soil from a flood protection embankment along the Bengawan Solo River in East Java, Indonesia. The highly-dense desiccation crack network observed in this man-made embankment may have an important role in the occurrence of the progressive failures detected frequently along the embankment. In a drying soil, drying causes shrinkage and a crack initiates when the tensile stresses exceed the soil strength. The tensile strength is dependent on the moisture content of the soil and the associated suction. In this thesis, keeping in mind of these influencing factors behind cracking behaviour, Bengawan Solo soil has been investigated experimentally under laboratory environment.

The investigation into desiccation cracks in soils is of significant importance to Civil, Geotechnical and Environmental Engineering on a global scale. Climate change may

increase the diversity and severity of current weather conditions to the point of extreme change. With temperatures in the tropical areas around the world predicted to increase and thus wetting and drying cycles expected to become more extreme, the importance of researching the effects and mechanisms of desiccation cracks in soils has become most topical. This research work makes significant improvements in laboratory testing procedures using modern technology to investigate cracking behaviour of soil so that effective interventions can be developed.

1.2 OBJECTIVES

The main aim of this research is to establish a better understanding on the physical processes and phenomena involved in desiccation and cracking of soils by new and properly developed experimental techniques.

More specific objectives are:

- To investigate the desiccation crack phenomenon in the Bengawan Solo soil
- To identify experimentally the mechanisms of cracking in soils
- Investigate the relationship between plate geometry and onset of cracking
- To determine the influence/effect of tensile strength on drying soil
- To study the evolution of soil microstructure during drying in reconstituted and compacted material
- To improve the experimental techniques currently used for the investigation of cracking in soil to gather information for variables during desiccation process (such as: crack aperture, cracks depth, crack geometry) that are difficult to measure with other typical technique currently used.

To achieve these objectives, following research methodology is adopted:

- Summarise the published data on desiccation and cracking of soils from all available sources and fields of research
- Find the basic cracking behaviour of the Bengawan Solo soil using conventional/current methods such as desiccation plate tests
- Apply image analysis techniques to quantitative analysis of the cracks and crack patterns
- Implementation of a compact 2D/3D Laser line scanner to achieve an improved and alternative experimental setup to all current available methods to study desiccation cracking in soil. This is the most important original contribution in this work
- Measure the tensile strength of the Bengawan Solo soil considering the effect of moisture content and density. The specimens are prepared at different moisture content within a defined range taking into account the variation of moisture content in a desiccation test both at reconstituted and compacted condition
- Undertaking fabric studies using Mercury Intrusion Porosimetry (MIP) and The Field Emission Scanning Electron Microscope (FESEM) to understand the microstructure of the Bengawan Solo fill. The fabric studies aim to support and better understanding of the mechanical behaviour on evolution of soil structure during drying

The experimental outcomes aim to gather relevant data associated with the behaviour of drying soils, more information than those typically gathered from current methods.

1.3 OUTLINE AND PUBLICATIONS

In order to address each of the research objectives, the thesis has been organised into seven chapters as detailed below.

Chapter 1 Introduction starts with a background to present this thesis which supports the importance of the findings as a contribution of the current knowledge on soil desiccation and cracking. The objectives and the outline of the thesis are briefly explained.

Chapter 2 State of Art presents a review of published research work related to desiccation, cracking and drying of soil. The concepts and experimental techniques previously and presently being used to investigate desiccation cracking in soil are discussed followed by a short discussion of available volume measurement methods of soil and microstructure of compacted and reconstituted soils.

Chapter 3 Soil Characterisation describes the research material Bengawan Solo soil, which was collected from an embankment along the Bengawan Solo River in East Java, Indonesia. Laboratory characterisation of the Bengawan Solo soil including information on the soil properties, particle size distribution, and soil mineralogy are given. The information is a summary of research conducted by El Mountassir (2011) at the University of Strathclyde, followed by test results of linear shrinkage and volumetric shrinkage characteristics performed within this research. Geotechnical failures due to cracking which have been observed along the embankments are described. Methods of sample preparation for all test conducted for this research is then discussed.

Chapter 4 Desiccation plate tests presents the desiccation test performed on reconstituted Bengawan solo soil. The tests explore the effect of specimen thickness and geometry on crack initiation and propagation towards the final crack network. To gather detail information about cracking mechanisms, digital image analysis technique has been used to analyse the desiccation plate tests. A detailed of digital image analysis is presented at the end of the chapter which includes explaining techniques to process sequence of images how information can be used by means of image analysis. Two conference papers has been published based on the of this chapter in Proceedings of 2nd International Conference on Environmental Science and Technology-ICEST 2011 and Proceedings of 4th Asia-Pacific Conference on Unsaturated Soils, 23-25 November 2009.

Chapter 5 Desiccation tests with compact 2D/3D laser scanner presents the development of an improved technique and alternative to current experimental set up for investigating soil desiccation and cracking. This method allows for the reconstruction of crack formation and propagation in three-dimensions. The results show the applicability of laser technology to study desiccation cracks in soil and provide a foundation for larger scale experiments in future. A paper on this research entitled ‘Compact 2D/3D profile laser sensor to study the behavior of drying soils’ has just been accepted to ACTA GEOTECHNICA. .

Chapter 6 Tensile strength and micromechanical state describes determination of tensile strength of Bengawan Solo Soil at both reconstituted and compacted condition. These results are supported by a micro-structural study conducted using Mercury Intrusion Porosimetry (MIP) and The Field Emission Scanning Electron Microscope (FESEM). A journal paper is under preparation, tentatively titled ‘*The effect of desiccation on tensile strength of drying soil: reconstituted versus compacted state*’ from the results of this chapter.

Chapter 7 Conclusions outlines the main conclusions and contributions of the research presented in this thesis. Suggestions for further study are also presented.

Chapter 2: State of the art

2.1 INTRODUCTION

The desiccation of a natural soil usually involves gradual moisture content reduction induced by evaporation from the soil surface. Desiccation cracking significantly affects soil performance. The recent advancement in experimental geomechanics has increased attention towards this subject area, driven by the fact that the presence of cracks in many geotechnical engineering applications affects soil performance. The mechanisms of desiccation cracking can only be well understood by adopting a systematic research approach to continuous experimentation and analysis.

This chapter begins with a brief discussion on soil desiccation and cracks. The classifications of cracks and causes/factors influencing cracking behaviour of soil are discussed shortly. Experimental works and techniques investigating desiccation cracking in soil are explored later on, followed by available literature on soil testing relevant to this research. The concepts and definitions presented herein will be used for interpreting data in *Chapter 4 'Desiccation plate tests'* and *Chapter 6 'Tensile strength and micromechanical state'*.

2.2 DESICCATION CRACKS

Desiccation is a process in drying soil, and cracking is one of the results of this process. Desiccation cracks in soil are a common phenomenon and are frequently observed in many natural and man-made earth structures.

Previous studies on desiccation cracking date back to the early twentieth century. The general meaning of desiccation cracking of soil was defined in a variety in literature. The definitions and examples given below are based on available literature on the mechanism of desiccation cracking of soil given by various researchers:

Shrinking soil often cracks when they dry. Cracking occurs under different conditions and it cannot be explained in the same way (Towner, 1987a).

Cracking in soil that are undergoing drying is controlled by soil suctions and by soil properties such as compression modulus, Poisson's ratio, shear strength, tensile strength and specific surface energy (Morris et al., 1994).

Desiccation cracks usually initiate on the surface and propagate downwards, which causes cracked soil columns to have a desiccated surface (Abu-hejleh and Znidarcic, 1995).

The cracks are a result of an internal energy imbalance in the soil mass caused by non-uniform moisture distribution, temperature distribution, or distribution of compaction energy during construction (Fang, 1997b).

The interchange of moisture required for the soil water balance to adjust itself both seasonally and in the long term takes place mainly by the transfer of energy and water through the soil surface. As this transfer takes place, the soil is alternatively wetted & dried, and swells & shrinks in sympathy. The shrinkage results in surface cracking, and the subsequent wetting and swelling causes the cracks to close again (Blight and 1997).

Cracking in muddy sediments during drying is a commonly observed phenomenon in drying puddles, river-flood plains, man-made embankments and lake

margins during droughts. The arising cracks are known as mud crack or desiccation crack (Weinberger, 1999).

Cracking mechanisms are highly complex phenomena influenced by the strong coupling between the hydrological and mechanical behaviour of soils. Water loss during evaporation induces a rise of capillary forces. This process is basically controlled by the hydraulic properties of the soil mass, and affects the mechanical behaviour because the soil tends to contract under increasing suction. During shrinkage, soil particles tend to reconfigure to support the changes in the stress state and at a certain point of the drying process, the crack generation begins.

The usual terms generally associated to cracking mechanism will be discussed further in *Chapter 4, Desiccation plate tests* due to their relevance on the desiccation plate tests.

2.3 CLASSIFICATION OF SOIL CRACKING

It is important to classify cracking for eventual engineering analysis of cracking behaviour. This section is focused on classification for soil cracking given by previous researchers:

- Classification after Fookes and Denness (1969)
- Classification after Fang (1997b)

2.3.1 Classification after Fookes and Denness

According to British Standards institution (BS2742C:1957, 1957) the word cracks and joints are regarded to refer to large discontinuities such as open and closed and

discontinuous fissures. The classification for soil cracking proposed by (Fookes and Denness, 1969) was based on size (e.g. very large fissure, large fissure, normal fissure, small fissure, very small fissure), surface geometry (e.g. planar, semi-curved, curved, hinged, semi-undulose, undulose, conchoidal), surface roughness (e.g. slickensided, very smooth, smooth, slightly rough, rough, very rough, pock marked, pitted), intensity (e.g. very low, low, moderated, high very high, excessive) and spacing (e.g. very thickly, thickly bedded, medium bedded, thinly bedded, very thinly bedded, laminated, thinly laminated) and was aimed to unravel these differences.

Tables 2.1, 2.2, 2.3, 2.4, and 2.5 show the classification system given by Fookes and Denness (1969) . Classifications include size, geometry, surface roughness, intensity, and spacing of cracks.

Table 2.1. Size classification of fissure.

Type	Size (area)
Very large fissure	$\geq 100 \text{ m}^2$
Large fissure	$1 - 100 \text{ m}^2$
Normal fissure	$0.01 - 1 \text{ m}^2$
Small fissure	$1 - 100 \text{ cm}^2$
Very small fissure	$\leq 1 \text{ cm}^2$

Table 2.2. Surface geometry classification of fissures

Type	Description
Planar	$L/R \leq \pi/8$
Semi-curved	$\pi/8 < L/R < \pi/4$
Curved	$L/R \geq \pi/4$
Hinged	Combination of planar and semi-curved
Semi-undulose	Combination of two or more alternatively convex and concave semi-curved
Undulose	Combination of two or more alternatively convex and concave curved
Conchoidal	As a conchoid

Table 2.3: Fissure surface roughness classification.

Type	Sand Paper Grade	Height of Asperity, H (above main plane of fissure, mm)
Slickensided	00	0
Very smooth	00	$0 < H \leq 2$
Smooth	00 – 01	$2 < H \leq 4$
Slightly rough	01 – 02	$2 < H \leq 4$
Rough	02 – 03	$4 < H \leq 6$
Very rough	03 – 04	$4 < H \leq 6$
Pock marked	04	$6 < H \leq 8$
Pitted	-	$H > 8$

Table 2.4: Intensity classification of fissure.

Intensity type	Area of fissure per unit volume (m^2/m^3)
Very low	≤ 3
Low	3 -10
Moderate	10 – 30
High	30 – 100
Very high	100 – 300
Excessive	≥ 300

Table 2.5: Spacing classification of fissure.

Description	Spacing of fissure
Very thickly	> 2 m
Thickly bedded	0.6 m – 2 m
Medium bedded	0.2 m – 0.6 m
Thinly bedded	60 mm – 200 mm
Very thinly bedded	20 mm – 60 mm
Laminated	6 mm – 20 mm
Thinly laminated	< 6 mm

2.3.2 Classification after Fang

Fang (1997b) classified four basic types of cracking in soil:

- Shrinkage cracking
- Thermal cracking
- Tensile cracking
- Fracture cracking

2.3.2.1 Shrinkage cracking

Shrinkage cracking is the most common cracking found in earth structures. This is the case particularly can be observed in drying mudflats. Tensile forces resulting from water loss in the drying surface layer causes formation of shrinkage cracks. The surface layer then breaks up into geometric shapes. The shapes of the cracks depend on the mineral composition, heating process, pore fluids, and other features. As shown in Figure 2.1, Illite shows finer cracking patterns than Muscovite, and also the cracking patterns between oven and air dried samples of Illite and Muscovite different due to the differences in the heating process.

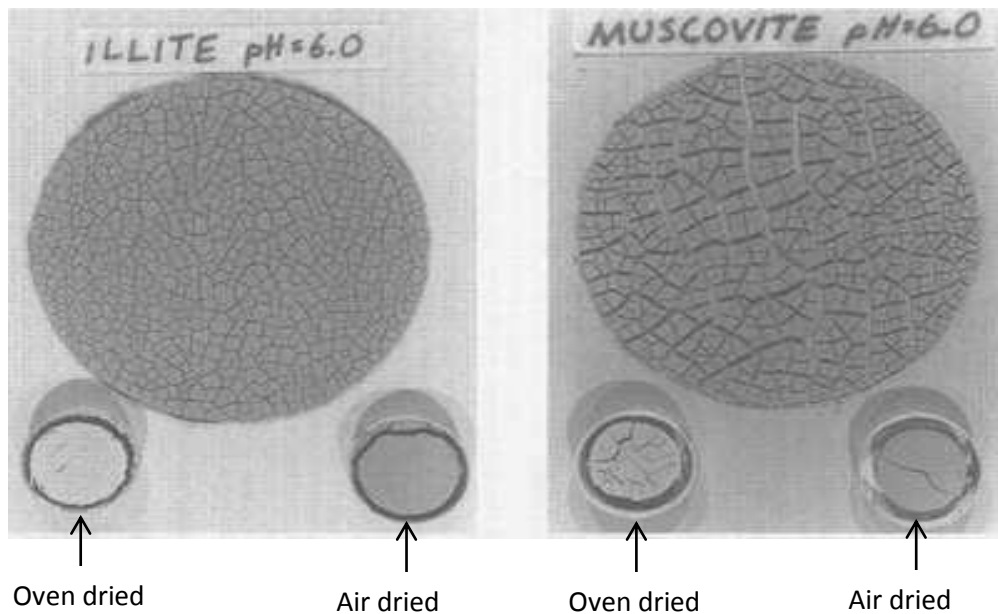


Figure 2.1: Cracking patterns comparison between oven and air dried samples of Illite and Muscovite clay (Fang, 1997b).

2.3.2.2 Thermal cracking

Thermal cracking is caused by changes in the thermal stresses of any material. When a material is heated and then cooled suddenly, stresses develop. These may be induced by cycles of freezing-thawing or wetting-drying, and also in pollution intrusion. The cracking pattern depends on drying process as well. As an example, from Figure 2.1, it is evident that the drying process in an oven is more intense and less uniform compared to air-dried processes.

2.3.2.3 Tensile cracking

Tensile cracks are caused by extreme pressures that may include: structural loading, rainfall, ice and snow loads, trees, vegetation and seasonal ground surface creep loads. It can also be caused because of changes in thermal stress and is related to fracture loads.

2.3.2.4 Fracture cracking

According to Fang (1997b), when a saturated soil mass dries, a meniscus develops in the voids of the soil structure, which produces tension in the soil-water system, and a corresponding compression force in the soil skeleton. This internal cyclic-type of load, caused by the combination of shrinkage or thermal stresses and the fluctuation of the pore water pressure between soil particles, is called a fracture load in soil. The cracks that caused by the fracture load are referred to as a fracture cracks.

2.3.3 Other forms of cracks

Cracks can also occur during the compaction process. Compaction machinery impose lateral stress component when compacting clay on steep slope. These lateral stresses can cause horizontal cracks. These cracks are frequently observed near surface and decrease in frequency with depth (Harrison et al., 1992). Clay sticks together in clumps. The original cracks are preserved in the clumps when the compactive effort is applied. Brittle clay and ductile clay with an angled crack in the middle of the specimen were compacted by Vallejo (1988). Different results were found in the two cases. The crack in the brittle clay did not close under initial loading, and then started to propagate as the load increased until the cracks reached the ends of the specimen and failure occurred. The crack in the ductile clay closed under an initial loading, but reopened during load increment. The cracks propagated, but the specimen failed in shear before the crack reached towards the ends of the specimen (Vallejo, 1988). This results show that cracks existing in soils before compaction may still exist in the soil after completion of construction process. Cracks may also form due to tectonic stresses, relief of stresses, or large scale shifts in the clay layer, e.g. cracks caused by earthquakes. Chemical reactions within the clay matrix can also produce cracking. The bonding process of the clay particles is a chemical process that is very delicate. Unknown chemicals may change these bonds, creating weaknesses that lead to cracking in clay. Exposure to strong acids, organic solvents or other caustic chemicals found in waste sites are known to induce cracks (Harrison et al., 1992).

2.4 COMMON CAUSES FOR DESICCATION CRACKS IN SOIL

Since ages desiccation cracks had been an interesting object of study for many researchers. Researchers have focused on several causes for desiccation and cracking starting from local environmental changes such as wetting-drying and freezing-thawing cycles, pollution intrusion, in many cases considering over-consolidated clay

(Fang and Daniels, 2006). The following causes for fissures/cracking in clays were found (Vallejo and Liang, 1994, Lakshmikantha, 2009):

- Drying of clay
- Large lateral stress
- Consolidation process
- Swelling of the clay
- Chemical reaction within the soil clay material
- Tectonic stress during earthquakes
- Inherited from bed rock

Soil composition, compaction, water presence in soil, desiccation process and rate, tensile strength in soil and soil suction influence the shrinking and swelling properties of soil, which in turn influence the cracking behaviour.

2.4.1 Soil composition and structure

The amount of clay regulates the volumetric shrinkage strain in soil. Albrecht and Benson (2001) showed that volumetric shrinkage strain increases with increasing plasticity index and clay content. The mineralogy of the soil they work with contained larger percentages of Smectite. Figure 2.2 shows volumetric shrinkage strain increases with increasing clay content.

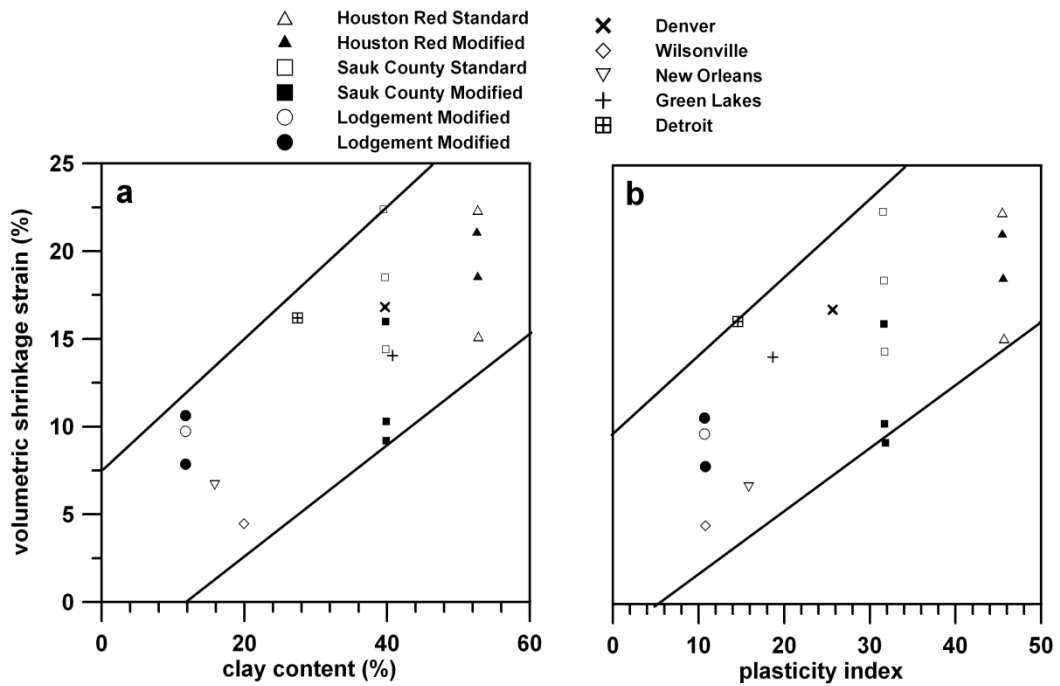


Figure 2.2: Volumetric shrinkage strain versus soil properties; (a) Clay content, (b) Plasticity index (Albrecht and Benson, 2001).

The minerals of the clay fraction play a central role on the properties of the soil, such as plasticity and strength (Mitchell, 1993a). There are certain clay fractions such as Smectite or mixed layer of Illite/Smectite that makes the soil highly attracted to absorb water, causing expansion of the material. Conversely, these soils develop significant change of volume (contraction) during drying. Albrecht and Benson (2001) and Omid et al. (1996) both observed that the shrinkage strains are smaller in soils with less Smectite and more Illite, Kaolinite and Quartz than soils with increased Smectite proportions. They also observed higher volumetric shrinkage for soil having lower dry density (Figure 2.3). Both crack initiation and cracking pattern are influenced by soil structure. Corte and Higashi (1960) did laboratory drying tests for soils with loose packing and close packing structure.

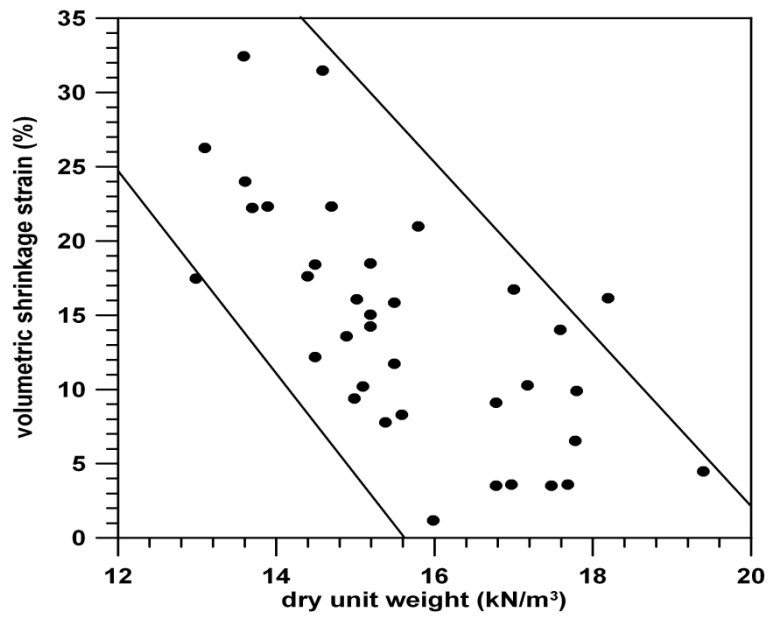


Figure 2.3: Volumetric shrinkage strain and dry density (Albrecht and Benson, 2001).

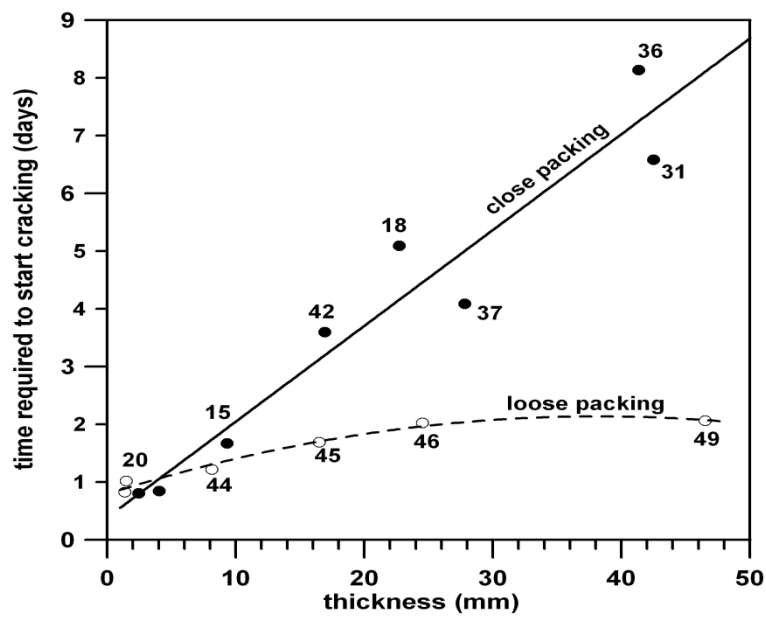


Figure 2.4: Influence of thickness of soil on crack initiation (Corte and Higashi, 1960).

Figure 2.4 shows the laboratory results of Corte and Higashi (1960) on drying soil with two different arrangements of soil particles. They proposed a linear relationship

in between the crack initiation and the thickness of soil layer for densely packed soil. For loosely packed soil this relation was non-linear. Furthermore, cracking in loosely packed soil started at higher water content than the densely packed soil.

Andrews et al. (1967), Fang (1997a), Alther et al. (1985), (Fang, 1997b) showed differences in desiccation cracking behaviour in flocculent (refers to edge to face arrangements) or dispersive (refers to face to face arrangements) soil structure (Figure 2.5). Flocculated structure means larger cracking area compared to dispersed structure.

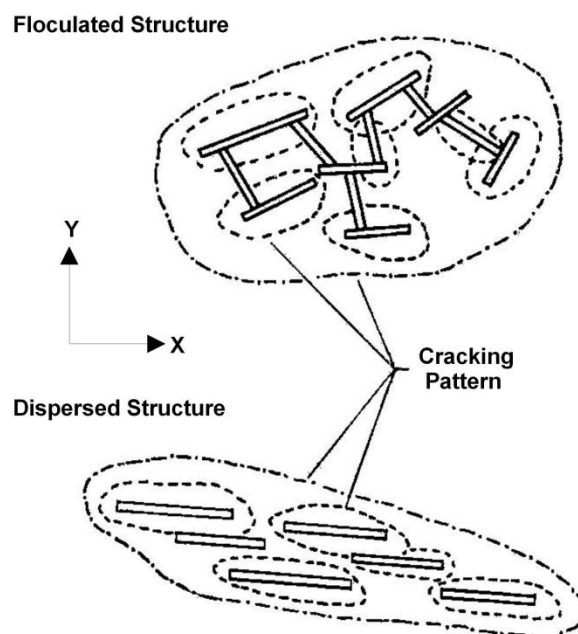


Figure 2.5: effect of soil structures on cracking patterns; (a) Flocculated structure, and (b) Dispersed structure (Fang, 1997b).

For compacted soils, compaction effort and variation of soil water content in soil are important parameters for desiccation cracking found on the work of previous

researchers, see e.g. Omidi et al. (1996), Albrecht and Benson (2001), Babu and Gartung (2001), Omidi et al. (1996) .

2.4.2 Tensile strength

In certain types of soil, crack initiation occur under saturated condition, and in other soils under different climatic conditions, the crack initiation occurs in unsaturated condition. This is why for the application in the study of desiccation cracking, it is important to determine the tensile strength of soil in both conditions. There are different test methods for determining tensile strength in soil. Table 2.1 summarises the variation in tensile strength for different test method observed by Harison et al. (1994).

Table 2.6: Variation of tensile strength with test method by Harison et al. (1994) and after Lakshmikantha (2009).

Test method	Specimen dimension (mm)	V_{95} (mm ³)	Strength ratio
Ring test	$R_o / R_i = 8; R_o = 50; t = 25$	8.29	1
Three-point bending	$200 \times 50 \times 25; 100 \times 50 \times 25$	156; 78.1	1.78; 1.56
Four-point bending	$200 \times 50 \times 25$	2187	3
Brazilian test	$R_o = 50; t = 25$	10596	4.10
Direct-pull dog bone	$d = 25; L = 35$	17181	4.5

where, R_o = Outside radius; R_i = Inside radius; t = Thickness; d = Diameter; L = Length; and V_{95} = Volume of the part of the specimen subjected to at least 95% of maximum tensile stress.

Towner (1987a) explains how the tensile strength depends on soil water content using remoulded clay bars. Figure 2.6 shows the tensile load at failure vs. water content from his work: the trend found was increasing tensile load at failure with decreasing water content.

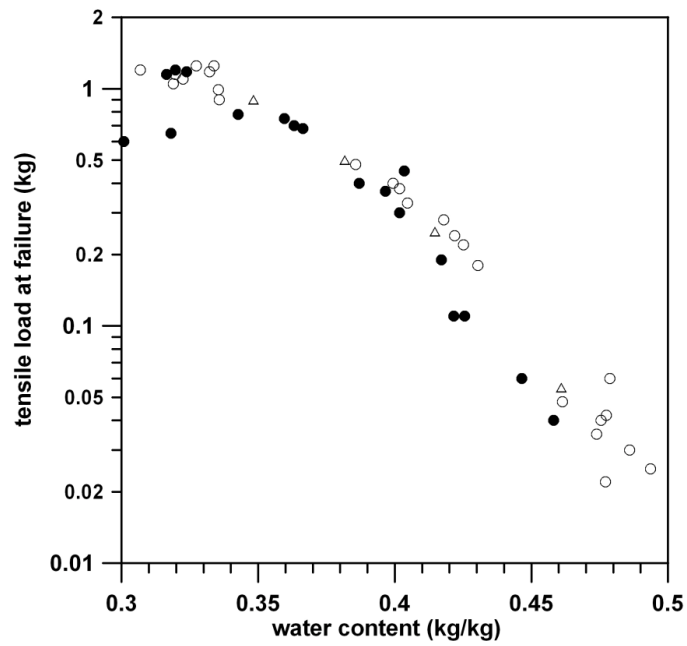


Figure 2.6: Tensile strength variation with degree of saturation (Towner, 1987a).

2.4.3 Soil suction

Konrad and Ayad (1997b) and Abu-hejleh and Znidarcic (1995) explained in their work that the critical suction at crack initiation near the soil surface during the shrinkage desiccation process depends on the soil tensile strength, initial stress state, total and effective stress path and the stress history of the soil. Many geotechnical problems are associated with volume change and moisture change; and suction is one of the major parameter that controls these phenomenon in soil (Fleureau et al., 1993).

2.4.4 Vegetation

Ravina (1983) described vegetation can also cause shrinkage and cracking, influenced by the process called transpiration. Depending on the water requirement of different species of plants, the drying pattern of the clay also varies. This affects the shrinkage behaviour of the clay. This phenomenon was studied by Biddle (1983). The effect of vegetation on shrinkage was further studied by e.g. Richards et al. (1983), Driscoll (1983) and Holtz (1983) and they all concluded the vegetation causes the increasing rate of shrinkage within soil. Alonso and Lloret (1995) also agreed on the fact that vegetation causes faster moisture loss of soil.

2.5 EXPERIMENTAL STUDIES INVESTIGATING SOIL DESICCATION AND CRACKING

2.5.1 Laboratory Experiments

A number of laboratory experiments have been performed to study the development of desiccation cracks, generally by using slurries of several centimetres thickness or compacted clay in a container/plate (Shorlin et al., 2000, Colina and Ronux, 2000, Kodikara and Choi, 2006). When the specimen starts to contract upon drying, this leads to a build-up of tensile stress in soil, and when the stress exceeds the local tensile strength, the soil cracks. The drying process of a starch-water mixture was investigated by Mizuguchi et al. (2005). The results suggested a polygonal structure in the horizontal sections (see in Figure 2.7, which is a snapshot in stage 3 as

described below). The distribution function of the angle between cracks had a single peak near 120° . The size of cracks found to be increased with depth.

Three stages were noticed during the drying process in order to clarify the mechanism of crack formation:

Stage 1: Water content decreases uniformly;

Stage 2: A sudden change of water content occurs and primary cracks are formed between the mixture and the side wall of the container or plate. The water content distribution remains approximately uniform;

Stage 3: The water content decrease slows down and the distribution is non-uniform. In other words, the soil has a drying front. The front propagates inward and the mixture shrinks non-uniformly. Secondary cracks are formed in this stage. Polygonal structures are observed to form at and above the water front at this stage. Below the front, on the contrary, the distribution is uniform. That concludes the water content in the soil is very important to the crack formation.

Mizuguchi et al. (2005) observed two types of cracks: smooth cracks (Type I) and sinuous cracks (Type II). Type I cracks were believed to be made by the difference of concentration ratio between the mixture and the container and frictional force between them. Type II was considered to be made by the non-uniformity of the local shrinkage in the mixture. Type I cracks were formed at stage 2 and Type II cracks were formed at stage 3. During formation of Type II cracks, the pattern seemed to emerge at the surface and cracks propagate inwards simultaneously.

In the field, natural soils are subjected to weather changes and shrinkage is a very common phenomena observed during drying. Crack formation and propagation would be expected follow these mechanisms in the field. Type I cracks are formed sequentially followed by Type II cracks contributing three-dimensional, prismatic structure at the surface and vertical propagation inwards. The presence of infrastructure or existing cracks in the soil may serve as points of weakness for Stage 2 and Stage 3 cracks to form.

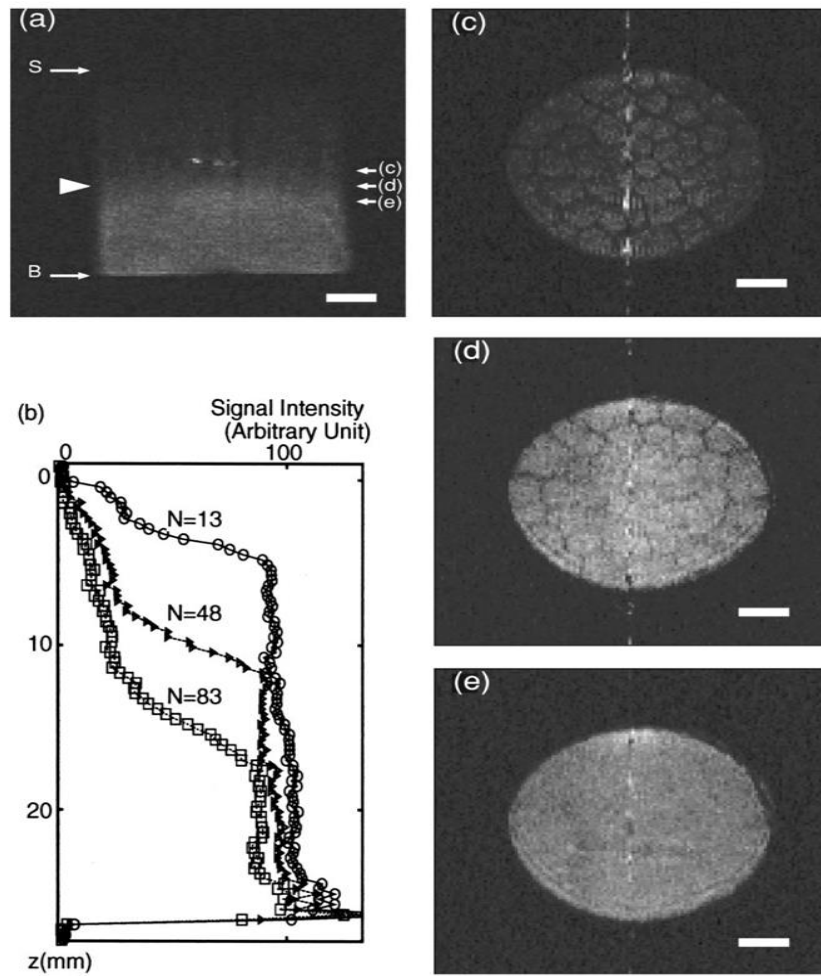


Figure 2.7: (a) Image of vertical section of the sample at $N=83$. White bar represents 5 mm length. Arrows with S and B denote the position of the surface and bottom, respectively. The symbols (c), (d), and (e) represent the position of horizontal slices, which is indicated by the same symbol; (b) Snapshots of signal intensity along vertical direction. The vertical axis corresponds to the depth from the surface and the horizontal axis represents the intensity; Horizontal images (c), (d), and (e) are averaged snapshots around $N=83$ at the position indicated by the symbol in (a) (Mizuguchi et al., 2005).

According to Shorlin et al. (2000), crack morphology is influenced by isotropic drying (in which drying process is controlled by isotropic or uniform conditions) and

directional drying (in which a one-dimensional pattern of cracks propagates due to a moving drying front). Isotropic drying process causes **arching** phenomena in cracks, so named because of their arch-like structure (Shorlin et al., 2000) . This creates a new crack that propagates away from existing cracks, which then curves back on itself in a roughly parabolic path and eventually terminates as it coincides into another crack (Figure 2.8). On the other hand, directional drying processes result in laddering phenomena. During this process, two or more cracks propagate almost parallel to each other, following a local drying front. As the layer behind the moving crack tips dries, a perpendicular cracks forms joining the two parallel cracks like the rungs of a ladder (Figure 2.9).

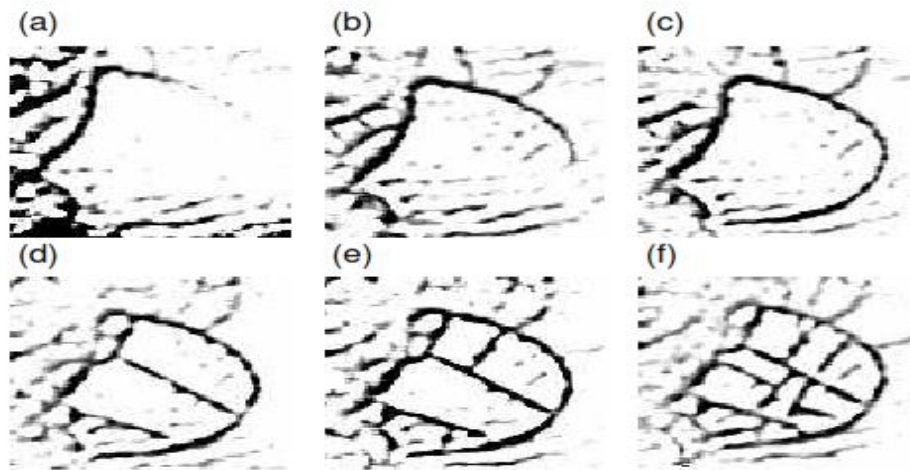


Figure 2.8: A sequence of images of a crack-portion pattern forming in a layer of final depth at 1.51 ± 0.06 mm with a *Teflon coated* substrate and with field of view 5.1 cm x 4.8 cm. Image (a) is 33 hours after the start of the run and the elapsed time between (a) and (f) is 6 hours. This sequence illustrates the **arching** process (Shorlin et al., 2000).

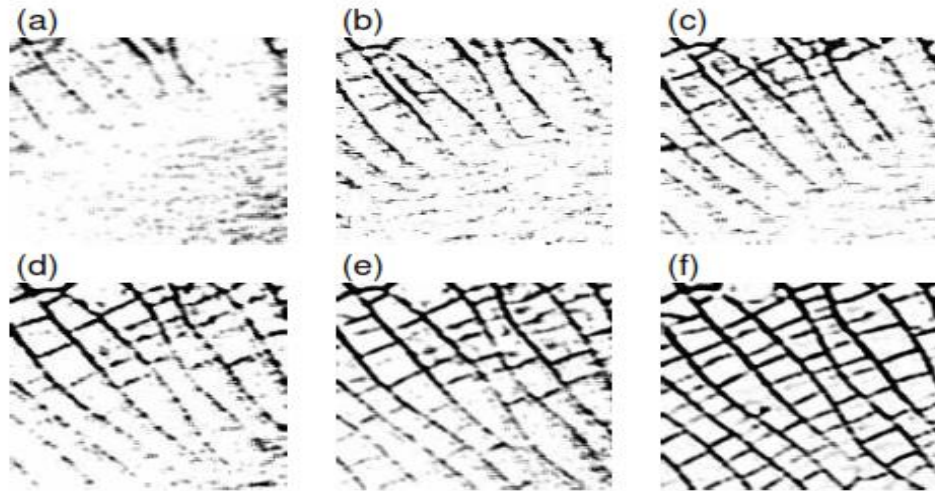


Figure 2.9: A sequence of images of a crack-portion pattern forming in a layer of final depth at 1.88 ± 0.10 mm with an uncoated substrate and with field of view 7.1 cm^2 . Image (a) is 67 hours after the start of the run and the elapsed time between (a) and (f) is 17 hours. This sequence illustrates the *laddering* process (Shorlin et al., 2000).

Crack opening and crack spacing increases with increasing thickness of the specimen (Colina and Roux, 2000). Kodikara and Choi (2006) and Péron et al. (2006) observed that once a crack initiates, subsequent subdivision of the layer takes place rapidly until a number of cracks that are equilibrium with the test conditions have emerged within (Figure 2.10).

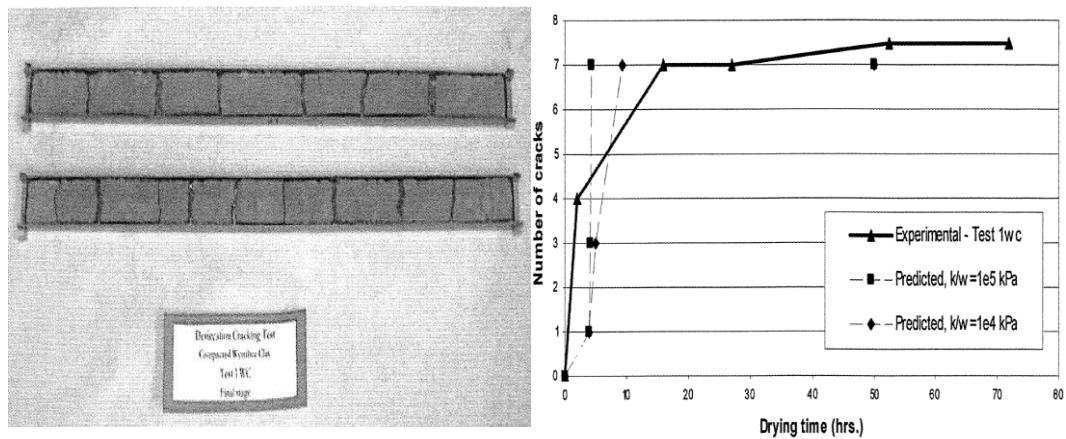


Figure 2.10: *Left*: Cracking pattern of compacted clay at the end of test (desiccation time: 144 hours); *Right*: Development of number of cracks with drying time for compacted clay (Kodikara and Choi 2006).

The experiments mentioned above cannot represent the field conditions with much larger sample size and soil variation. Wells et al. (2003) found that the development of cracks in soils is greatly affected by rainstorms, evaporation, and soil properties in the field. The artificial soil mixtures used in some experiments are not representative of the condition, but the mechanisms of crack formation will be consistent.

It is difficult to find experiments focusing on desiccation and cracking at a larger scale. Among available published work, the experimental work of Corte and Higashi (1960) was found to be most comprehensive series of laboratory tests focusing desiccation of soil layers. The soil used was Bloomington till obtained from a till deposit near Lily Lakes, Illinois. Experiments were carried out in large containers to avoid any boundary effect. Mechanisms of crack formation were analysed by measuring water content at various stages of crack initiation and also by taking images. After the specimen/soil completely dried, various features were determined: shape, size distribution of the cracking cells, total length of crack, area of crack etc. Temperature, relative humidity, thickness of soil layer, material of the bottom of the desiccation containers were considered as important parameters in terms of cracking behaviour/pattern. Around sixty experiments were performed with the soil both in slurry state and loosely compacted state.

Lloret et al. (1998) performed two series desiccation test on compacted and slurry state; a cylindrical specimen and on circular specimens under laboratory conditions. Different soil thickness and bottom contact surface of the holding tray was considered to be important variables. The material used as specimen was mining waste.

Albrecht and Benson (2001) performed desiccation tests on eight types of soil. The specimens were compacted at standard, modified and reduced proctor effort. Each specimen was saturated by permeation before drying at laboratory condition. A wide range of compaction conditions and soil properties were achieved in this work.

Towner (1987b) proposed a theory to explain the mechanisms of cracking of a drying clay. As the clay dries, the tensile stress and the tensile strength increase with decreasing water content (increasing suction), while the clay is assumed to be saturated. This assumption is made because the greatest amount of shrinkage is observed during initial drying (Towner, 1987b) Cracks form when stress induced by drying is equal to or exceeds the tensile strength drawing the clay particles close together. The magnitude of the induced stress is equal to that of the change in soil-water suction for isotropic shrinkage but considerably less for enforced anisotropic shrinkage (Snyder and Miller, 1985). The presence of boundaries (that are typical in laboratory experiments) prevent shrinkage in one or more directions and influence crack formation (Towner, 1987b).

Phenomena observed in laboratory experiments are relevant to field conditions because they capture similar phenomena. For example, temperature control and drying-wetting cycle are applicable in laboratory and field observations. Weather changes and different base condition could have similar effect due to the friction between two soil layers. Vertical cracking in the field during drying corresponds to uniaxial compression in the oedometer (Snyder and Miller, 1985). The cracking experiments by Towner (1987b) showed that constrained clay bars of initially the same length cracked at essentially the same water content irrespective of their initial water contents. When drying clays are prevented from shrinking in one direction, they do not crack until the stress induced in that direction is equal to or greater than the corresponding tensile strength. The induced stress found in the constrained

direction is approximately a function only of the water content and independent of the state of anisotropy.

More recently, Lakshmikantha (2009) focused on experimental and theoretical aspects of the cracking in drying soils incorporating fracture mechanics, classical soil mechanics and image analysis techniques. Desiccation tests in controlled laboratory environment were performed; tensile strength and fracture toughness were measured. Moreover, equipment capable of simulating the different combinations of climatic conditions with monitoring by sensors and a digital camera was designed and constructed named as environmental chamber. This approach allowed experiments on large specimens at laboratory conditions. The morphology of cracks and fissures was explored within.

Published measurements on tensile strength are poor due to lack of a systematic approach of initial sample conditions, increases in tensile strength following a drying path, and observational limitations during cracking. This work seeks to address these weaknesses by systematically evaluating desiccation cracking in three dimensions in a laboratory environment.

2.5.2 Field Experiments

Field experiments on cracking behaviour mostly involved measuring the geometrical parameters of crack. This measurement can be done in-situ by direct methods and indirect methods. Fracture data on exposed surfaces and subsurface are obtained separately in direct methods. Traditional methods for obtaining fracture data on exposed rock surfaces are scanline surveys (ISRM, 1978, Priest and Hudson, 1981), window sampling (Priest, 1993), and digital imaging (Kemeny and Post, 2003). A scanline survey provides fracture information along a line on a rock face. In window sampling, after identifying the rock face, information such as orientation, spacing,

and length are determined for each set of fractures. In digital imaging, surface photographs are taken at specific intervals in order to quantify the surface geometry. Digital imaging can also be used to analyse surface cracking pattern without disturbing the soil specimen. Borehole wall imaging methods are used when detecting subsurface fractures in rock masses using various optical devices, e.g., photoelectric transformers, conventional cameras, and television cameras. Indirect fracture detection methods like elastic methods, electrical and electromagnetic methods, and radar methods are also used to obtain the fracture information in rocks (National Research Council, 1996). Dasog et al. (1988) observed the crack geometries in field by scanline surveys. Konrad and Ayad (1997b) conducted field tests to observe the crack formation using digital imaging.

Konrad and Ayad (1997a) excavated three test sections with different soil properties and depths. Figure 2.11 shows plan view and the longitudinal cross section of the excavation. The first level was the top soil, the second level was weathered clay and the third level was intact clay. During the test, the excavations were covered with a roof to avoid rain water infiltration and the test sections were exposed to the air. The main objective of the experiment was investigating the behaviour of intact clay which was not exposed to any desiccation-drying or freeze-thaw cycle.

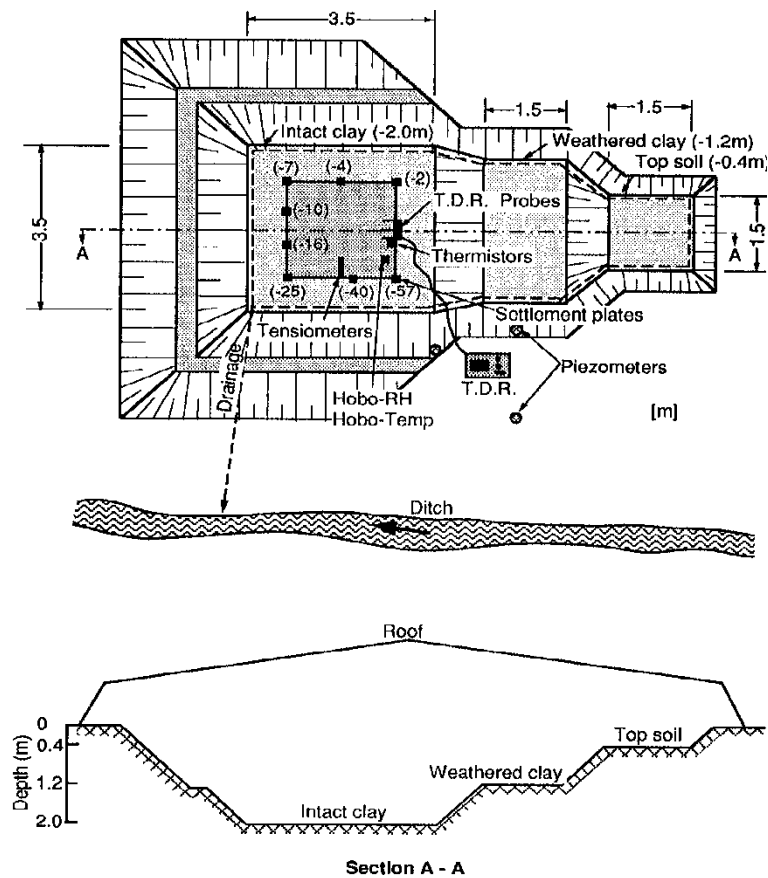


Figure 2.11: Characteristics of test sections.

The fracture characteristics of mud cracks in dehydrating mud puddles in the Dead Sea region, Israel, was investigated by Weinberger (1999). Figures 2.12-2.14 show some of the observed cracks. The morphology showed surface discontinuity between the upper desiccated mud layer and the lower layer which was not cracked. Most importantly it was observed that the crack initiates from the bottom of the desiccated layer and propagate upward vertically towards the free surface and laterally outward toward the adjacent cracks. Interestingly, these findings contradicted previous literature that document cracks initiation at or near the surface.(Lachenbruch, 1961, Morris et al., 1992b, Morris et al., 1994, Prat et al., 2002), or from the middle of the drying soil layer (Corte and Higashi, 1960). In most cases, the cracks propagates downwards.

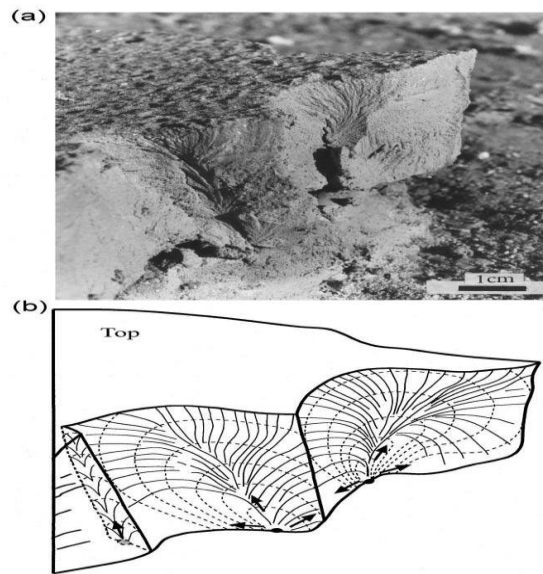


Figure 2.12: (a) Oblique view of two adjacent mud cracks, (b) Their surface morphology interpretation. Crack origins (solid dots) are located at the bottom (Weinberger, 1999).

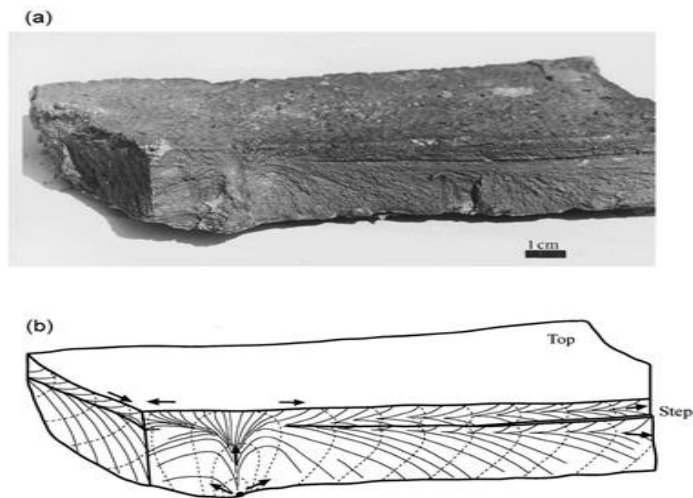


Figure 2.13: (a) Oblique view of a recovered polygon, (b) Surface morphology interpretation of an associated bounded crack. A single vertical plume axis branches in to separate sub-horizontal axes (along which cracks are propagated at opposite direction) that are obliquely oriented with respect to bedding (Weinberger, 1999).

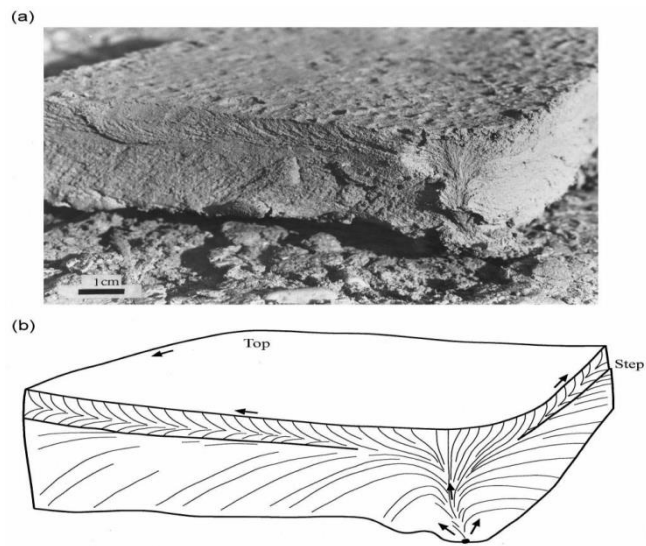


Figure 2.14: (a) Oblique view of a polygon, (b) Interpretation of surface morphology of an associated mud crack. The crack nucleates at depth, ruptures the desiccated layers and subsequently propagates bi-laterally away from the origin along curved paths (Weinberger, 1999).

Several documents are available investigating average spacing and opening for cracks in intact and weathered marine clay. Water content in the soil was observed to be an important parameter to the crack formation. Nishimoto et al. (2007) used stress field and water content field to investigate the formation of 3D cracks by numerical analysis. Moe et al. (2003) prepared two patches of Maryland expansive soil in the field which were air-dried in open air. Crack spacing, cell size, and cell separation were observed for twenty days during drying. The important findings were that between 80-90% of all cracks appeared in the first two days and between 60-80% of crack bounded blocks were formed in this period. The crack network mostly established after six days. Generally, a fully developed crack network had an average cracked block size of around 60 mm, an average crack width of 2 mm and a maximum crack width of about 15 mm (Moe et al., 2003). Wells et al. (2001) used expansive soil from Mississippi delta to study modes of cracking and their impact on filtration. A rectangular box (20 cm x 94.3 cm x 20 cm) with a sub-surface drainage system was used for that test purpose.

2.6 SOIL SHRINKAGE

This Section provides information on work based on soil shrinkage as shrinkage behaviour is closely involved in soil desiccation processes.

Most of the previous studies regarding soil shrinkage were concerned with agricultural aspects. The first relevant work within soil mechanics was by Tempany (1917). He used compacted soils to investigate the relationship between shrinkage and water loss. He suggested the existence of a shrinkage phase, where for fully saturated samples the volume change of the sample is equal to the water volume evaporated. This phase exists for contraction without any restriction by friction in between the internal particles. This contraction continues until a point is reached at which the soil starts developing inter particle friction and resist the shrinkage. The water content at which soil stops contracting further is the shrinkage limit. Shrinkage limit and total volume change were observed by Tempany (1917) as a function of the amount of colloids in the solid.

Haines (1923a) presented a complete interpretation of shrinkage behaviour. He observed that the shrinkage curve (Figure 2.15) consists of two straight lines:

Point C: This is the starting point of drying.

Segment CB: Corresponds to normal shrinkage, the stage where the volume of water evaporated is equal to the reduction of the total volume of the samples.

Second phase BA: This is the second phase, residual shrinkage and represents the stage where part of the water loss is replaced by air.

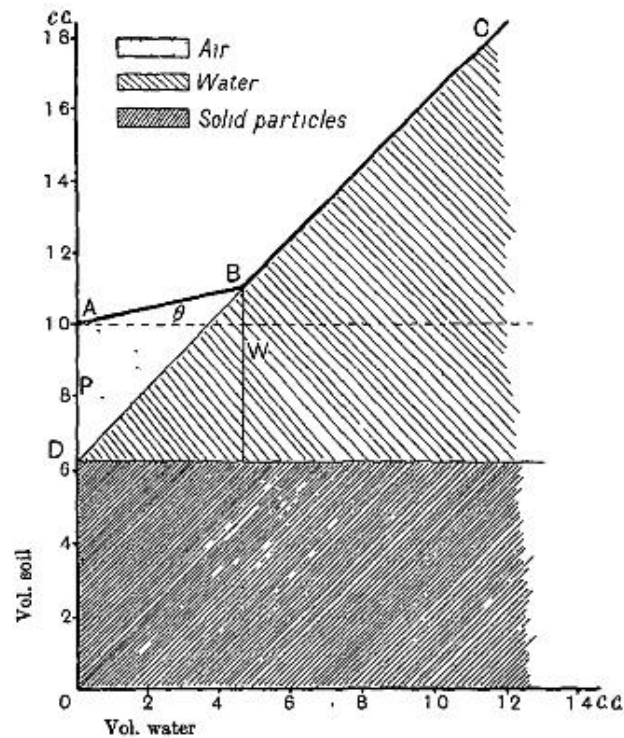


Figure 2.15: Interpretation of shrinkage behaviour (Haines, 1923a).

Eventually shrinkage phenomenon of soil was reviewed by many other researchers (Terzaghi, 1925, Lauritzen and Stewart, 1941, Stirk, 1954, De Jong and Warketin, 1965). Terzaghi (1925) was the first who review shrinkage from an engineering point of view. Lauritzen and Stewart (1941) studied shrinkage of an undisturbed sample and observed a phase prior to normal shrinkage. This kind of phase is available in soil with particular structure. Later this was termed as structural shrinkage by Stirk (1954).

The first model of the soil shrinkage in terms of soil shrinkage was presented by Poulouvas.A (1970). Soil shrinkage was presented in terms of volume of water in soil and suction (Figure 2.16):

AGRB: Saturation boundary drying curve

BEC: Ultimate boundary wetting curve

CDB: Ultimate boundary drying curve

In Figure 2.16, between the ultimate boundary wetting and the saturation boundary drying curves, there are primary wetting curves GHM and RN as well as drying curves MG and NFR.

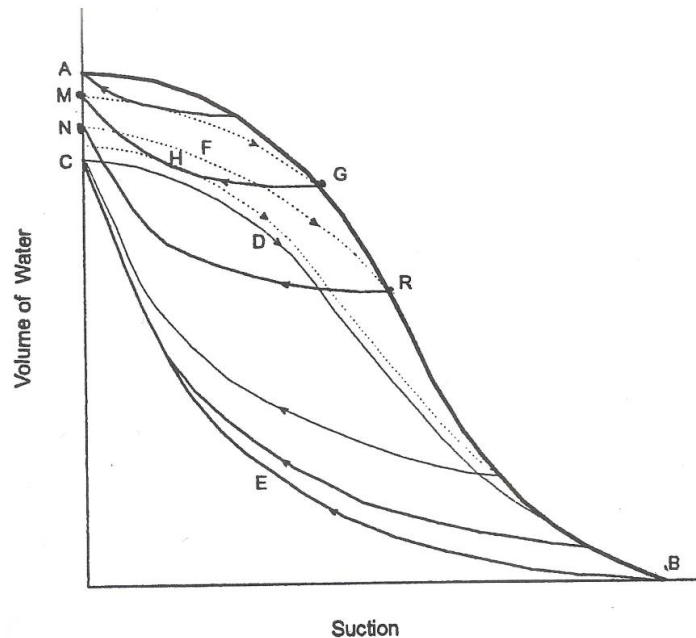


Figure 2.16: Behaviour of soils during drying and wetting process presented originally (Poulovas.A, 1970).

The phases during shrinkage were distinguished as structural shrinkage, normal shrinkage, residual shrinkage, and zero shrinkage (Bronswijk, 1990, Bronswijk, 1991a, Bronswijk, 1991b). Another important publication of interests on shrinkage phenomenon is by Sridharan and Prakash (2000). They considered the process of shrinkage as volume reduction which takes place due to capillary pressures induced by the evaporation of water from the soil. They also suggested that the shrinkage limit of a soil is not a plasticity characteristic of the soil but is the result of packing phenomenon and controlled primarily by the relative grain size distribution of the soil.

2.7 WATER RETENTION BEHAVIOUR

The relationship between the water content retained within the pores of soil over a range of suctions can be expressed by a curve most popularly known as ‘retention curve’. Soil suction and water content are important parameters that control important geotechnical properties such as permeability, volume change, deformability and shear strength (Barbour, 1998). Soil science and geotechnical engineers have acknowledged the importance of soil suction and water content and developed several test techniques to study these phenomena. These techniques have different ranges of applicability, and only the electrical resistance and sensors have been found to be capable of determining the full range of suction values. Most of the procedures are time consuming in comparison to other soil testing. Most of the available studies use granular soil or artificial soil mixture to study the testing procedure. Relatively little data are available for natural clayey soil.

2.7.1 Testing techniques

Depending on suction type, such as matric suction or total suction, and suction range, appropriate test method should be carefully selected. Soil suction can be measured by two types of methods:

- i) Direct methods measure the negative pore water pressure due to suction directly. These methods require good contact between suction sensors and soil sample and measure only matric suction. Available direct methods are tensiometers and axis translations techniques. The tensiometer is the most widely-used instrument for measurement of suction in field and typically measures suction up to 100 kPa, whereas the axis translations technique is a commonly used laboratory method with a suction range from 0-1500 kPa (Nam et al., 2010).

ii) Indirect methods require measurement of other parameters (e.g. water content, relative humidity, resistivity or conductivity) and then relate results to the suction through calibration (Agus and Schanz, 2007, Ridley and Wray, 1995, Agus and Schanz, 2005). This type of technique can be used to measure both total and matric suction. Examples of indirect methods are filter paper technique (Chandler and Gutierrez, 1986, Chandler et al., 1992, Bulut et al., 2001), thermal conductivity sensors technique, chilled-mirror dew-point technique (Leong et al., 2003, Tang and Cui, 2005, Leong et al., 2007) and use of capacitance sensors that measure water content. Chilled-mirror dew-point technique was used in order to obtain water retention curve within this research.

2.7.2 Variation of retention behaviour

Water retention behaviour can be influenced by the type of soil and void ratio. Different types of soil exhibit different ability to retain water, which is clearly evident in Figure 2.17. Figure 2.17 presents water retention curves for four different types of soil; sand, silt and clay (Barbour, 1998, Vanapalli et al., 1999). Ragina clay retained water within soil up to suction of hundreds of MPa and sand sample is largely desaturated at around 100 kPa.

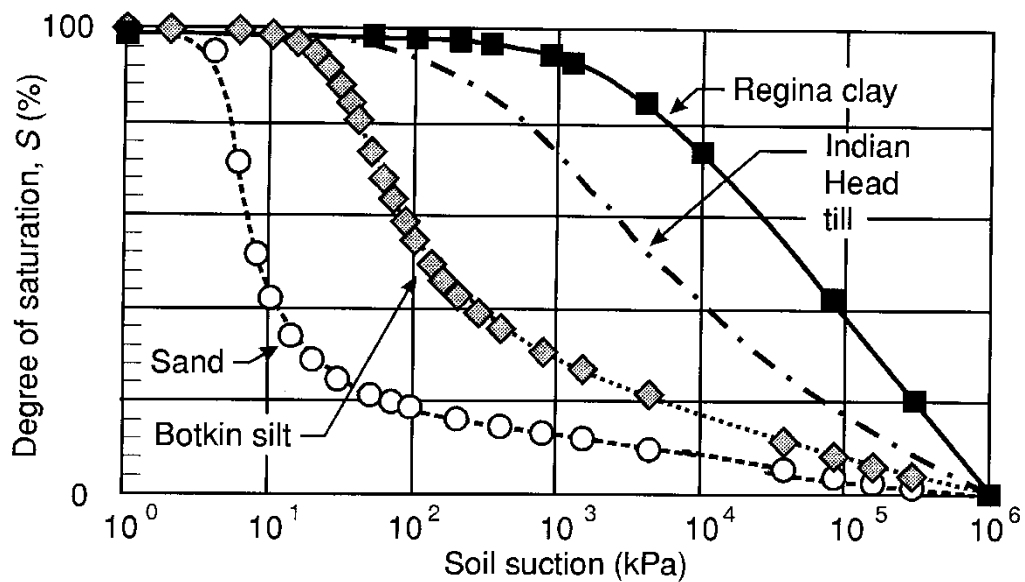


Figure 2.17: Influence of soil type on water retention behaviour (Barbour, 1998, Vanapalli et al., 1999).

Water retention behaviour is also influenced by void ratio even for the same soil. Figure 2.18 presents the water retention behaviour of three soil samples of compacted Boom clay, following a drying path each at a different initial void ratio (Romero, 1999, Nuth and Laloui, 2008). The shift of the retention curve in Figure 2.18 can be explained by a reduction in void ratio that corresponds to an increase in the dry density of the soil. Also, the shape of the curve for the sample with a high initial void ratio is different from the other two samples. It is proposed that this difference is due to soil type; deformable soil undergoes significant changes in volume during drying, which affects the soil structure, and subsequently shifts the retention curve (Nuth and Laloui, 2008).

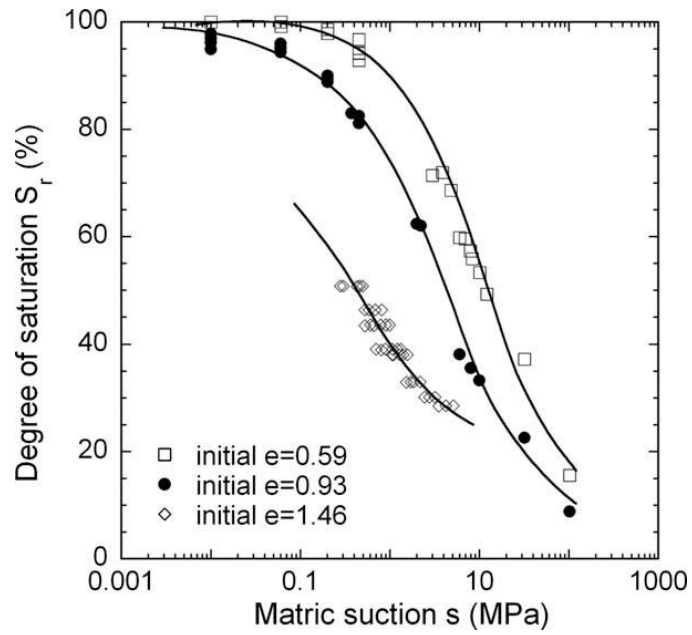


Figure 2.18 : Influence of void ratio and structure on soil water retention behaviour of Boom clay (Romero, 1999, Nuth and Laloui, 2008).

Apart from different soil type and void ratio, soil structure has also been found to influence water retention behaviour (Vanapalli et al., 1999). Figure 2.19 shows that despite of having similar void ratio and same soil, a different air entry value is exhibited for the retention behaviour for sample compacted dry of optimum compared to those compacted wet of optimum. This is due to the different soil structure that is created during compaction at different moisture content.

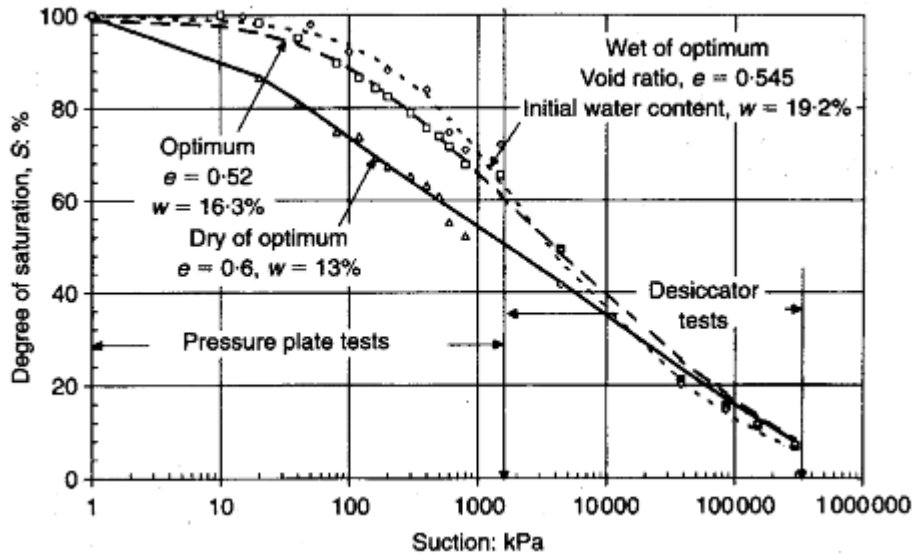


Figure 2.19: Soil–water characteristics for specimen compacted at different initial water content (Vanapalli et al., 1999).

2.8 METHODS TO MEASURE VOLUME CHANGE IN SOIL TESTING

Measuring *volume* of samples in soil testing is a very important measure as the parameter *volume* is used to calculate various geotechnical properties such as dry density, porosity, void ratio etc. In previous and recent years, significant contributions have been made by various researchers in measuring/monitoring volume change in soil testing, but most of these advances are limited to a conventional triaxial soil sample. This section refers to a number of different volume measurement techniques, which are mainly used for measuring volume change in triaxial tests. In this thesis, the use of the laser for measuring volume changes in soils undergoing drying paths will be investigated. Volume measurements in soil testing,

and available measurement techniques will be further discussed in *Chapter 5 'Desiccation Tests using 3D compact Laser Scanner'*.

2.8.1 Contact methods

Available methods for measuring volume changes by local measurements can be referred as contact methods. The most common use is the vernier callipers. They are widely used in research laboratory for all kind of experimental measurements in small scale, for example the measurement of small compacted soil samples. : linear variable differential transformer (LVDT), Hall effects transducers (Clayton and Khatrush, 1986, Maâtouk et al., 1995, Geiser et al., 2000), stain gauges (Lo Presti et al., 1995, Kolymbas and Wu, 1989), proximity sensors (Cole, 1978, Khan and Hoag, 1979.), and opto-electronic sensors (Baumgartl et al., 1995.). There are several problems associated with contact methods such as they involve measurements between two points and often the average of several reading are taken to achieve accurate measurements. Also, the shape and size of the sample sometimes create problems as the readings are accurate over the small scale but at large scale, this method gives unrepresentative readings. An example is given regarding this last phenomenon in *Chapter 6*.

2.8.2 Non-contact methods

The first suction controlled triaxial apparatus developed by Bishop and Donald (1961) is of major historical and scientific interest (Figure 2.20). In this method, control of the volume change of the sample was solved by optically monitoring the

level of mercury contained in a glass cylinder that surrounds the sample. More recently, the use of mercury became restricted due to health and safety reasons; the method was modified later as it was found to have various disadvantages (Geiser et al., 2000). Several researcher introduced important changes within the test setup to achieve an improved technique to measure volume change of triaxial soil samples. Automatic monitoring of the mercury level was proposed by Josa et al. (1987). Cui and Delage (1996) used water instead of mercury. Rampino et al. (1999) used air as a confining fluid and designed a cylinder to improve the precision. Aversa and Nicotera (2002) worked with a similar concept as Rampino et al. (1999). The system by Bishop and Donald (1961) was modified later by Wheeler (1988) using a double cell triaxial cell (Figure 2.21).

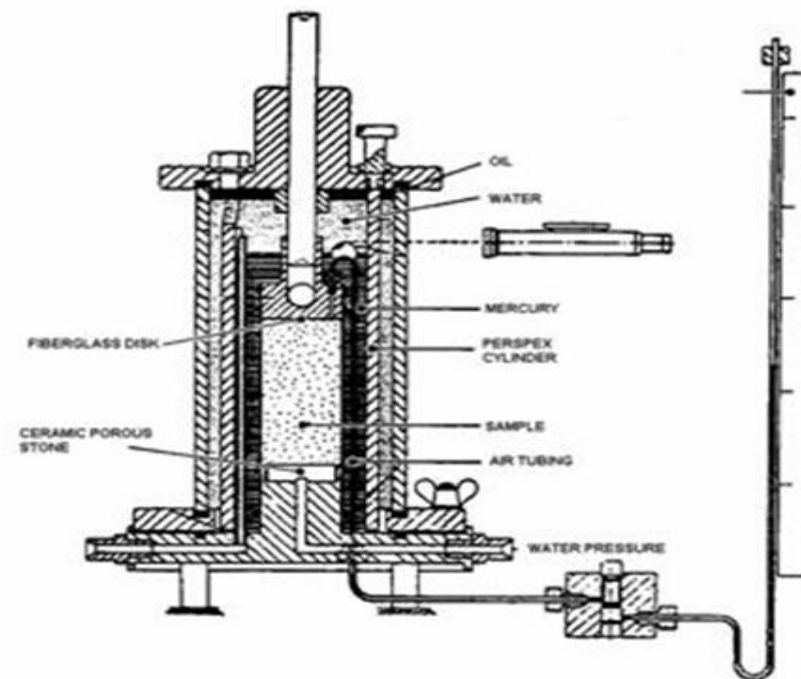


Figure 2.20: Suction controlled triaxial apparatus (Bishop and Donald, 1961).

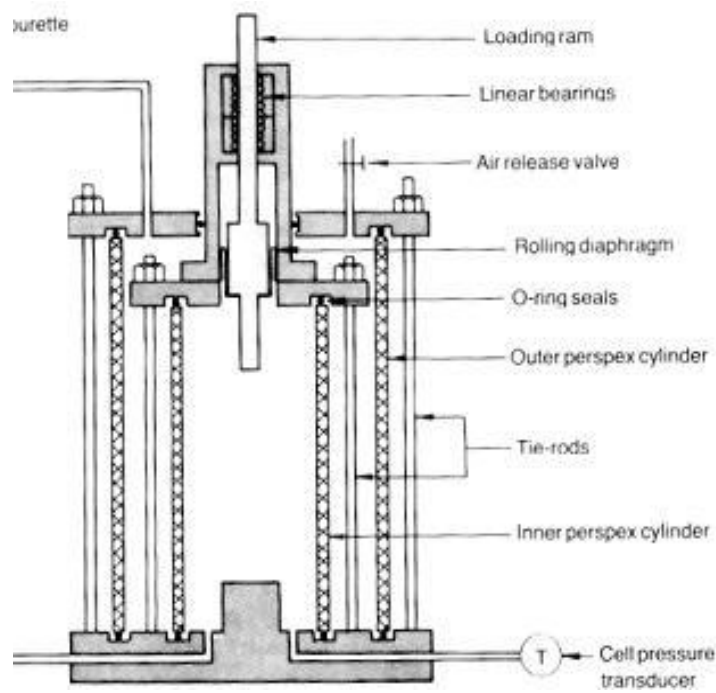


Figure 2.21: Double wall triaxial cell (Wheeler, 1988).

Accurate measurements of volume changes in unsaturated soil is, however, more difficult than in saturated soil (Ng et al., 2002). In saturated soil testing, it is assumed that the total change in volume of a sample is equal to the change in the volume of water in the sample (Head, 1998). This assumption does not apply any more in unsaturated soil testing, as the volume change of a sample depends on changes in volume of both the pore water and pore air phase. A comprehensive description and evaluation of existing methods of measuring volume changes in triaxial testing is provided by Geiser et al. (2000). Geiser et al. (2000) classified these techniques into three groups:

- i. Measurement of the cell fluid
- ii. Measurements of the changes in water and air volumes separately
- iii. Direct measurement of the soil sample

Laser scanners have been used with success in measuring the volume of solid in recent years. Romero (1999) and Romero et al. (1997) developed a successful laser

technique that provided a complete description of the profile of the triaxial sample during shearing. Digital image processing techniques have also been used to measure displacements, volume change and deformations in soil testing. Image processing techniques in triaxial testing were introduced by Macari et al. (1997a).

2.9 FABRIC STUDY

Microstructural studies are increasingly used to improve the understanding of macroscopic behaviour and physical properties of compacted and natural soils. The development of experimental techniques such as Scanning Electron Microscopy (SEM), Environmental Scanning Electron Microscopy (ESEM) and Mercury Intrusion Porosimetry (MIP) enhance the opportunity in geotechnical research to study arrangement of soil particles (Collins and McGown, 1974a, Barden and Sides, 1970, Barden et al., 1973a, Juang and Holtz, 1986a, Delage and Lefebvre, 1984a, Romero et al., 1999). Pore size distribution is an essential element for soil fabric study (Romero, 1999). Particle size distribution, void ratio and dry density are equally important. Pore size distribution may be the parameter responsible for permeability, compressibility and strength (Juang and Holtz, 1986a). ESEM provides a qualitative observation of soil fabric arrangement and MIP techniques give a quantitative data on the soil porosity.

Microstructural features of soil can be investigated by using SEM and MIP independently or together (Barden et al., 1973a, Collins and McGown, 1974a, Delage and Lefebvre, 1984a, Griffiths and Joshi, 1989a, Prapaharan et al., 1991, Jommi and Sciotti, 2003). ESEM has an obvious advantage over conventional SEM as sample can be examine in its natural wet condition (Romero and Simms, 2008b). Zhang et al. (2005) investigated in the change in fabric of a double porosity tropical soil along drying and wetting path. Microstructural investigation with special attention to MIP and ESEM have been presented in Romero and Simms (2008b)).

2.9.1 Classification in soil fabric

Collins and McGown (1974b) developed a classification for soil fabric based on SEM investigation for a wide range of natural soil. The main structural features observed were:

i) Elementary particle arrangement: These consist of individual clay platelet interactions or individual silt/sand grain interactions

ii) Particle assemblages: Groups of elementary particle arrangement. Figure 2.22 illustrates different types of particle assemblages (Collins and McGown, 1974b).

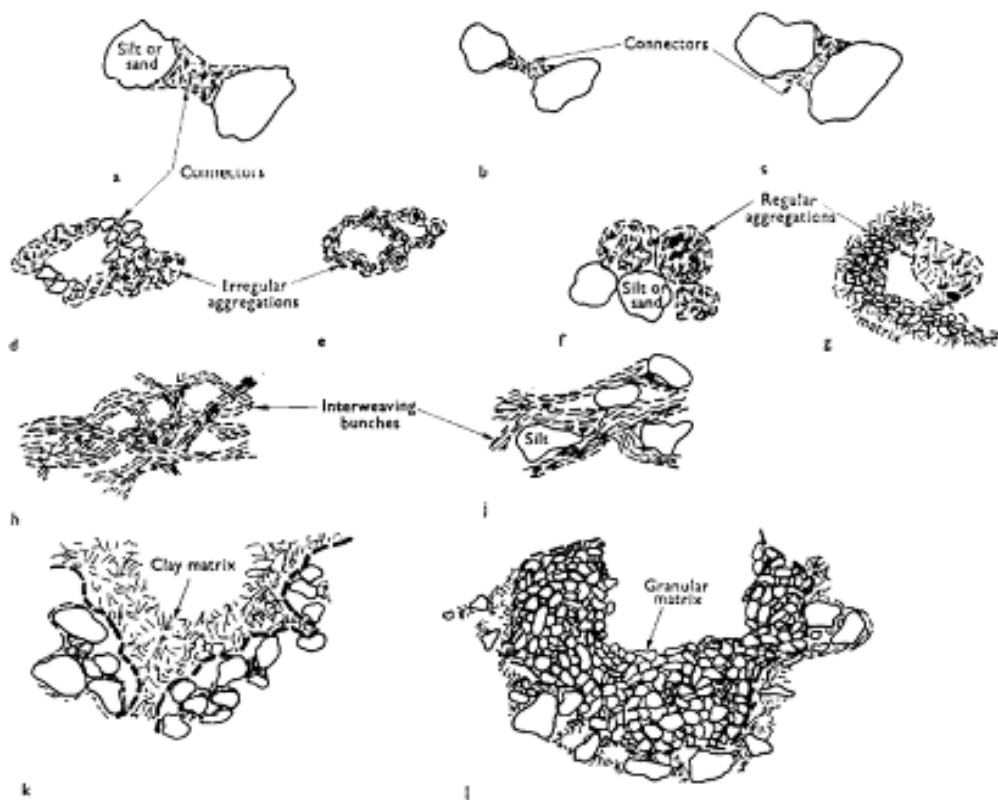


Figure 2.22: Different types of particle assemblages (Collins and McGown, 1974a).

iii) Pore spaces: Collins and McGown (1974a) identify four groups of pore space (Figure 2.23):

- a) *Intra-element pores* are located within the elementary particle arrangement
- b) *Intra-assembly pores* occur within particle assemblies
- c) *Inter-assembly pores* occur between assemblies
- d) *Trans-assembly pores* traverse the soil fabric

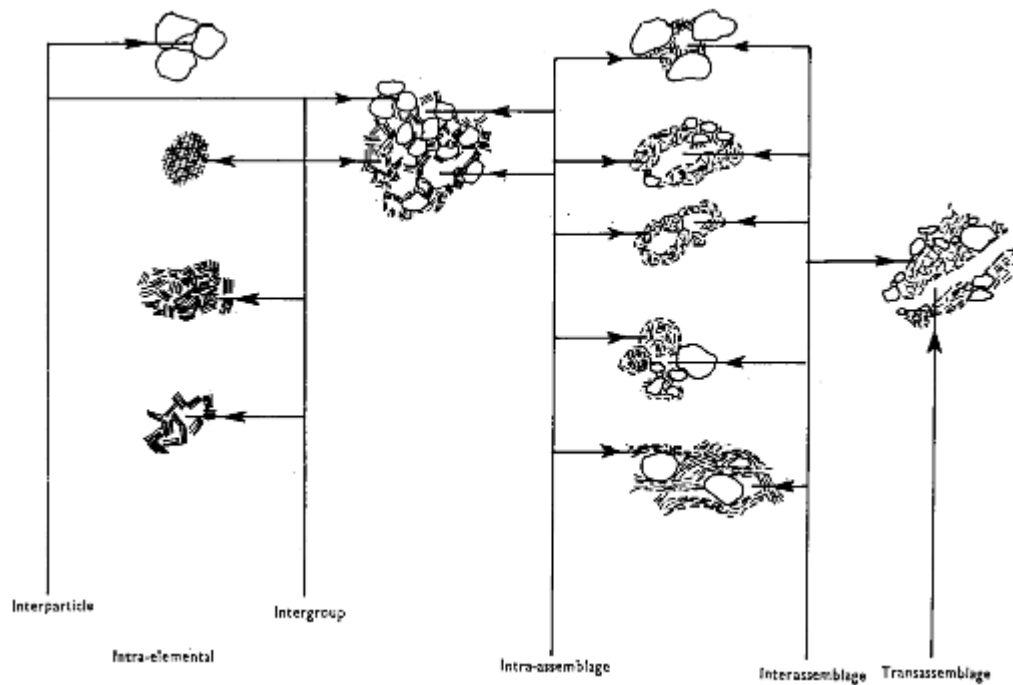


Figure 2.23: Schematic representation of types of pore space (Collins and McGown, 1974a).

A schematic representation of microfabric of compacted soils is shown in Figure 2.24 by Alonso et al. (1987). According to Alonso et al. (1987) in natural and compacted clayey soils the basic unit is not the single clay platelet but domains

which are constituted by groups of clay platelet. Fabric classifications according to Alonso et al. (1987) are as follows:

- a) *Intra-element pores* are intra-domain pores as shown in Figure 2.24a, d.
- b) *Intra-aggregate pores* form domains who group together to form aggregates and pores within the aggregates (Figure 2.24b).
- c) *Inter-aggregate pores* exist between the aggregates (Figure 2.24b). They are also referred as *inter-assemblage pores* (Romero, 1999, Lloret et al., 2003).

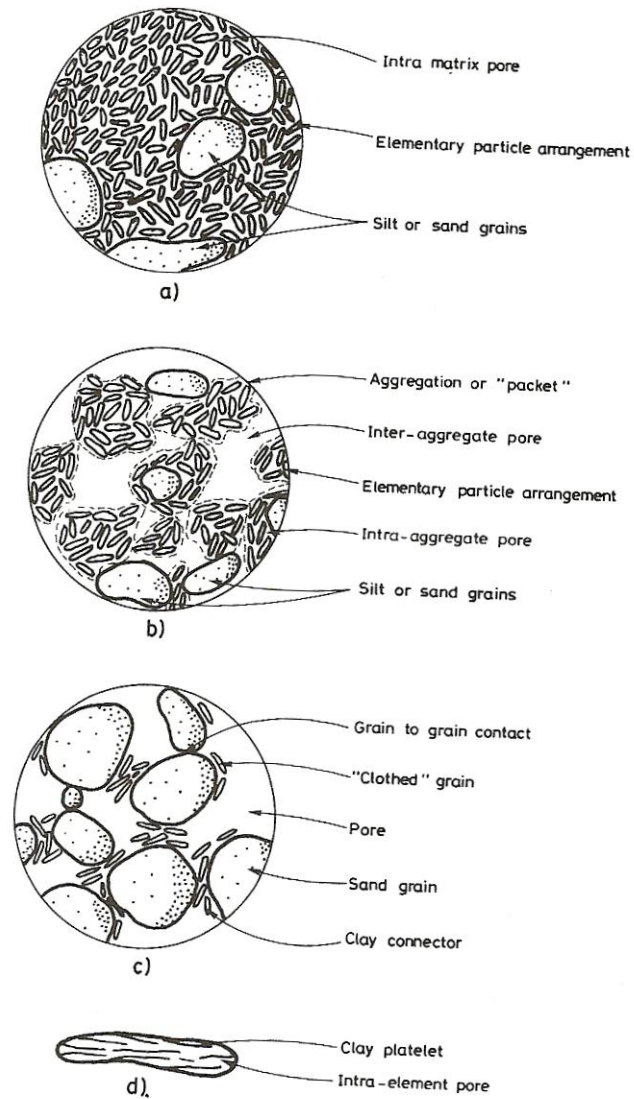


Figure 2.24: Types of microfabric; a) Clay matrix predominantly integrated by elementary particles of clay platelets and a few grains of slit or sand, b) Microfabric of a clay predominantly integrated by aggregations of elementary particle arrangements, c) Sand or slit matrix with clay connectors between individual grains, and d) Elementary particle arrangement in a parallel configuration (Alonso et al., 1987).

A description of pores found at different microstructural levels in clay was presented by Delage et al. (2006) as:

- a) *Intra-element pores* are Inter-layer spaces, pores inside clay particles.
- b) *Intra-aggregate pores* are Inter-particle voids inside clay aggregates.
- c) *Inter-aggregate pores* are pores between clay aggregates.

2.9.2 Microstructural study: compacted versus reconstituted states

At this stage it is important to define the term ‘reconstituted soil’. Burland (1990) defined reconstituted clay as one that has been thoroughly mixed at a water content equal to or greater than the liquid limit. Burland (1990) used the term ‘intrinsic’ which referred to clay reconstituted at a water content in between W_L and $1.5 W_L$ (preferably $1.25 W_L$). The term ‘reconstituted soil’ used within this thesis referred to soil specimen based on definition given by Burland (1990). The liquid limit (W_L) of Bengawan Solo Soil was found 55% by El Mountassir (2011) and in this research for reconstituted state the specimen was always prepared at 55% or higher than 55% (mostly $W_L - 1.25 W_L$).

Most commonly it is assumed that the reconstituted and compacted soil exhibit different behaviour due to their different microstructures. There are number of experimental studies available in literature which focuses on hydraulic and mechanical behaviour of soil at both compacted and reconstituted state (Marinho, 1994, Jotisankasa, 2005, Monroy, 2006, Boso, 2005, Tarantino and Tombolato, 2005, Tarantino, 2009, Koliji, 2008). These publications are useful in order to understand the microstructure of compacted soils, and offer as a basis to differentiate the microstructure similarities and dissimilarities in between compacted and reconstituted state of soil.

Soil compacted on the wet side of optimum and having an initial mono-model pore size distribution (PSD) may evolve to a bi-model size distribution upon drying (Gens et al., 1995, Simms and Yanful, 2001). On the other hand, soil compacted on the dry side of optimum having a bi-model pore size distribution (PSD) initially, can evolve to a mono-model pore size distribution (PSD) upon wetting (Monroy et al.). Again, soil having initial bi-model pore size distribution (PSD) which is compacted on the dry side of optimum may evolve to a mono-model pore size distribution (PSD) (Gomez et al., 2009). However reconstituted normally consolidated soil may exhibit bi-model pore size distribution at low stresses (Griffiths and Joshi, 1989a) and also a bi-model pore-size distribution can appear in saturated natural clays in an over-consolidated state (Ninjarav et al., 2007).

Figure 2.25 shows the pore size distribution (PSD) comparison of Speswhite Kaolin at same suction level for two states: statically compacted to 1200 kPa and reconstituted from slurry and subsequently air-dried. The reconstituted soil exhibits the same modal size as the intra-aggregate modal size of the compacted soil. These findings can be concluded that the aggregates are made of reconstituted soil and are the link between reconstituted and compacted soils (Tarantino, 2010).

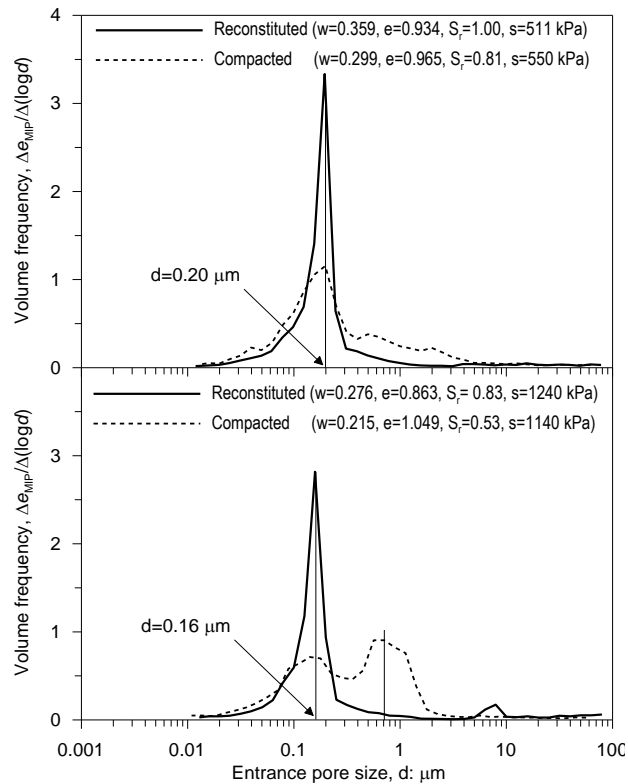


Figure 2.25: Comparison of PSD of compacted and reconstituted samples of Speswhite kaolin at similar suction (Tarantino, 2010).

A similar observation is apparent from Figure 2.26 which shows the PSD of Barcelona red clay in compacted and reconstituted states. The reconstituted soil sample show mono-modal PSD with modal size that decreases when suction increases and void ratio decreases. The two compacted soil sample exhibit a bi-modal PSD with only the inter-aggregate pore affected noticeably by compaction.

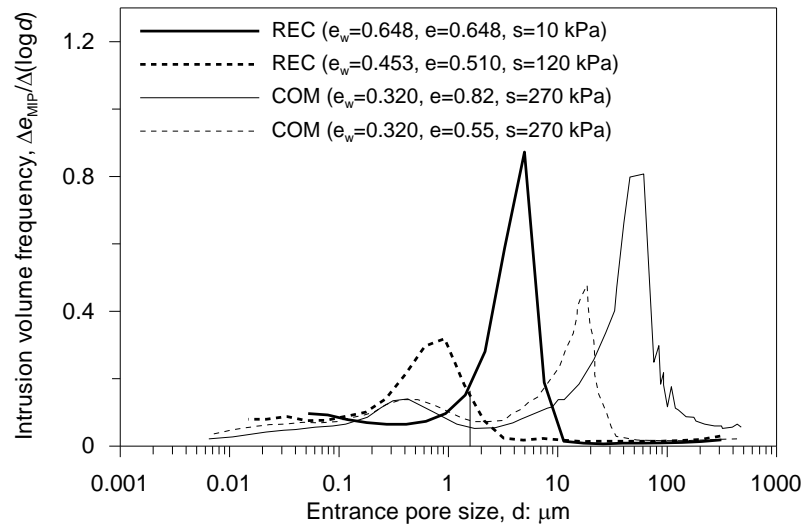


Figure 2.26: Comparison of PSD of compacted and reconstituted Barcelona red clayey silt (Tarantino, 2010).

Koliji et al. (2010) also had similar findings during MIP investigation on compacted and reconstituted soil samples (Figure 2.27). The modal size of mono-modal PSD of the reconstituted soil sample is similar to the intra-aggregate modal size of the compacted sample.

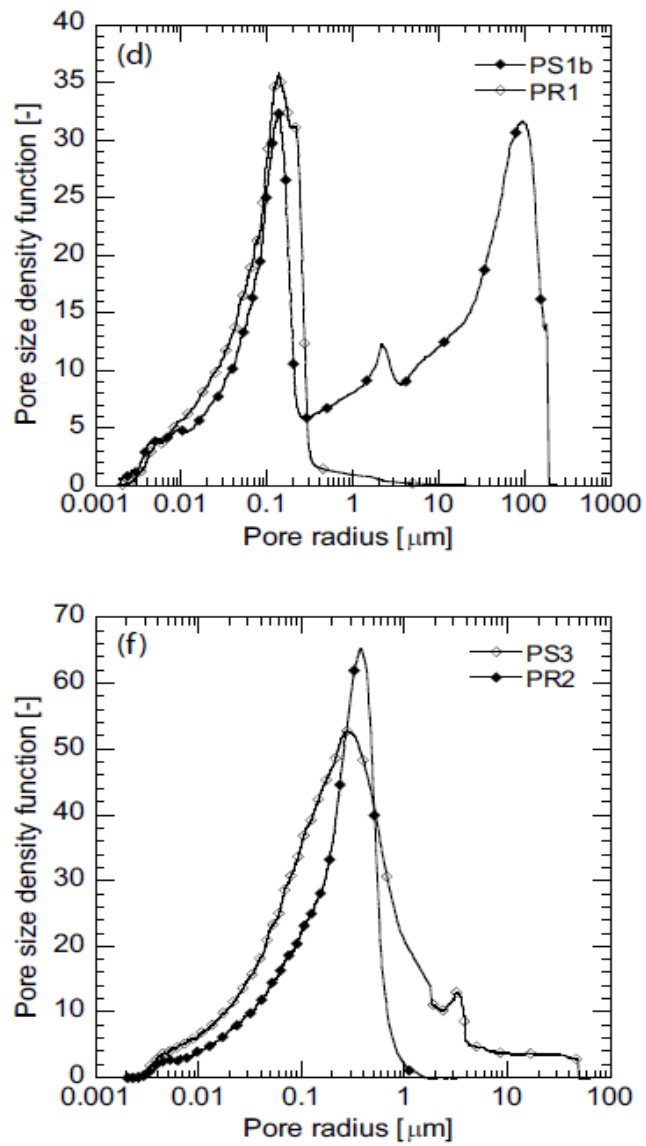


Figure 2.27: Comparison of PSD of compacted (PS) and reconstituted (PR) samples of Bioley silt at zero suction (PR2 and PS3) and a suction of 500 kPa and a vertical stress of 500 kPa (PR1 and PS1b) (Koliji et al., 2010).

2.10 CONCLUSION

Laboratory investigation on desiccation cracks of soil has improved significantly in recent years; e.g (Tang and Graham, 2000, Lakshmikantha et al., 2006, Rodriguez et al., 2007, Peron et al., 2009, Trabelsi et al., 2010). There is, however, not a laboratory reference test to study soil desiccation and cracks. Unfortunately, the investigation remains limited on several cracking parameters. Laboratory investigation on desiccation cracks can be improved with several new techniques, which helped in describing new knowledge regarding soil cracking mechanism. Some of these techniques will be discussed later on in *Chapter 4 Desiccation plate tests* and *Chapter 5 Desiccation tests with compact 2D/3D laser*

The crack development observed in the laboratory tests is often for small-size samples which cannot represent field conditions. Field tests mainly focus on the mean value of crack geometric characteristics because field survey on crack development is time consuming and also expensive in terms of research. Little information can be found on crack patterns in natural soils exposed to the atmosphere. Furthermore the desiccation tests performed in the laboratory are often made on artificial mixtures. Using a soil sample from a field site with corresponding desiccation cracking problem could contribute essentially in this field.

Chapter 3: Soil characterisation

3.1 INTRODUCTION

The research in this thesis investigates the desiccation cracks of a drying soil. The material used for this purpose is sampled from a flood embankment, located along the Bengawan Solo River in East Java, Indonesia. This chapter starts with a short description of the embankment site with specific references to cracking and its impact on the embankment. A full characterisation of Bengawan Solo soil including basic properties and mineralogy is presented. The characterisation data presented in this chapter is a condensation of the PhD thesis by El Mountassir (2011) at University of Strathclyde. Additionally, tests for the linear and volumetric shrinkage characteristics of the material were carried out by the author of this thesis. This chapter concludes by discussing the methods adopted to prepare soil samples for all laboratory tests for this research.

3.2 BENGAWAN SOLO EMBANKMENT

3.2.1 Geological Origin

The geology of the Bengawan Solo River Basin is presented in Figure 3.1. The site relevant to this study is characterised by alluvial deposits, which are materials deposited by rivers. It can consist of a wide range of particle sizes, from boulders down through cobbles, pebbles, gravel, sand, silt to clay. River plains are made entirely of alluvial deposits. More detail of the founding layers can be found in the thesis completed by El Mountassir (2011).

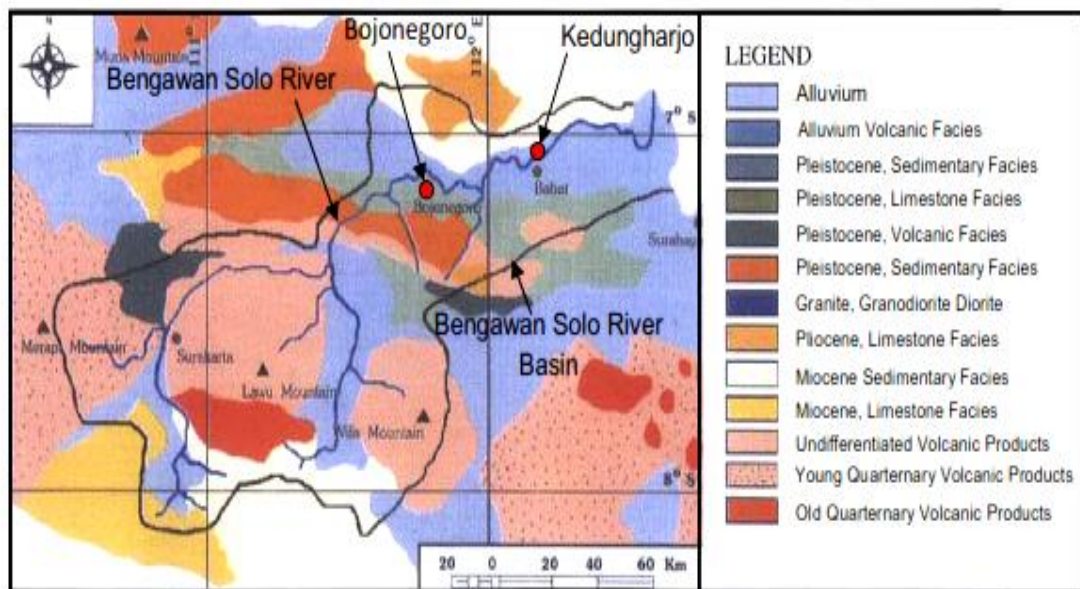


Figure 3.1: Geological map of Bengawan Solo River Basin, East Java, Indonesia (Takeuchi et al., 1995).

3.2.2 Site Description

This research has been conducted on a soil sampled from a flood protection embankment located along Bengawan Solo River in Java, Indonesia (Figure 3.2).

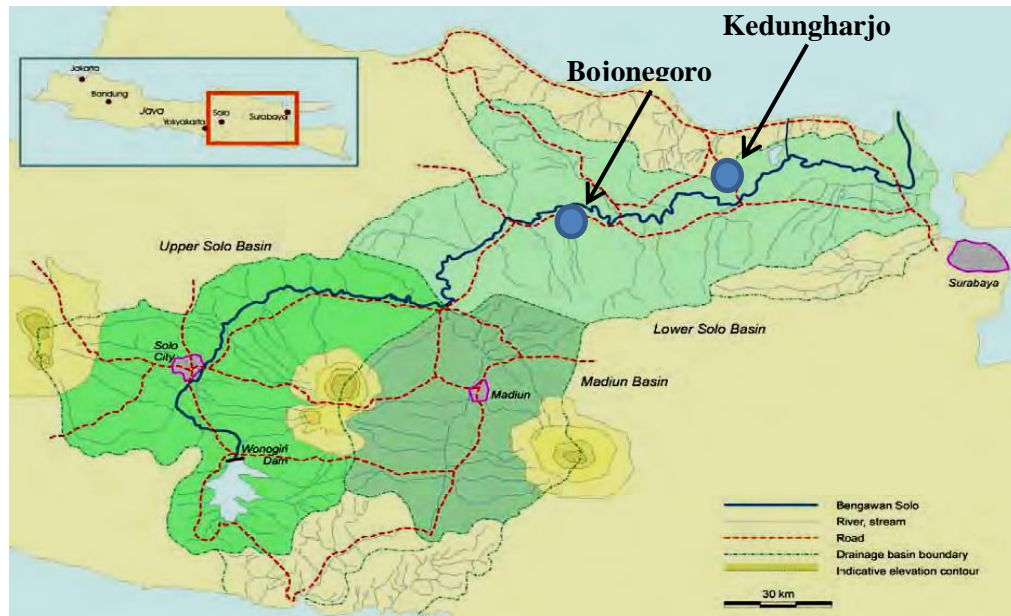


Figure 3.2: Site location within the Bengawan Solo River Basin (Sudarsono, 2009).

The source of the river lies in the Sewu Mountain Range in Central Java and it enters the sea, north of Surabaya in East Java (Figure 3.2). The Bengawan Solo River basin is the largest river basin on the island of Java, between 110°18' and 112°45' East Longitude and 6°49' and 8°08' South Latitude (Hidayat et al., 2008). This river, with a length of 600 km, is the longest in Java (Sudarsono, 2009).

According to UN (2004), the seasonal variation in Indonesia primarily consists of the dry season (between May and October) and the wet season (between November and April). Indonesia has an average relative humidity between 70% and 90%, with an average of 87%. The average rainfall is 2,100 mm/year (Sudarsono, 2009). Approximately 8% of the basin is flood-prone. The population in the river basin is

estimated at 16.03 million in 2005. The river catchment area is approximately 19,778 km² in total (Hidayat et al., 2008).

There are parts of the basin that are exposed to erosion due to different kinds of land use and degradation of the vegetation cover. This causes damage to the infrastructure, siltation in the reservoirs, and increases the flood risk. Flooding along the Bengawan Solo River is not an uncommon event and flooding has negative impacts on local people and agriculture, due to the loss of crops as a result of inundation. Hidayat et al. (2008) reported in detail the damages and impact of the flooding on Bengawan Solo basin, discussed the flooding and landslides incident between late December 2007 and early January 2008. JP (2009) reported the inundation incident in February 2009 flooding along Bengawan Solo river.

The section of flood defence embankment investigated within this research is located in the village of Kedungharjo, in the city region of Bojonegoro (see Figure 3.1 and 3.2). Figure 3.3 shows few pictures of Bengawan Solo embankment where the soil was sampled. At these locations, the embankments were frequently overtopped or breached, resulting in the evacuation of Kedungharjo village. Repairs of the embankments can only take place during the dry season due to the high river water level during the wet season. The river water level variation between the dry and wet seasons can vary as much as 10m.



(a)



(b)



(c)



(d)

Figure 3.3: (a) Embankment; (b) Concrete slabs used as a surface protection to prevent erosion of the outward slope; (c) Man-made embankment; (d) River meandering (El Mountassir, 2011).

Availability of construction materials is one of the major considerations in the design of any large infrastructure design system. In most cases, local material is used as a construction material, as this is an economic option. This large, man-made embankment is made from various compositions of soil: sand, clay and rock sourced from the river bed.

The material was compacted dry to an optimum of 80-85% of the maximum Proctor dry density (Soemitro, 2005) which is equivalent to BS Light test, 596 kJ/m^3 .

3.2.3 Geotechnical Failures along Bengawan solo

embankment

The embankment site was visited by El Mountassir (2011) in May 2006. This corresponds to the end of wet season of Indonesia, which is between November and April (Takeuchi et al., 1995). During the site investigation, the embankment along Bengawan Solo embankment showed signs of many different types of failure. The important features observed likely to contribute to embankment failures were (Figure 3.4):

- Erosion of embankments
- Failure due to desiccation cracks
- Rapid drawdown failures
- Shallow slip failures
- Global slip failures
- Failures due to secondary uses

The very dense desiccation crack networks observed in this man-made embankment may have an important role in the occurrence of small progressive failures frequently detected along the embankment.

For the purpose of this research, the failure due to desiccation cracks within the embankment site has been given attention. The data available investigating desiccation is mostly regarding clays used in landfill applications; e.g. (Basnett and Brungard, 1992, Miller and Mishra, 1989, Montgomery and Parsons, 1989). Furthermore, the data investigating desiccation cracks in embankment is minimal (Sherard, 1973). It is important to study this problem in detail order to preserve the primary purpose of a flood embankment serving as a water barrier.

3.2.4 Evidence of Desiccation Cracks

Figure 3.4 shows some evidence of crack desiccation that was found at the site of the embankment at different forms. Figure 3.4 (a), (b) and (c) shows the beginning of the widespread cracking across the stepped surface of the embankment. Drying and shrinkage at the upper surface of the embankment may be not as harmful as longitudinal cracking as shown in Figure 3.4 (d), (e) and (f); which can cause the slide of a big mass from the upper portion of the embankment (Jansen, 1988). The pictures were taken during the wet season and therefore it is expected that during a drier period, desiccation cracks would extend at even greater depths and be widespread throughout the embankment.

Desiccation in the form of cracks up to a depth of approximately 35 cm was found during the visual inspection of the embankment. It was known that the embankment had overtopped completely the week previous to the site visit; during the site visit, the embankment soil still retained high degree of saturation.

Figure 3.4 (g) and (h) shows the cracking patterns formed on the outward slope of the embankment during drying. This might also be the case during the dry season when the water level of the river is very low and the stepped surface of the embankment remains exposed to the hot sun. The visual state of the soil from the pictures suggested that this part of the embankment was covered with water when the water level was higher than at the time of inspection. The embankment soil still contains high moisture content at this stage, which makes the material very soft and easily eroded away in blocks. This creates water pathways within embankment fill material. The soil at lowest part of the embankment fill will be removed when too soft. As the embankment relies on the weight of the soil mass to counteract the force of water, which means erosion can be a major cause for embankment failure.



(a)



(b)



(c)



(d)



(e)



(f)



(g)



(h)

Figure 3.4: Widespread desiccation cracking across the stepped surface (images (a), (b), and (c)), longitudinal cracking (images (d), (e) and (f)) and interfaces with the receding flood water (images (g) and (h)) (El Mountassir, 2011).

Table 3.1: Summary of soil properties (some data after (El Mountassir, 2011)).

Properties	Depth: 0.5-1.0m	Properties	Depth: 0.5-1.0m
Particle density (Mg/mm ³)	2.73	Linear Shrinkage Limit (%)	14
Sand content (%)	30	Volumetric Shrinkage (%)	17.35
Silt content (%)	57	Plasticity index (%)	18
Clay content (%)	13	Activity	1.4
Uniformity coefficient	29	Organic content (%)	8
Liquid Limit (%)	54	British Soil Classification System (BSCS)	Organic silt of high plasticity (MHO)
Plastic Limit (%)	36		

Table 3.2: Methods used for determining soil property of Bengawan Solo soil.

Soil property	Method used	British standard reference
Liquid Limit	Cone Penetrometer method	BS1377-2:1990
Plastic Limit	Traditional method of rolling threads	BS1377-2:1990
Organic content	Ignition method	BS1377-3:1990

3.3.1 Soil mineralogy

The soil mineralogy studies of the Bengawan Solo soil were carried out at CIEMAT in Madrid, Spain, under the direction of Dr Ana María Fernández Díaz. The mineralogical information of the soil is thought to be important in interpreting to macro-scale testing result on the soil. Figure 3.6 presents the X-ray diffractograms of random powder samples using the total soil fraction which proves the presence of different minerals in the soil. Figure 3.6 presents the X-ray diffractograms of oriented samples in the < 2 μm fraction at 0.5-1.0 m depth. Although the amount of clay is not very high (around 13 %, see Table. 3.1), the orientated diffractograms

highlight that montmorillonite and kaolinite are the main clay minerals presents in Bengawan Solo soil.

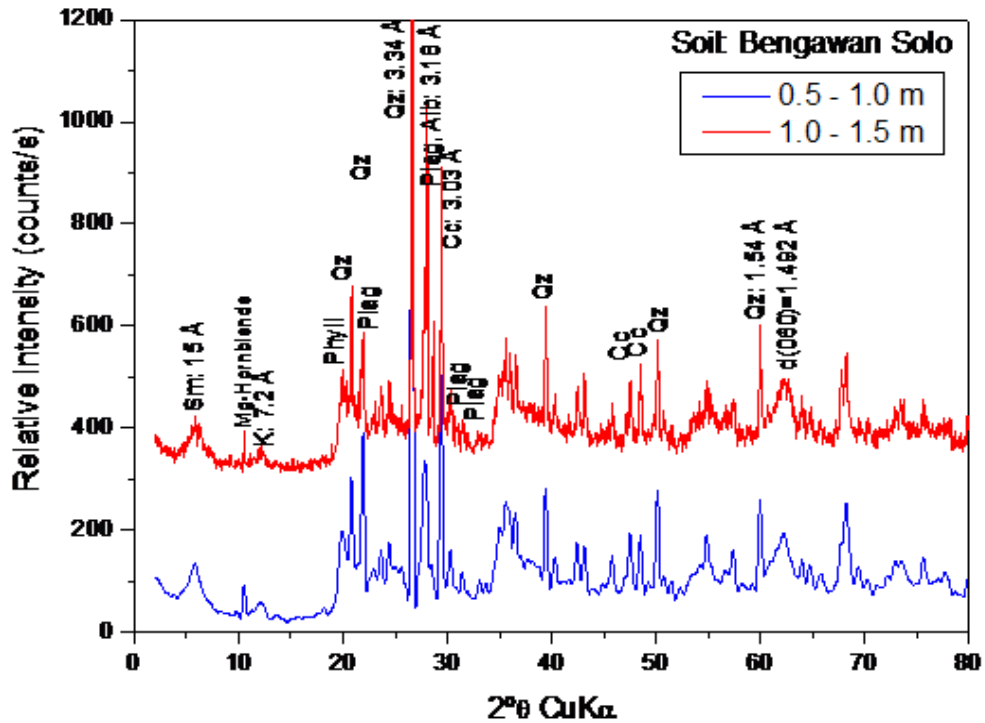


Figure 3.6: XRD-patterns of random powder samples (total fraction) (Sm: montmorillonite, K: kaolinite; Phyll: total phyllosilicates; Qz: quartz; Plag: plagioclases; Cc: Calcite). D1=0.5-1.0 m and D2=1.0-1.5 m.

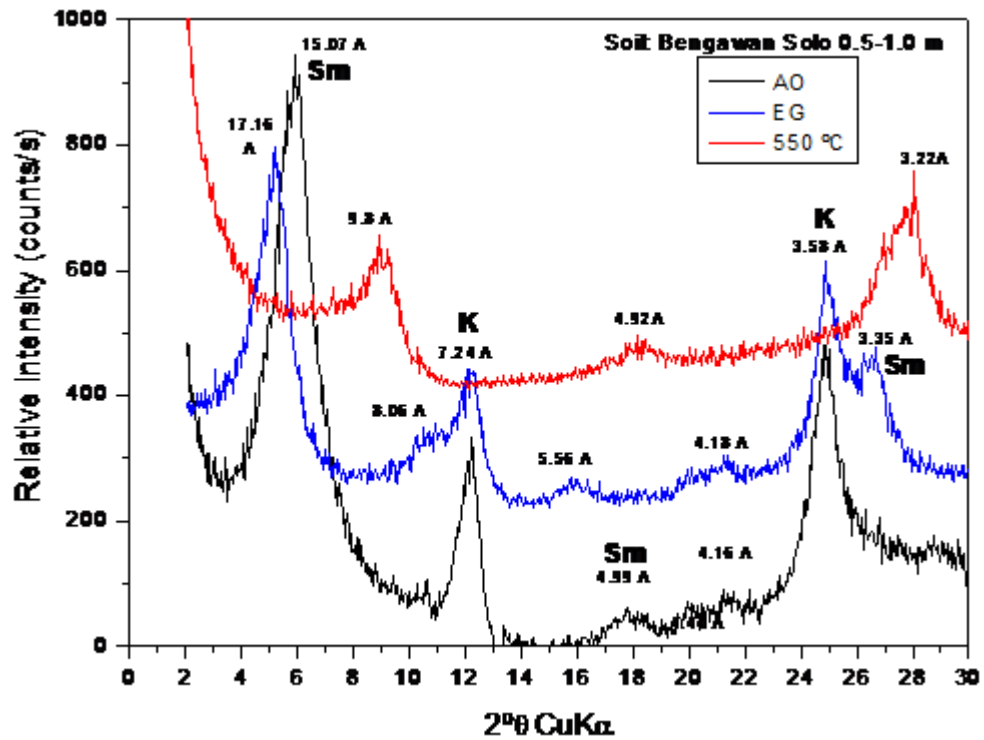


Figure 3.7: X-Ray diffractograms of oriented samples (< 2 μm fraction)
(Sm:montmorillonite; K: kaolinite).

Table 3.3 presents the mineralogical quantification of total fraction and table 3.4 presents the quantification of the clay minerals present by (% mass) and indicates that the clay fraction is made up of 88% of montmorillonite at 0.5-1.0 m depth.

Table 3.3: Soil mineralogy - Total fraction mineralogical semi-quantification by means of X-ray diffraction (% weight).

Minerals*	Total Phyllosilicates	Quartz	Calcite	Plagioclases	Mg-hornblende
Depth 0.5-1.0 m	60	18	12	9	1

*Sample <63 μm prepared

Table 3.4: Clay fraction (<2 μ m fraction) mineralogical semi-quantification by means of X-ray diffraction (% weight).

Minerals	Smectite	Kaolinite
Depth 0.5-1.0 m	88	12

From the clay mineralogy of this soil it has found that the clay is rich in smectite minerals (montmorillonites) which makes the soil highly attracted to absorb water and causing high shrinkage of the material (Whitlow, 1995). These soils develop significant change of volume during drying. The type of minerals forming the clay fraction play a central role on the properties of the soil, such as plasticity and strength (Mitchell, 1993b).

3.3.2 Shrinkage, shrinkage limit and shrinkage characteristics of Bengawan solo soil

Shrinkage limit is the least-commonly tested Atterberg Limit. Although it is not used directly in soil classification because liquid and plastic limit are used, shrinkage limit provide some indication of the particulate structure of the soil. For example a dispersed structure will generally exhibit low shrinkage limit and a flocculated structure a high shrinkage limit (Whitlow, 1983). Shrinkage is the major reason for volume change associated with water content variation in soil (Haines, 1923b, Hogentogler, 1937).

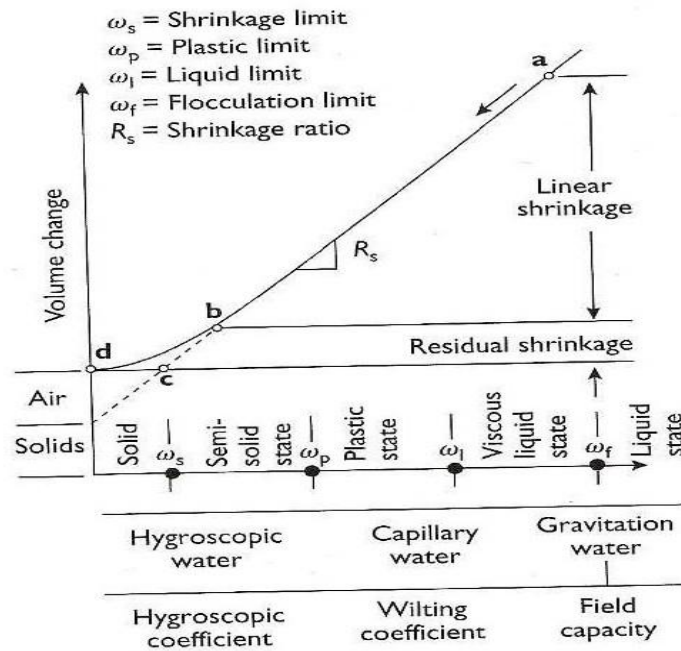


Figure 3.8: Correlation of soil volume change and consistency (Haines, 1923b, Hogentogler, 1937).

The moisture content at which a saturated soil will cease to contract upon drying is defined as shrinkage limit of the soil. It is the lower limit of the semi-solid state, and also this state represents the point of minimum volume for the soil (Figure 3.8). The amount of shrinkage measured depends to some extent upon the size as well as the type of the sample. For example, with a large sample, there may be an appreciable difference in the moisture content at the surface and at the centre of the sample and consequent variations in the amount of shrinkage. The moisture content represents the average (Akroyd, 1964).

The types of soil cracking have been classified into four types: shrinkage, thermal, tensile, and fracture cracks (Fang and Daniels, 2006). Shrinkage cracking is the most common cracking found in earth structures and the phenomenon can be observed in drying mud-fields. Hence, it can be seen as an essential element into the investigation of desiccation of clay soils. Yesiller et al. (2000) suggested that the comparative

difference between the plasticity index and the shrinkage limit acts as an indicator for a soil's potential to shrink and propagate cracks.

However, there is also an effect of soil composition on the desiccation process. Soil is a product of weathering; soil inherits the original and as well modified properties of the parent rock or mineral. Soil composition has a direct bearing on the shrinkage and swelling properties, which, in turn, influence the cracking behaviour. Shrinkage is one of the major causes for volume change associated with variations of water content in soil (Fang and Daniels, 2006). Due to that reason, it was important to measure the volumetric shrinkage of Bengawan Solo soil as part of this research.

Both linear shrinkage and volumetric shrinkage tests were carried out for Bengawan Solo soil in accordance with BS 1377-2:1990 and BS 1377-4:1990 following the detailed procedures presented in Head (1992).

3.3.2.1 Linear shrinkage test

Linear shrinkage is the one dimensional decrease in soil mass which is expressed as a percentage of the original dimension, when the water content is reduced from a given value to the shrinkage limit. The linear shrinkage test was carried out according to BS 1377-2:1990:6.5 Head (1992) using two different methods: *air dried and oven dried*. The soil is dried in oven at standard oven temperature (105°C) in the oven dried method and left exposed to dry in ambient air in the air dried method. It was important to check at what extent the results differ because there was a possibility to reuse the oven dried soil if the air dried soil samples run out during the research period.

The specimens were air dried in a well-ventilated room and oven dried at 105° C. Their external dimensions were measured periodically using a vernier calliper until no further decrease in their dimension was found in average (Figure 3.9). The linear shrinkage limit was calculated using the following equation:

The linear shrinkage of the soil as a percentage of the original length of the specimen,

$$L_s = \left(1 - \frac{L_D}{L_o}\right) \times 100 \quad (3.1)$$

where,

L_o = Original length of the specimen.

L_D = Length of the air-dried or oven-dry specimen.

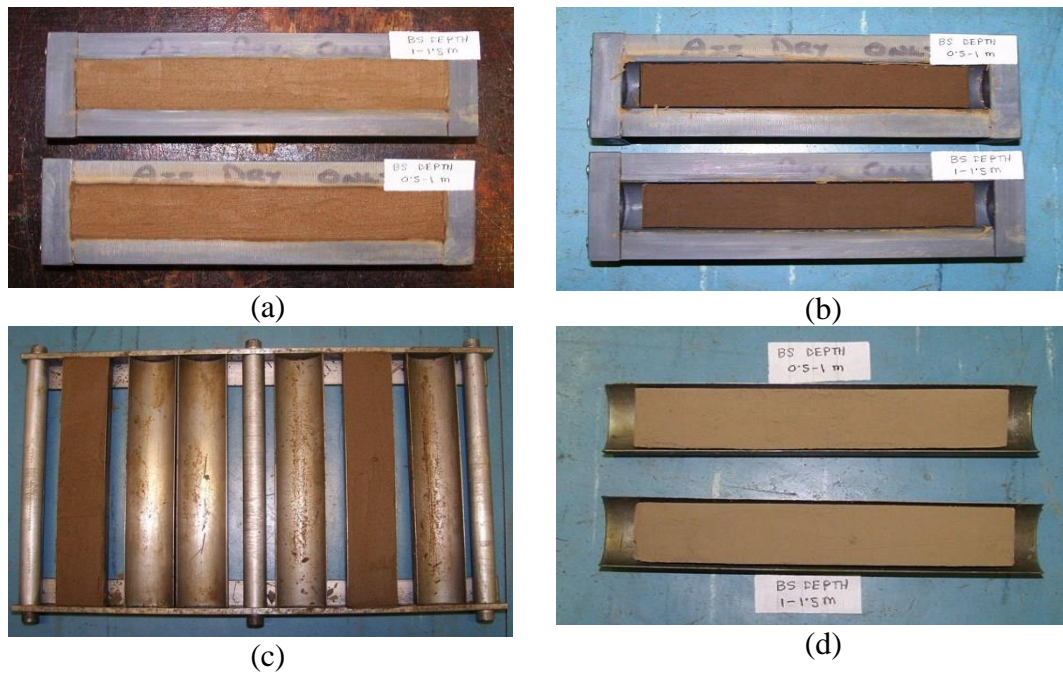


Figure 3.9: (a) Samples on linear shrinkage mould at initial state, air dried; (b) Samples on linear shrinkage mould started to shrink, air dried; (c) Samples on linear shrinkage mould at initial state, oven dried; (d) Samples on linear shrinkage mould shrank after oven drying.

The linear shrinkage was found to be 14.2% and 14.8% for air dried and oven dried samples, respectively. In general, a decrease in shrinkage limit means increase in clay content. For sand that contains some silt and clay, the shrinkage limit is about 12-24, and for clay shrinkage limit ranges from 4-12 (Fang and Daniels, 2006). According to soil classification tests, Bengawan Solo soil is also classified as *silty clay*.

3.3.2.2 Volumetric Shrinkage

Volumetric shrinkage of soil is the decrease in volume and expressed as the percentage of soil mass, when water content is reduced from a given percentage to the shrinkage limit. The specimen for volumetric shrinkage test was prepared according to BS 1377-4:1990 (Head, 1992). The test was performed on a small cylindrical specimen of 91.41 mm diameter and 17.45 mm height. Shrinkage tests using small cylindrical specimens and similar procedures were performed by many other researchers (Kleppe and Olson, 1985, Briaud et al., 2003, Boivin et al., 2004, Indrawan et al., 2006, Krisdani et al., 2008). In a well-ventilated room, the specimen was air-dried naturally without speeding up the drying process by any other means, to avoid the formation of shrinkage cracks. Periodically the mass of the specimen was measured using 0.01 g electronic balance and the results were used to calculate the moisture content change resulting from evaporation from the specimen. The external dimensions were measured using a Vernier calliper until no further decrease in moisture contents was observed. Considering the drying around the specimen is not uniform, in order to obtain an accurate calculation of volume change, 8 sets of measurements of height and diameter were taken for the specimen. Since the shrinkage curve of a soil is not affected by the different drying rate (Krisdani et al., 2008), the experiment was performed in laboratory controlled temperature room where all the other tests took place throughout the research.

The parameters that can be obtained from a shrinkage curve are the shrinkage limit and air-entry value which can be correlated with the point where the shrinkage curve starts to deviate from the saturation line. From the shrinkage curve (Figure 3.10), the shrinkage limit for Bengawan Solo soil was found as 17.35% which again comparable to Fang's general index of clay content (Fang and Daniels, 2006). According to USBR (1974) the degree of expansion of Bengawan Solo soil falls into 'medium' category. The degree of saturation for the shrinkage test was not started from 100% degree of saturation; it was calculated as 94%. Therefore the air-entry value could not be obtained from the shrinkage curve.

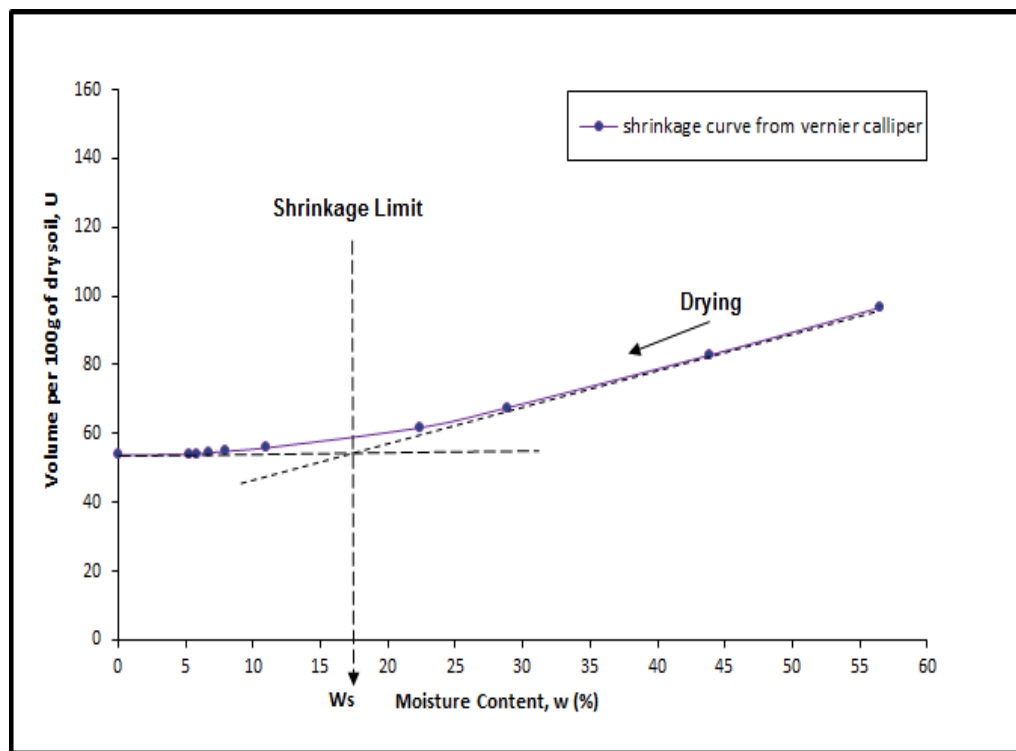


Figure 3.10: Shrinkage curve for Bengawan Solo soil.

The ratio of the liquid limit to shrinkage limit (LL/SL) of soil gives an idea about its shrinkage properties. Generally if LL/SL is large it means the soil may undergo an undesirable volume change due to a change in the moisture in the field. Newly

constructed foundation on these soils may show crack due to shrinking and swelling of the soil resulted from the seasonal change in moisture content (Das, 2009) . For Bengawan solo soil the LL/SL is calculated as 3.283; is hence considered not very high.

3.4 COMPACTION CURVES

For construction of any structure, it is necessary to compact the soil to improve its strength. Table 3.5 gives the summary of the compaction tests done by El Mountassir (2011).

Table 3.5: Procedures used to achieve different compactive efforts; after El Mountassir (2011).

Test name	Rammer mass (kg)	Rammer drop (mm)	No of layers	Blows per layer	Compactive effort
Extreme light	2.5	300	2	9	132
BS light	2.5	300	3	27	596
BS heavy	4.5	450	5	27	2682

Figure 3.11 shows the compaction curves of Bengawan Solo soil performed at different compactive effort. The Bengawan Solo embankment soil was compacted to 80-85% of the optimum dry density of the standard proctor test. The standard proctor test (593kJ/m^3) is equivalent to the BS Light test (596kJ/m^3) and 80-85% of the optimum dry density of the BS Light test lies within the range of densities covered by the Extreme Light tests (Figure 3.11).

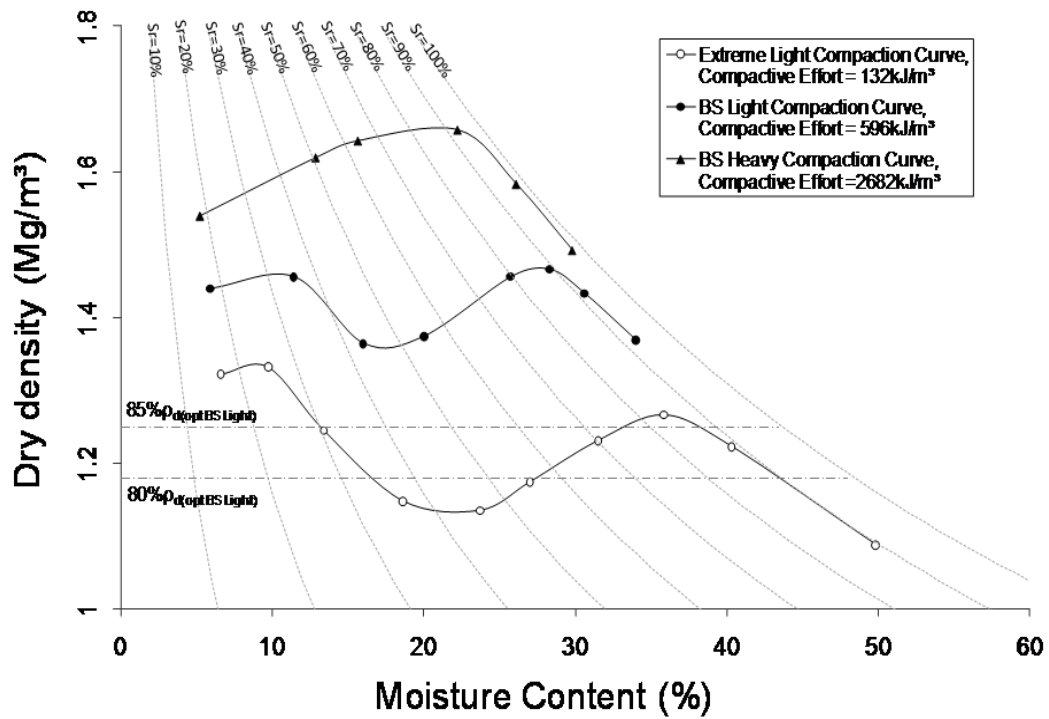


Figure 3.11: Compaction curves at three different compactive efforts (El Mountassir, 2011); (i) Extreme Light, 132 kJ/m³, (ii) BS Light, 596 kJ/m³ and (iii) BS Heavy, 2682 kJ/m³.

In this thesis, the Bengawan Solo compaction curve was used to find the tensile strength characteristics of the embankment soil at different moisture contents and dry densities in *Chapter 6 'Tensile strength and micromechanical state'*.

3.5 SAMPLE PREPARATION

In this section the method adopted for specimen preparation for all the tests performed within this research is described shortly. Please note that the description

of the initial conditions for each test will be presented as a test reference at the beginning of individual test/chapter.

3.5.1 Soil Mixing

Bengawan Solo soil was air dried at first and the air dried materials were broken to a smaller size using a plastic hammer. Next the materials were crushed in a crushing machine and the crushed materials were sieved through 2 mm for preparing sample for all tests (Figure 3.12).

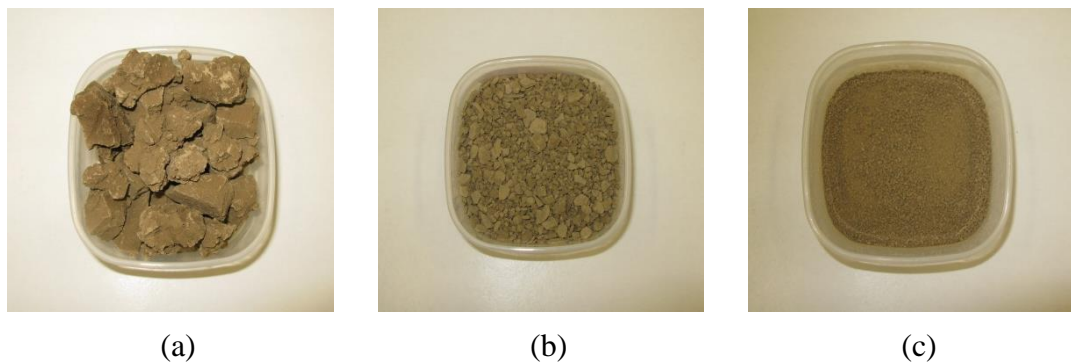


Figure 3.12: Different stages of soil preparation before sampling; (a) Air dried hand broken large soil particle; (b) Crushed soil in a crushing machine; (c) 2 mm sieved soil ready to use for sampling.

Sieved soil was then mixed with pure water to achieve desired water content according to the test requirement. Then the specimens were kept inside a closed air tight container in a temperature controlled room for at-least 24 hours to achieve a homogenized soil paste. In some cases where series of tests were performed in a row, the samples were prepared in one volume in order to avoid the variation in the initial

condition among the specimens. The mixed soil was then sealed in an air tight container until required.

The amount of water added to prepare a sample at desired moisture content was found using the following equation (Head, 1989):

$$\Delta m_w = \frac{m_t}{(1 + w_i)} \times (w_f - w_a) \quad (3.2)$$

where, Δm_w = amount of water to be added, m_t = Total amount of air-dried material, w_f = the desired moisture content, and w_a = the air dried moisture content.

Pure water was added to the air-dried soil slowly with a fine nozzle spray and hand-mixed using a spatula until the required amount of water, Δm_w was delivered from the nozzle spray bottle. A moisture content test was performed according to Head (1992) at the beginning and end of each test to validate this procedure.

The tensile tests discussed in *Chapter 6* were performed upon reconstituted and compacted samples. It was believed that the reconstituted soil could provide useful information to understand the soil in terms of its nature, structure and strength. However the desiccation plate test discussed in Chapters 4 and 5 were performed only on reconstituted soil.

3.5.2 Preparing Reconstituted Soil

Ideally, a reconstituted material can be described as restoring the state of a dehydrated material to its full liquid form by adding water. The liquid limit of Bengawan Solo soil is 54%. In preparation of reconstituted soil the samples was made at or above its liquid limit (55%-60%) to achieve a slurry state or to ensure full saturation.

In the desiccation plate tests and all the tests using the laser scanner, this slurry was then poured into specific moulds according to test requirements and left exposed to air in a temperature controlled room to continue drying. For tensile strength tests of reconstituted soil, the prepared slurry was poured into the tensile mould and allowed to dry naturally, taking periodic measurements of the water content. When the soil batch reached the desired water content, the soil specimen was carefully removed from the mould and tested immediately or stored in an airtight container. The soil prepared and used this way termed as '*reconstituted soil*' within this thesis.

3.5.3 Preparing Compacted Soil

To prepare the compacted samples, the mass of soil (m) to be added in order to reach a required dry density (ρ_d) was calculated as follows:

$$m = \frac{\rho_d(100 + w)}{100} \times V \quad (3.3)$$

where, V is the volume of any mould used, usually a mould with defined geometric shape.

The mass of soil required was added to the mould in three layers. The specimens were compacted using a tamping rod and a small light hammer after each layer was added; the number of blows varied depending on the desired dry density. The mass and volume was measured and noted after the sample preparation. A moisture content test was performed to measure the actual dry density ρ_d of the prepared sample.

In preparation of compacted samples for the tensile strength measurement of Bengawan Solo Soil, it was important to adopt specific preparation method according to the test requirement. This will be discussed in more detail later in *Chapter 6*.

3.6 CONCLUSION

The characteristics of the Bengawan Solo embankment and the soil collected for testing were described in this chapter. The site is characterised by alluvial deposits and according to the soil classification tests the material is classified as organic silt of high plasticity. Although the linear shrinkage and volumetric shrinkage of the material were found to be moderate to high (Fang and Daniels, 2006), it is believed that the clay mineralogy of this soil plays a key role of shrinking behaviour of the material (Table 3.4, Figure 3.6-3.7). The soil was found rich in smectite minerals (montmorillonites) and the *LL/SL* ratio was found to be low, which indicates that the Bengawan solo soil does not exert undesirable volume change due to shrinkage during seasonal moisture change. The volumetric shrinkage curve presented in this chapter is compared in *Chapter 5* with volume change measured with 2D/3D compact laser. The tensile strength experimental campaign in *Chapter 6* was carried out with specific references to the compaction curve presented within this chapter to explain the evolution of the material from slurry to dried state. This is studied in terms of state, strength and structure later on in *Chapter 6 Tensile strength and micromechanical state*.

Chapter 4: Desiccation plate tests

4.1 INTRODUCTION

Desiccation cracking significantly affects the soil performance. Cracks create zone of weakness in a soil mass and reduce its overall strength and stability. Many examples can be found in various geotechnical, agricultural and environmental applications, e.g. irrigated land, tailing ponds for mining waste, landfill liners, earth embankments, reservoir beds (Colina and Ronux, 2000). Cracks can develop due to various processes such as desiccation and shrinkage, freezing, penetration by plant roots etc. This chapter investigates the potential for desiccation cracks in the Bengawan Solo soil, which was obtained from a flood protection embankment in East Java, Indonesia. The highly dense desiccation crack network observed in this man-made embankment may have an important role in the occurrence of the small progressive failures that are frequently detected along the embankment.

Shrinkage cracking is significant in earth embankments, slopes, foundations and roads. Although cracking in drying soil is a very common phenomenon, the causes

and mechanisms involved are very complex due to the interactions that take place during the drying process among material, the surrounding conditions, and boundary conditions of the embankment. Simultaneous and strongly-coupled hydro-mechanical, and sometime also thermal processes, take place during soil desiccation (Rodriguez, 2006). Accurate, direct measurement of geometrical parameters of soil shrinkage cracks is not easy. Large measurement errors are expectable due to the irregular shapes and complex cracks patterns. In recent years, image analysis techniques have been used extensively to characterise the crack networks with improved accuracy (Lakshmikantha et al., 2009, Tang et al., 2008b).

This chapter presents desiccation plate tests for Bengawan Solo soil with three different shapes and thicknesses. The cracking pattern, the time of crack initiation, and the crack network due to drying shrinkage were analysed and interpreted to identify influences on test outcome. This chapter concludes with image analysis to determine the geometrical properties of crack network from desiccation plate tests.

4.2 CHARACTERISTICS OF SOIL CRACKING

At this stage, it is relevant to define the key terms used in this chapter for analysing soil cracking. This is necessary to provide a basis for quantifying observations.

The following definitions were given by Corte and Higashi (1960):

- ***Cracking moisture content:*** refers to the moisture content of the soil at the crack initiation. This is measured by sampling the soil when the cracking started, (with modern technology improving now the electronic balance can measure continuous moisture change within samples) or by interpolation on a desiccation curve. If the soil layer is thick, this moisture content measurement is taken as the one at surface.

- **Thickness of the soil** is defined as the thickness of the soil after complete drying. The thickness does not change much once the cracking has initiated.
- **Cells are** fragments of soil, separated by cracks which intersect each other.
- **Size of cell** generally refers to the area after the cracked soil is completely dry, unless it is mentioned that the change of cell size during desiccation is considered.
- **Area of cracks** is equal to the area of the container (in which the tests are carried out) minus the total area of cells.
- **Length of cracks** is the total linear dimension which is measured along the cracks.

Typical cracking patterns are shown in Figure 4.1. The following definitions were given by Kodikara et al. (2000a):

- ✓ **Primary cracks** are cracks that develop at first forming large blocks.
- ✓ **Secondary cracks** are cracks that develop after primary cracks during subsequent drying and subdivision of the larger blocks further.
- ✓ **Crack pattern:** The observed field cracking pattern was divided into two broad categories by Kodikara et al. (2000a).

Orthogonal pattern: In orthogonal patterns, crack tends to meet at right angles.

Non-orthogonal pattern: In non-orthogonal patterns, cracks do not meet at right angles.

- ✓ **Crack intersection:** The point where two or more crack intersects. Crack intersection angle defines the cracking pattern.

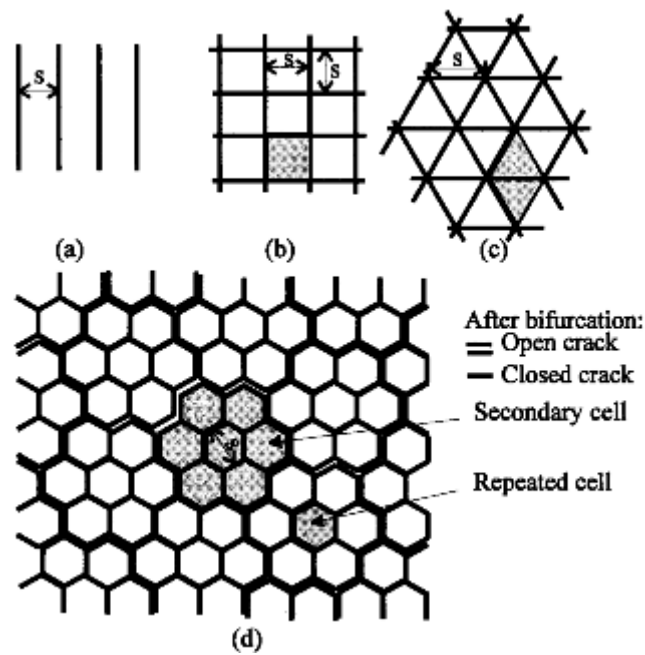


Figure 4.1: Theoretical cracking pattern as suggested by Kodikara et al. (2000a); (a) is 2D cracking pattern, (b), (c) and (d) are essentially 3D cracking pattern.

To quantify the amount of cracking, the parameter of *Crack Intensity Factor (CIF)* was developed. The CIF (or crack density factor CDF) was introduced as a descriptor of the extent of surface cracking by Miller et al. (1998a). CIF is defined as the ratio of the surface crack area, to the total surface area of the drying specimen. Image analysis process was used to determine CIF values from photographs of the desiccation process within this research and was found to be a powerful, efficient tool for the determination of the CIF for soil under drying conditions.

4.3 DESICCATION PLATE TESTS

4.3.1 Objectives

The desiccation tests were performed upon reconstituted Bengawan Solo Soil. The results focus and explore various cracking parameters.

The specific objectives for this experimental campaign were:

- To investigate the potential for desiccation cracks in the Bengawan Solo soil
- To identify experimentally the mechanisms and main causes of cracking
- To investigate the relationship between plate geometry and onset of cracking in terms of cracking parameters

This research investigates desiccation cracking in drying soil. For this purpose, it was important to investigate the potentiality for cracking of the material used within the research at laboratory conditions. The findings behind the mechanisms and main causes of cracking may lead to new understanding and the development of precautions or guidance to avoid soil cracking in the field.

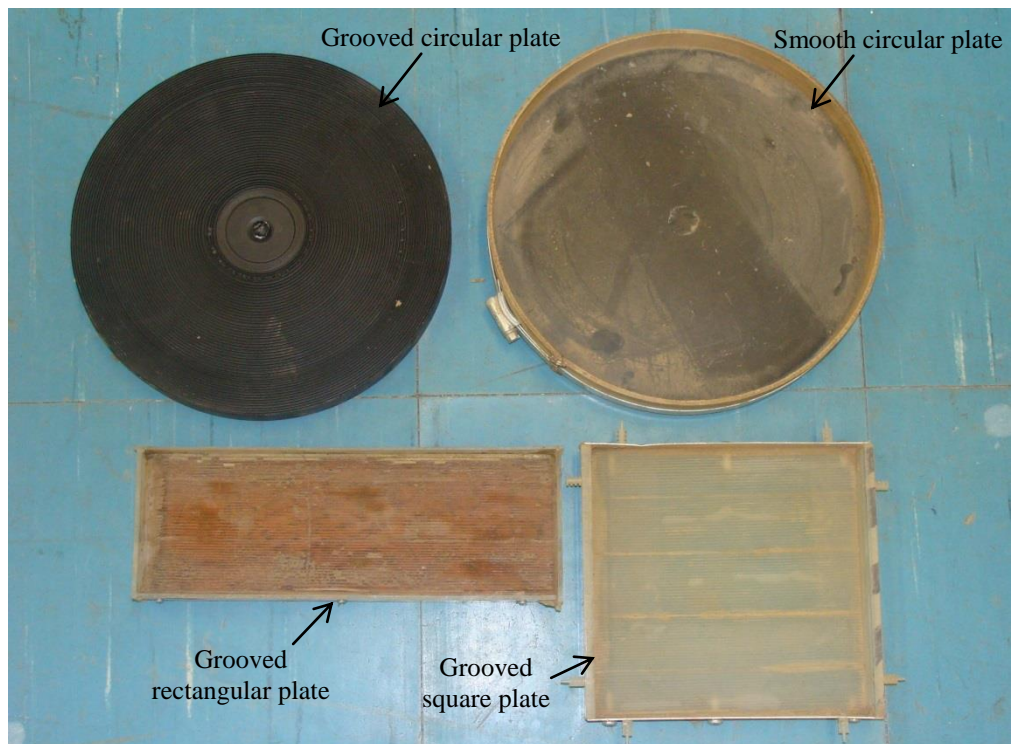
4.3.2 Experimental Methodology

Soil is a highly-complex material and its desiccation cracking behaviour is assumed to be governed by number of factors. These factors include mineral composition, clay content, relative humidity, shrinkage characteristics of the particular soil, layer thickness, size of the soil sample, and boundary conditions (Fang, 1997b). Many works have already focused on this issue in the last two decades. Water content is the

parameter that controls crack initiation; water content depends on temperature, relative humidity, and the thickness of the soil layer. All these factors were taken consideration during investigation of desiccation cracks for Bengawan Solo soil.

4.3.2.1 Desiccation test methodology

Three different plates (square, rectangular, and circular) of 5 mm, 10 mm and 20 mm thickness were used for these experiments. Perspex was used as a mould material for each of the plate due to availability of this material. The plate dimensions and test references are given in Table 4.1. The tests, namely DPTS, DPTR and DPTC, refer to desiccation plate test for square plate, rectangular plate and circular plate respectively and '01' refers desiccation plate test series number (01 in this case). Figure 4.2 shows the desiccation plates together with the groove patterns used for all the tests. The grooves were made by cutting them into the plate as required.



(a)



(b)



(c)

Figure 4.2: Different desiccation plates used for the tests; (a) Grooved and smooth plates with different shapes, (b) Groove pattern in circular plate, and (c) Groove pattern in square and rectangular plate.

The samples have been prepared manually by placing the soil into the mould using a spatula. The tests were performed for reconstituted specimen. In order to avoid

adhesion of the soil to the side walls of the mould, the side walls were greased before the soil was emplaced. The bases of the square and rectangular desiccation plates have been grooved parallel and the circular plate has been grooved in a circular manner to avoid soil sliding at the contact between the bottom of the plate and the sample. However, the bases have not been greased in order to allow full adhesion to take place between the soil and the mould (Costa et al., 2008). An additional Perspex scale has been used carefully to control thickness of the soil layer for different tests.

To avoid trapping air inside the sample, the mould was tapped a few times after placing all soil inside the mould. Samples were kept on an electronic balance, which measured and recorded the mass of the specimen continuously at predefined intervals until the samples dried completely. The vertical contraction of the sample during the drying process was recorded with a vernier calliper.

Table 4.1: Test reference for desiccation plate test.

Test No	Test Reference	Plate Type	Plate dimension(mm)	Plate thickness (mm)	Base condition	Specimen Type
1	DPTS01	Square	175x175	10&20	} grooved	reconstituted
2	DPTR02	Rectangular	295x95	10&20		
3	DPTC03	Circular	ø =125	5	} grooved and smooth	
4	DPTC04	Circular	ø =125	10		
5	DPTC05	Circular	ø =125	20		

The cracking moisture content was recorded as soon as the first crack appeared. First the cracking moisture content was calculated by taking a small part of the specimen at the onset the cracking. However, it was observed that this affected the natural cracking propagation the sample (Figure 4.3). Therefore precision balance (Mettler Toledo, Model SB-8001) was used as a high capacity precision weighing balance. It features 8100 grams of maximum weighing capacity and 0.1 gram readability. RS232 interface gives the balances the option of connecting to a computer, printer or

other device. The balance was programmed with Windmill software (Data acquisition and control *software* for Windows) for continuous monitoring and recording the weigh at predefined intervals during the total test period without interfering test condition.



Figure 4.3: Example of measuring cracking water content during desiccation test and how it effects the natural cracking propagation.

A high-resolution digital camera (Canon Powershot G9, 12MP, 6x optical zoom) was mounted at the top of the set up for capturing pictures at defined intervals to capture photograph the crack occurrence, crack propagation information and crack pattern. The camera was connected with a computer and programmed to capture the images at 60 minutes interval time during the total test period. The sequence of images captured the crack initiations, propagation and crack network etc. Specific images were chosen to perform image analysis later on from different stages of crack propagations. In order to gather detail information about the cracking mechanism, image analysis was performed on the captured 2D images.

The room temperature and relative humidity were also recorded with humidity-temperature data logger (Figure 4.4). The data logger used (Model RH520) is a graphical data logger for Humidity/Temperature measurements and Dew Point calculation which provides simultaneous numerical and graphical display of humidity and temperature readings, time and date. It measures humidity ranges from 10 to 95% RH and temperature ranges from -28 to 60° C(-20.0°F to 140.0°F). The basic accuracy is 3% RH, 1.8°F/1°C. Internal memory records up to 49,000 data points and can be transferred to a PC via RS-232 serial port for further data analysis. For the experiment the data logger was programmed to record temperature and humidity at one hour interval during the total test period. Recorded data was then plotted and analysed in MS Excel. The room was only temperature controlled, so it was important to measure if the humidity varies a wide extent or not. The temperature found to be around 20.0°C and the relative RH found ranges from around 28%-36%. The repeatability of most of the tests were checked and for RH 28%-36% the results did not varied significantly. Figure 4.5 shows the schematic test setup for desiccation plate tests.

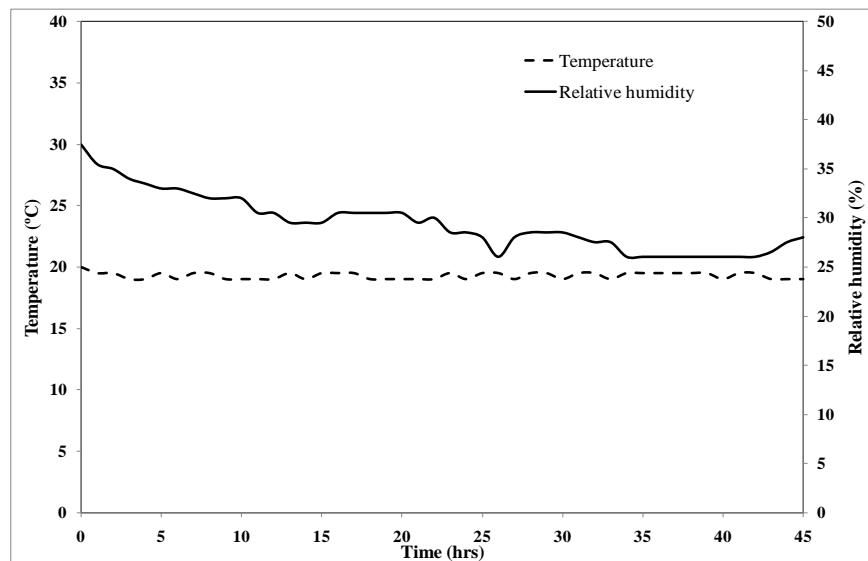


Figure 4.4: Temperature and relative humidity measurements during experiment.

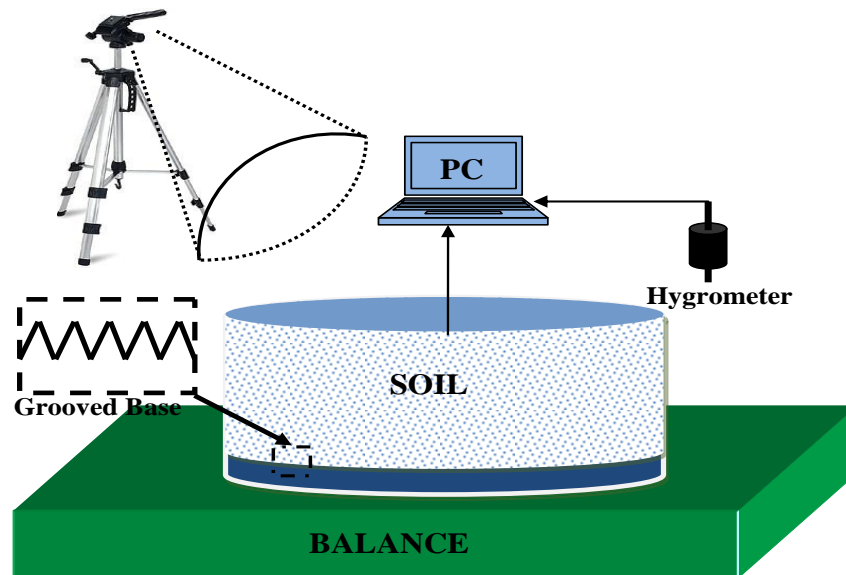


Figure 4.5: Desiccation plate test setup.

4.3.3 Quantitative analysis of cracks by digital image analysis technique

In recent years, image analysis techniques have been used extensively to characterise crack networks with improved accuracy and overcame the measuring obstacles of irregular shape and complex cracks pattern within the drying soil specimen. (Lakshmikantha et al., 2009, Tang et al., 2008b, Yan et al., 2002). In this work, image analyses were performed using Matlab programme to determine the geometrical properties of crack network. This tool has been used to extract the crack network parameters, such as the number of crack intersections, the number of crack segments, the average crack length, the average crack width and the average crack area. Digital image analysis was performed with square and rectangular plate for 10 mm soil thickness and with circular plate for 5, 10 and 20 mm soil thickness. Similar procedures were used by previous researchers to explain the soil sample size effect on cracking mechanism (Prat et al., 2006, Lakshmikantha et al., 2006). The procedure adopted for image analysis is shown in Figure 4.6-4.7. First, the digital

image (truecolor) of cracks acquired by camera was converted to grayscale intensity image. In this process, conversion from true colour image to grayscale was done by eliminating the hue and saturation information while retaining the luminance. Then, image segmentation process was done by thresholding techniques, converting grayscale image to binary black-and-white (B&W) image. In this process, the binary B&W image has replaced all pixels in the grayscale image with luminance greater than a threshold value with the value 1 (white) and has replaced all other pixels with the value 0 (black). Hence, the binary image data consists of only 1's and 0's, which represent cracks and un-cracked surface respectively. In this way, all crack parameters can be extracted accurately with program algorithm. Finally, a skeletonisation operation has been performed where all cracks with different width were converted to lines, without changing the essential structure of the crack network. After the image was skeletonised, the total length of each crack was determined by calculating the distance between intersections.

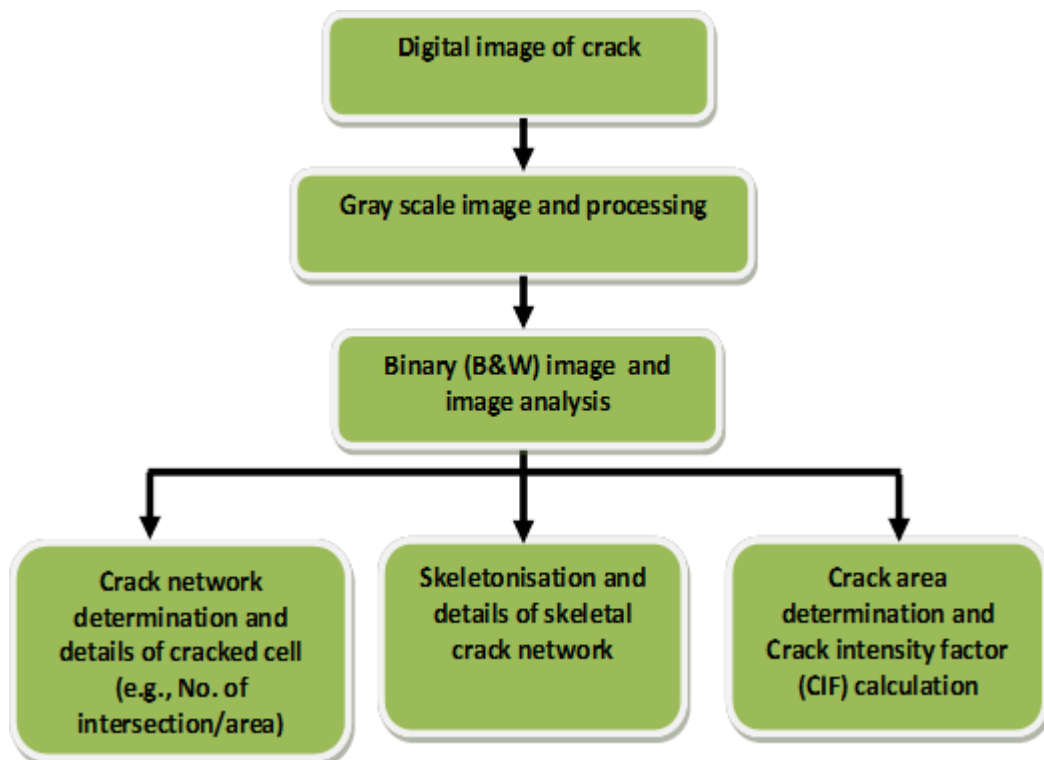


Figure 4.6: Flow chart showing the image processing and analysis.

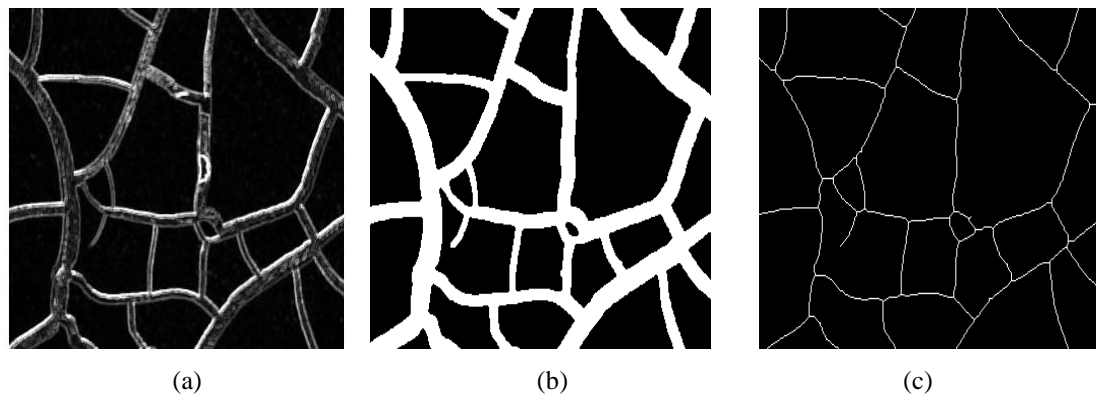


Figure 4.7: Image processing of crack network; (a) Greyscale image, (b) Binary image, (c) Skeleton of crack network (Atique and Sanchez, 2009).

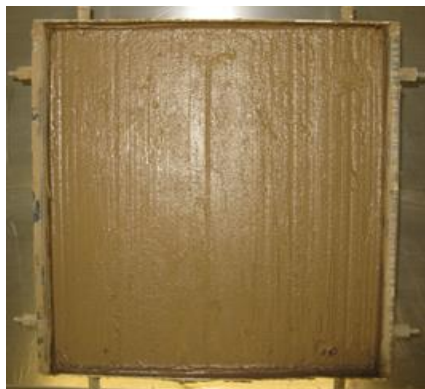
4.4 OBSERVATIONS OF EXPERIMENTAL RESULTS

The results of the tests are described here in separately for different desiccation plates. Time-lapse video clips have been produced from the testing to capture the evolution of desiccation cracking in laboratory test sample. The test duration was determined simply by running the test until soil sample was completely dried and the weight of the soil sample from the electronic balance does vary anymore. The test duration varied depending on the desiccation plate shape, the thickness of the soil sample and of course the initial water content of the sample.

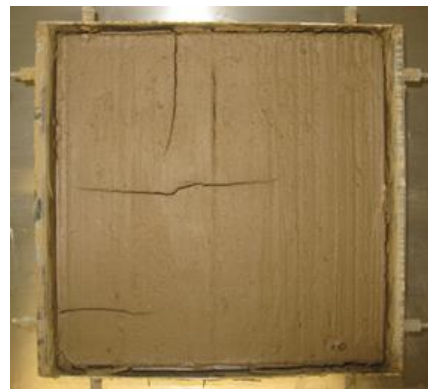
4.4.1 Square desiccation plate

4.4.1.1 Cracking Pattern

It was observed that approximately after 20 hour time from the test started soil sample tends to shrink at first and then crack growth occurs in orthogonal and sequential manner with sequential subdivision is the primary mode of the crack development during the test. Primary cracks were formed initially and secondary cracks have subdivided the initial crack pattern (see figure 4.8). 90% crack developed during 20-30 hour time period of the total test duration. The crack intersection found creating ‘+’ or ‘T’ was noticeable always. For 10 mm sample, the primary crack developed was dominant, dividing the sample into larger blocks.



(a) 0 hrs



(b) 21 hrs



(c) 24 hrs



(d) 150 hrs

Figure 4.8: Orthogonal cracking Sequence in square plate.

4.4.1.2 Effect of wetting and drying on the crack pattern

In order to investigate the effect of wetting and drying on geometric structures of desiccation crack patterns and network, a 20 mm soil sample in square plate was investigated. The sample was inundated with water after completely drying. The desiccation plate was made to drain excess water through 8 rubber tubes, after the dried soil sample absorbed enough of water to flood the sample. The sample was photographed at 60 minute interval during drying and wetting to observe the formation and growth of cracks. Figure 4.9 shows the experimental setup.

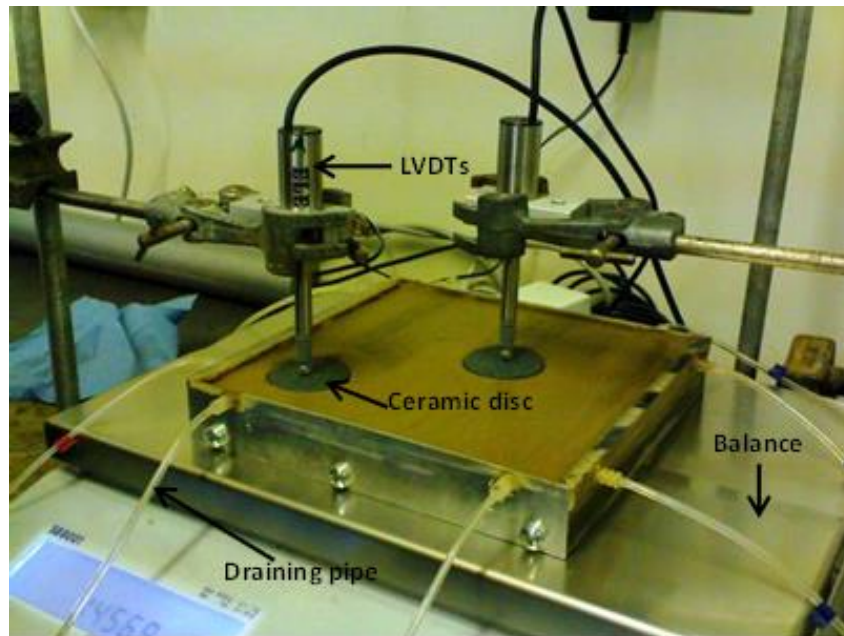


Figure 4.9: Experimental set-up.

Water inundation resulted in the apparent closure of all the visible cracks after the first drying. The cracking network seemed to help the added water to seep through the dried soil parts/cell without changing the cracking network/pattern. Another important observation was that the fine soil particles mixed with water formed a paste-like solution, which blocked the draining path in the rubber tube. Consequently, the dried soil cell eventually turned into wet lumps with no definite shape with the previous network apparently filled with soft soil. During the second

drying the cracking network did not change, which was expected as this part of the soil was already weakened due to previous cracking network from first drying. The second drying resulted re-opening of the large cracks created previously, and no more new cracks were observed. Also after reopening, the crack network was not as defined as first time, but irregular in nature, due to fine soil particles that were covering parts of the crack paths.

In order to observe the surface shrinkage pattern and the influences of wetting and drying on soil thickness, two LVDTs were placed at the surface of the specimen. It was found that the LVDTs were not effective in order to investigate these features, because they are contact devices and were affecting the cracking pattern. The LVDTs needed strong supports in order to measure the shrinkage changes within soil thickness due to drying and wetting. Unfortunately, the reconstituted specimen was too soft for this hardware and the LVDTs sank into the specimen. More importantly, LVDT placement influenced the test outcome. Cracking was always observed to start where ever the LVDTs were placed. Figure 4.10 shows this effect. Further tests did not use LVDTs because of these problems.

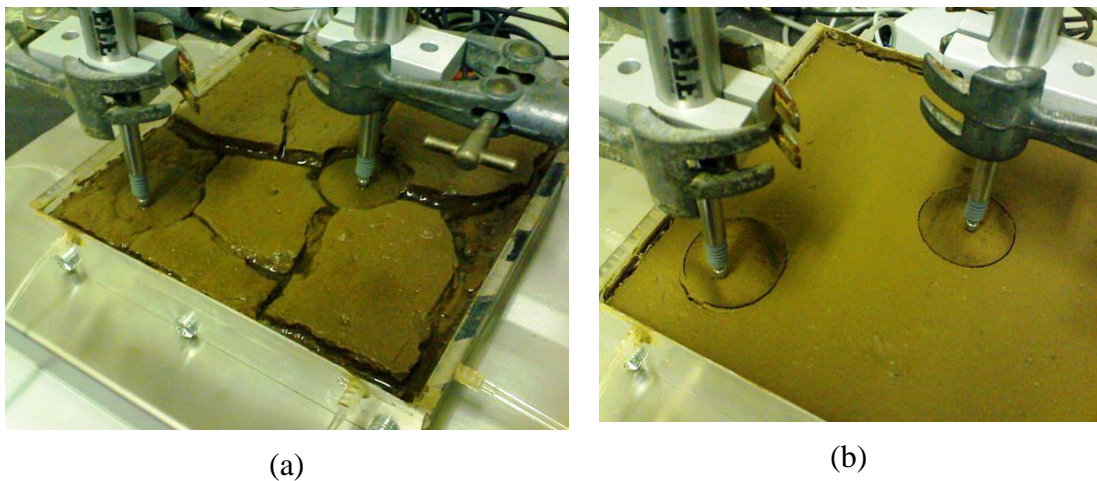


Figure 4.10: (a) Cracking pattern not affected by wetting cycle, (b) Ceramic plate sinking in soft soil failing to measure vertical deformation of soil layer.

4.4.2 Rectangular desiccation plate

4.4.2.1 Cracking Pattern

For the rectangular desiccation plate, the initiation of the first crack was found to be around the center of the mould. The crack then propagated slightly curved forward, backwards, and along with a downward propagation to the full depth of soil layer thickness. Initial cracking divided the whole sample into two large blocks (Figure 4.11a). Parallel cracking was observed during secondary crack development (Figure 4.11b).

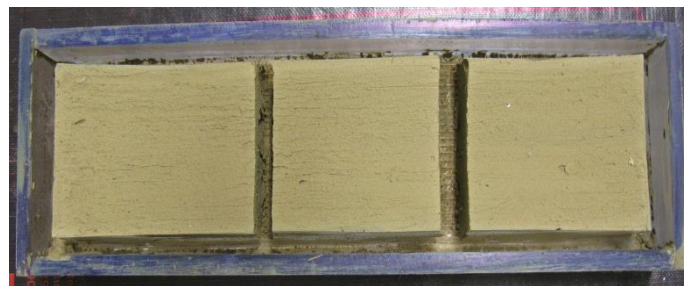
In the rectangular desiccation plate, the crack also initiated around the center of the mould, but propagated in an opposite direction of the grooves in the base. Some of the tests were done 3-4 times to ensure consistency. According to the analytical model proposed by Kodikara and Choi (2006), the maximum stress occurs at the center of the layer, thus facilitating the crack initiation. But interestingly for 20 mm soil layer thickness, the specimen cracked into three equal block (Figure 4.10b); this cracking pattern was quite similar to the work done by Peron et al. (2007a).



(a)



(b)



(c)

Figure 4.11: (a) Primary crack in rectangular plate dividing the soil sample into two large blocks, 10 mm soil layer thickness, (b) Rectangular 10 mm final cracking pattern, (c) Final crack in rectangular plate dividing the soil sample into three large blocks, 20 mm soil layer thickness.

4.4.3 Circular desiccation plate

4.4.3.1 Cracking Pattern for different soil thickness

Circular desiccation plate tests were performed for three different soil thicknesses: 5 mm, 10 mm and 20 mm. Table 4.2 gives the summary of the tests for circular plate. Figure 4.12 shows the final cracking pattern for circular specimen with three thicknesses.

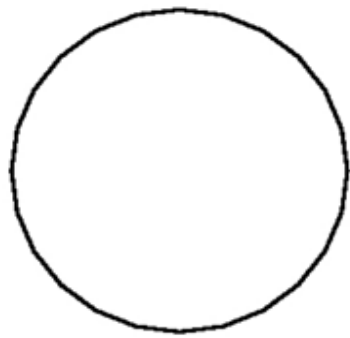
All samples produced predominantly sequential, orthogonal crack patterns, leading to subdivisions of the crack area into smaller cells. For the 10 mm and 20 mm samples the crack initiated from the side wall. However, for 5 mm samples, non-orthogonal crack patterns evolved at the primary cracking stage and they occurred simultaneously and relatively fast all over the soil surface.

Table 4.2: Summary of the desiccation test for circular plate in grooved based at three different soil layer thicknesses.

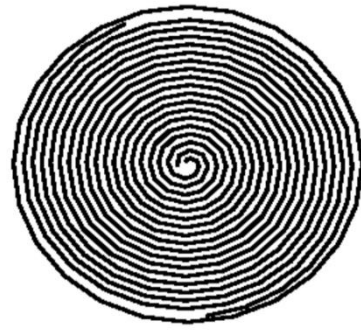
Desiccation plate shape	Plate Dimension (mm)	Base condition	Initial sample thickness (mm)	Final sample thickness (mm)	Test duration (days)	Initial water content (W%)	Cracking water content (W%)
Circular	175x175	Grooved	5	4.38	3	56.767	52.000
	295x95	Grooved	10	8.94	5	56.380	47.000
	125	Grooved	20	16.21	7	56.380	45.000
Circular	175x175	smooth	5	4.00	2	57.000	51.255
	295x95	smooth	10	8.33	5	56.452	50.911
	125	smooth	20	15.67	8	56.000	No crack

4.4.3.2 Influence of the base pattern and thickness on cracking

Circular specimen was tested with two different bottom contact surfaces: smooth and circular grooves with 5 mm, 10 mm and 20 mm soil layer. Tests were performed in triplicate to ensure consistency. The smooth surface offered less friction than the grooved surface. The cracking pattern seemed to be influenced by the base condition. For the 10 mm soil layer, the cell number was higher for smooth base with smaller sizes of cells than plate with grooved base. Interestingly, for the 5 mm soil thickness the opposite results was observed. Smooth base specimen has lower numbers of cells and larger cells; however, the cracking pattern followed the grooved surface pattern within the plate for 5 mm soil layer (Figure 4.11). More interestingly, the 20 mm grooved specimen cracked with few numbers of large cell compared to the 5 and 10 mm grooved specimens. The 20 mm smooth base specimen experienced shrinkage with no cracks at all. Figure 4.12c shows the 20 mm sample in smooth base with shrinkage from the side wall and and colour change. For all cracked specimens, non-orthogonal and predominantly 120° crack patterns were observed at the primary cracking stage. These cracks appeared to occur simultaneously and relatively quickly over the soil surface for both contact surfaces.



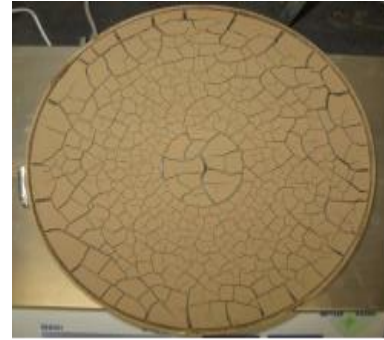
Smooth base



Grooved base



(a)



(a)



(b)



(b)



(c)



(c)

Figure 4.12: Final cracking pattern for circular plate in different base; *Left*: Smooth base, *Right*: Grooved base; (a) 5 mm plate, (b) 10 mm plate and (c) 20 mm.

Figure 4.13 shows the evolution of moisture content for specimen in circular plate with grooved base 3 different soil layers.

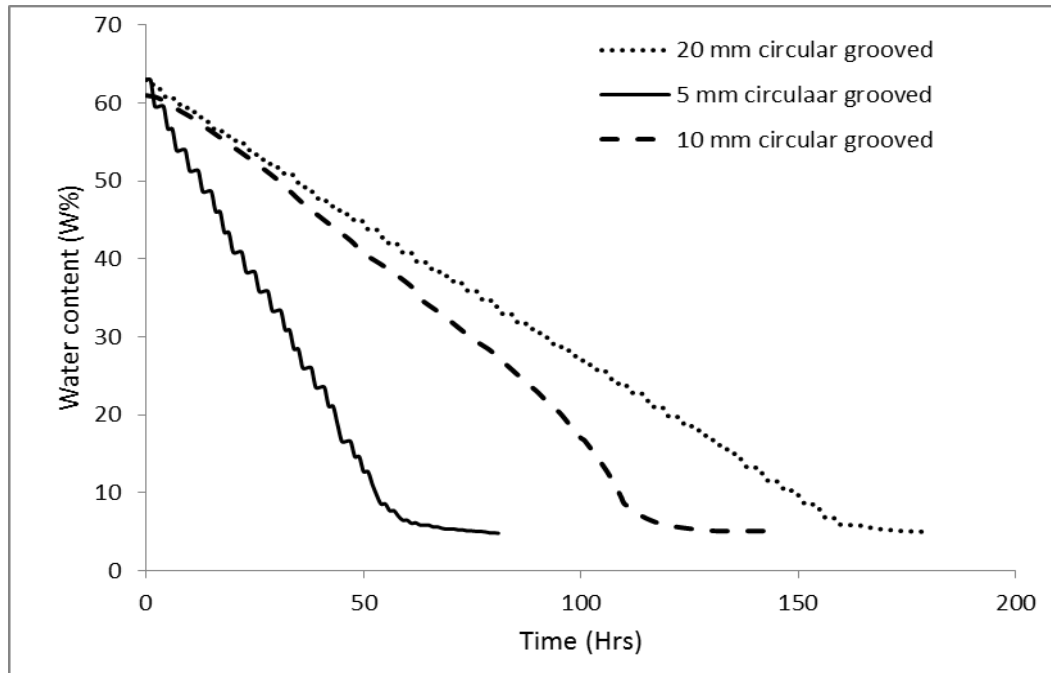


Figure 4.13: Variation of water content over time (circular plate).

4.4.3.3 Cracking moisture content

Figure 4.14 shows the cracking moisture content for circular plate for 3 soil layer thicknesses. The cracking moisture contents for 5 mm, 10 mm and 20 mm samples were 52%, 47% and 45%. Cracking moisture content seemed to increase as soil layer thicknesses decreased (Figure 4.14). This observation contrasts with the hypothesis made by Corte and Higashi (1960).

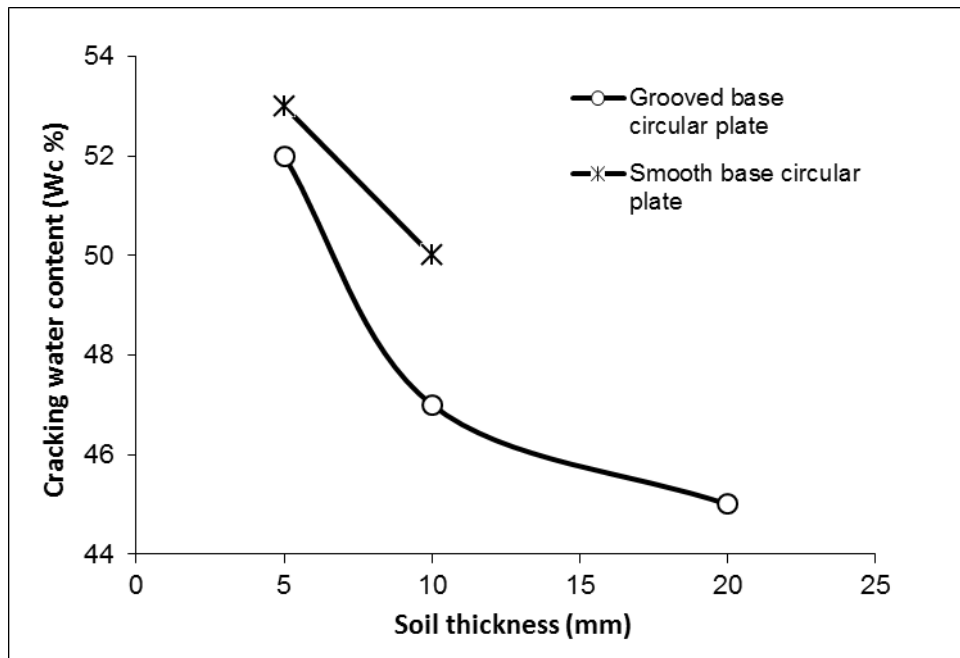


Figure 4.14: Effect of soil layer thickness on cracking water content (circular plate).

4.4.4 Effect of different Plate Shape

Figure 4.15 shows the final crack pattern for 10 mm soil samples performed on square, rectangular and circular plate. The visual observations from the images showed that number of cells after cracking was higher in a square plate than circular or rectangular plates. The crack patterns were mostly orthogonal in rectangular plates, whereas they were mixtures of orthogonal and non-orthogonal in square and circular plates.

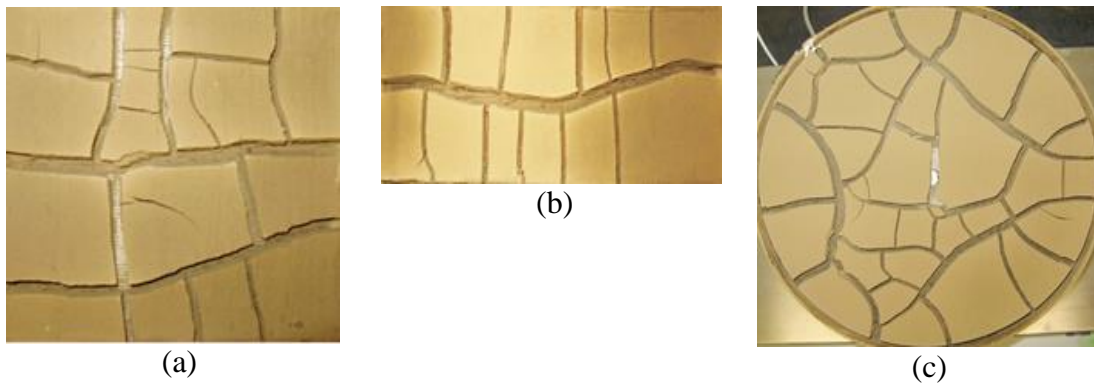


Figure 4.15: Final crack network pattern in 10 mm thickness sample; (a) Square plate; (b) Rectangular plate; (c) Circular plate.

Figure 4.16 shows the evolution of moisture content for specimen in three different shaped grooved base desiccation plates for similar soil layer thickness. The evolution of moisture content for two plates does not differ significantly for rectangular and square plate. The duration for circular plate test was less than the other two.

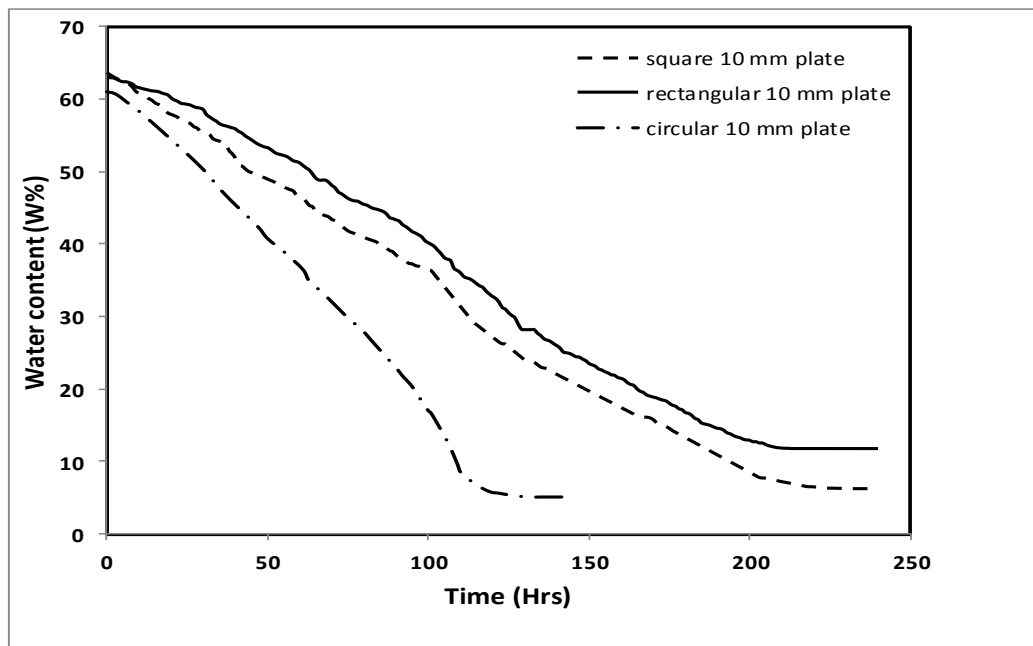


Figure 4.16: Water content variation curve for three different shaped desiccation plates with 10 mm thickness.

Table 4.3-4.4 show the summary of the analysis of desiccation test for three different plate shapes.

Table 4.3: Summary of the desiccation test for different plate geometry.

Desiccation plate Shape	Plate dimension (mm)	Base condition	Initial sample thickness (mm)	Final sample thickness (mm)	No. of crack/area (m ⁻²)	No. of cell/area (m ⁻²)	Initial water content (W %)	Cracking water content (W %)
Square	175x175	Grooved	10	8.29	620	555	64	57
Rectangular	295x95	Grooved	10	8.94	428	428	61	59
Circular	125	Grooved	10	6.21	489	305	61	58

Table 4.4: Crack network parameters for three different plate geometries at similar soil layer thickness.

Plate structure	Soil thickness (mm)	No. of crack Intersection/area (m ⁻²)	No. of crack segment/area (m ⁻²)	Total length of Cracks (mm)	Crack Intensity Factor (CIF) (%)	Average width of crack (mm)
Square	10	751	1306	1060	17.81	5.14
Rectangular	10	393	785	763	21.45	7.87
Circular	10	1060	1487	1967	19.69	4.91

The effect of different geometry of specimen on desiccation cracking was first studied by Lakshmikantha (2009) in an elaborate manner. Although this research work is not as elaborate in regards to geometry, it was interesting to see the effect of three different plate shapes on desiccation cracking pattern even in a small scale. It is clear that for the same soil layer thickness the CIF does not vary significantly for

different geometry of the specimens (Table 4.4). However the different geometries had an effect on the final cracking pattern (Figure 4.15). This observation is consistent with previously published studies (Lakshmikantha, 2009). For 5 mm and 10 mm soil layer thicknesses with the same areas (circular plate, Table 4.5) had similar results as well, but 20 mm thickness showed lower CIF compared to the other two, suggesting an influence of the lower boundary on laboratory results.

Table 4.5: Crack network parameters for three different thickness circular plate grooved base (D = 125 mm).

Soil thickness (mm)	No. of crack/area (m ⁻²)	No. of crack intersection/area (m ⁻²)	No. of crack segment/area (m ⁻²)	Total length of cracks (mm)	CIF (%)	Average width of crack (mm)
5	23480	16448	10517	7713	21.43	1.36
10	489	1060	1487	1967	19.69	4.91
20	265	122	163	772.5	11.18	7.10

4.4.5 Summary of Desiccation plate test results

The desiccation plate tests aimed to study some relevant factors that affect the behaviour of soils subjected to drying. The experimental research has been performed on samples from Bengawan Solo River of Indonesia.

The observations from the desiccation plate test were that most samples produced predominantly sequential, orthogonal crack patterns (i.e., cracks that tends to meet at right angles) leading to subdivision of the crack area into smaller cells (Figure 4.8). The dynamics of the crack formation showed, that in the first stage of crack-pattern development cracks, the cracks tend to meet at a small number of points. These cracks then propagate in fairly straight lines occasionally meeting another crack

moving in a similar manner forming a polygonal pattern along with vertical propagation. Similar observations were made by Shorlin et al. (2000) and Mizuguchi et al. (2005). The final stage of drying was governed by vertical propagation and completes drying of the soil without any observable new crack formation.

The shape of the crack nodes at an intersection was always '+' or 'T' regardless of experimental conditions (Figure 4.8 and Figure 4.12). Similar observations were found in the work by Tang et al. (2008b).

Nearly 90% of the crack development occurred during a 20-30 hour time period, although the total duration of the desiccation cycle was approximately 170-250 hours. Cracking was found in the field while the embankment soil retained high degree of saturation (during wet season). Based on these observations, the Bengawan Solo soil may start to crack at quite high water content. Seasonal variations may trigger this process at more intense states.

Higher desiccation rates were observed for smaller thicknesses. Non-orthogonal crack patterns evolved at the primary cracking stage and they occurred simultaneously and relatively fast across the soil surface (Figure 4.12 a). This phenomenon is extensively reported in literature by Corte and Higashi (1960), Nahlawi and Kodikara (2006). Nahlawi and Kodikara (2006) reported that if the thickness increases the with same drying area, the water content loss will decrease because the water has to travel greater distance for evaporation.

Cracking pattern was found to be influenced by the base condition of the desiccation plate (Figure 4.12). This indicates the friction between two soil layers has an effect on cracking pattern. Natural soil consists of different sizes of soil particles, which always have frictional effects between two soil layer. This is true in laboratory test samples and embankments in the field. The sources of cracking may come from similar and different sources in field applications relative to laboratory studies, but the underlying phenomena of grain-grain and grain-water interactions are the same. In the present work, only circular specimens were tested with different bottom conditions. The smooth surface offered the least friction, which is quite significant in

20 mm soil thickness in smooth base with no cracking. Similar observation was made by Groisman and Kaplan (1994)

Cracking water content does not appear to be influenced much by plate geometry if the soil layer thickness is same (for 64%, 61% and 61% initial water content 57%, 59% and 58% cracking water content was found for square, rectangular and circular plate respectively). For same initial length but different initial water content, Towner (1987b) found cracking water content is independent of initial water content. Although the tests were not performed for wide range of initial water content and thickness, it can be assumed from the findings that the Bengawan Solo Soil tends to crack at high degree of saturation. This was evident during site investigation (see Figure 3.4 in *Chapter 3*). Since Indonesia has two main seasons, wet and dry, the cracking created during the wet season will be more intense. These cracks may propagate and widen during the dry season, which risks triggering various kinds of embankment failures. However cracking water content was found increasing with decreasing soil layer thickness for same drying area (Figure 4.14) which again supports by Nahlawi and Kodikara (2006)

Different geometries had an effect largely on final cracking pattern. Unfortunately the CIF was only measured for final cracking pattern and not at different stages of cracking formation. The key aspect from this would be to know an overall picture of crack initiation, severe cracking period, rate of crack growth and end of cracking. However CIF for the final cracking pattern suggests the extent of surface cracking is not varies a lot for similar thickness with different geometry. This finding support the findings by Lakshmikantha et al. (2009). However for same drying area with different thickness the CIF varies higher with higher thickness difference. These observations indicate that CIF is dependent on specimen thickness, which limits its applicability in comparing laboratory and field-scale behaviours. It would be realistic to compare evolution of CIF at different stage of drying also in order to complement this limitation. Manmade embankments are subjected to erosion for various reason which makes the embankment unevenly thick throughout its length. Field observations would need to take these factors into account and compare cracking at many areas to ultimately establish a relationship.

4.5 CONCLUSION

This chapter presented the laboratory experiments carried out on the desiccation cracking of Bengawan Solo soil at higher water content states, for reconstituted specimen. The soil experienced shrinkage which leads the sample to cracking due to desiccation. It is believed that the presence of montmorillonites within Bengawan solo soil influences its desiccation property significantly. It has been observed that the cracking pattern evolved sequentially. First the crack divides the soil surface into large cells and subsequent drying causes these cells into smaller cells. It has been found that the higher the soil thickness, the lower the number of cells. This was at least evident for 5 mm, 10 mm and 20 mm circular plate with smooth base. Image analysis showed that the parameters that govern crack pattern varied with plate geometry. Also, CIF values were similar for three plate geometries. Significantly more research is needed for further understanding of the influences of base conditions on desiccation processes as that could reflect the picture of friction effects between two soil layers in practical field.

The findings from the tests reported in this chapter also agreed with the findings from previous researchers in terms of crack initiation, propagation, and other parameters. However, these methods provide no information about the vertical propagation/deformation of cracking. This information is probably the most significant in practice for various geotechnical applications. The research presented here in finds the necessity for improving experimental techniques to better understand the mechanisms of cracking, particularly in the vertical direction.

The next chapter, *Chapter 5, Desiccation Tests using 3D compact Laser Scanner*, will discuss desiccation testing with an improved setup to capture vertical cracking, which is the most important achievement of this research.

Chapter 5: Desiccation Tests using 2D/3D compact Laser Scanner

5.1 INTRODUCTION

One of the main objectives of this research was to develop an experimental technique to investigate cracking behaviour in soil in three dimensions. This chapter proposes a new measurement technique to study desiccation cracks in soil by the use a 2D/3D compact laser scanner. Desiccation plate test as explained in *Chapter 4* were performed with this test setup using a glass desiccation plate. The chapter starts with a short background of necessity of introducing a new test setup to study desiccation cracks in soil. The experimental equipment used and the experimental procedures are then described. A calibration process was performed to investigate the accuracy of this 2D/3D laser scanner. For this purpose, volume of a toy Lego was measured by water displacement method. Surface cracking parameters were measured using image analysis and 3D scanner in order to compare the variation of the results. Experiments have been performed to validate the functionality of the device and a comparison between laser scanning techniques has been also performed. The experimental outcomes showed that the proposed experimental technique of measuring cracked soil parameters using a laser scanner was faster and more precise

than the currently used method. Furthermore it provided more information than the currently used methods. It is, in summary, a promising experimental technique that could assist to advance current knowledge in this complex subject.

5.2 BACKGROUND

5.2.1 Why new technique?

Desiccation cracks in soils are a highly complex phenomenon due to the strong coupling between the hydrological and mechanical behaviour of soils. There is not a consensus on the kind of theory or model that should be used to correctly describe cracking phenomena. A number of different theories have been proposed in the last few years (Morris et al., 1992b, Konrad and Ayad, 1997a, Hallet and Newson, 2005, Rodriguez et al., 2007, Trabelsi et al., 2010, Trabelsi et al., 2011). As for the experimental investigation, different laboratory protocols have been followed focusing mainly on the volumetric response on drying, tensile strength properties, as well as on crack initiation and propagation (Tang and Graham, 2000, Lakshmikantha et al., 2006, Rodriguez et al., 2007, Peron et al., 2009, Trabelsi et al., 2010). However, there is not a laboratory reference test to study desiccation cracking of soil.

Desiccation experiments focusing on soil cracking phenomena are generally performed on slurry samples prepared in either rectangular or circular plates (Peron et al., 2009, Lakshmikantha et al., 2009, Tang et al., 2011). Current methods/techniques to estimate the volume change under such conditions present severe limitations. LVDT is a contact measurement device; hence it is not useful where non-contact measurements are desired to prevent any perturbation in the stress field that could alter the natural evolution of the test. Furthermore, the initially fully-saturated soil cannot support the weight of the LVDT sensor head, which settles (or penetrates) in the soil mass and thus invalidates the measurement. Non-contact

magnetic sensors (Clayton and Khatrush, 1986, Jardine et al., 1984) require the inclusion of reflecting elements on the soil surface; which would significantly alter the stress state in its vicinity, affecting the crack formation process, and the subsequent crack propagation (Obidat and Attom, 1998). Peron et al. (2009) used a measurement system based on callipers, which is not easy to operate and it also provides a crude estimation of the volume change. Furthermore, those devices (i.e. LVDTs, callipers and non-contact magnetic sensors) provide local measurements only, from which is difficult to obtain an accurate estimation of the volume change in drying soils due to soil curling and the presence of desiccation cracks. Digital image processing has also been used to measure displacements, volume change and deformations in soil testing (Obidat and Attom, 1998, Alshibli and Sture, 2000, White et al., 2001, Ören et al., 2006). In particular, digital image analysis have been used to track the movement of displaced particles in direct shear tests (Guler et al., 1999) and to characterize soil fabric changes in micro-scale during testing (Adamcewicz et al., 1997, Romero and Simms, 2008a, Airò Farulla et al., 2010) as well as for analysing surface cracking patterns (Lakshmikantha et al., 2006). Macari et al. (1997b), Alshibli and Al-Hamdan (2001) and Gachet et al. (2006) studied volume changes of specimens in conventional triaxial tests using digital image processing. In general terms, it was shown that the results obtained from digital and manual measurements matched well. However, the measurement of vertical and horizontal displacements from digital images is not very precise from one camera. Moreover, the use of image processing technique to estimate volume change in drying soils has a number of limitations. For example, due to the shadows in the 'crack valleys' it is difficult to detect the actual (3D) geometry of the cracks from a digital image (i.e. crack depth and variation of crack aperture with depth). Furthermore, from digital images it is not possible to detect soil curling and surface settlements either.

From above, it is evident that the device to be used in the study of drying soils should be able to accurately track the evolution of the main global hydraulic (e.g. water loss) and mechanical (e.g. volume change) variables associated with this phenomenon. It would be also recommended to gather relevant information associated with the

evolving crack network, for example changes in its geometrical properties, morphology, crack aperture and depth.

Current experimental investigations in this area primarily concentrate on the study of slurries prepared in plates and subjected to drying under controlled laboratory conditions. In those tests, quite accurate measurements of the water loss during desiccation can be gathered by means of high precision balances. The measurement of the volume change under such conditions is more complicated. Conventional devices used in the laboratory to measure displacements, such as contact ones (e.g. linear variable differential transformer, LVDT) and non-contact ones (e.g. Hall effect, Eddy current) are not suitable for these kinds of experiments due to the perturbation that they may induce in stress field (Gachet et al., 2006). Digital image analyses are generally used to study the nature of soil crack propagation and also to obtain useful parameters to characterize the morphology of the crack network (Miller et al., 1998b, Velde, 1999, Vogel et al., 2005b, Vogel et al., 2005a, Lakshmikantha et al., 2009, Tang et al., 2008a, Tang et al., 2011). A rough estimation of the vertical settlement can be obtained from image analyses from one camera (Shin and Santamarina, 2011). More accurate measurements will require more advanced systems such as 2- and 3-component setups described by Brossard et al. (2009).

This chapter proposes the use of a 2D/3D laser device as an alternative to current methods to study drying cracks in soils. Laser scanners have been used with success in measuring the volume of solid materials (Zhang and Morris, 2005) and in soil and rock testing to measure displacements and other geometrical properties (Hong et al., 2006, Romero and Simms, 2008b). However, their effectiveness in studying desiccation cracks in soils has not been determined yet. Experimental setup of laser scanning technique is compact which includes, amongst others, data acquisition from electronic balance for continuous water loss monitoring as well as a motion controller for precise laser movement. The name 2D/3D is because the 3D representation of the soil sample is obtained after compiling subsequent linear (2D) profiles data. A series of experiments were performed to evaluate the functionality of the proposed device to study soil desiccation. The main soil properties, the proposed

device and methodology, and experiment results are discussed in the following sections.

5.3 OBJECTIVES AND EXPERIMENTAL CAMPAIGN

The aim of this experimental campaign was to introduce a new and improved/alternative test setup for investigating desiccation cracks behaviour in drying soil. The specific objectives were: (i) to validate the functionality of the 2D/3D laser scanner device in investigating soil desiccation and crack (ii) to examine the advantage using lasers scanning technique over existing techniques generally used for analysis of cracking behaviour in soil.

Desiccation plate tests were performed on reconstituted Bengawan Solo Soil what was allowed to dry in a laboratory controlled environment. Table 5.1 gives the test details and initial condition. LDT 01 refers to Laser Desiccation Test no1 and so on. LDT01 was performed to measure the volumetric shrinkage which was then compared with the volumetric shrinkage curve described in *Chapter 3 “Soil Characterisation”*.

Table 5.1: Desiccation Test details using 3D compact Laser Scanner.

Test Ref.	Initial moisture content, w_0 (%)	Aim of the test	Plate
LDT01	53.37	Measuring volumetric shrinkage	Circular glass plate
LDT02	54.75	Analysing cracking parameter	
LDT03	57.689	Analysing cracking parameter	

5.4 EXPERIMENTAL SET-UP

The experimental set-up consisted of the following main components: i) compact 2D/3D laser-scanner (ScanControl 2700-100, Micro-Epsilon Messtechnik GmbH & Co, Ortenburg, Germany); ii) laser motion controller; iii) electronic balance with the soil sample on it; iv) relative humidity and temperature sensor; v) digital camera and vi) a computer with data acquisition system (DAS). Figure 5.1 presents a schematic representation of this setup and the main components are briefly described below.

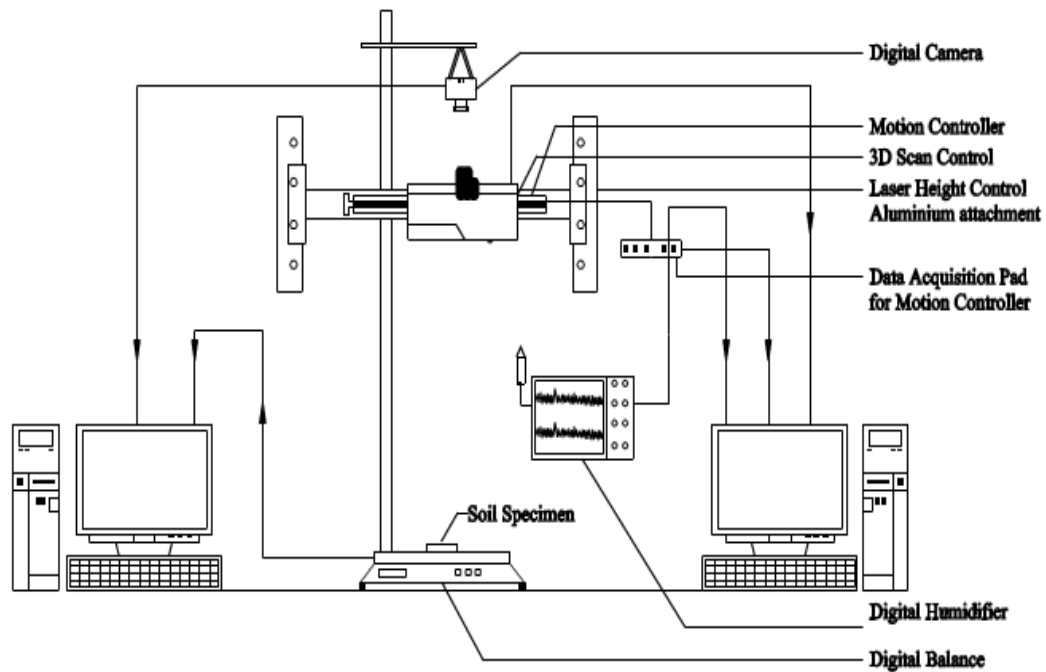


Figure 5.1: Schematic of set up of Desiccation plate tests using 3D compact Laser Scanner.

The laser unit was fixed to the wall using a frame designed to allow positioning of the laser at different heights (Figure 5.2). In order to obtain a 3D representation of the sample, the laser was coupled with a motion controller (model OWIS PS-10) that moves horizontally (x-axis) at a constant speed perpendicular to the laser line. This is a single axis position controller with a 2-phase stepper motor including open loop functionality which has an USB interface to communicate with the computer. The Software tool *OWISoft* was used to configure and control this unit. While scanning over the surface of the sample, the soil profiles were transferred to the computer as an array of points. Scanned data was transferred to the computer for processing using the software *ICONNECT* from Microepsilon-Website (2011). Each of these profiles consists of a certain number of calibrated measuring points, including additional information like intensity, time and counter information. To measure the water loss during desiccation, a high capacity precision weighing balance was used (*Mettler Toledo model SB-8001*). It features 8.1 kg of maximum weighing capacity which

offers 1×10^{-4} kg readability. Via a RS232 interface, the balance was connected to a computer and programmed (using Windmill software) for continuous monitoring.

A data logger (Model RH520) was used for relative humidity (RH) and temperature measurements. The RH measurement range is from 10 to 95% and temperature from -28 to 60°C. The basic accuracy is 3% RH and 1°C. Measurements were transferred to a computer via a RS-232 serial port for further data analysis. A 12.1 MP digital camera was mounted on the laboratory stand to take images of the sample during desiccation. A desktop computer was used for data acquisition and devices control.

The laser frame is a vital part as the motion controller and the laser scanner itself is attached with this. The laser frame was manufactured by the mechanical laboratory within University of Strathclyde. There are three holes at each side of the frame in order to hang the frame with wall to achieve three different Z-resolution of the laser line towards the test sample. The bracket was carefully mounted to wall in order to maintain the proper alignment of the laser. After attaching the laser, the alignment was checked using a level. Figure 5.2 showing the image of the complete set up.

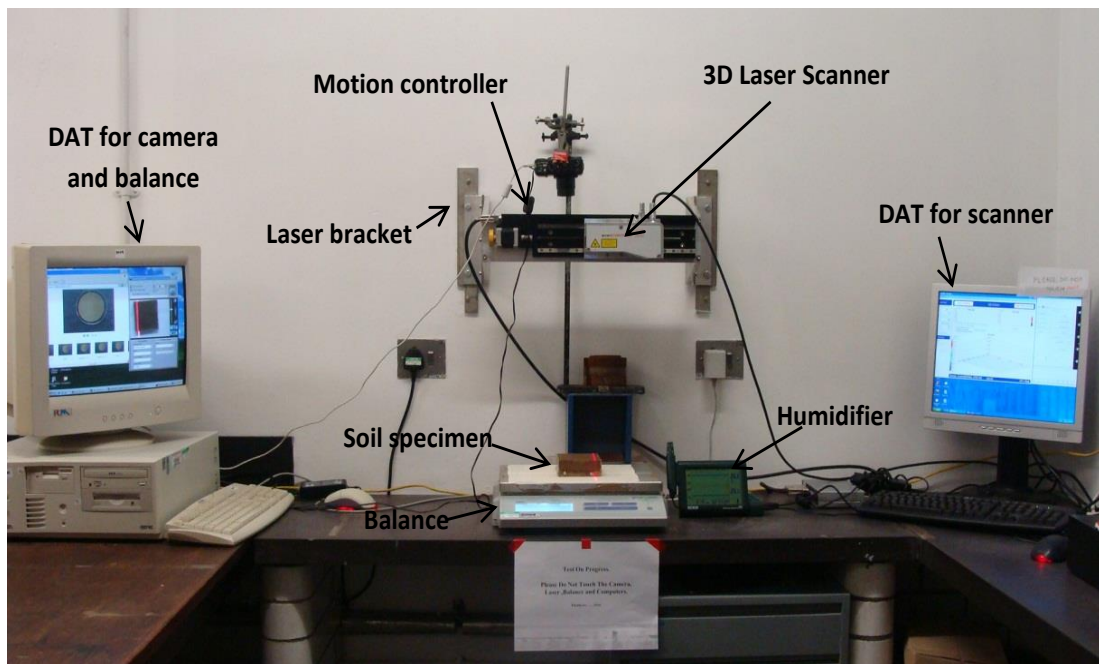


Figure 5.2: Photo of desiccation test set-up using 3D compact Laser Scanner.

5.4.1 Scan CONTROL 2700-100: Compact 2D/3D profile sensor with integrated controller

ScanControl 2700-100 from *Micro-Epsilon* (Microepsilon-Website, 2011) was used to do the tests. The general specification of the laser scanner ScanControl 2700-100 is given in Table 5.2.

Table 5.2: Scan CONTROL 2700-100 scanner specification.

Light source	semiconductor laser; wavelength 658nm; aperture angle laser line 20°; output power 10 mW
Operating temperature	0°C to 50°C
Storage temperature	-20°C to 70°C
Measuring range x-axis	100mm
Start of measuring range z-axis	350mm
End of measuring range z-axis	450mm
Start of extended measuring range z-axis	300mm
End of extended measuring range z-axis	600mm
Linearity z-axis [%]	±0.2% (3σ) FSO (Full scale output)
Linearity z-axis	±200 μm
Resolution x-axis	640 points/profile
Reference resolution z-axis	15 μm
Profile frequency	100Hz (standard measuring field)

The measuring principle of the laser line scanner was the triangulation principle for a 2D acquisition of a height profile of various target surfaces (Figure 5.3). A laser line was generated by a special lance and projected onto the target surface. A high-quality optical system projected the diffusely-reflected light of this laser line back onto a highly sensitive sensor matrix. In addition to the calibrated distance information (z-axis), the controller, integrated into the sensor head, used this matrix image to calculate the position along the laser line (x-axis). This generates calibrated matched measurement values (z, x) which are then output as a precise line profile. The profile sensor scanCONTROL 2700-100 delivers 64,000 points/sec or 100 line frames/sec with an absolute consistent and reliable rate.

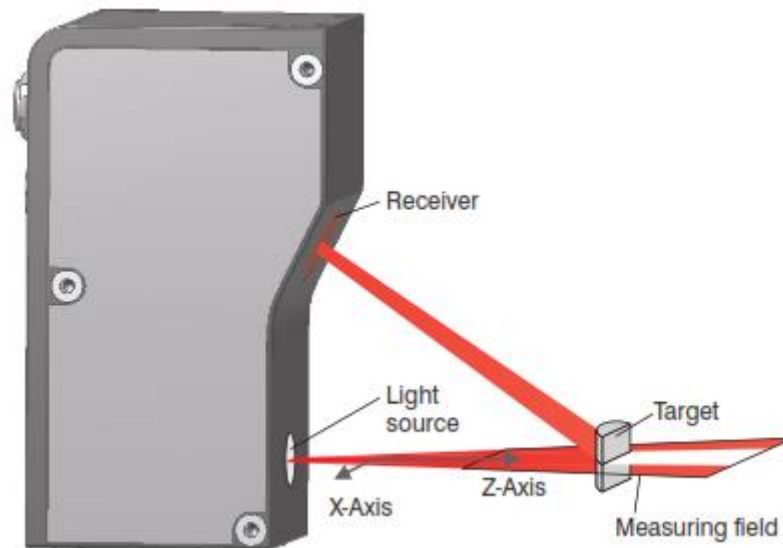


Figure 5.3: Measuring principle of the laser.

5.4.2 Laser 2D/3D Resolution

Z-axis resolution corresponds to the elevation resolution (i.e. the one concerning the distance from surface to sensor). Any points in the surface point cloud (A point cloud is a description of a set of points, usually specified in a three-dimensional coordinate system X , Y , and Z and are intended to be representative of the external surface of an object) separated by this amount or more can be identified by scanner. The laser scanner used in this research has a z-axis resolution of $15\ \mu\text{m}$. Therefore, the sensor is able to measure steps of up to $15\ \mu\text{m}$ height, taking a reference line of 640 points, at the manufactured specified standard measuring target. X-axis resolution corresponds to the resolution along the laser line. Higher resolution means a greater amount of acquired data along the laser line, hence more information about the surface. The adopted laser has a pre-defined parameter for this purpose, which is in the form of points/profile. The width of the laser line depends on the actual distance of the sensor to the target. For example, for surface to laser distance of 400 mm, the laser line width would be 100 mm. Y-axis resolution corresponds to the

resolution normal to laser line axis. This lateral resolution does not have any pre-defined value. It depends on several laser scanner parameters, e.g., exposure time, profiles/sec, scanning distance in y-axis. With other parameter fixed, higher profiles/sec gives higher y-axis resolution.

5.5 EXPERIMENTAL METHODOLOGY

The reconstituted specimen specimens were prepared according to the procedure as described in *Chapter 3 'Soil Characterisation'*. All specimens were prepared at around the Liquid Limit of Bengawan Solo soil (55%) to ensure a slurry state. Only reconstituted specimens were used for the tests described in this chapter. A slurried sample was chosen in order to allow analysing evolution of drying soil.

The desiccation tests were performed in a small room under controlled temperature and relative humidity conditions. The room has no windows and the lighting was strictly controlled to facilitate constant conditions during testing. The soil sample was prepared close to its liquid limit and allowed to dry in a circular glass desiccation plate (9.689 cm diameter, 1.292 cm height; Figure 5.4). The moisture content was determined before and after the test. Humidity data logger was continuously monitoring the temperature and relative humidity of the room. The average temperature during the test was 19.5°C ($\pm 0.30^\circ\text{C}$) and the average RH was 37% ($\pm 3\%$). The sample was placed on the balance, which was programmed to record water loss continuously.

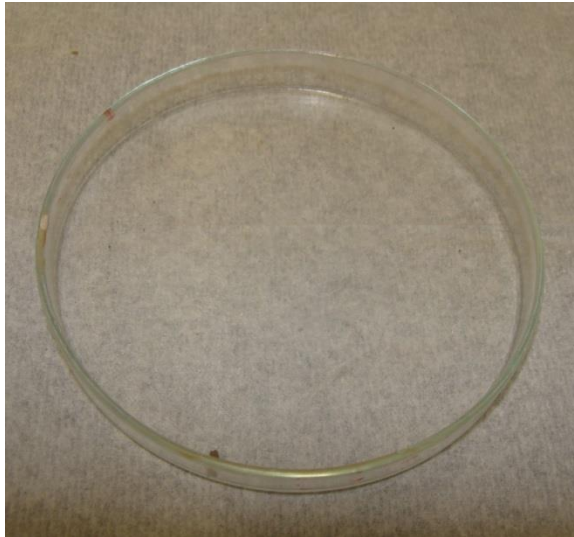


Figure 5.4: Glass desiccation plate used for laser scanner.

As with the desiccation tests, the change of the volume of the soil specimen was one of the interests; the whole experimental set up remained untouched until the end of the test to avoid interfering with the test conditions. The scan time was noted and captured image from the camera at the same time was taken to perform image analysis for the comparison in measurement of crack networks between two methods. The volume change of the sample was measured from the scanner data using Surfer software. The scanning was performed at every two hours during until most cracking initiates and the interval time was increased to 3 to 4 hours at the very end of the tests when no significant changes occurred within the specimen. The scan frequency was increased after LDT 02 (4 scans) because more scans were found to be useful to achieve detailed information. Therefore, LDT 03 was performed with 15 scans.

A calibration process was performed to investigate the accuracy of the laser scanner in the context of particular application which is volume change. For this purpose, we measured volume of a toy *Lego* by the water displacement method. We then compared the measurement with the volume found by laser scanner system.

5.6 GENERAL SET-UP AND ANALYSIS PROCEDURES

5.6.1 Setting up the scanner and Motion Controller

After the desiccation plate was ready to start the test with specimen in it, the plate was placed at the top of the balance. It was done by displaying image data within the scanCONTROL configuration tools (Figure 5.5-5.6). The motion controller software was set at 3.88×10^{-3} m/s and the travel distance was controlled as required (Figure 5.7). The travelling distance was then calculated to select the buffered profiles in scanCONTROL 2700. This parameter defined the number of profiles that make up a point cloud (i.e. to determine the resolution in the Y/T direction with this parameter.). The minimum adjustable value was 100 and the maximum adjustable value depended on the parameter *points/profile*. This setup was kept constant until the test finished. The scanning position was important at each scan in order to avoid unexpected noise around and within the desiccation plate which could lead to incorrect calculations of the cracking parameters.

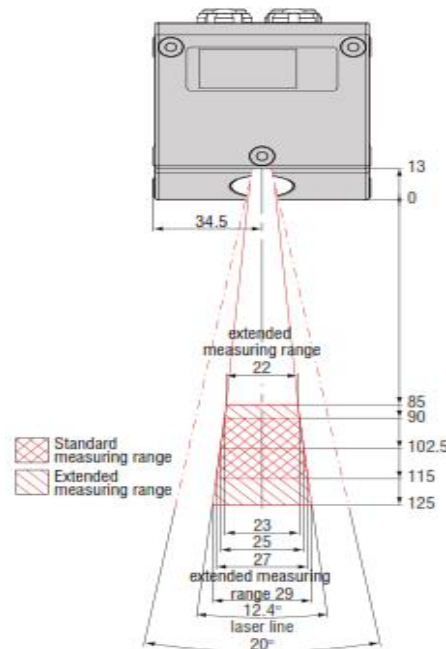


Figure 5.5: Laser resolution measurement region (Microepsilon-Website, 2011).

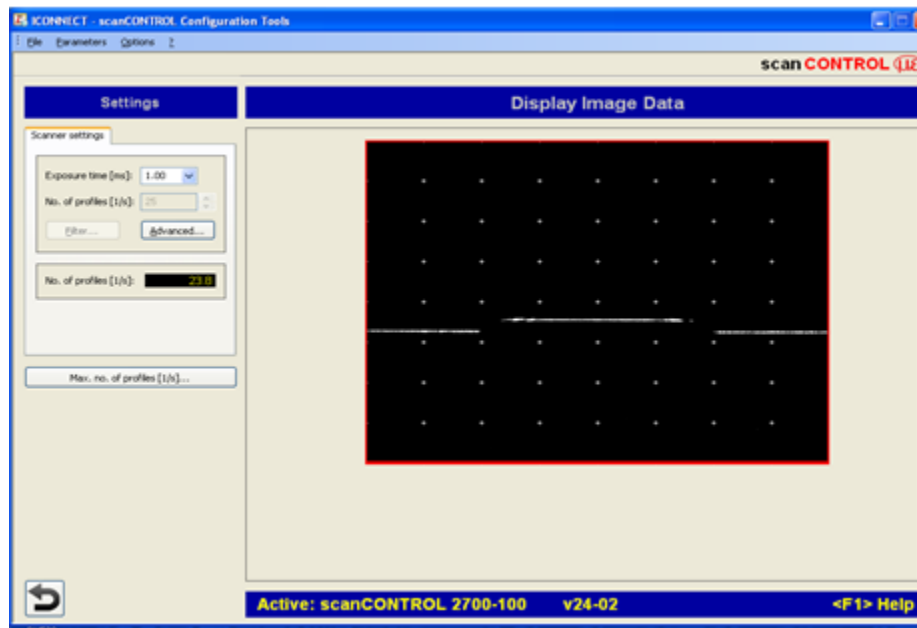


Figure 5.6: Positioning the desiccation plate within the laser resolution region.

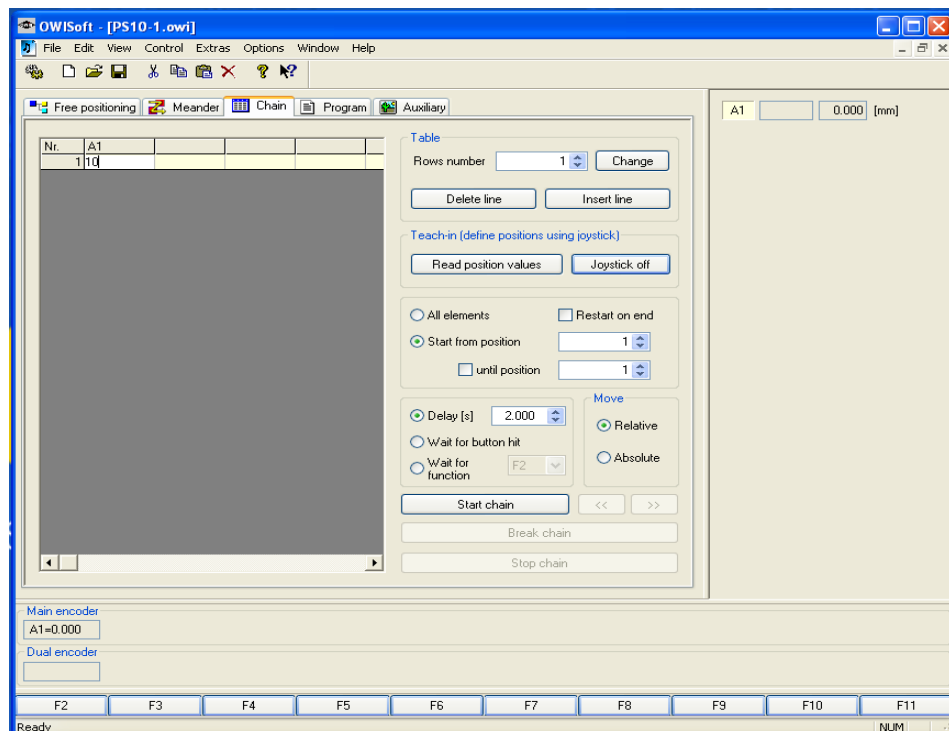


Figure 5.7: Motion controller lab software screen.

The sequence of setting up the 3D compact Laser Scanner is illustrated as a flow chart Figure 5.8. The position of the desiccation plate under the scanner is important to achieve a better scanning resolution zone. The travel distance of the laser line for scan depends on the size of the desiccation plate, the laser line length and finally on the motion controller. For the tests performed here the travel distance was selected based on the diameter of the desiccation plate. The next step was to calculate the buffered profile which can be calculated from travel distance. Finally the sample was ready for scanning and the scan continued until the test finished.

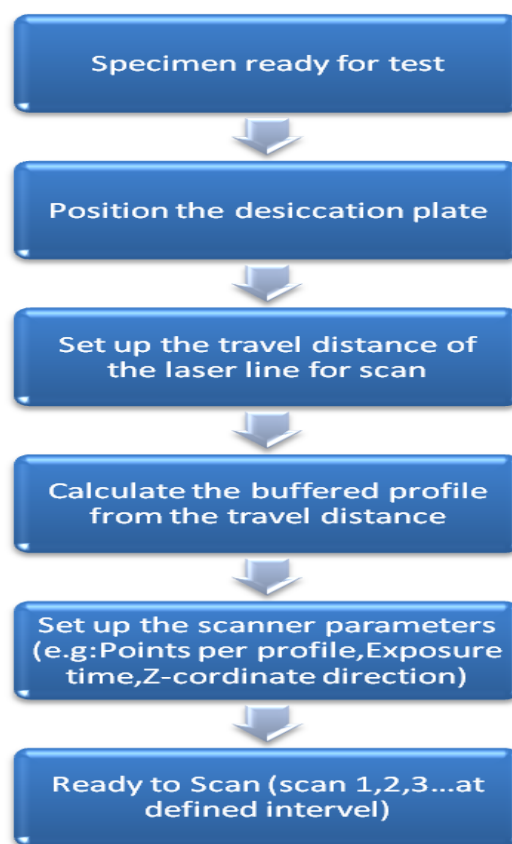


Figure 5.8: Set up flow chart of laser scanner desiccation test.

5.6.2 Data acquisition system for scanCONTROL 2700 and

Software operation

The laser was attached with the motion control unit for scanning on the move. The laser was operated to move at a speed of 3.88×10^{-3} m/s which allowed taking linear measurements at 38 μm increments. Moreover, with a standard laser line width of 100 mm, it produced a 312.5 μm point-to point distance in the axial direction. The sample was scanned at time intervals depending on the crack appearance in the sample. The whole experimental set up remained untouched until the end of the test, allowing for the accurate recording of experimental data during the test without perturbation of the sample position and condition. The exported 3D data of the surface profile from laser scanner is reconstructed and analysed using *Surfer*. Laser scanner surface 3D data represents point clouds distributed in a non-uniformly spaced grid. In *Surfer*, the first step was to create a uniform spaced grid from these non-uniformly spaced vectors (X,Y,Z). For the purpose of this study, and in order to achieve high precision measurements, our data sets were additionally densified in both the x and y directions during gridding. This is a standard feature of *Surfer* which facilitates the creation of a very fine grid. Equidistant spacing of 40 μm in x and y axis was used. The surface was then interpolated at the points specified by uniform spaced grid using natural neighbour linear interpolation method. It calculates the weighted average of neighbouring observations using weights determined by Voronoi polygon concepts (Okabe et al., 2008). Nearest neighbour algorithm was useful for converting regularly spaced XYZ dense datasets to *Surfer* grid files. A module in *Surfer* software allows the calculation the volume below the interpolated surface. Volume change during two different times was then calculated as the difference between the corresponding volumes. Any other program able to process a file containing the digital information of the sample (X,Y,Z) can be used instead of *Surfer* (e.g. Matlab) for this type of analysis.

5.7 CALIBRATION OF THE LASER SCANNER

For calibration purpose two rectangular aluminium brick with deep square groove at the top surface of them were manufactured by the mechanical laboratory of Strathclyde University. The rectangular aluminium brick is referred as a dummy brick in the discussion that follows. The grooves were precisely machine-made with a difference in width no more than 100 μm . The volumes for dummy bricks were known from the manufacturing process and verified by vernier calliper measurements. Figure 5.9 shows the schematic of the dummy sample.

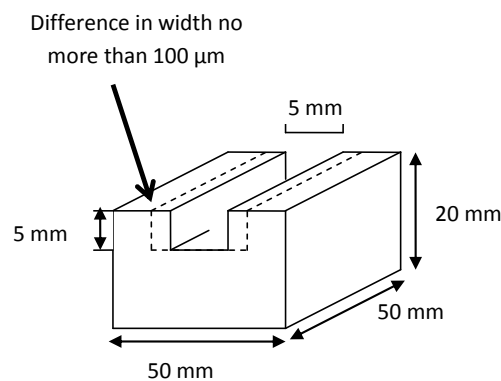


Figure 5.9: Schematic of dummy sample.

The aim was to scan both of the dummy bricks and determine the volume changes in between them from scanner result. A Perspex plate was also made in order to ensure to have the same scanning positioning. After the first scan the 2nd brick is placed in the same position and get another scan. Figure 5.10 and Figure 5.11 shows the aluminium dummy sample and the Perspex positioning plate.



Figure 5.10: Aluminium Dummy sample.

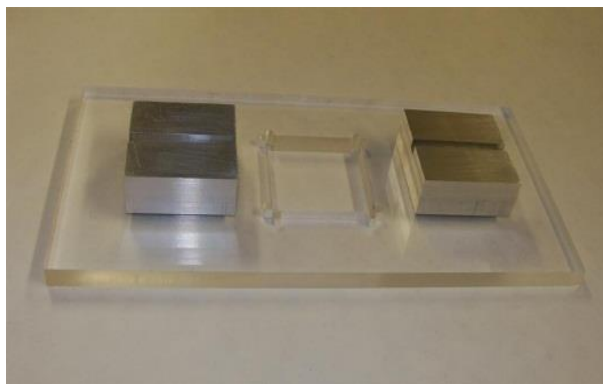


Figure 5.11: Aluminium dummy sample with positioning place.

Unfortunately, the scanner result was not acceptable for the dummy brick as there was some noise present, especially at the sharp edges, because of reflections from the shining surface and the inability of the laser line to reach the sharp and steep edge of the dummy. There was also some reflection from the transparent Perspex plate. The parameters for exposure time and the filter settings were adopted to avoid the noise, but it was found that the error was in all measuring direction (X, Y, Z axis). Figure 5.12 shows a dummy sample in lab software screen with noise all around the dummy after a scan. Figure 5.13 is the reconstructed view of the scan illustrating that these problems could not be overcome.

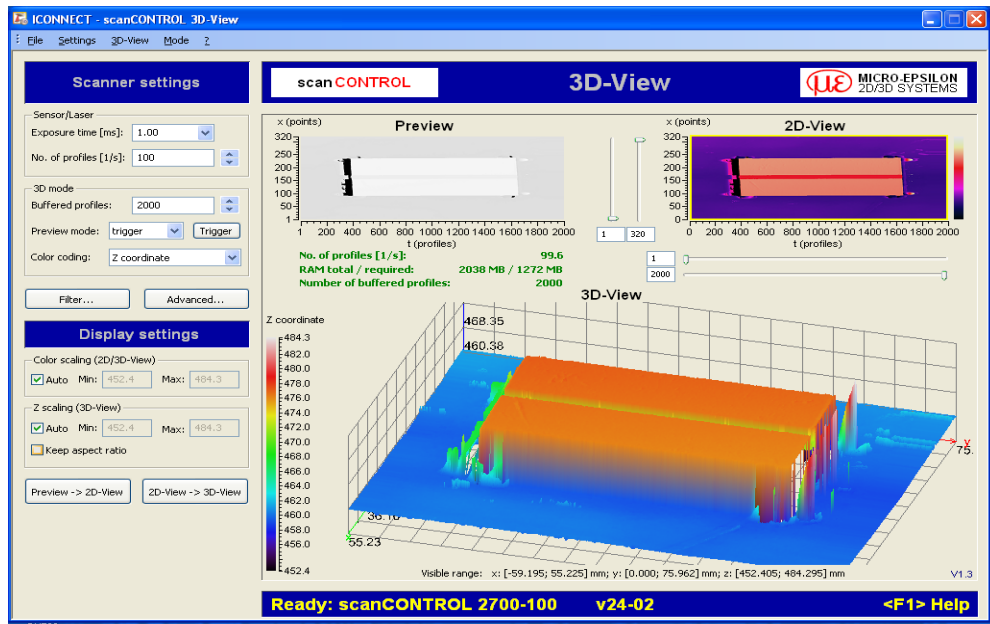


Figure 5.12: 3D image of scanned dummy sample with lots of noise.

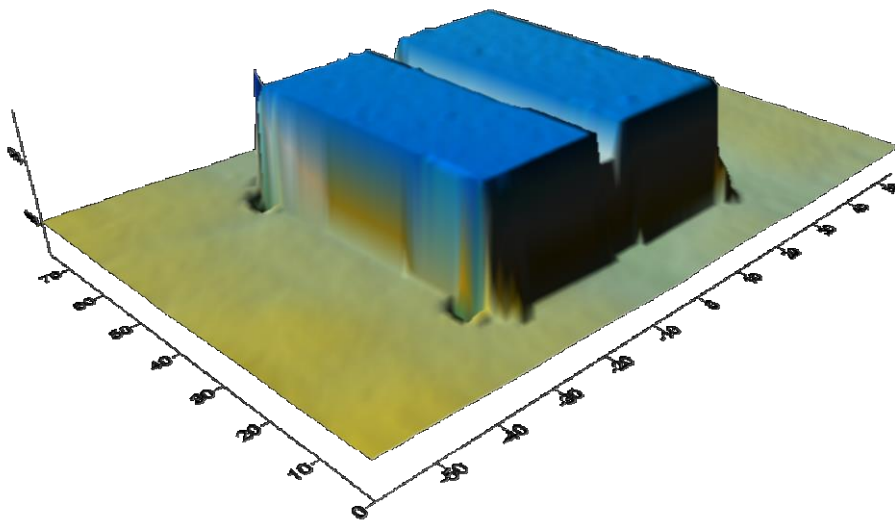


Figure 5.13: Surfer view of the dummy with measuring error at all direction.

To see the scanning accuracy in more detail, the groove width of the dummy was measured with laser scanner which was supposed to be 5 mm. But as it was found, the scanner results showed the groove width not to be uniform. This was probably because of the discontinuity and shining of the surface. Figure 5.14, the left figure

represents a zoom version of the scanning of the groove of the dummy sample and the discontinuity of the line proves the inaccuracy of the scanning results.

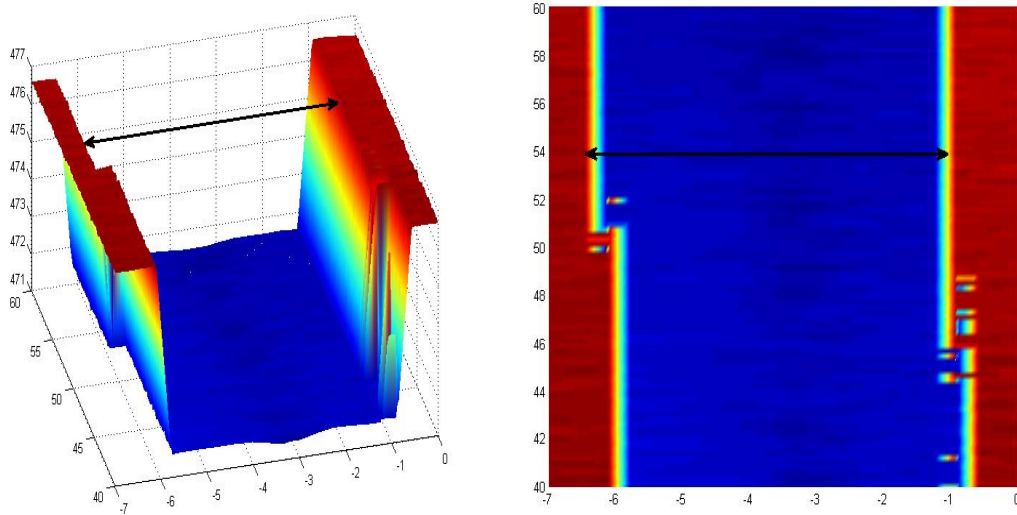


Figure 5.14: *Left*: Scanned output of groove of the dummy sample; *Right*: Zoomed version.

Measurement errors can also result from laser scanner and analysis software/method. We need to consider the laser scanner resolution as well. For the 3D measurement, there are three aspects of resolutions; Z-axis resolution, X-axis resolution, Y-axis resolution. Measurement error source can be divided into following two categories: laser scanner setup error and computational error. These error sources effects in every way and the output differs from the actual input surface.

5.7.1 Calibration of laser scanner for volume change estimation with an alternative method

Considering all the problems associated with the aluminium dummy bricks it was then thought to take an object with no shining surface for the calibration and yet with specific dimension that could help measuring desiccation cracking features as well. To check the accuracy of the laser scanner for volume measurement and other measuring features, we took a children's lego-type brick (Figure 5.15).

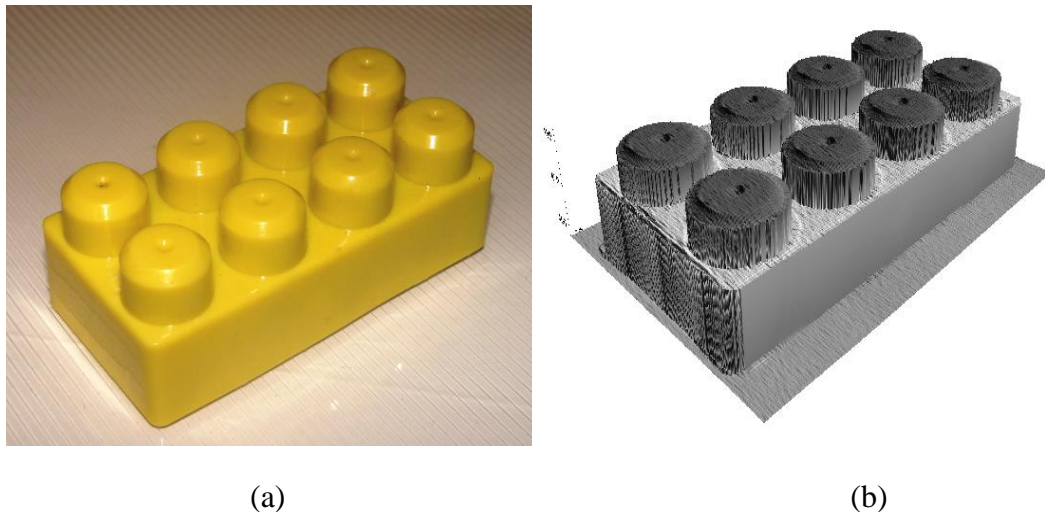


Figure 5.15: (a) Image of the children's lego-type brick used for the volume calibration, (b) 3D image of the lego-type brick from surfer using scan data.

The volume of the Lego brick was measured with the water displacement method (Head, 1992, BS1377-2:1990, 1990) and vernier calliper (measurement to 0.01 mm) to compare to the laser scanning data. This was a challenging thing to do as it was just a toy but it has the real advantage of capturing the irregular crack valleys of desiccated soil specimen. One other advantage of the brick is that the sides are steep.

Although not recommended by the laser manufacturer, the steep sides reflect the real data, since the real crack sides are also steep.

Due to the complex and irregular shape of the lego piece the volume measurement was performed by *water displacement method*. The volume was found 36600 mm^3 . The vernier calliper measurement was not accepted. The Lego piece had curves with shape too complex to be measured accurately by callipers. The measurement from the water displacement method agreed well with the volume calculated from the 3D reconstruction. Also, the reproduction of the dimples on top of each knob was found precise. Figure 5.16 shows the 2D visualisation of the scanner data.

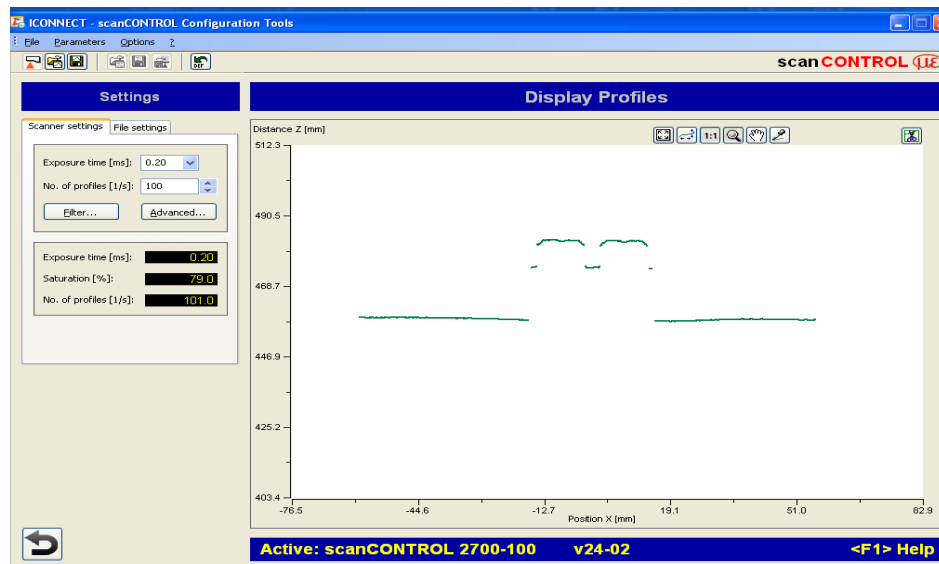


Figure 5.16: 2D visualisation of the Lego in scanCONTROL software screen.

The actual height of the lego-type brick was with Vernier calliper measurement 25.42 mm. Each measurement was taken eight times and the average was taken. The height of the lego measured from 2D scan data was found 24.697 mm (Figure 5.15). Thus, height was found 0.723 mm less than the actual height. Therefore, volumetric resolution was calculated as $72.3 \text{ mm}^3/\text{cm}^2$. The volume ($V_{\text{lego-surfer}}$) measurement by surfer using 3D scanner data was found 36917.24 mm^3 . Whereas the volume measured by water displacement method ($V_{\text{lego-actual}}$) was as 36600 mm^3 which is 317.24 mm^3 less. So the percentage (%) error can be calculated as 0.87%. Therefore,

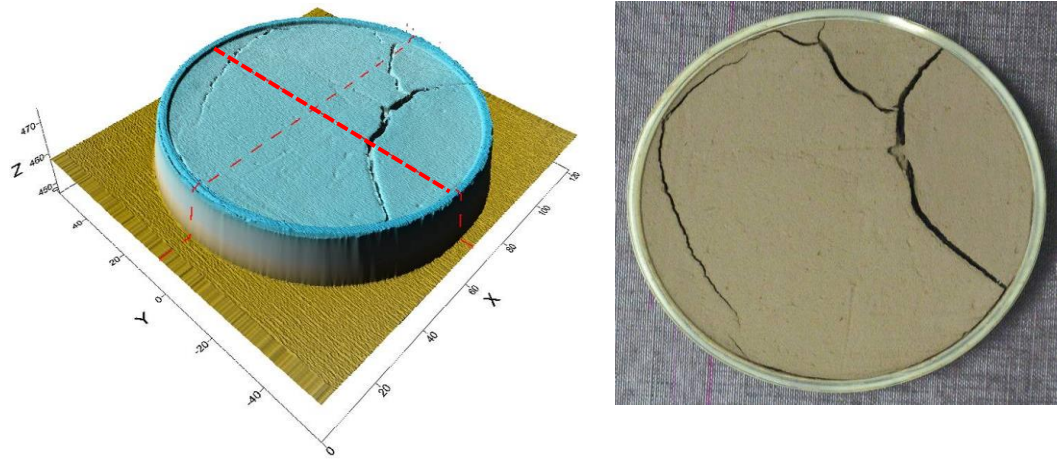
for the scan area of 27.0345 cm^2 , the volumetric accuracy per unit area was found $1.17 \times 10^{-2} \text{ cm}^3/\text{cm}^2$.

The width was also checked from above scan data which was 31.985 mm. The actual width was 31.05 mm which was an average of eight measurements taken by vernier calliper. The height was underestimated by 0.723 mm, for the range of 450 mm, but the width was overestimated, probably because of the edge discontinuity. This is why we found volume measurement overestimated.

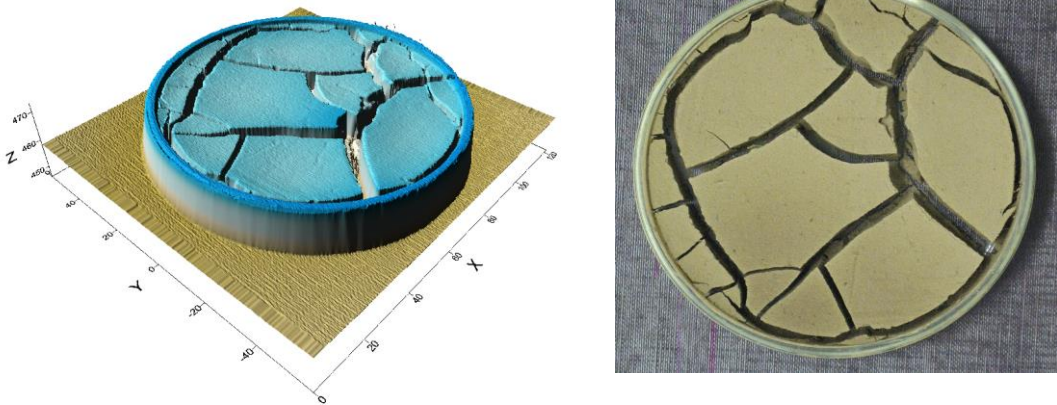
5.8 RESULTS AND DISCUSSION

5.8.1 Digital model

Figure 5.17 presents the 3D digital image of the sample at two different times: (a) 6 hours and (b) 23 hours. The corresponding digital images are presented alongside. The capability of the proposed device to capture the actual pattern observed in the tests is apparent from the Figures; only a few small fissures are not perfectly reproduced by the model.



(a)

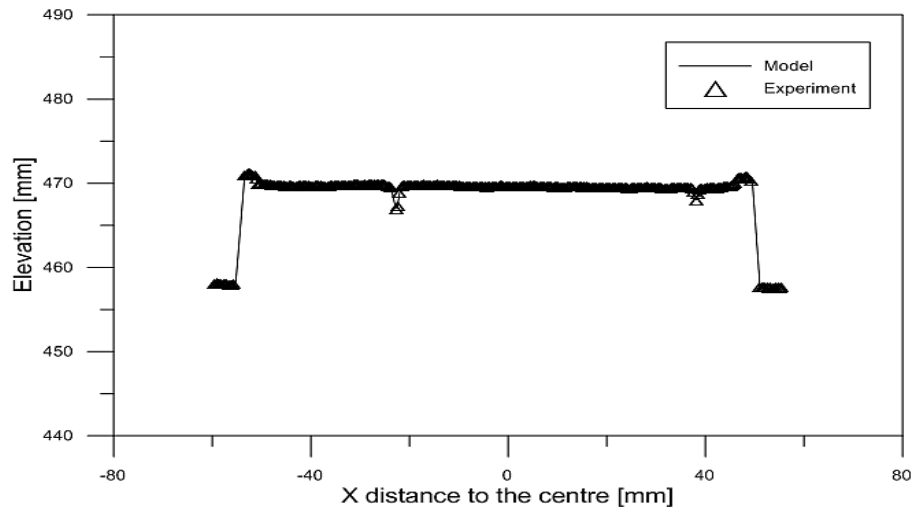


(b)

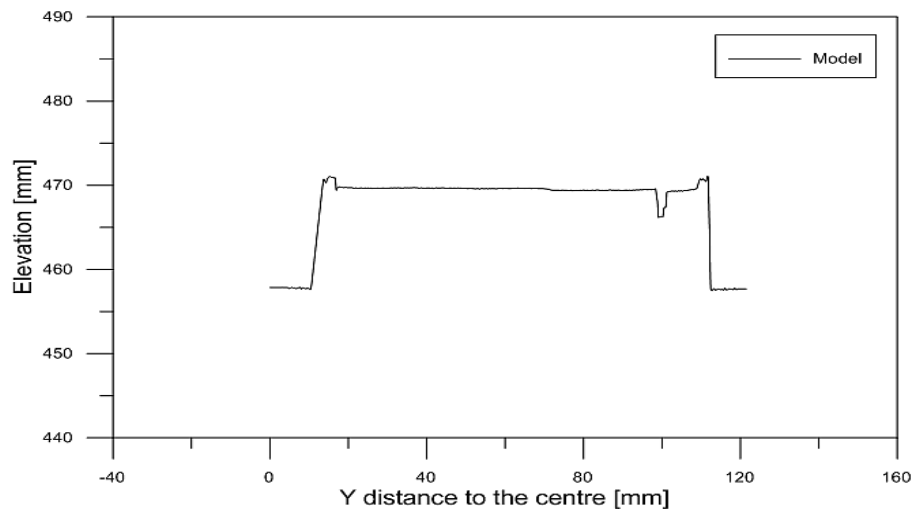
Figure 5.17: 3D images of the soil sample at two different time of drying, generated by Surfer after scanning (left) and digital images taken by camera (right) : (a) 6 hours and (b) 23 hours of drying.

Once the digital image/model of the soil is generated, it can be used to explore other features/properties of drying soils which are difficult to study using other available techniques; for example, the depth of the cracks and their morphology below the soil surface are observed in this digital model. Figure 5.18 presents the vertical profiles associated with the two cross sections indicated in Figure 5.17 (i.e. the two dashed lines, parallel to 'X' and 'Y' axes). Symbols in Figure 5.18 correspond to the actual points scanned with the laser in the Y-direction (i.e. along the laser line). In the same figure, the digital model obtained with *Surfer* is represented by a continuous line. As

expected, the digital model closely fits the scanned points. Figure 5.18b presents the profile of a vertical in the X-direction obtained with the digital model.



(a)



(b)

Figure 5.18: Evolution of typical cross section during drying showing the section profiles at different times (a) Cross-sectional profile along Y axis (model and experiment after 6h of drying), (b) Cross-sectional profile along X axis (model after 6h of drying).

5.8.2 Cracking mechanism observed from scanner result

Figure 5.19 presents the time evolution of the vertical profile in the Y-direction. This kind of information is very useful in learning about the dynamic of crack propagation with depth, which is not possible to obtain with other available experimental techniques. It can be observed that at the beginning, the shrinkage is associated with settlement only (Figure 5.19 from initial to 2hrs). The first crack appears around 4 hours after drying and starts to widen at the tip followed by vertical propagation with sharp local drying front (Figure 5.19 at 6hrs). This process continues until 16 to 18 hours with a settled surface cracking pattern. Vertical crack propagation and widening continued until approximately 24 hours of drying. At 24 hours, the initial cracks seemed to have reached the maximum depth first. The total test duration was 60 hours. From 18 hours to 60 hours, the average spacing of these cracks did not vary much. The extent of cracking vertically seems to depend of the thickness of the plate/soil layer. Similar observations were made by Shorlin et al. (2000).

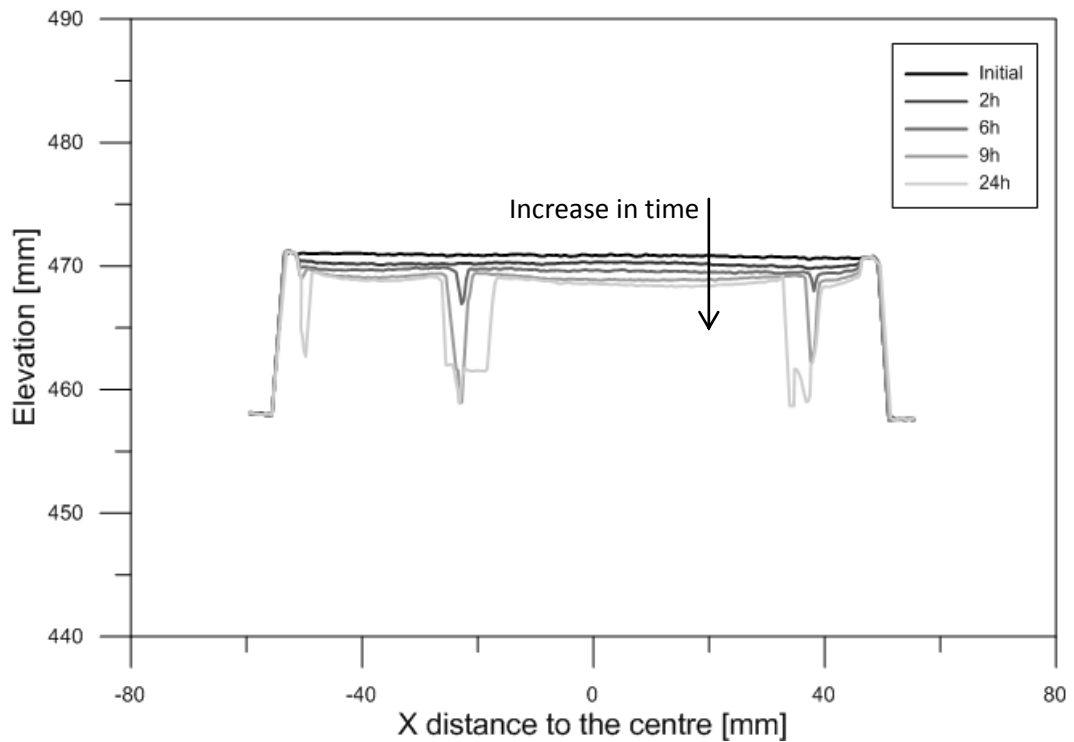


Figure 5.19: Evolution of the central cross-section along Y axis during drying, showing the section profiles at different times.

5.8.3 Estimation of volume change of the drying soil specimen

Following the procedure explained in Section 5.6.2, the information from the digital images at different times can be used to calculate the volume change of the sample. This is one of the main advantages of this device and methodology. The advantage of knowing volume change is that volume change during shrinkage can be associated with vertical deformation at the surface, lateral shrinkage, and cracking. It allows for the calculation of the variations in the void ratio/porosity that takes place during shrinkage. Changes in porosity of intact soil can be used to estimate the changes in its permeability. The changes in crack geometry can also be tracked and then used to develop models accounting for the effect of cracks on flow and evaporation. Future

work can use this method to study the volume changes associated with each stage of the desiccation and cracking processes in high resolution.

Figure 5.20(a) presents the evolution of volume change in time. After 24 hours of drying, the volume remained nearly constant. The proposed device allows recording the water loss during desiccation; from which the water content can be calculated. Figure 5.20(b) presents the corresponding results.

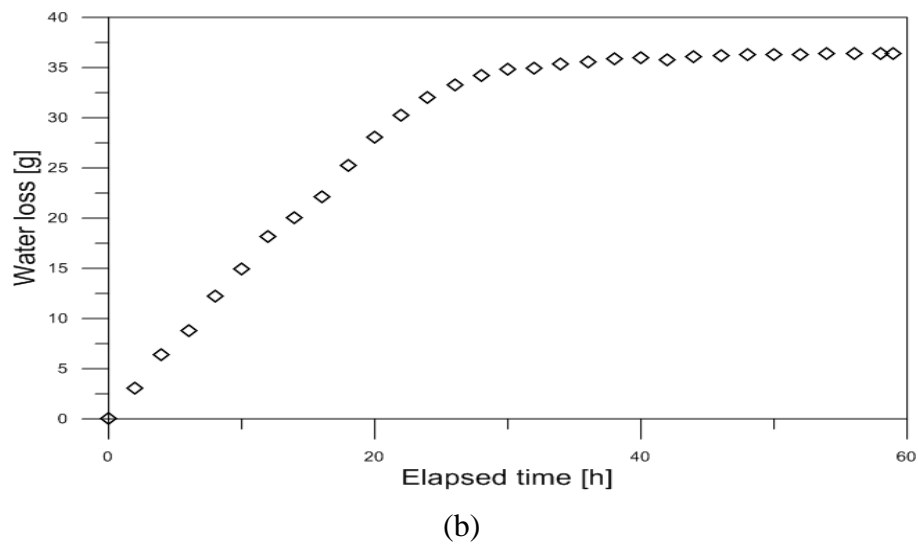
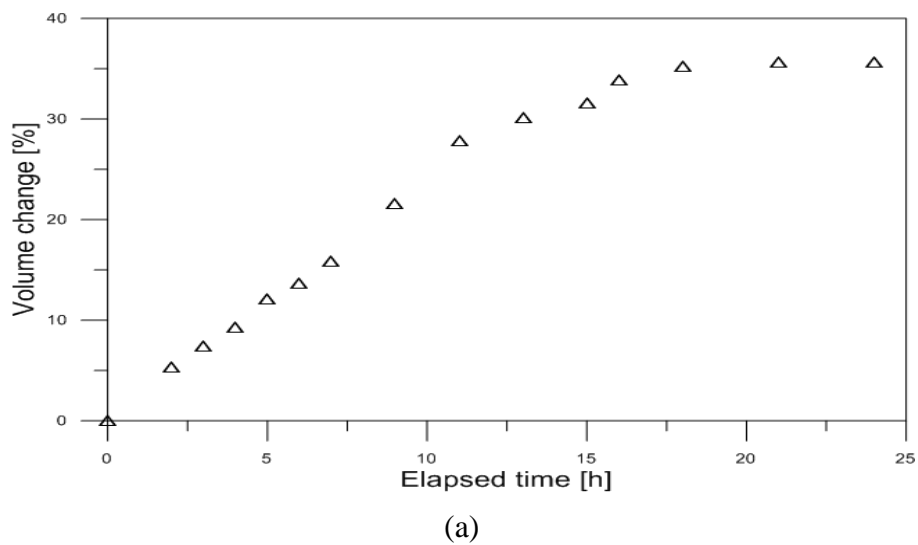


Figure 5.20: Time evolution of (a) volume change, (b) water content.

5.8.4 Evolution of the drying desiccated soil specimen

Detailed information about the shrinkage evolution and how settlements and cracks are distributed in the soil sample during drying can easily be obtained from the digital model of the soil. Figure 5.21 presents the contour levels at different times, from which it is possible to study how settlements and cracks evolve during drying. A contour plot has been used to describe the vertical deformation of the drying and cracked soil. Contours are one of several common methods used to denote elevation or altitude and depth on maps. Generally, a contour line for a function of two variables is a curve connecting points where the function has the same particular value. A contour line joins points of equal elevation (height) above a given level. From these contours, a sense of the general terrain can be determined.

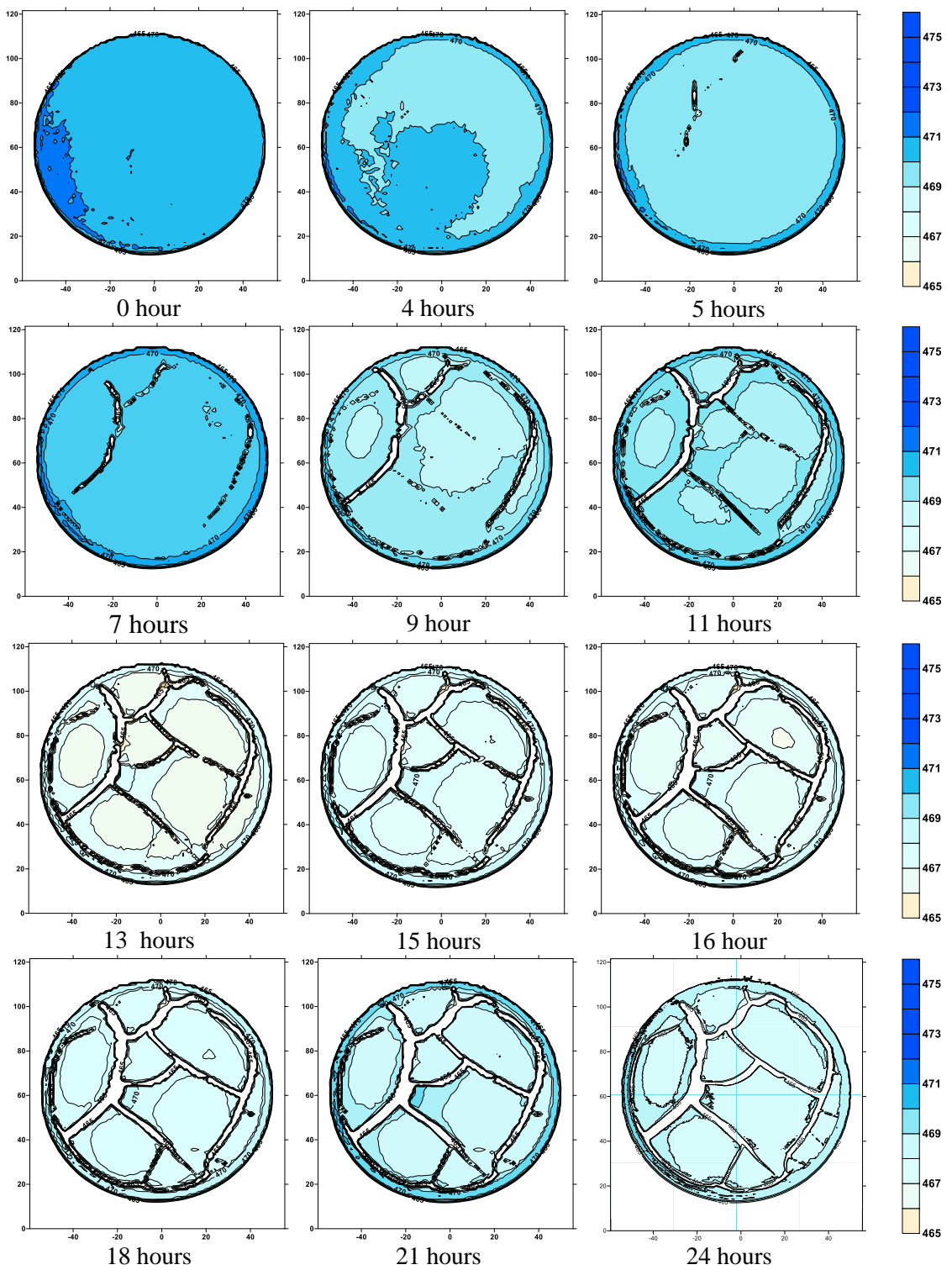


Figure 5.21: Contour levels at different times.

The evolution of the volume change was thought to be important during the first stage of the test until the crack initiates to describe at what stage of the specimen the cracking starts. The crack initiated just after 4 hours of the test. The water content at that point was 48% and the volume of the specimen was calculated to be 86 cm³.

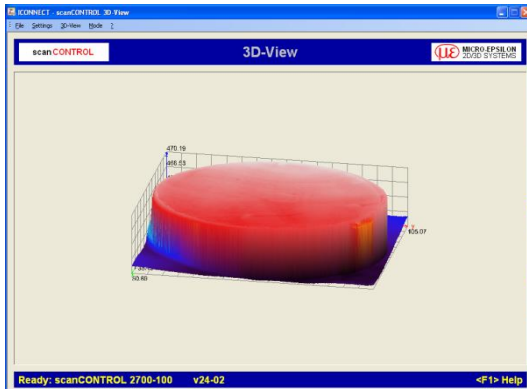
From hour 4 to hour 16, the soil continued to generate new crack and propagated until connected to another new or previously formed crack. After 16 hour the cracking pattern for the specimen was clear and settled. Assuming the crack network was completed, further scans were performed every 2-3 hours until the test finished. The total test duration was 60 hour. From 18 hour to 60 hour, the volume did not change significantly. No new cracks formed. The previously-formed crack increased in size as a result water loss from the specimen from the additional surfaces exposed to ambient air.

5.8.5 Analysis of crack network propagation from 3D scanner

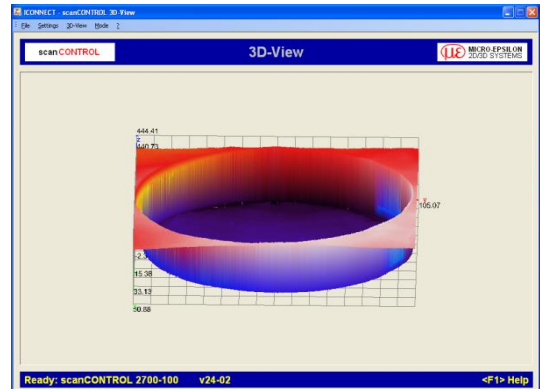
In order to analyse crack morphology, four sets of images were taken from test, which included image directly from the 3D scanner and image captured by the camera at the same time. These images were carefully studied to explain crack network.

Each scan was performed with two scan configuration; Z-inverted and Z-not inverted. Figure 5.22 shows two set of the scanned specimen performed at both inverted in Z-direction and not inverted in Z-direction to examine visually the propagation of cracks on the surface and in the vertical direction over time. As camera capture 2D image, the surface analysis is possible from the image only. Any information regarding vertical deformation has to be ignored here.

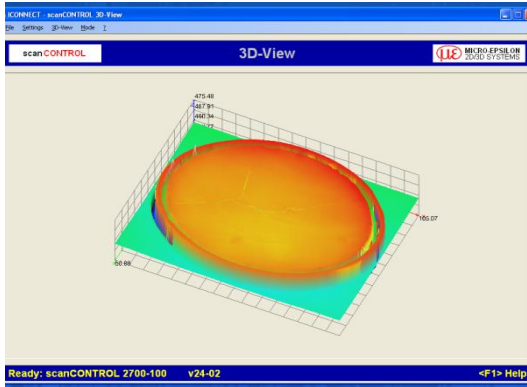
The scan image Figures 5.22 a1, 5.22 b1, 5.22 c1 and 5.22 d1 show the nature and evolution of crack propagation at the upper surface of the specimen. Figures 5.22 a2, 5.22 b2, 5.22 c2 and 5.22 d2, on the other hand, show the crack propagation information towards the bottom of the desiccation plate. The visual observation from the scanner image shows the crack which initiates at first also approaches first towards the bottom of the plate. Interestingly this propagation was not linear throughout the crack as can be seen in Figures 5.22 b2 and 5.22 c2. Eventually in time, the cracks propagated toward the bottom of the plate (Figure 5.22 d2).



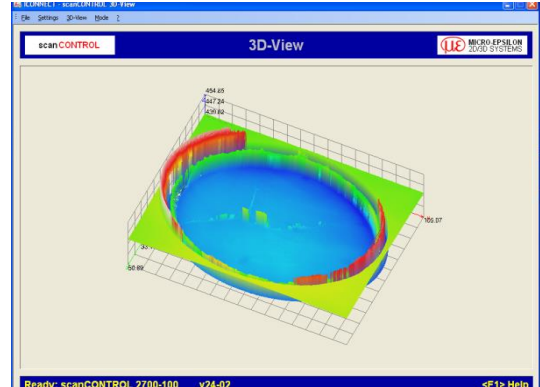
(a1) 0 hour



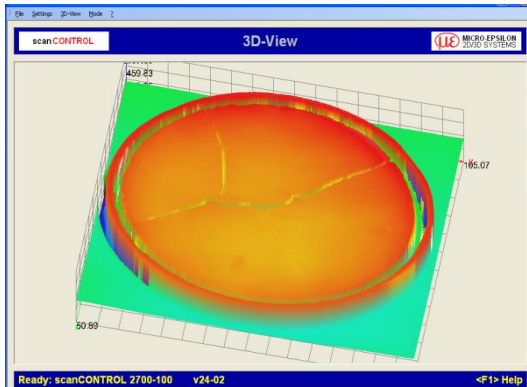
(a2) 0 hour



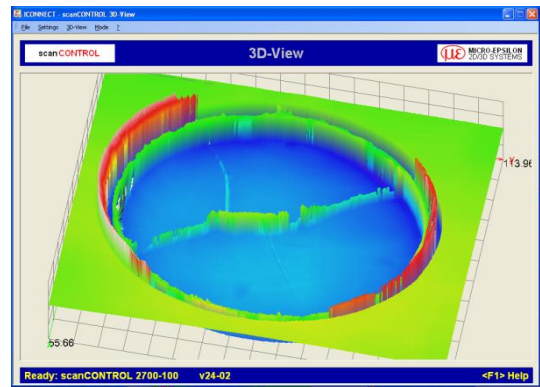
(b1) 21st hour



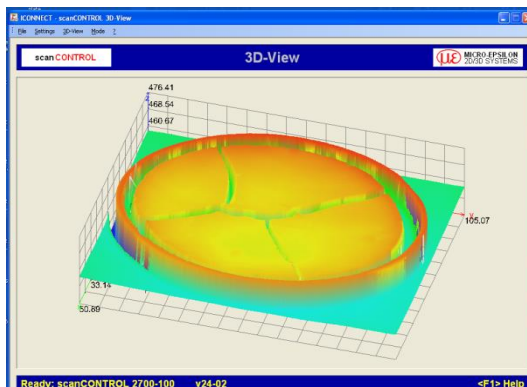
(b2) 21st hour



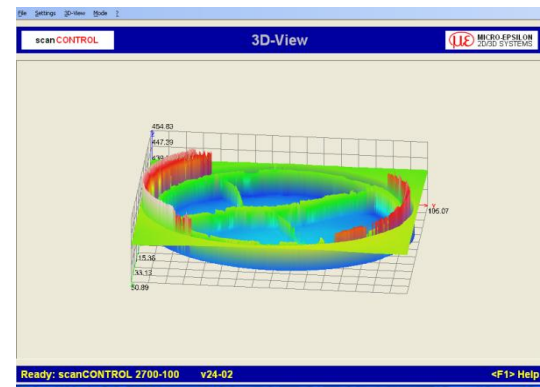
(c1) 26th hour



(c2) 26th hour



(d1) 50th hour



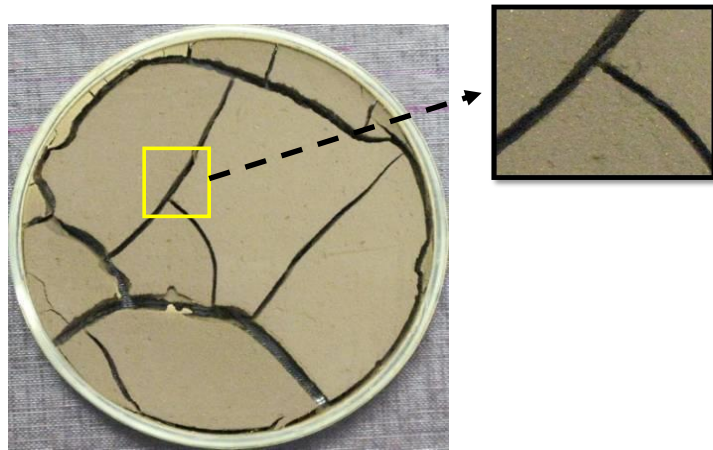
(d2) 50th hour

Figure 5.22: Crack propagation over time; *Left* Z-inverted, *Right* non-inverted.

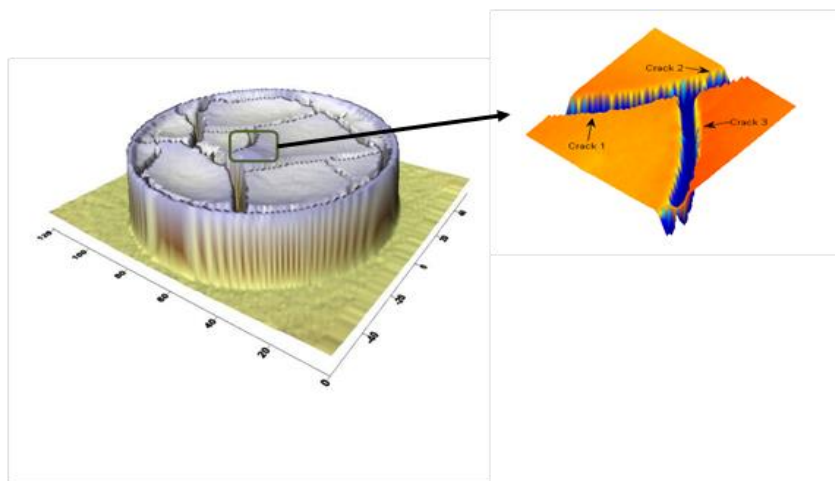
The image sequences of the test captured by the camera gave valuable additional information such as the time of each crack initiation and the propagation of the crack towards the adjacent crack to complete the final cracking pattern within the sample. This data allowed for a full reconstruction of crack formation over time.

5.8.6 Cracking parameter: 3D scanner vs. image analysis

The formation and propagation of cracks were explored in detail from the data provided by the 2D/3D laser scanner in experiment LLT02. For simplicity of analysis, a square vertical segment from the centre of the plate was cropped to perform the analysis (Figures 5.23a-5.23b). The cracks in this section of the experiment are shown in Figure 5.24a-5.24b. The length, crack width and crack area were determined for the three major cracks (1, 2, and 3) in this analysis area. The results for the parameter are shown in Table 5.3-5.5.



(a)



(b)

Figure 5.23: (a) Region of interest which has been analysed for crack information by image analysis technique; (b) Region of interest which has been analysed for crack information by laser scanning technique.

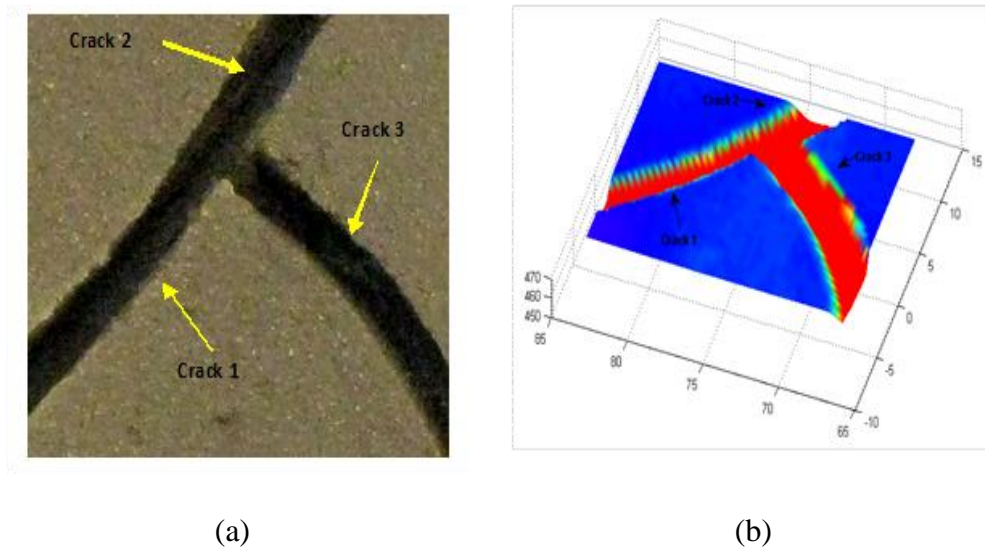


Figure 5.24: Crack identification for the comparison analysis.

The data found from both analyses are comparable. The intensity distribution in the image analysis of the surface gives noise about the crack. In order to extract the cracking parameters, various morphological operations (erosion, dilation, opening, removing, etc.) needed to be performed. The process is time consuming and manual operation of removal unwanted noise leads to inaccurate results. Laser scanner completes scanning within very short time and the achieved intensity information for the surface is more precise than 2D camera image. The operation to calculate cracking information is processed by programme software which makes the whole process much faster than compared to the image analysis.

Table 5.3a: Crack network analysis by Image analysis from LDT02.

	Crack no.	Width (mm)	Length (mm)	Avg width (mm)	Total length (mm)	Total crack area (mm²)
Stage 1	1	0.706	50.28	0.687	86.05	177.35
	2	0.395	26.16			
	3	0.960	9.61			
	4	-	-			
Stage 2	1	1.469	51.98	1.127	114.65	129.15
	2	1.003	28.20			
	3	1.638	9.61			
	4	0.396	24.86			
Stage 3	1	3.616	52.15	3.192	113.45	362.16
	2	2.881	28.31			
	3	4.294	10.11			
	4	1.978	22.88			

Table 5.3b: Crack network analysis by Laser scanner 3D image from test LDT02.

	Crack No.	Width (mm)	Length (mm)	Avg width (mm)	Total length (mm)	Total crack area (mm²)
Stage 1	1	1.989	50.26	1.94	84.57	164.43
	2	1.375	25.42			
	3	2.487	8.89			
	4	-	-			
Stage 2	1	2.792	51.54	2.014	105.87	213.22
	2	1.997	26.43			
	3	2.327	5.98			
	4	0.940	21.92			
Stage 3	1	5.120	49.72	3.733	102.98	384.42
	2	3.055	25.10			
	3	5.110	7.90			
	4	1.650	20.26			

Table 5.4a: Crack network analysis by Image analysis from LDT03.





			Width (mm)	Length (mm)	Avg width (mm)	Total length (mm)	Total crack area (mm²)
	9 Hr.	Crack 1	1.42	11.36			
		Crack 2	1.69	5.50	1.36	28.20	38.35
		Crack 3	0.95	13.53			
	13 Hr.	Crack 1	2.2	11.36			
		Crack 2	2.26	5.41	2.32	30.47	70.71
		Crack 3	2.50	12.36			
	18 Hr.	Crack 1	2.21	12			
		Crack 2	2.89	5.19	2.71	29.13	78.94
		Crack 3	3.02	11.01			
	22 Hr.	Crack 1	2.44	12.27			
		Crack 2	3.07	5.1	3.01	30.39	91.47
		Crack 3	3.52	10.92			

Table 5.4b: Crack network analysis by Laser scanner 3D image from LDT03.

		Width (mm)	Length (mm)	Avg width (mm)	Total length (mm)	Total crack area (mm²)
Stage 8	Crack 1	1.38	12.21			
	Crack 2	1.73	4.32	1.34	31.69	42.47
	Crack 3	0.92	15.16			
Stage 10	Crack 1	2.18	12.18			
	Crack 2	2.41	4.69	2.42	32.01	77.47
	Crack 3	2.68	15.14			
Stage 13	Crack 1	2.23	12.98			
	Crack 2	2.49	4.85	2.62	32.99	86.44
	Crack 3	3.15	15.16			
Stage 15	Crack 1	2.33	13.16			
	Crack 2	2.94	4.75	3.01	33.87	101.94
	Crack 3	3.78	15.96			

Table 5.5: Comparison table: image analysis vs laser scanner results.

	Scan_15 at 22 Hr.						
	Width			Length			Area
	Crack 1	Crack 2	Crack 3	Crack 1	Crack 2	Crack 3	Total
2D image	2.44	3.07	3.52	12.27	5.1	10.92	91.47
3D data	2.33	2.94	3.78	13.16	4.75	15.96	101.94
	Scan_13 at 18 Hr.						
	Width			Length			Area
	Crack 1	Crack 2	Crack 3	Crack 1	Crack 2	Crack 3	Total
2D image	2.21	2.89	3.02	12	5.19	11.01	78.94
3D data	2.23	2.49	3.15	12.98	4.85	15.16	86.44
	Scan_10 at 13 Hr.						
	Width			Length			Area
	Crack 1	Crack 2	Crack 3	Crack 1	Crack 2	Crack 3	Total
2D image	2.2	2.41	2.68	11.36	5.41	12.36	70.71
3D data	2.18	2.41	2.68	12.18	4.69	15.14	77.47
	Scan_8 at 8 Hr.						
	Width			Length			Area
	Crack 1	Crack 2	Crack 3	Crack 1	Crack 2	Crack 3	Total
2D image	1.42	1.69	0.95	11.36	5.5	13.53	38.35
3D data	1.38	1.73	0.92	12.21	4.32	15.16	42.47

5.8.7 Measuring volumetric shrinkage form laser scanner

data

Based on the success of measuring volume change, volumetric shrinkage of Bengawan Solo soil was determined by this method as well. To check the accuracy the volumetric shrinkage curve was then compared with the volumetric shrinkage curve achieved by using conventional calliper method. A glass circular desiccation plate of 12 mm of height and having 48 mm of diameter was taken. The specimen was prepared at 54% water content close to the liquid limit of the soil and let dry in the laboratory environment (LTD01). In order to achieve a good evolution of the volume change, the specimen was scanned at 2-3 hrs. intervals until there was not

any more change in the volume of the specimen. Figure 5.25 shows the volumetric shrinkage curve measured by two different methods. The volumetric shrinkage measured by vernier calliper was found 17.35% and volumetric shrinkage measured by 3D laser scanner was found 18.43%.

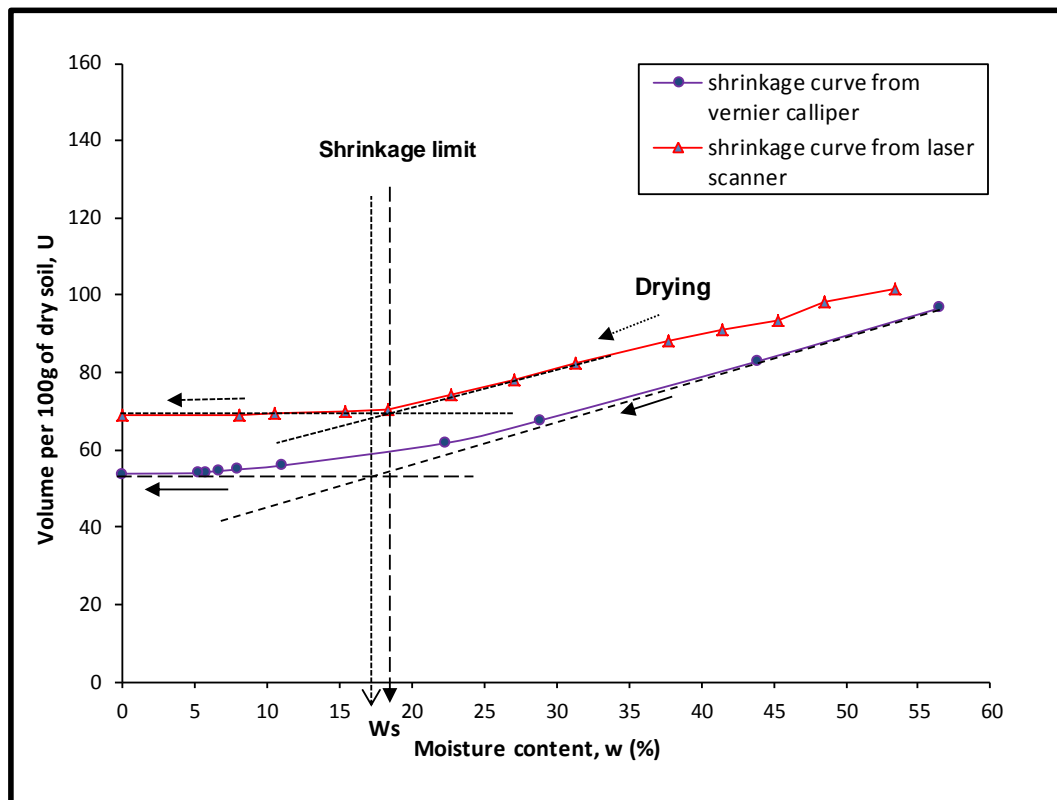


Figure 5.25: Volumetric shrinkage curve for Bengawan Solo Soil found using two methods, from laser scanner measurements and vernier calliper measurements.

5.9 CONCLUSION

A new device to experimentally study the behavior of drying soils based on precision 2D/3D laser scanning is presented in this chapter. Valuable information was obtained from the digital model of the soil, including volume change, distribution of settlements on the soil surface, crack aperture and morphology in depth. Scans at different times allow learning about the volume changes at the onset of crack formation and how the phenomena of crack propagation evolve in time at the soil surface and depth. The experimental outcomes show that the laser scanning technique achieves significantly more information than those typically gathered from current methods. Because this method allowed for the accurate measurement of volume change without disturbing specimen condition at any point of the test, volumetric shrinkage of Bengawan Solo soil was captured with precision. The result was also compared with previously measured volumetric shrinkage curve as a comparison and believed to be very good alternative procedure of measuring volumetric shrinkage of soil specimens. This technique can be applied to a wide range of soils and can be useful in other fields of engineering where precise volume change measurements are important.

Chapter 6: Tensile strength and micromechanical state

6.1 INTRODUCTION

Tensile strength is a useful and sensitive indicator of soil condition and plays significant role in various engineering application (Kodikara et al., 2000b, Dexter and Kroesbergen, 1985). Many failures of earthen structures are related to tensile characteristics of soil and attempts to explain the mechanism of tensile failure has been taken into account by several researchers over the years.

In this chapter, the tensile strength of soil is measured at different drying conditions. The soil tested, namely Bengawan Solo soil, is taken from a flood defence embankment along the Bengawan Solo River in Indonesia. Tensile strength was determined using direct tensile strength equipment (direct method) on both reconstituted and compacted specimens. Four different initial conditions starting from saturated towards drying condition were chosen from the compaction curve and have been presented herein. The tests permit measurement of tensile strength at crack

initiation of the specimen. Modern micro structural testing techniques of mercury intrusion porosimetry (MIP) and environmental scanning electron microscopy (ESEM) were carried out to explore the microstructural changes along different hydro-mechanical paths for same specimens at their initial conditions.

Many geotechnical problems arise from volume and moisture changes due to capillarity; for example shrinkage and swelling of expansive clays. This Chapter describes the influence of soil structure/condition on the tensile strength of reconstituted and compacted soil. An attempt has been taken to point out fundamental mechanisms involved during soil drying process and significant comparison of evolution of soil behaviour at reconstituted and compacted condition while drying.

6.2 BACKGROUND

Although tensile strength is an important indicator in expression of material strength, in case of soil tensile strength also depends on various other properties of soil (e.g., moisture content, density etc.). In most case of engineering practice tensile strength of soil is assumed to be negligible. A limit with zero suction and zero tensile strength is the conservative estimation of strength. In contrast there are so many problems associated with soil arises, as the soil starts to dry (i.e. becomes de-saturated or partially saturated). Desiccation cracking is a classic example in this case. It is believed that in drying soil tensile crack initiates, when the tensile stresses exceeds the soil tensile strength. Most importantly, soil cracking is one of the major causes of the progressive failure of earth slopes, erosion and other premature failures of earth structures because cracked zones are weaker and more permeable (Jamei et al., 2008) than intact soil. Compacted soil layers in dams and clayey liners in waste disposal facilities can fail from cracking due to tensile failure (Morris et al., 1992b). The cracks also become preferential paths for leakage and organic gas migration in

clay liners used for waste isolation (Alonso et al., 2006). In construction, materials such as cement stabilized crushed rocks used in road pavement construction can undergo cracking due to tensile failure (Nahlawi et al., 2004). Tensile strength greatly affects soil bearing capacity (Lu and Likos, 2004), slope stability (Griffiths and Lu, 2005) and failure of road bases and retaining walls (Heath et al., 2004). Three modes of cracking are considered in fracture mechanics, which are, i) tension, ii) shear and iii) tearing (Vallejo and Liang, 1994). According to (Vallejo and Liang, 1994) unsaturated soil in slopes, desiccated soils and fissured soils in general can be subjected to tensile-shear state of stresses which produce crack propagation in modes 1 and 2.

In unsaturated soil mechanics, tensile strength of soil has been studied widely (Bishop and Garga, 1969, Snyder and Miller, 1985, Alonso et al., 1990, Delage and Graham, 1995, Tang and Graham, 2000, Tang et al., 2002). Desiccation occurs at unsaturated condition of soil. Applying unsaturated soil mechanics to desiccation cracking of clays in various geotechnical applications requires knowledge of tensile strength (Fang and Hirst, 1973, Morris et al., 1992b). The existing common experimental methods for measuring tensile strength can be categorised as direct methods (Peters and Leavell, 1987, Towner, 1987b, Leavell and Peters, 1987, Wallace, 1998, Hannant et al., 1999, Tang and Graham, 2000, Munkholm et al., 2002, Tamrakar et al., 2005, Lu et al., 2007) and indirect methods (Brazilian tensile test (Frydman, 1964), flexure beam test (Krishnayya et al., 1974a), hollow cylinder test (AL-Hussaini, 1981), and double punch test method (Fang, 1997b)). Various hypotheses that have been proposed so far remain unsatisfactory and unproven. All the direct tensile testing methods are well accepted and assume to produce consistent test results. The tensile strength of soil been analysed in literature also had variable initial conditions.

It was considered important to investigate the potential of tensile cracking occurrence within Bengawan Solo embankment as evidence of cracking being found during site investigation. The analysis of test results is helpful in understanding the behaviour of soils subjected to tensile strength conditions which may lead to formation and propagations of cracks at the site.

This chapter investigates tensile strength of Bengawan Solo soil at different drying condition together with micro-structural analysis of the soil in both reconstituted and compacted condition. This test campaign aims to significantly contribute to existing experimental and theoretical knowledge in the analysis of tensile strength of soil in relation to cracking.

6.3 OBJECTIVES AND EXPERIMENTAL CAMPAIGN

Continuous moisture changes during drying of soil cause phase changes within the soil structure and soil state (from slurry to plastic and from plastic to solid state). There are three stages of moisture content of soil: i) Dry stage ii) Partially saturated stage and iii) Saturated stage. The tensile strength varies with the moisture content of soil. The main aim of the tests performed in this Chapter was to determine how the evolution of water change within the soil influences/effects the tensile strength of soil.

Compacted soil is used for most engineering practices. The tests were performed on compacted soil as well as a reconstituted soil to provide information on evolution of tensile strength for two different soil structures. To compare the results, the specimens were prepared at same initial conditions. More specific objectives of the tests were:

- To measure tensile strength of soil at crack initiation by direct measurement method
- To compare the tensile strength for reconstituted and compacted soil at crack initiation

- To perform microstructural investigation of reconstituted and compacted soil as an influence on tensile strength of soil.

6.4 EXPERIMENTAL METHODOLOGY

6.4.1 Specimen preparation

In preparation for specimen for tensile test campaign a special mould was designed (see Figure 6.1). It was built at the Science Faculty Workshop of Strathclyde University. This mould will be referred here as the tensile mould. The tensile mould is rectangular in shape and matches the total length and width of direct tensile strength measurement equipment.

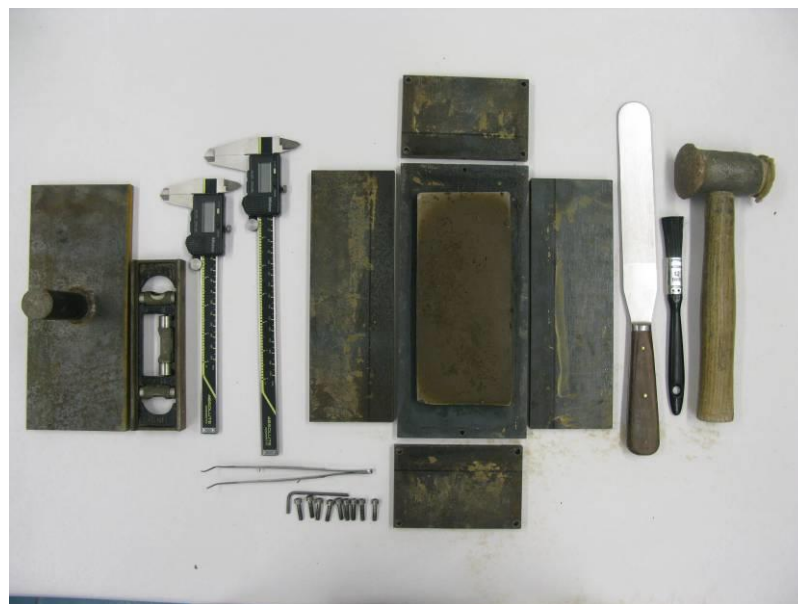


Figure 6.1: Photograph of the accessories used for tensile strength test specimen.

It consists of two parts. The first part is where the specimen is placed for air drying or compaction. The walls around the specimen are removable, and therefore it is easy to remove the specimen afterwards without disturbing the specimen. The second part of the mould was used for compacted specimen only (for compaction) and can be referred to as a tensile compaction tool (see Figure 6.1). The direct tensile test equipment is complex in shape and it was important to maintain the same initial condition for the specimen in order to meet the objectives of the test campaign. Compacted soil specimens at higher density could not be achieved by using the special mould, so the soil was Proctor compacted for such cases. For a reconstituted specimen, once the soil was prepared at its liquid limit, the specimen was then allowed to dry within the mould until the required density was achieved. For a compacted specimen, once the specimen was prepared at the desired water content, it was then compacted at the required dry density. After carefully removing the soil specimen from the mould, it was cut into the shape of the direct tensile test equipment mould for testing purposes.

One of the main difficulties was to cut the specimen according to the complex size of the tensile device. Many repetitions were made to adjust the specimen condition. At very wet conditions, it was hard to cut the specimen into shape and mould them into the device. Yet again, it was hard to compact very wet soil at the required dry density. Moreover, sometimes the compacted specimen was too dry and crumbly at low moisture content and just fell apart during cutting into shape. Figure 6.2 shows some examples of failures.

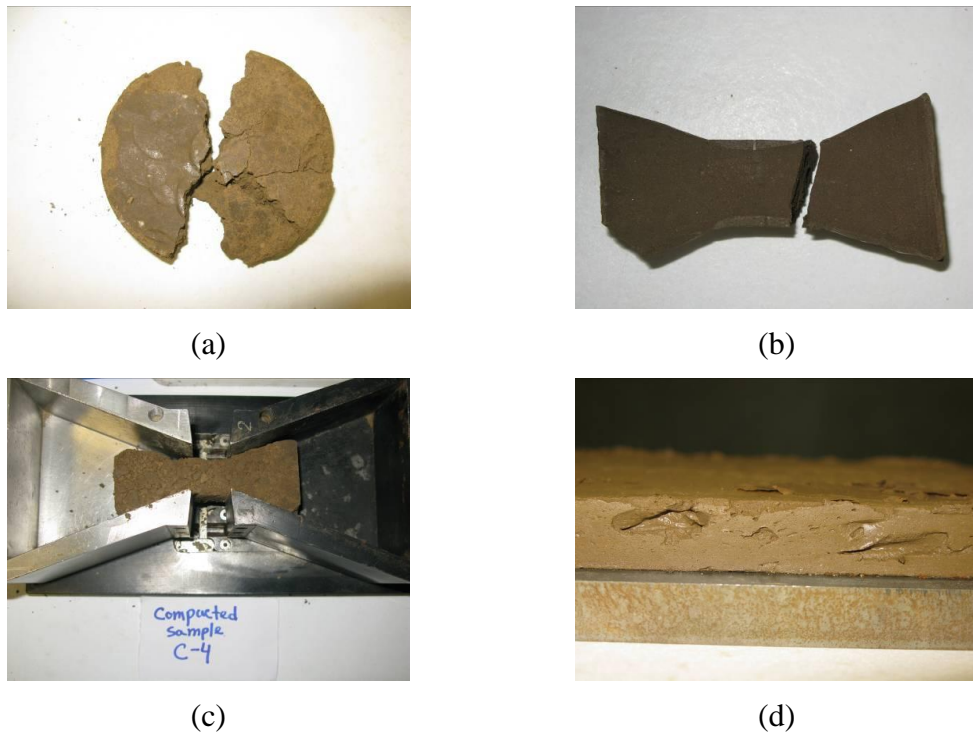


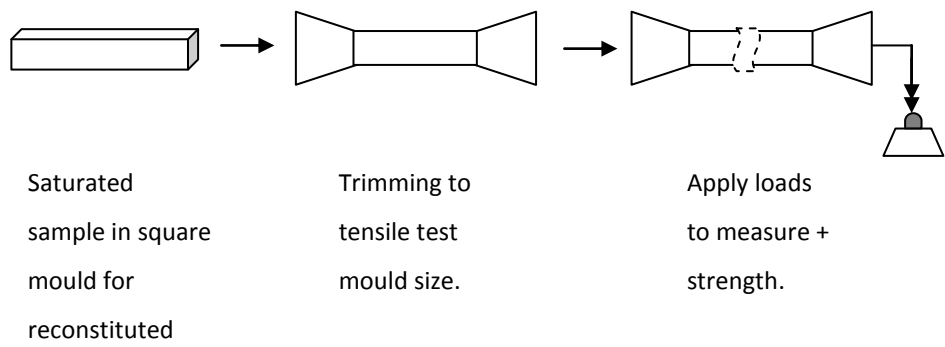
Figure 6.2: Difficulties in specimen preparation; (a) Crumbly compacted specimen at lower water content, (b) Specimen broke during cutting into shape to fit into complex shaped tensile mould, (c) The cut specimen does not fit properly inside the mould for test requirement, (d) Evidence of air-bubbles within specimen during drying in preparation of reconstituted specimen.

Previous researchers, e.g., Rodríguez (2002), Lakshmikantha (2009), Peron et al. (2007a), Lakshmikantha (2009) who used the same the tensile strength device, used a different method for preparing specimens. Most of them prepared specimen inside the device. In this research work, the aim was to achieve specific points from compaction curve of the soil and follow a drying path. It was essential to prepare compacted specimens at the same initial condition as reconstituted specimens and these conditions could not be achieved by preparing the specimens in the device.

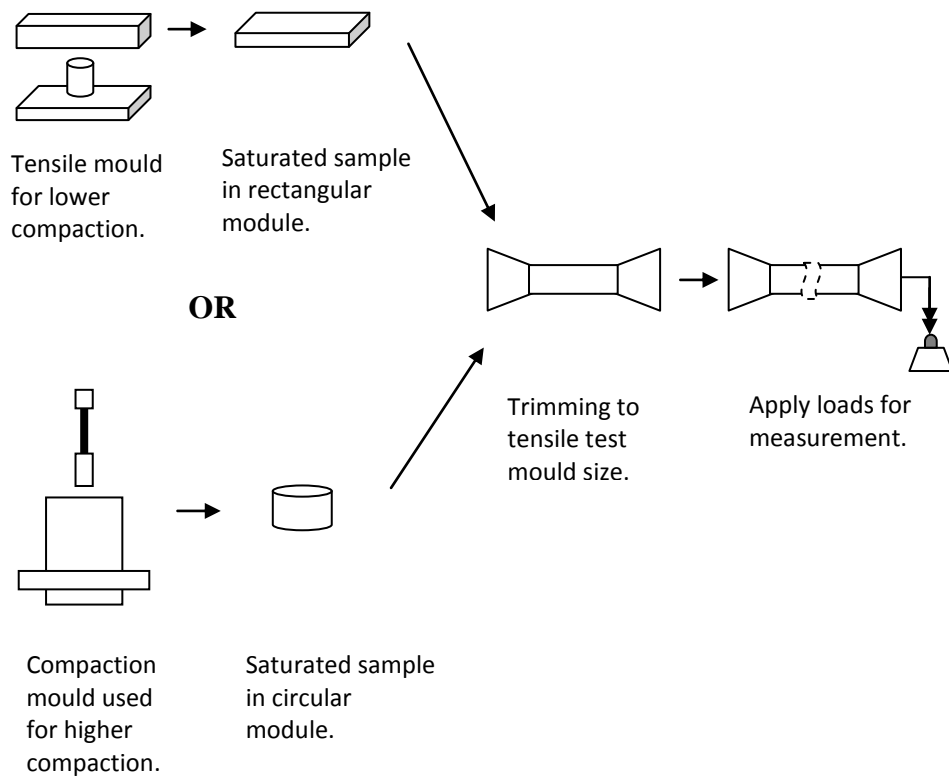
The rate and extent of cracking in clayey soil were dependent on plasticity, dry density and initial moisture content (Morris et al., 1992a, Kodikara et al., 2000a, Peron et al., 2007b). In addition, the tensile strength highly affects the desiccation

process and also the cracking rate (Yesiller et al., 2000, Albrecht and Benson, 2001). Considering the importance of these physical properties in relevance to the tensile strength of soil, each specimen was made always with special care. The slurried soil was always measured for volume change. Due to the complex shape of the device it could not be done accurately as the specimen dried/shrank away from the wall. Moreover, the central part of the specimen was the most important part as this was the part where the tension is applied to. In order to compare the results consistently, the area of this central part needed to be maintained constant. Taking into consideration of these matters, the specimen was always prepared outside and later on trimmed into specific shape of the tensile strength device.

The trimmed soil was used for moisture content test to measure the exact water content of the test specimen. The test procedure was simple, but the sample preparation needed practice. Figure 6.3 shows the schematic of sample preparation.



(a)



(b)

Figure 6.3: Schematic of sample preparation; (a) Reconstituted specimen preparation, (b) Compacted specimen preparation.

6.4.2 Selection of the initial condition for tensile test specimen

To meet the objectives of tensile test campaign, it was important to choose the specimen points for water content (w_0) and dry density (p_d) very carefully so that they actually follow the drying path from slurry to drying state of the soil. For that, three steps were followed:

- i) Choosing moisture content and dry density from compaction curve; moisture content and dry density values were chosen from the compaction curve (Figure 3.11 in *Chapter 3*).
- ii) Making reconstituted soil specimen.
- iii) Making compacted specimen with similar initial condition as reconstituted soil specimen.

Although the aim was to achieve the same initial condition for both specimen (reconstituted and compacted), it was not always possible due to specimen preparation difficulties. The reconstituted specimen was prepared at its liquid limit and allowed to dry until it was safe to handle, so that the compacted specimen can be made at similar conditions. Table 6.1 shows the initial conditions for all specimens used for tensile test campaign. The test reference assigned as TTR01 and TTC01 meaning tensile test for reconstituted specimen, test no-1 and tensile test for compacted specimen, test no-1. The tensile test has been performed three times for each test condition.

Table 6.1: Initial condition of specimens used for tensile strength test campaign.

Test reference for Reconstituted series	W_o (%)	ρ_{d0} (mg/m ³)	e_o	S_r (%)
TTR01	37.929	1.32	1.07	96.936
TTR02	31.073	1.45	0.88	96.095
TTR03	24.005	1.57	0.73	88.765
TTR04	21.39	1.61	0.68	85.874
Test reference for Compacted series	W_o (%)	ρ_{d0} (mg/m ³)	e_o	S_r (%)
TTC01	36.119	1.32	1.07	92.310
TTC02	30.432	1.43	0.91	91.387
TTC03	23.600	1.56	0.74	86.904
TTC04	20.056	1.64	0.66	82.958

Throughout the campaign the test reconstituted specimens were prepared at first and then the compacted specimens were prepared at same initial condition. There were many repetitions making the specimens and adjusting these values (ρ_{d0} and W_o). With practice and by changing procedures (for example, moving to a standard compaction mould to reach higher density values instead of using the tensile mould; preparing the reconstituted specimen before making the compacted specimen.), the values for W_o and ρ_{d0} for all reconstituted and compacted specimen were adopted for tensile test campaign. Figure 6.4 shows the points selected for the tensile tests in the compaction curve.

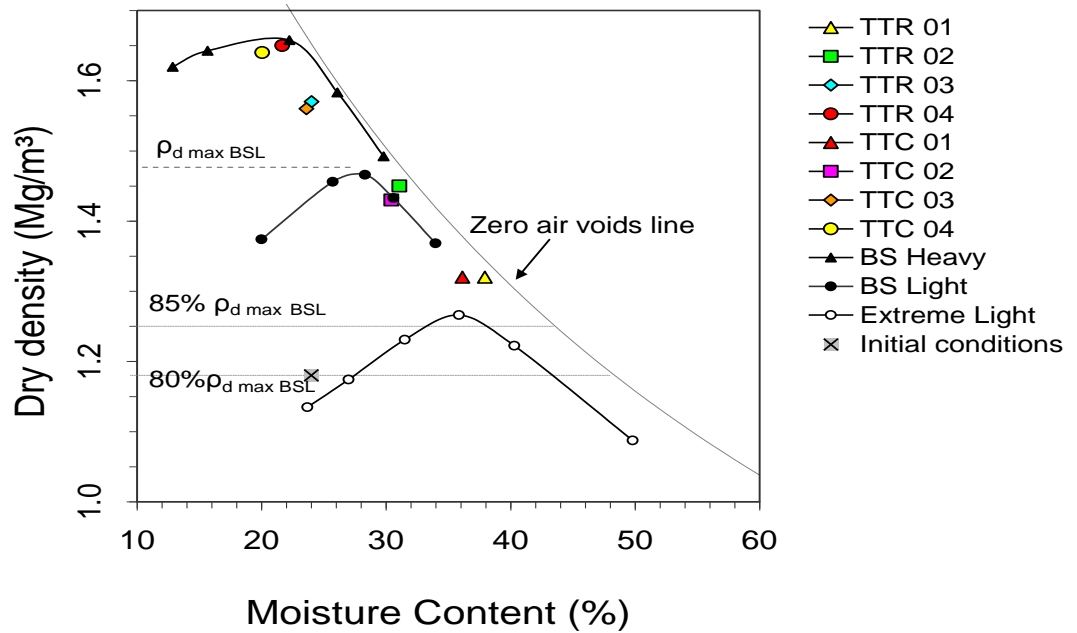


Figure 6.4: Selection of points for tensile test specimens from compaction curve of Bengawan Solo soil.

6.4.3 Preparing reconstituted specimen

In preparation of reconstituted specimens, the slurry form of the soil was prepared at around its liquid limit (55%) following the same procedure as mention in Section 3.5.2. Using a spatula, the slurry was placed inside the tensile mould in three stages and slightly tapped two to three times each time to level the soil surface and remove any entrapped air bubbles inside the specimen. In order to avoid adhesion of the soil to the side walls of the moulds, the side walls were greased before the soil was emplaced.

The mould was then left within a temperature controlled room for air drying and allowed to dry naturally. When the soil sample had shrunk and dried enough to

handle safely, the side wall of the mould was removed. The soil sample was allowed to dry until the required dry density was achieved. Four reconstituted samples were prepared following the same procedure at four different moisture contents (Table 6.1). The initial condition of all specimens were carefully selected the compaction curve of Bengawan Solo soil. The water content and dry density were measured at this stage and carefully noted. The moulded soil was then cut into shape required for the tensile test equipment using a sharp paper knife. The trimmed soil was used for moisture content test and also saved in an air tight container for mercury intrusion porosimetry (MIP) and the Field Emission Scanning Electron Microscope (FESEM) testing.

6.4.4 Preparing compacted specimen

In preparation of compacted specimen at same water content and dry density as reconstituted sample, two steps were followed. A large amount of soil was prepared at the required moisture content using the procedure explained in Section 3.5.2 and then compacted within tensile mould. The specimens were compacted in three layers for better distribution and uniformity. Special care needed to be taken in measuring the volume of the tensile mould. The mould was large in volume and a small measuring mistake would result in the specimen lying outside the zero air void line of the compaction curve (Figure 6.5).

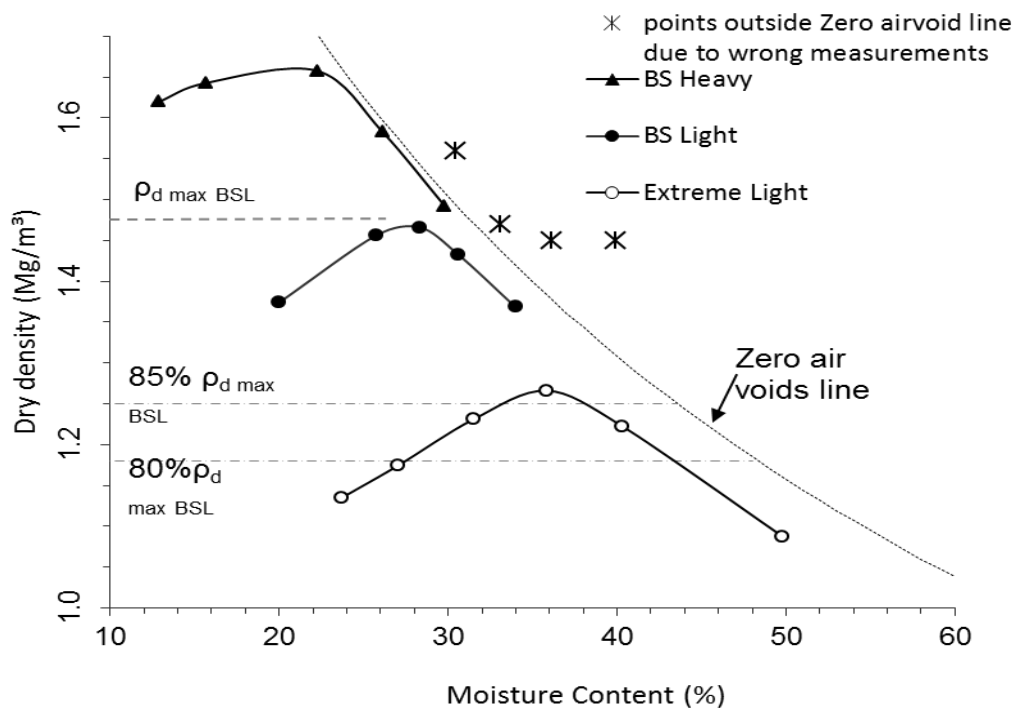


Figure 6.5: Points at compaction curve outside the zero air void line due to mistake in volume calculation of the tensile mould.

Through proper practice during specimen preparation by carefully taking average during measurement of the compacted specimen, each volume was calculated. Large scale vernier callipers were used for to measure the longer side of the rectangular tensile mould. At higher moisture content, the required dry densities for specimen TTC01 and TTC02 were 1.32 g/cm³ (36%) and 1.43 g/cm³ (30%). These values were difficult to achieve by standard proctor mould, but were achieved with a moderate compactive effort by using a hand hammer. Figure 6.6 shows the image for preparation of one of the compacted specimens at lower moisture content.

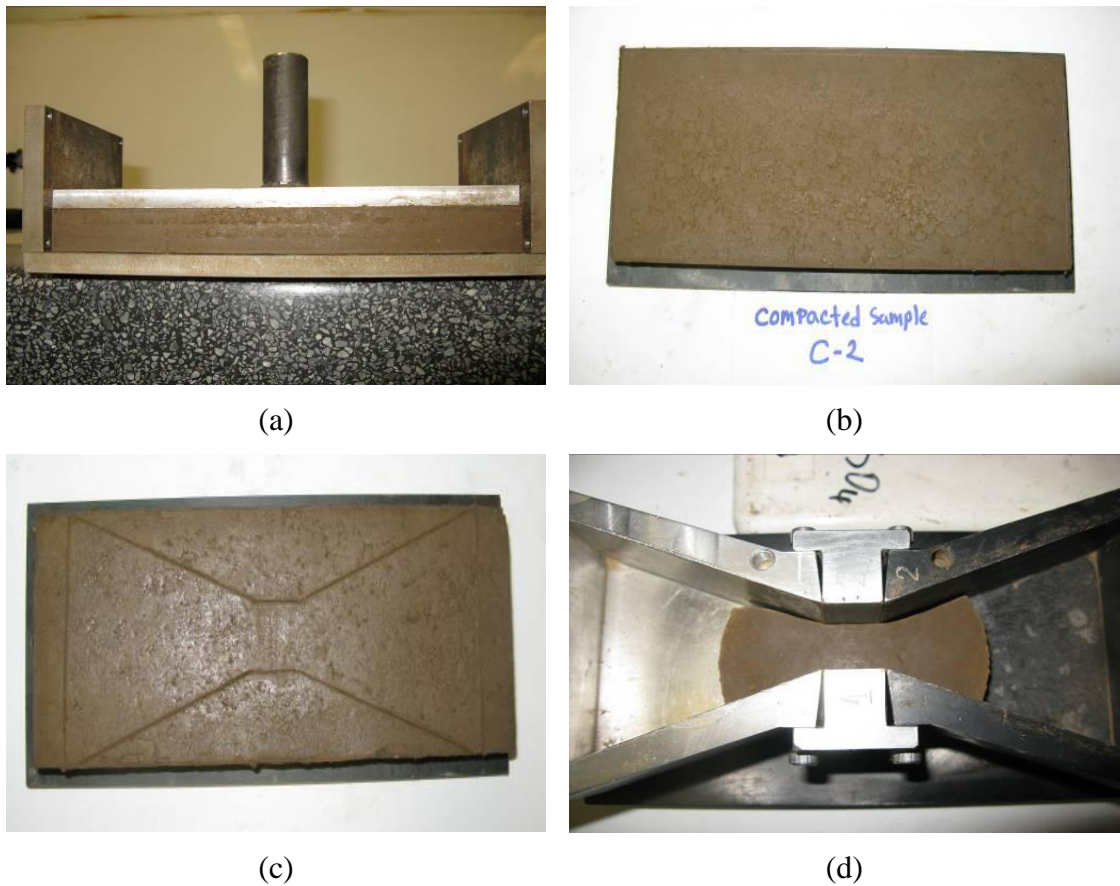


Figure 6.6: Image showing preparation of compacted specimen by tensile mould; (a) Compaction by tensile compaction tool in three layers, (b) Finished compacted specimen, (c) Specimen prepared for cutting into shape, (d) Cut compacted specimen placed inside the tensile testing device.

Specimens TTC03 and TTC04 were prepared using standard BS light compaction mould (see Figure 6.7). With this low moisture content it was harder to compact the specimen at this higher density. The compactive effort was adopted to achieve the required dry density. The specimens were cut into the shape to fitted inside the tensile equipment. The moisture content test was always performed with the trimmed soil, and the rest of trimmings were saved in a sealed airtight container for MIP and FESEM testing.

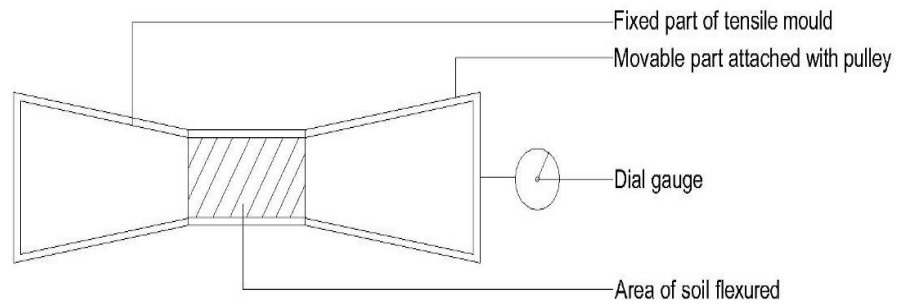


Figure 6.7: BS light compaction mould to prepare compacted specimen at higher dry density.

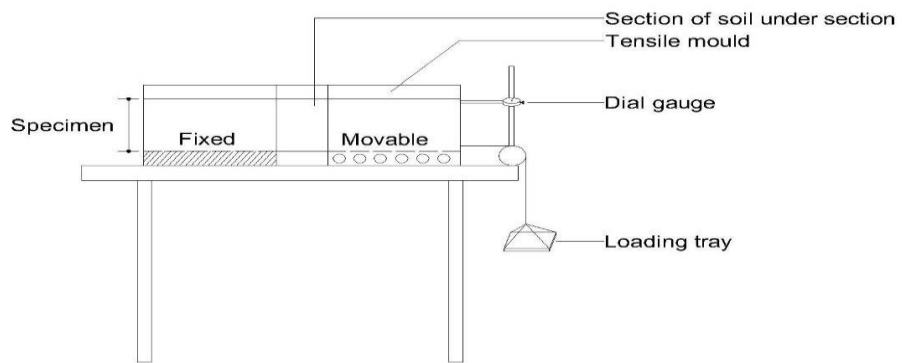
6.4.4 Tensile strength testing device

The tensile tests were performed by direct tensile strength equipment (see Figure 6.8 and 6.9). This was designed by Rodríguez (2002) and is similar to one by Mikulitsch and Gudehus (1995). The same equipment was used by Lakshmikantha (2009) as a part of his PhD work. The equipment was brought to Geotechnical laboratory at Strathclyde University from the Soil Mechanics Laboratory of UPC for this research for a period of time. The equipment is consisting of three parts (Figure 6.10):

1. ***The central part*** where the specimen is subjected to tension during test. The central part is surrounded by two removable solid blocks (marked as part 1 and 2) which helps to place the soil specimen securely in place and removed just before the application of the load. There two other rectangular solid blocks used here which placed below the central part of the soil specimen just to support the specimen before loading application.
2. ***The two trapezoidal parts***, one of which is fixed and the other is movable freely and attached with a loading pan. Displacement is allowed on the movable part by means of a tensile force imposed by the application of different weights on this loading pan. 0.01 mm precision dial gauge is used to measure the displacement.
3. ***The loading pan*** is the third part and is flexible with pulley to be able to pull the movable trapezoidal part downward.

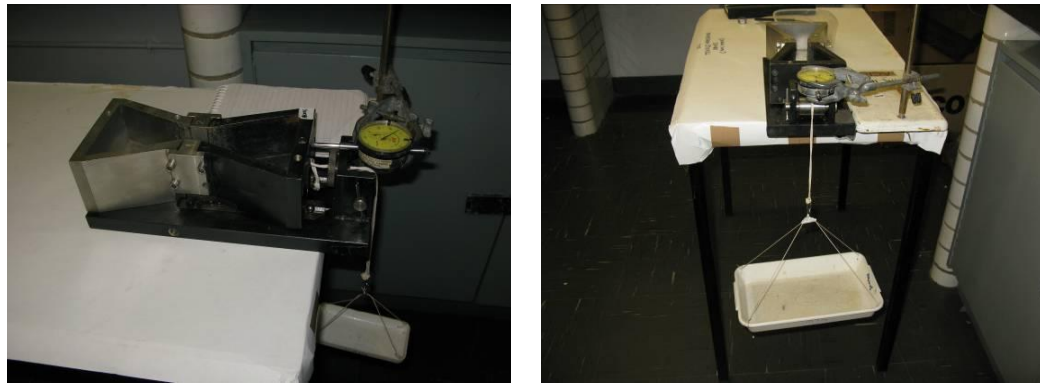


(a)



(b)

Figure 6.8: Schematic of direct tensile strength equipment; (a) Top view, (b) Front view.



Front view

Side view

Figure 6.9: Laboratory set-up for tensile test.

6.4.5 Mounting of specimen within the device and testing procedure

After cutting the specimen into shape as required to tensile testing mould, the steps in order for mounting the specimen into the tensile testing mould was as follows (see Figure 6.10):

- Assemble the three major parts of the tensile mould described in Section 6.4.4.
- Attach the dial gauge at mid-point of movable part of the tensile mould. LVDT can be use also instead of dial gauge. Record the initial point at dial gauge.
- Place the shaped soil specimen carefully inside the mould.

- Unscrew all the screws from the '1' and '2' marked solid part (Figure 6.10) and detach that from the central part of the soil specimen.
- Carefully remove the two rectangular solid blocks from below the soil specimen at the central part. As soon as it is completed, the specimen is under test condition with '0' load.
- Measure area of the soil subjected to tensile stress (which is the central part of the soil specimen).
- Attach the loading pan and note the pan weight and the displacement in mm from the dial gauge as the first measurement.
- Start adding weights into the loading pan and note as well. Weights were placed with care and with a constant frequency. For wet soil at high moisture content lower weight were used and increased gradually until the tensile failure occurred, whereas for soil with lower water content, which is drier, took higher weight to reach the failure. Figure 6.11 shows some of the photographs taken during the tests. Figure 6.11a shows the initiations of a cracking and Figure 6.11b is the front view of the same specimen.

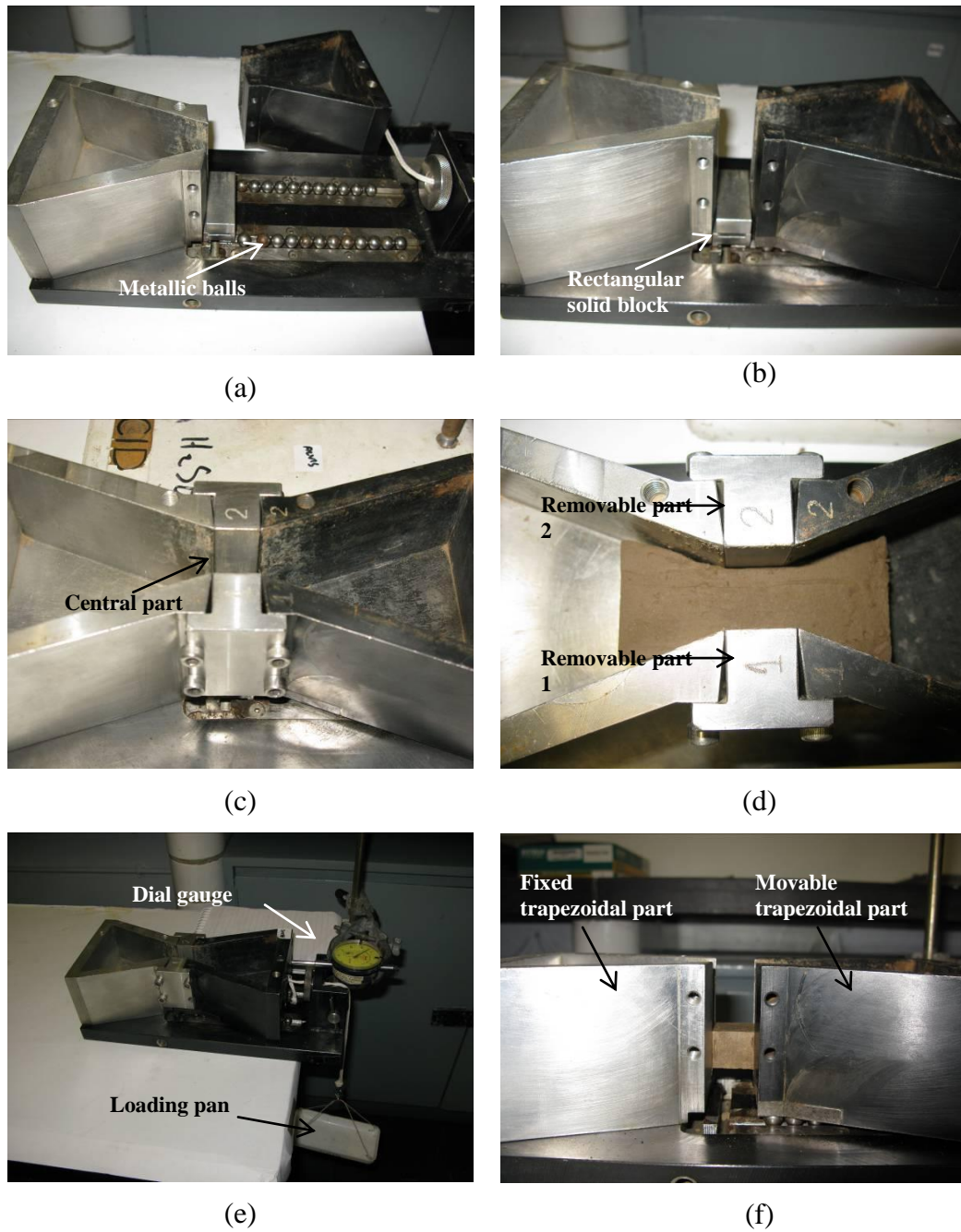


Figure 6.10: Assembling different parts of the tensile device and mounting the specimen step by step.

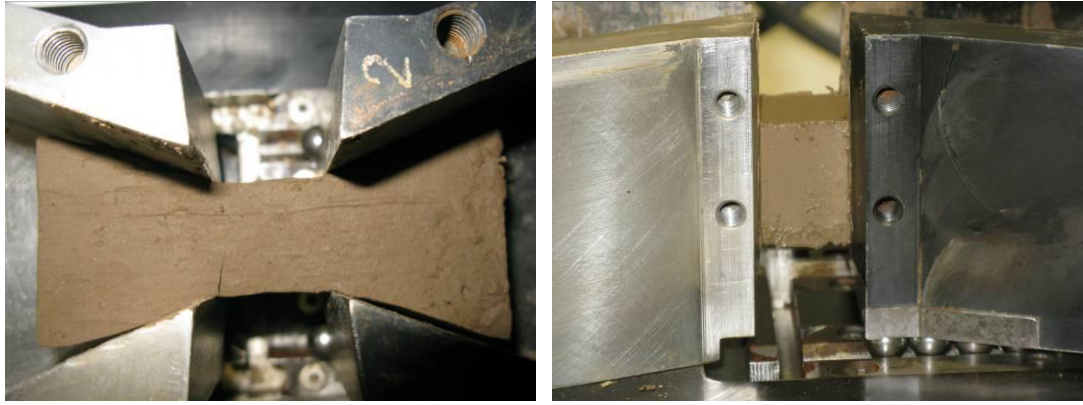


Figure 6.11: Tensile test specimen during test: Starting of a crack in the failure zone (left); Front view of a test specimen (right)

The tensile strength was calculated at each stage of the loading addition. The following equation was used to measure the tensile strength:

$$T = \frac{W \times g}{A} \quad (6.1)$$

where, T= tensile strength

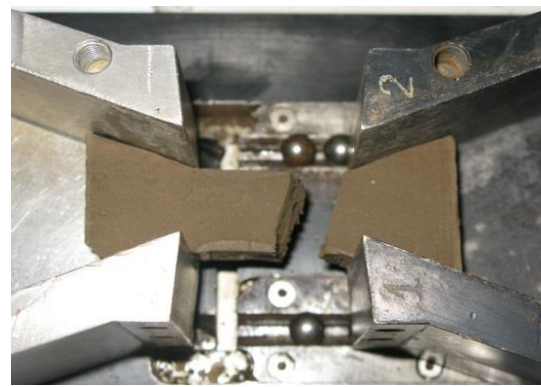
W= weight added in the loading pan

A= area of the soil specimen subjected to tension.

Figure 6.12 shows both specimens at the tensile test after failure. The images show differences between the failure mode and surface texture between specimens at both states and also at lower and higher water content.



(a)



(b)



(c)



(d)

Figure 6.12: Tensile test after failure; (a) Reconstituted specimen at lower water content, (b) Reconstituted specimen at higher water content, (c) Compacted specimen at lower water content, (d) Compacted specimen at higher water content.

6.5 RESULTS

6.5.1 Tensile strength for reconstituted and compacted specimen

Two series of tests were done for the tensile strength testing campaign. First one was for reconstituted specimen and the second one was for compacted specimen. Each series consist of four tests starting from saturated/slurried condition towards dried condition. The results of these tests are presented in Table 6.2.

Table 6.2: Details of tensile strength tests.

Test no	Test ref	Sample type	W%	P_d mg/m ³	e_0	S_r %	T (kPa)	A (m ²)
1	TTR 01	Reconstituted	37.929	1.32	1.06	96	12.8	0.0004
2	TTR 02		31.073	1.45	0.88	96	35.649	0.00044
3	TTR 03		24.005	1.57	0.73	88	68.803	0.00041
4	TTR 04		21.39	1.61	0.68	85	122.33	0.00048
5	TTC 01	Compacted	36.119	1.32	1.06	92	8	0.00041
6	TTC 02		30.432	1.43	0.9	91	13.288	0.0004
7	TTC 03		23.6	1.56	0.74	86	57.931	0.00045
8	TTC 04		20.056	1.65	0.66	82	92	0.00044

Figure 6.13 shows the load deformation curve for reconstituted and compacted specimen at four different moisture content and dry density. The load deformation curve corresponds to the moisture content shown in Table 6.2. The curves show relatively large deformation at higher moisture content then at lower moisture content for both series. The slope of the curves gradually increases with decreasing moisture content.

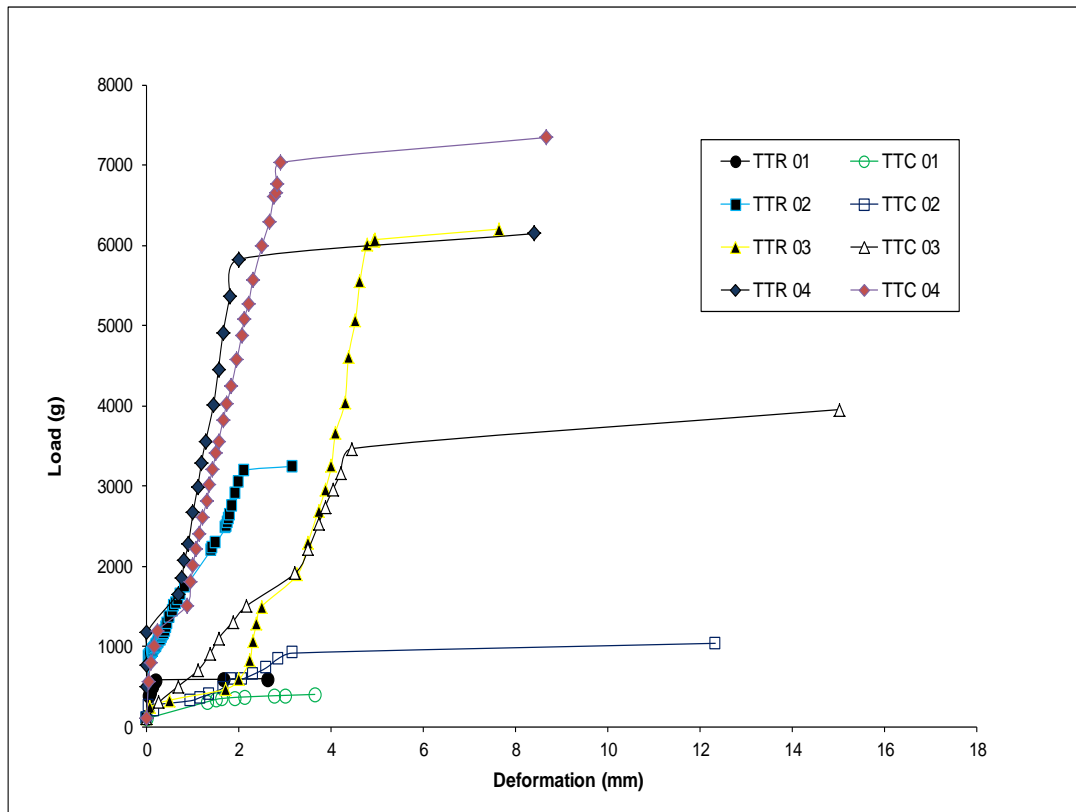


Figure 6.13: Load deformation curve for reconstituted and compacted specimen during drying from higher water content towards lower water content.

Figure 6.14 shows the relation between the tensile strength and water content for all tests (reconstituted and compacted). Tensile strength generally seemed to increase with the decrease of moisture content. Similar trends were observed by Krishnayya et al. (1974b), Ajaz and Parry (1975) and Tang and Graham (2000). The relationship between soil tensile strength and moisture content was studied by Nahlawi et al. (2004), Al-Alshayea (2001), and they suggested that tensile strength decreases nonlinearly with an increase in water content.

In Figure 6.14 the reconstituted specimen shows higher tensile strength compared to the compacted specimen. This indicates Bengawan Solo clay might experience important changes during drying which may be responsible for higher tensile strength values observed for reconstituted specimen than compacted specimen.

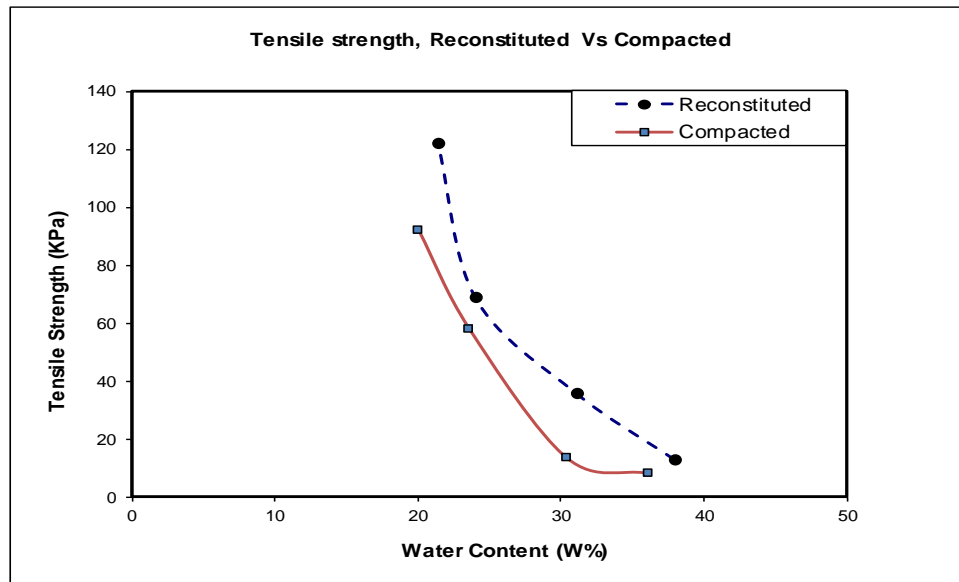


Figure 6.14: Evolution of tensile strength of Bengawan Solo soil during drying at reconstituted and compacted states.

6.6 PROBLEM ASSOCIATED WITH DIRECT TENSILE TESTING DEVICE

Tensile strength is essentially determined assuming that uniform tensile stress is achieved on the failure plane. As a result, the commonly used methods are more suitable for brittle and elastic materials than for ductile materials. The direct tensile test device used for this research is already tested by several researchers; e.g. (Rodríguez, 2002, Lakshmikantha, 2009, Trabelsi et al., 2010, Trabelsi et al., 2011, Lakshmikantha et al.) and can be considered to be well established. However the technique followed needed a self-supported specimen, which required trimming to place it properly into the mould. This method is, therefore, not suitable for very soft clay, as mentioned earlier. Few more difficulties during the testing procedure involved were:

1. Previous researchers, who used this device, compact the soil specimen within the device. The author of this research found it hard and in some

cases inaccurate to the specimen requirements. The compaction must have been done at three different stages as the device consists of 3 parts. At higher compaction level it is not easy to be consistent with the compaction mould, especially with the mid-section of the device/specimen. Yet, this is the most important part, as the tensile force is applied in this section. In the field compaction is never homogeneous as well and so this is quite expected. The author of this thesis suggested an improved compaction procedure, particularly for the tests required for the tensile test campaign and achieved better specimen specifications.

2. The weir that holds the loading tray was not strong enough to bear the load that was required for the tensile failure of the dried reconstituted specimen at lower water content. It tore off a few times during the middle of the test. Sometime this occurred just after the test completion before dial gauge had read the final reading. This was very inconvenient considering the steps for specimen preparation for the tests. The author also did not find the any specific length anywhere in the previous literature for the weir length, and the author found the result could vary a bit for different length of the weir. However the author measured the existing weir length that was attached already and maintained this throughout the test campaign.
3. The area subjected to tensile strength should be taken into consideration very carefully since this particular area was used to calculate the tensile strength. The significant difference between areas would not be a proper representation of the results when comparing. As the specimen was trimmed to cut into the shape to place it within the tensile mould, there was slight difference between the areas (see Table 6.2) which could be ignored. Similar differences was also found in the work done by Trabelsi et al. (2011), because they prepared specimen within the mould and allowed them to dry within. As a result, a small gap was created between the specimen and the sides of the mould, because of shrinkage, and that resulted in the differences in the areas.

6.7 FABRIC STUDY

A microstructural investigation was carried out for Bengawan Solo soil for reconstituted and compacted soil specimens. FESEM was only performed for TTR 01, TTR 03, TTC 01, and TTC 03. These specimens were detailed in Table 6.1 and Figure 6.5. Experimental techniques such as Scanning Electron Microscopy (SEM), Environmental Scanning Electron Microscopy (ESEM), Field Emission Scanning Electron Microscope (FESEM) and Mercury Intrusion Porosimetry (MIP) have already achieved their reliability in fabric study in various geotechnical investigations. The ESEM provides a direct and qualitative observation of the soil fabric arrangement and MIP gives a quantitative data on soil porosity and pore size distribution. Pore size distribution is an essential element of soil fabric investigation (Romero, 1999) and can be responsible for differences in permeability, compressibility and strength (Juang and Holtz, 1986b). Carter (1990), Guérif (1990) and Munkholma et al. (2002) showed that microporosity has a significant effect on tensile strength. SEM and MIP have been used independently or together in previous microstructural investigation of soils (Barden et al., 1973b, Collins and McGown, 1974b, Delage and Lefebvre, 1984b, Griffiths and Joshi, 1989, Prapaharan et al., 1991, Jommi and Sciotti, 2003). The study presented in this section was carried out using both FESEM and MIP in order to investigate the following features:

- To investigate/compare the fabric of the Bengawan Solo soil at two different conditions: reconstituted and compacted
- To investigate the evolution/deformation of fabric Bengawan Solo soil the drying path from saturated condition

6.7.1 Mercury Intrusion Porosimetry (MIP) tests

6.7.1.1 Principle

The MIP technique is based on the capillary laws which govern the entrance of a non-wetting liquid into the smallest pores. For liquids like mercury, Washburn (1921) gave an equation that related the pore entrance diameter d to the absolute pressure P .

$$P = \frac{-4\sigma_{Hg} \cos \theta_{nw}}{d} \quad (6.2)$$

where θ_{nw} is the non-wetting angle between mercury and the solid particle and σ_{Hg} is the surface tension of mercury.

The surface tension of the mercury used for this investigation was $\sigma_{Hg}=0.484$ N/m at 25°C and contact angle $\theta_{nw}=140^{\circ}$ was used ((Diamond (Diamond, 1970) adopted the contact angle between 139° for montmorillonite and to 147° for other clay minerals.)

There are number of limitations in the ability of the MIP technique. They are listed below:

1. Equation 6.2 by Washburn (1921) assumes that all pores are cylindrical and are identically parallel in form. As the real pores in soil are seldom cylindrical, the assumption is an over simplification of the pore network within the soil.
2. The extrusion curve is different from that of the intrusion curve due to the entrapped mercury within the pores of soil with contraction because of the difference in contact angle of mercury for entrance and exit.
3. There are also some isolated pores which are completely surrounded by solid particle and the mercury cannot be forced in those. However, this

enclosed porosity is not thought to be significant by Romero and Simms (2008a).

4. The smallest pores of the soil specimen might not also be intruded due to the pressure capacity of the MIP equipment. This is referred as non-intruded porosity. Again the minimum pressure of the equipment limits the maximum pore diameter which can be detected. This is referred to as non-detected porosity (Romero and Simms, 2008a). This is the reason why the intruded void ratio determined by MIP might not be the same as void ratio of the soil specimen under test.
5. There is restriction on the specimen volume used in the MIP equipment. A maximum volume of 5000 mm^3 for the specimen and a maximum pore volume of 292 mm^3 can be tested.
6. The high pressure used in MIP technique applied during Mercury intrusion might damages or change the structure of the soil specimen. However this limitation is considerably overcomes in the work presented by previous researchers (Lawrence, 1878, Delage and Lefebvre, 1984a, Reed et al., 1980, Griffiths and Joshi, 1989b, Romero and Simms, 2008a). Lawrence (1878) presented data that suggested virtually no damage to the sample occurred upon mercury intrusion. Delage and Lefebvre (1984a) presented data showing agreement between the pore size diameters measured using by SEM and MIP analysis which indicates mercury intrusion does not damage soil structure.

6.7.1.2 MIP Equipment

The porosimeter used in the Department of Geotechnical Engineering and Geosciences at UPC Geotechnical Laboratory is the AutoPore IV 9500. This instrument could reach a maximum pressure of 223 MPa covering the pore diameter

range from approximately 900 to 0.005 μm . It has two low-pressure ports and one high-pressure chamber (Figure 6.15).



Figure 6.15: MIP equipment used for the tests.

6.7.1.3 Specimen Preparation

For the MIP analysis the specimen preparation is vital to accurately determine the pore size distribution. The specimen is dried using freeze-drying technique (Delage et al., 1982), which has become the standard method, as oven drying or air drying can cause significant changes in soil structure (Ahmed et al., 1974). The specimens were trimmed to approximately 1 cm^3 and freeze dried for the period depending on how much saturation the specimen was. It took up to three days to freeze dry the samples with high saturation. Freeze dried specimens were stored inside a desiccator until testing.

6.7.1.4 Experimental methodology

Before performing an analysis, it was necessary to weigh the freeze dried specimen (Figure 6.15), record the mass, and create a specimen information file in the computer that controls the analysis software for MIP instrument. This file also included a pressure table that specified the pressure values for data collection during the analysis.

To begin the analysis, it was necessary to load the sample into the penetrometer and then install the loaded penetrometer in a low pressure port. Penetrometer 950-61711-00 was used for all these tests with a bulb volume of 50 cm³. The first phase of the low pressure analysis was the evacuation of gases from the penetrometer. The penetrometer was then backfilled automatically with mercury. The second phase of the low pressure analysis was the collection of data at pressures up to the last low pressure point specified in the pressure table. The low pressure intrusion stage which involved increasing mercury pressure up to 345 kPa lasted approximately 2 hours.

After the low pressure analysis had been completed, the penetrometer was removed from the low pressure port and installed in a high pressure chamber (Figure 6.15). The high pressure analysis collected data at pressures indicated in the high pressure portion of the pressure table (in particular, up to 223 MPa for this apparatus). In the high pressure intrusion stage, mercury pressure was increased continuously to 223 MPa, lasting typically 12hrs, after which an extrusion cycle followed.

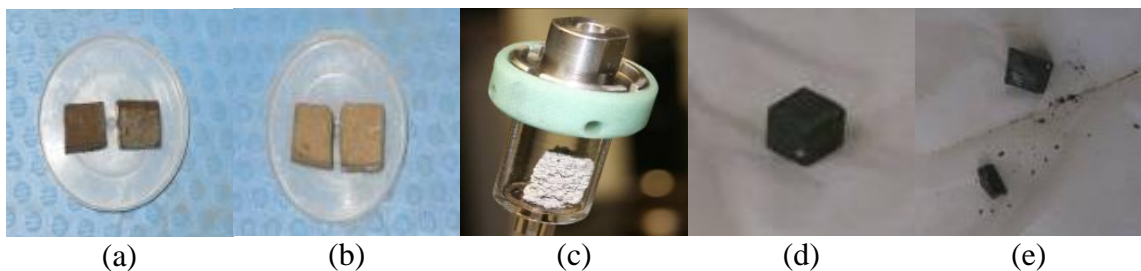


Figure 6.16: (a) MIP specimen wet, (b) MIP specimen freeze dried, (c) MIP specimen just before test, (d) MIP specimen after test, (e) MIP specimen broken after test in order to check proper mercury penetration during test.

Figure 6.16 shows a complete picture of the MIP specimen before and after test; and penetrometer tool to tighten the penetrometer lid or to dismantle the lid.

6.7.1.5 Calculations

Equation 6.2 was used to determine the pore entrance diameter, which by a simple rearrangement gives the following equations:

$$e_{intr} = \frac{V_{v(intr)}}{V_s} = \rho_s \bar{v} = \frac{M_s}{V_s} \times \frac{V_{v(intr)}}{M_s} \quad (6.3)$$

where,

e_{intr} = void ratio of specimen intruded with mercury

V_s = volume of solids

$V_{v(intr)}$ = volume of voids intruded with mercury

ρ_s = particle density

\bar{v} = cumulative intrusion volume

M_s = specimen mass

The equation for measuring intruded porosity (n_{intr}) can be written as

$$n_{intr} = \frac{V_{v(intr)}}{V} = \frac{e_{intr}}{1 + e_{intr}} \quad (6.4)$$

and the equation for measuring the degree of saturation ($S_{r_{nw}}$) of mercury can be expressed as

$$S r_{nw} = \frac{V_{v(intr)}}{V_{v(total)}} = \frac{n_{intr}}{(n_{intr})_{max}} \quad (6.5)$$

6.7.1.6 Results

Figure 6.17 shows the evolution of clear bi-model PSD (pore size distribution) functions for reconstituted specimens TTR01 and TTR02 during drying path. For TTR03 the macroporosity (pores above 1 microns) were not adequately captured, and the TTR04 plot did not show clear bi-model PSD (pore size distribution). A pore mode corresponding to 34-42 nm was found for all four specimens. This pore mode was found in all the specimens and may correspond to the intra aggregate porosity; the pore space between clay particles. The dominant modes were found between 1-3 μm and shifted towards smaller pore diameter range with decreasing water content, as expected. From here, a boundary between intra-aggregate and inter-aggregate porosity was observed at around 150 nm as pores smaller than this magnitude appear not to be affected by higher dry density of the soil. Lloret et al. (2003) did similar classification but the boundaries between the inter-aggregate and the intra-aggregate pores were found to be present around 200 nm, based on the pores that do not change when increasing the compactive effort and observing the swelling behaviour of compacted soil.

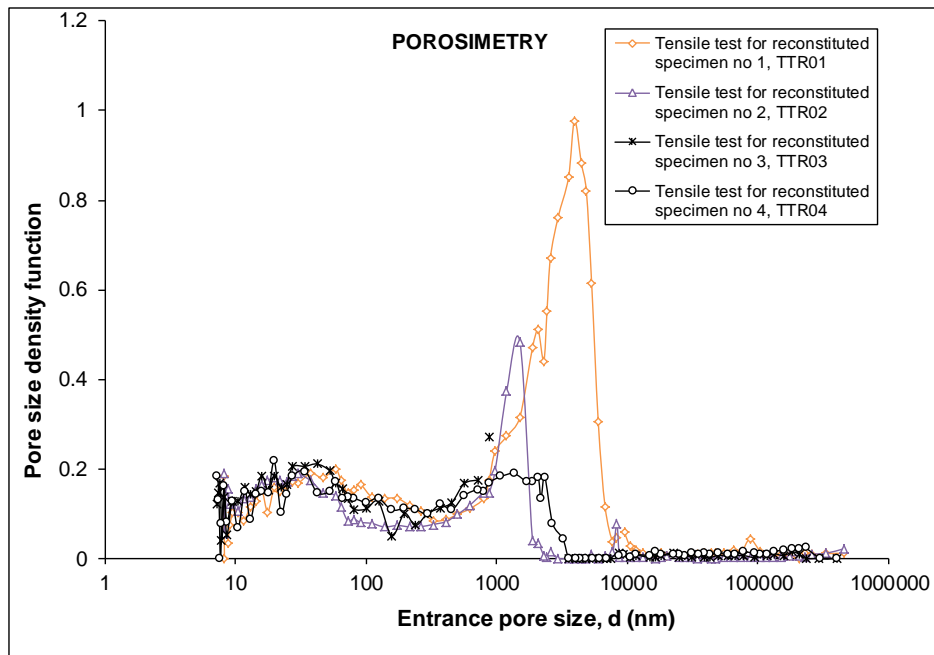


Figure 6.17: MIP results for all reconstituted specimen at four different initial conditions to capture the evolution of soil microstructure during drying.

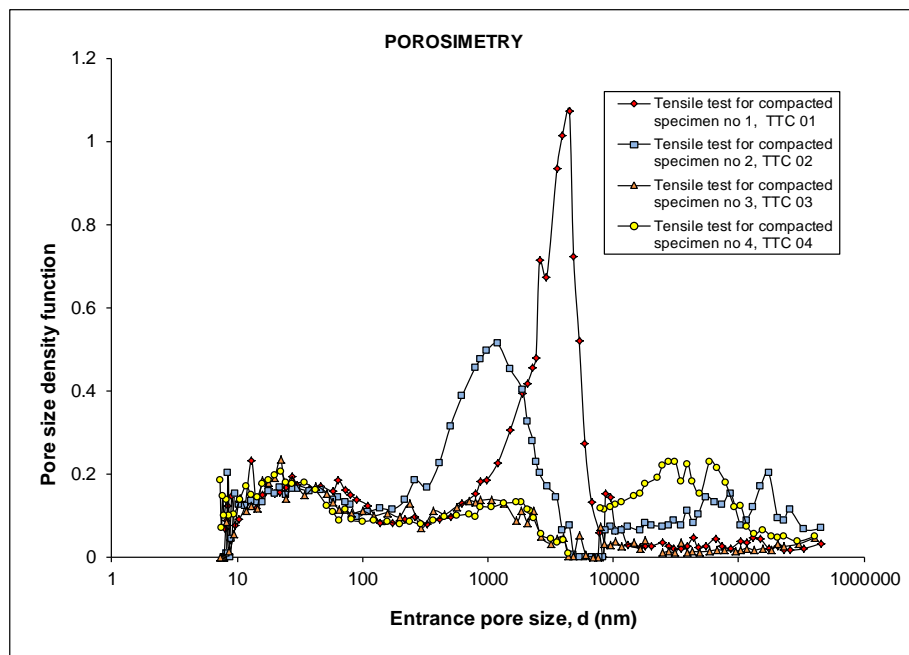


Figure 6.18: MIP results for all compacted specimen at four different initial conditions to capture the evolution of soil microstructure during drying.

Figure 6.18 shows the evolution of bi-model PSD functions for compacted specimen TTC01 and TTC02 during drying path. Yet again, TTC03 and TTR04 plot did not show clear bi-model PSD. It was observed that for all four specimens a pore mode corresponded to 22-27 nm. Again the boundary between inter-aggregate and intra-aggregate was observed at 150 nm, similar to reconstituted specimens. The dominant modes or the inter-aggregate pores were found between 1-4 μm and shifting towards smaller pore diameter range with decreasing water content as expected. As expected, the inter-aggregate pores region only is effected by the different magnitude of compaction, which supports the findings by Lloret et al. (2003).

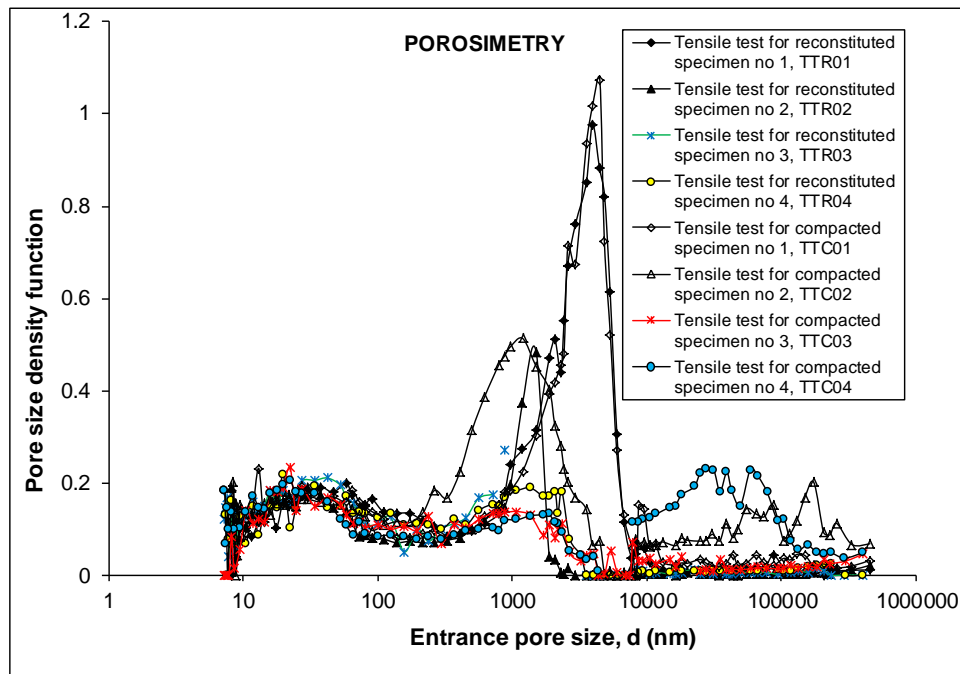


Figure 6.19: MIP results for all reconstituted vs. compacted specimens.

Figure 6.19 includes all the MIP plots for both types of specimens (reconstituted and compacted). For all the specimens; reconstituted and compacted curves follows almost similar pattern which was interesting. For both cases, it is interesting to note that the reduction of certain class of micropores is accompanied by an increase in

certain class of micro pores, leading towards a bi-modal distribution (except for specimen TTR03). A model to account this response on drying was proposed by Koliji et al. (2006). Kong et al. (2005) also analysed the PSD evolution of compacted clay at different stages of dehydration. Generally, good agreement is obtained between both reconstituted specimen TTR03 and TTR04, which displayed two modes (below 3 microns). On the other hand, the compacted sample TTC-04 displayed larger macroporosity with a dominant pore mode around 20-50 microns.

6.7.2 The Field Emission Scanning Electron Microscope

(FESEM) tests

6.7.2.1 Experimental equipment

The Field Emission Scanning Electron Microscope FESEM used is a 'JSM-7001 F' from JEOL (see Figure 6.20). Low voltage (3 kV) images were obtained with negligible electrical charging of samples. For magnifications up to x2000 and at moderate kV there is no need for placing conducting coating to prevent surface charging. Nevertheless, a thin conducting film of 2 nm platinum & palladium was used to improve the resolution. The author is grateful to Dr Enrique Romero for kindly conducting the tests for FESEM investigation at UPC, Barcelona.



(a)



(b)

Figure 6.20: FESEM (Field Emission SEM) equipment: JSM-7001F used for the tests.

6.7.2.2 Specimen preparation

The material was first freeze-dried, before the platinum-palladium coating and kept in high-vacuum for three days. This high vacuum allows using 3 kV (in SEM we have usually 15 to 20 kV at higher absolute pressure). Since FESEM uses high-vacuum (absolute pressure: 9.6×10^{-5} Pa), the samples were previously freeze-dried and then placed in the sample chamber under vacuum for three days before observation. Sample surfaces were prepared by fracturing and gentle blowing to maintain the intact the fabric. The specimen chamber handles specimens up to 200 mm in diameter. Figure 6.21 and 6.22 show specimen during tests.



Figure 6.21: Specimen holder with samples TTC01, TTR01, TTC03 and TTR03. Samples were freeze-dried and coated with 2 nm platinum and palladium.

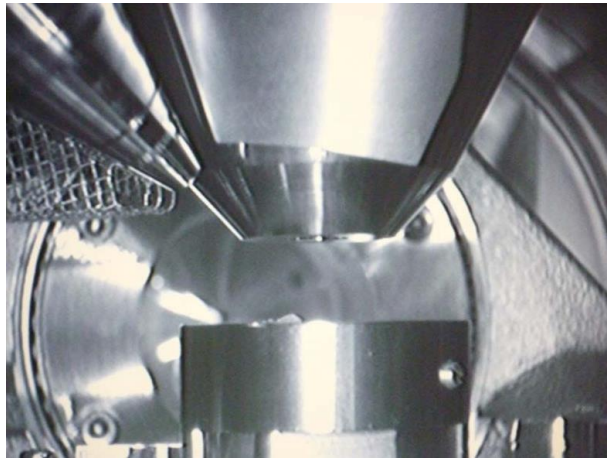


Figure 6.22: Sample inside the high-vacuum FESEM chamber (absolute pressure of 9.6×10^{-5} Pa).

6.7.2.3 Chamber condition

Absolute pressure of 9.6×10^{-5} Pa was maintained in observing the specimen inside the high-vacuum FESEM chamber. This high vacuum allows high resolution performance of a field emission SEM with the ability to image non-conductive samples at moderate to high kV and higher beam current. In this investigation, this was 3 kV (in SEM, we have usually 15 to 20 kV at higher absolute pressure).

6.7.2.4 FESEM results

Figures 6.23-6.25 presents the FESEM micrographs of the reconstituted and compacted specimen investigated. Figure 6.23 and Figure 6.24 present two images of compacted and reconstituted specimen prepared at similar conditions (moisture content and dry density). It is interesting that the compacted specimen shows an open structure by large inter-aggregate pores bridging connections whereas in contrast the reconstituted specimen shows no open structure. Instead, the image for the reconstituted specimen shows a complex soil matrix at very dense conditions where soil aggregation is not well-defined. No visual pores are observed.

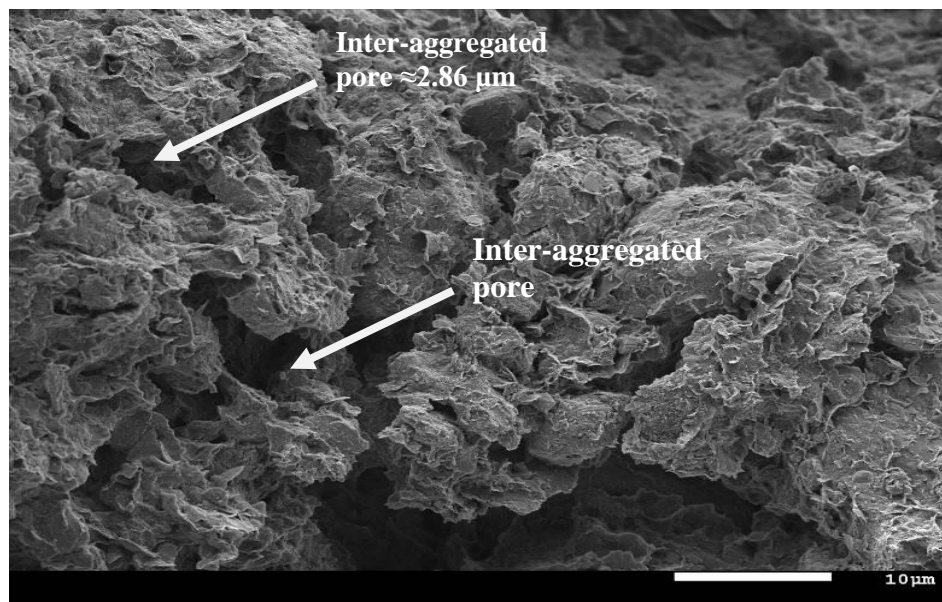


Figure 6.23: ESEM micrograph of inter-aggregate pore present in compacted specimen ($\approx 2.86 \mu\text{m}$ and $3.57 \mu\text{m}$); TTC01 (36.119%, 1.32 mg/m^3).

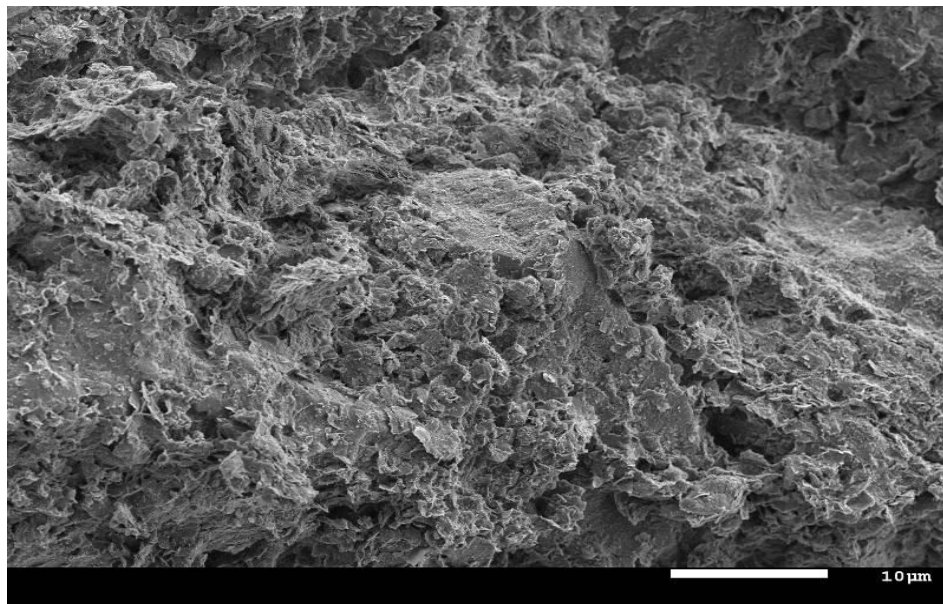


Figure 6.24: ESEM micrograph for reconstituted specimen TTR 01 (37.929%, 1.32 mg/m³), soil aggregate not well defined.

Moving to compacted TTR03 and reconstituted TTR03 specimens, the inter-aggregate pores of compacted TTC03 specimen is not well defined and more open. Yet again, the reconstituted specimen TTR03 shows no defined structure similarly to specimen TTR01. The comparison of Figure 6.23 and 6.25a for compacted specimens suggests that the outer covering of specimen TTC01 is softer than specimen TTC03. This is maybe because TTC01 contains higher moisture content than specimen TTC03. It is very interesting that the only difference between reconstituted TTR01 and TTR02 is that visually TTR01 look wetter than TTR03 as it should be. There is no significant visual presence of pores. The preparation method of the reconstituted specimen at 55% moisture content and subsequent drying intervals may influence the ability to distinguish the pores. The increasing suction during drying process led to clay particle drawn towards each other. However the FESEM requires very small size specimen for analysis, which could also miss some of the defined pore size that might have been lying outside the image analysis zone.

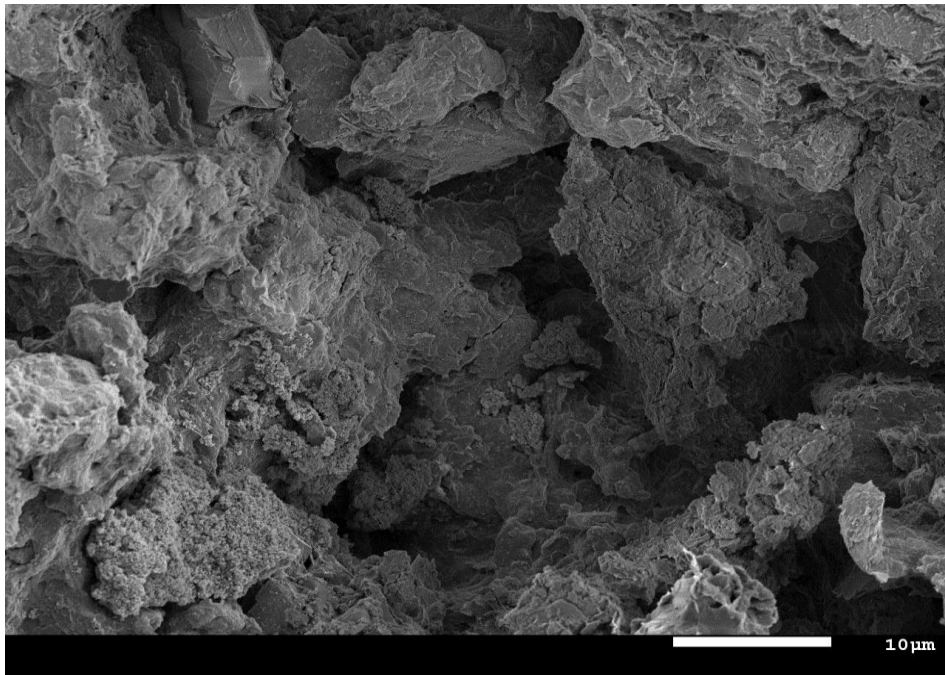


Figure 6.25a: ESEM micrograph for compacted specimen TTC03 (23.600 w%, 1.56 mg/m³).

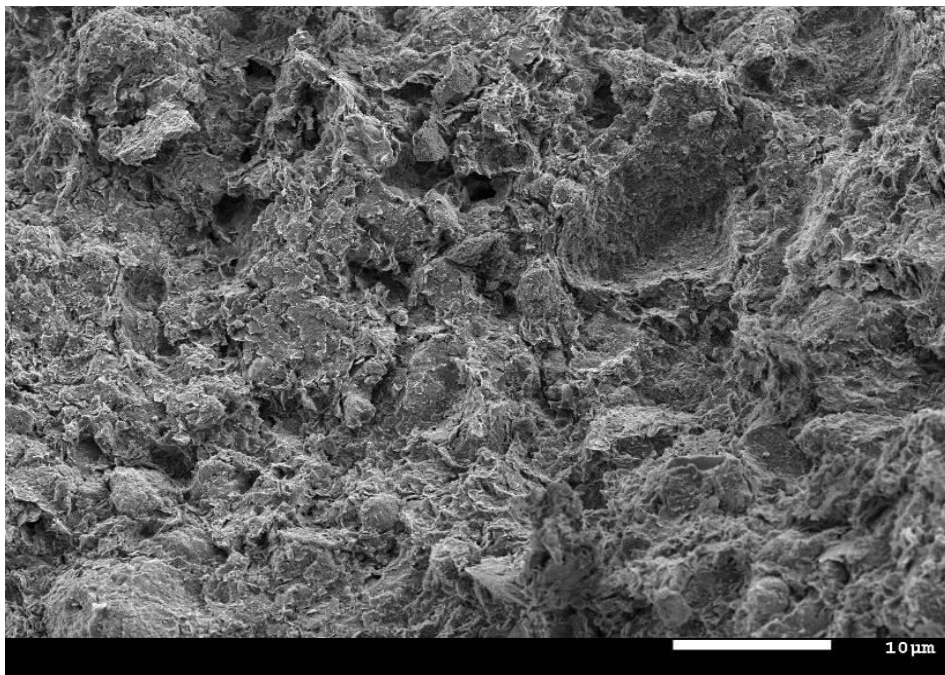


Figure 6.25b: ESEM micrograph for reconstituted specimen TTR03 (24.005 w%, 1.57 mg/m³); soil aggregate not well defined.

6.8 WATER RETENTION BEHAVIOUR

Suction was measured by WP4 potentiometer (Model WP4, Decagon Devices, 2003). This method determines total suction by measuring the dew point humidity of the space just above the sample. It provides a quick and accurate method for measuring larger suction values in the range of 1 to 100 MPa. Figure 6.27 shows the water retention behaviour (main retention wetting/drying path) for reconstituted specimen. As expected, the two pathways produce curves that are not identical. In most cases, these pathways are not identical and the drying curve is higher for a given suction than that in the wetting branch. This phenomenon in retention curve is known as hysteresis.

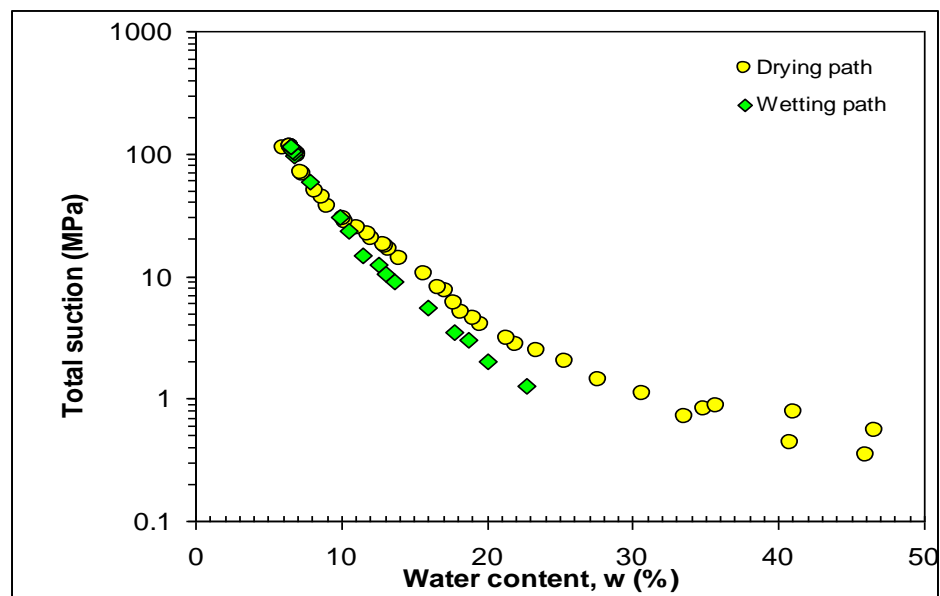


Figure 6.26: The main retention wetting/drying path for reconstituted specimen of Bengawan Solo soil.

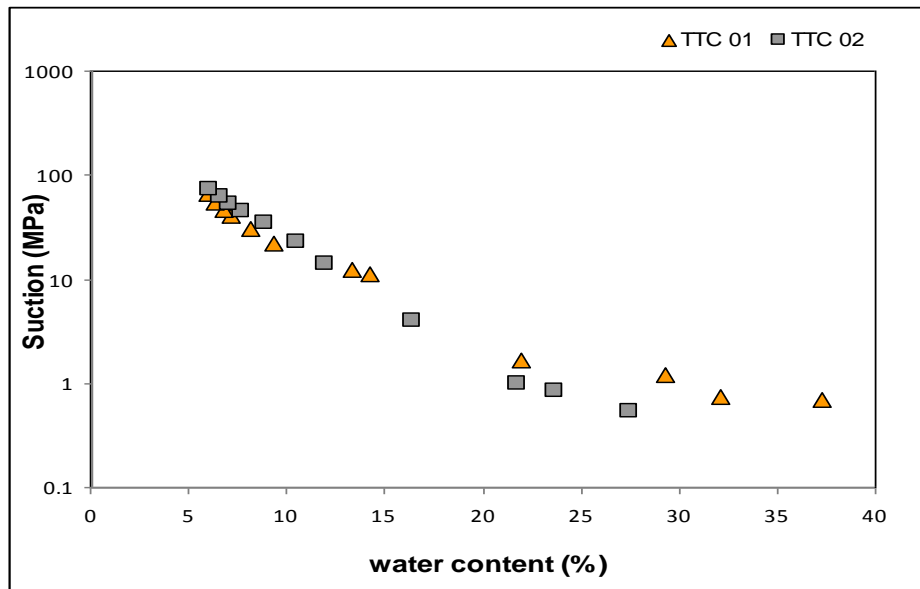


Figure 6.27: Water retention curve for Bengawan Solo soil compacted at different dry densities and water content.

Figure 6.27 shows the water retention curve for Bengawan Solo soil at different dry densities for compacted specimens. Figure 6.28 shows the suction for reconstituted and compacted specimen. Both samples have higher suction values around 100 MPa, though the curves for compacted specimen are steeper than that of the reconstituted specimen. For both curves, the moisture content increases as suction decreases. High suction values are principally controlled by the intra-aggregate pores. This can be observed with the characteristic curves (Figure 6.27) for different densities, where the compaction affects the macro-pore distribution, which has considerably little effect on high suction values for the soil. This was also reiterated in the work of Romero et al. (1999).

All the experimental results determined (retention curve for reconstituted and compacted specimen) are presented in Figure 6.28. It is evident that the curve for reconstituted specimen lies above the two compacted curves. This difference may be explained by the reconstituted specimen undergoing shrinkage during drying. This shrinkage results in higher dry densities during drying and may shift the curve

upwards from the compacted curves. In addition, reconstituted specimens contain higher water contents than compacted specimens as a result of the preparation method, so the initial evaporation rate from reconstituted specimens may have been higher compared to compacted specimen. At lower water content, the TTC01 curve almost matches with the curve of the reconstituted specimen.

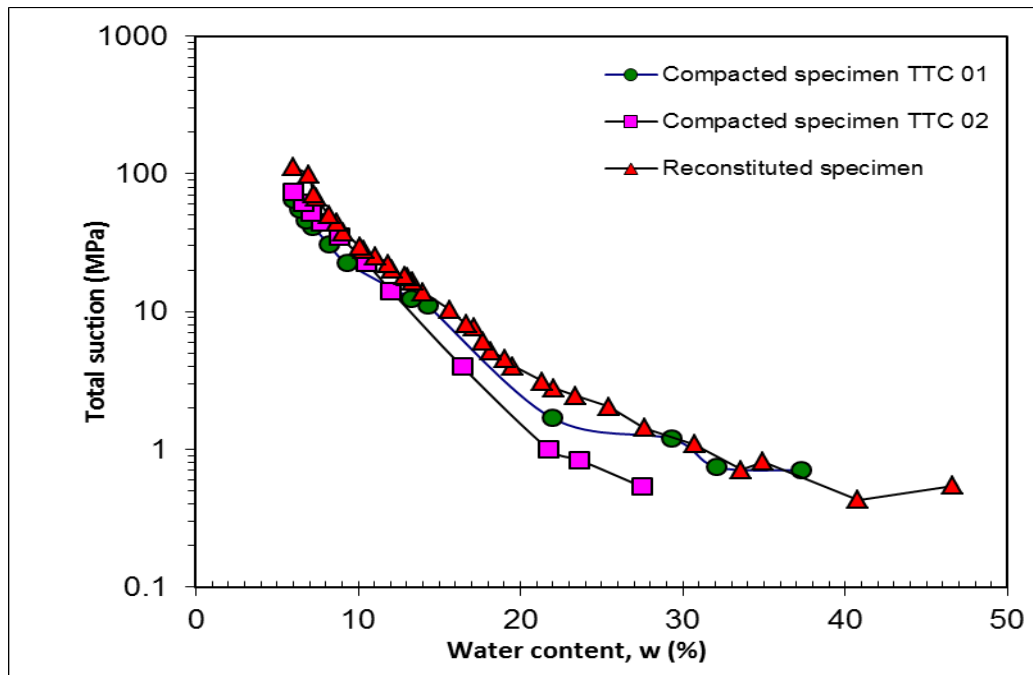
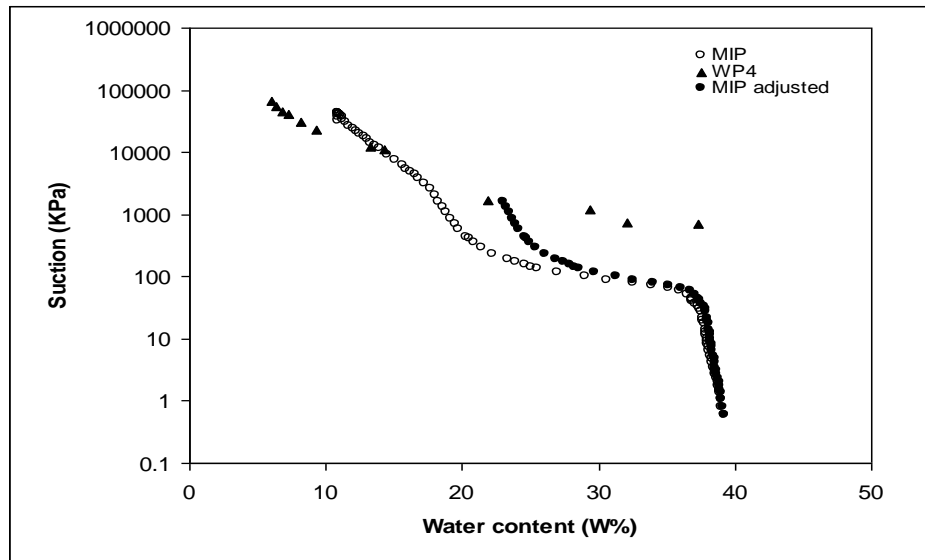


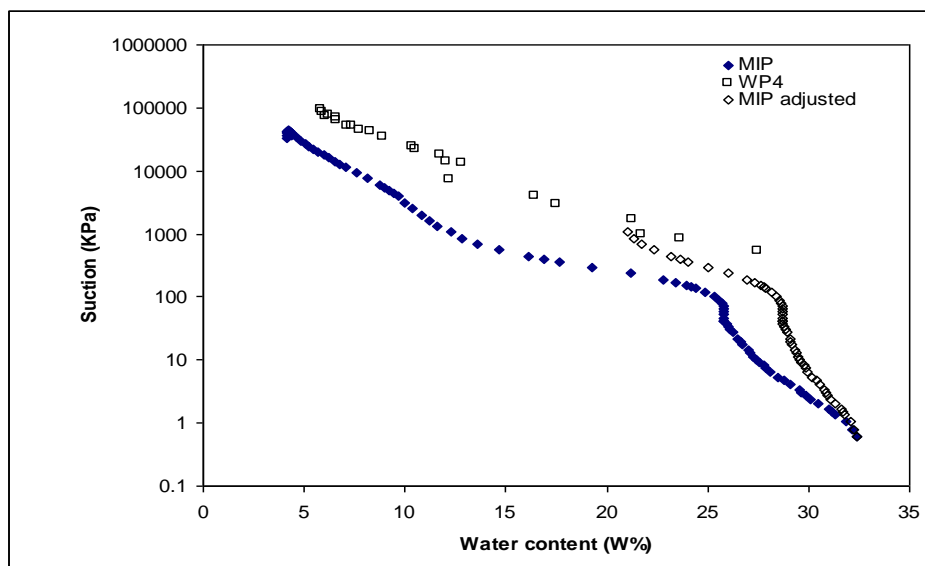
Figure 6.28: Retention curve for reconstituted specimen and compacted specimen at two dry densities and water content.

Retention curve was also estimated from MIP plot in order to have a comparison between the two methods. Figure 6.29 shows the water retention curves estimated from MIP and plotted together with the high suction range from psychrometer readings for compacted specimen TTC 01 and TTC 02. The retention behaviour determined using MIP and from experimental data might not be the same as in MIP technique only the retention of water due to the capillary effects is considered and any water held by adsorptive force is ignored. Also this technique assumes that the material is non-deformable under drying paths. This assumption is not true for expansive clays which undergo volume changes while drying. However, the adjusted

MIP plot matches the high suction range from psychrometer readings (Figure 6.29a, b).



Compacted specimen TTC 01 (36.119%, 1.32 mg/m³)



Compacted Specimen TTC2 (30.432%, 1.43 mg/m³)

Figure 6.29: Water retention curve for Bengawan Solo soil at compacted condition estimated from MIP.

In general, reasonable agreement was found with respect to the shape of the retention curves estimated from MIP and WP4 method. Figure 6.30 shows the water retention curves (estimated from MIP) for reconstituted specimen TTC04 and TTR04. They match the high suction range from psychrometer readings from El Mountassir's (2011) test results.

If one assumes tensile strength as two multiplicative functions, one dependent on void ratio and the other one suction (Trabelsi et al., 2011), then the term associated with suction (tensile strength increases with suction) will display a lower value for the compacted material. The variation of tensile strength with porosity has been observed previously (Trabelsi et al., 2011). As shown in the estimated water retention curves, for the same water content (ranging in the domain in which water retention curve is sensitive to void ratio), the compacted material will display a lower suction and consequently a lower tensile strength (for the same total porosity).

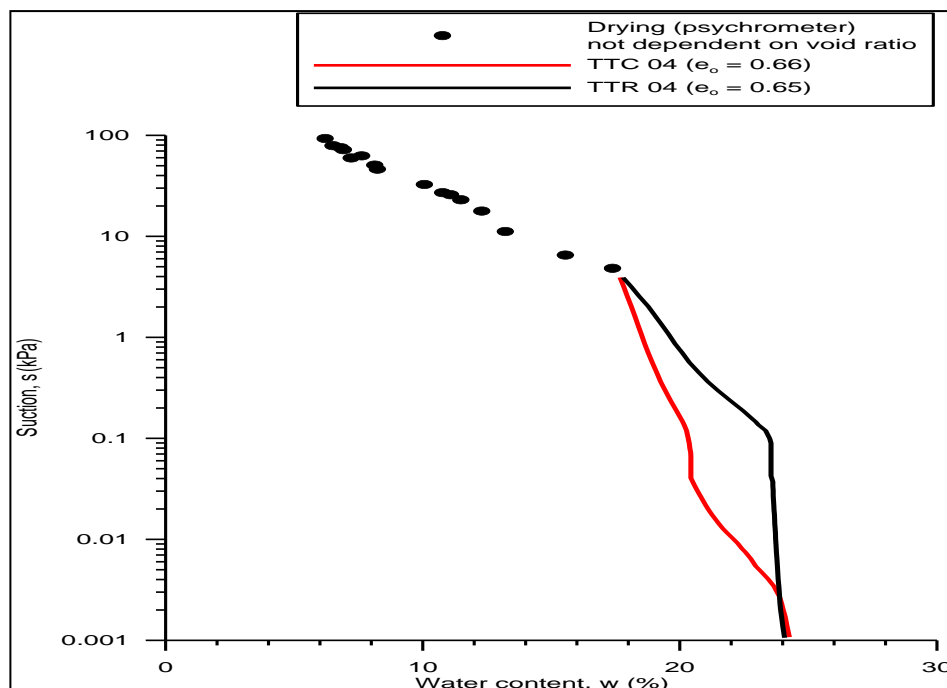
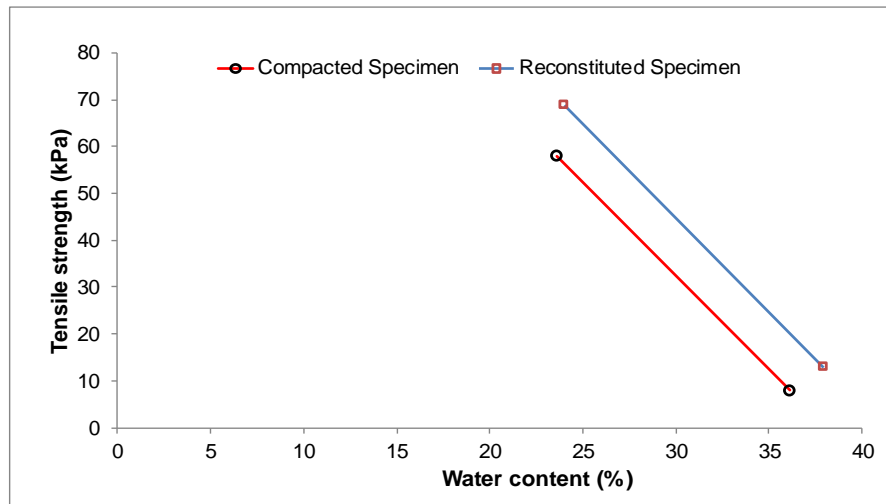


Figure 6.30: Water retention curve for Bengawan Solo soil at compacted and reconstituted condition for higher dry density estimated from MIP; compared with the test results of El Mountassir (2011).

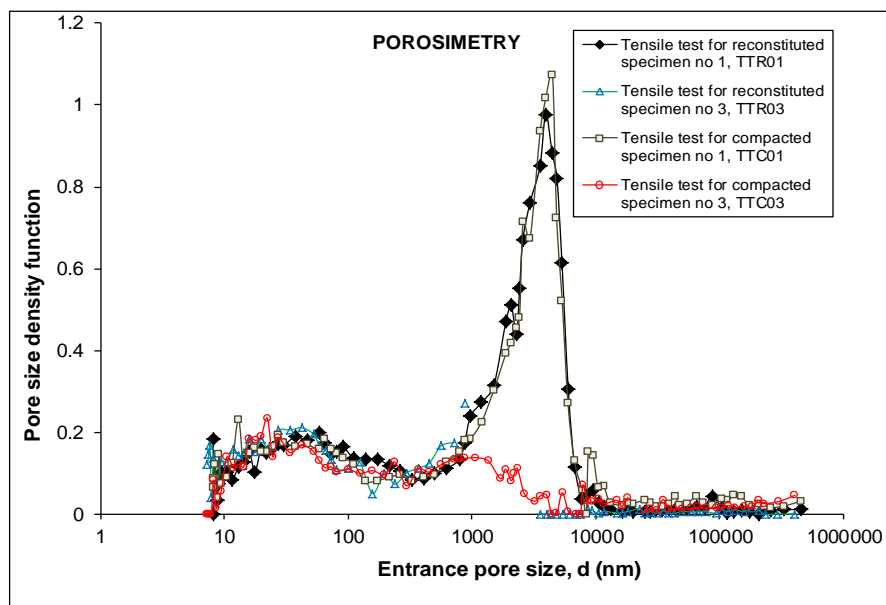
6.9 SUMMARY

A summary of the results is presented in Figure 6.31a, b, c for reconstituted samples TTR01, TTR03 and compacted samples TTC01, TTC03. The MIP of the compacted sample TTC01 displayed larger macroporosity than for TTR01 with a dominant pore mode around 5 μm . This larger pore size is associated with a lower air-entry value. In general, soils with small pores only exhibit higher strength than soil with large pores, and as well as soil with different pores. If tensile strength is assumed to be controlled by the loss of continuity of water (cavitation associated with the air-entry value), then the compacted specimen will display a lower value for tensile strength and this was consistent with experimental findings. This larger pore size is associated with a lower air-entry value. Evidence of these pore sizes found in the corresponding FESEM specimen especially in compacted specimens. Unfortunately, the FESEM for reconstituted specimen were unsatisfactory as the arrangement of the soil aggregates was impossible to see in both TTR01 and TTR03.

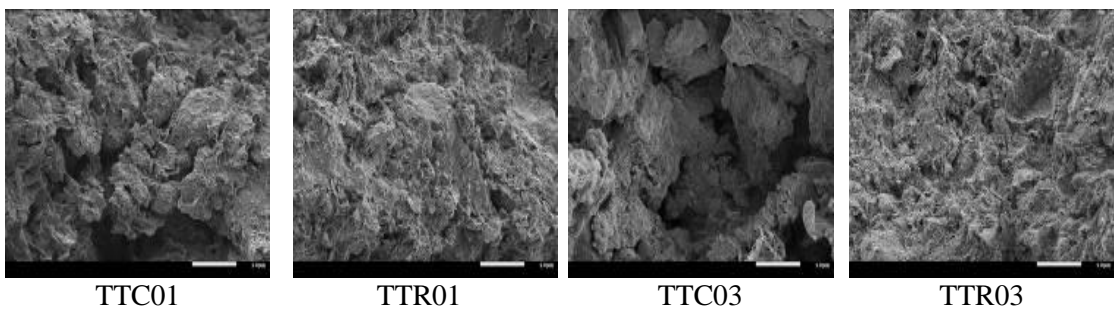
The MIP plots complement the fact that the number and size of the pores and aggregates are strongly influenced by the compaction energy for the compacted specimen. The MIP curve patterns for both specimen matches and yet interestingly the FESEM image does not show the inter-aggregate pore sizes for the reconstituted specimens. The image (Figure 6.31c) shows larger pores in compacted material than the reconstituted material. However, swelling clays such as smectites always cause higher strength than clays constituted of other minerals. The presence of montmorillonite in Bengawan Solo clay was evident X-ray diffraction. This might attribute to the fact that Bengawan Solo clay changes significantly during drying, which may be responsible for higher tensile strength values measured for reconstituted specimens than for compacted specimens.



(a)



(b)



(c)

Figure 6.31: Summary of tensile test campaign for Reconstituted and Compacted specimen; (a) Tensile strength, (b) MIP results at different dry densities, (c) FESEM micrograph at different dry densities.

6.10 CONCLUSION

In this chapter a series of test were performed to study the tensile strength of Bengawan Solo Soil. The tensile test results showed an increase in the tensile strength during drying. Specimens of different dry densities reached different magnitudes of tensile strength. A good agreement is obtained between reconstituted and compacted specimens. Compacted specimens were found to have larger pore sizes than reconstituted specimens. In general, soils with small pores only exhibit higher strength compared to soil with large pores as well as soil with different pores. Pore size distribution has a large effect of types of tensile failure (Snyder and Miller, 1985). According to Snyder and Miller (1985), soils at normal field conditions have a higher proportion of small pores and few large pores. In this case, sharp cracks will appear along the large pores and tensile failures will initiate in only few places within the soil mass. The high value of pore water within this type of soil structure explains the hard consistency exhibited by these soils and can be compared here with reconstituted soil. FESEM results complement this observation, showing a complex and dense soil matrix for reconstituted samples at two different water contents. Tensile failure that occurs in reconstituted soil is very defined. On the other hand, well-aggregated soil under normal field conditions possesses a large amount of unsaturated pores with correspondingly low values of tensile force (Snyder and Miller, 1985). This type of soil can be compared here in with compacted specimen that exhibit similar structure. In this research, the tensile strength for the compacted specimens was clearly lower than for reconstituted specimens, and this was consistent with previous experimental findings. According to Snyder and Miller (1985), cracking will occur at many points within the soil mass and result in a crumbling effect. Crumbling is evident in the tensile failure pattern of the soil here.

The presence of montmorillonite in Bengawan Solo clay results in important changes during drying that may be responsible for higher tensile strength values for reconstituted specimens than compacted specimens. During construction of earth fill embankments where traditional compaction methods are used as in the Bengawan Solo fill embankments, it is difficult to control water content and compactive effort. Seasonal variation could lead the soil structure to a reconstituted state fully and it is

difficult to maintain the soil at original compacted state. That means the soil throughout the embankments contains variable water content, dry densities and structure. These results are important from practical perspective for this kind of construction work. Testing should be carried out for a wide range of soil to develop detailed information of soil structure.

Chapter 7: Conclusions and recommendations for future work

7.1 CONCLUSIONS

A novel, 2D/3D laser scanning system was developed to study desiccation cracking in the clay-rich Bengawan Solo embankment soil. This device combines the laser scanner with a computerized motion controller and an electronic balance to capture precise images during all stages of desiccation cracking. This technique allowed for the capture of the evolution of key local variables associated with the desiccation cracks: crack initiation, crack propagation, volume change, and distribution of settlements on the soil surface over time, crack aperture, and three-dimensional crack network morphology during drying. This system makes significant improvements over previous techniques that relied solely on image surfaces or destructive sampling methods.

The 2D/3D laser scanner was found to yield similar information on changes to the soil surface as to digital camera images. The 3D reconstructions of crack formation and propagation provided a significant advance over digital camera images that are inherently limited to the soil surface.

The test results showed that initially, shrinkage was associated with settlement only. The first crack appeared consistently around 4 hours of drying, at the early stages of shrinkage. It was evident from the results that the first crack to appear reached the maximum depth first. Further cracks formed as drying time increased. Once formed, cracks continued to extend downward, limited by the plate boundaries. This process continued for 16 to 18 hours until a settled surface cracking pattern was established. When the water content approached the shrinkage limit, the crack development approached a steady state. From 18 hours to 60 hours, the average spacing of these cracks did not change very much.

The volumetric shrinkage measured by the laser was found to closely agree with the value determined using one of the traditional volumetric shrinkage measurement procedures given in BS 1377-4:1990. The experimental outcomes demonstrated that the laser scanning technique achieved significantly more information in less time than can be obtained using current methods.

Tensile strength was experimentally determined for both reconstituted and compacted samples using a direct method. Preparation of specimens and transfer to the testing device allowed for the study of the evolution of tensile strength at cracking following a drying path. Previous methods of preparing the specimens in the testing apparatus would not have been appropriate for this study. Cutting the specimens to fit the testing device required precision. Soil moisture content and dry density were found to influence the tensile strength. As dry density of the soil increased moisture content at cracking Decreased. This effect was found most significant for specimens at lower water content compared to specimens at higher water content.

Aggregate formation during soil specimen preparation seemed to affect the microstructure. Mercury Intrusion Porosimetry (MIP) and the Field Emission

Scanning Electron Microscope (FESEM) showed that macroporosity was evident in compacted specimens and absent in reconstituted specimens. The tensile strength for the compacted specimens was found to have lower values than the reconstituted specimens. The pore size distribution had a significant effect on the type of tensile failure. Well-aggregated soil consisted of large amounts of unsaturated pores with correspondingly low values of tensile strength.

Desiccation plate tests showed that at the initial stage of drying the sample tended to dry with a fast and gradual decrease of water content. Cracking initiated at different places on the surface at high water content, close to the soil's liquid limit. In the first stage of crack-pattern development, cracks tended to meet at a small number of points. These cracks then propagated laterally in fairly straight lines, occasionally meeting another crack moving in a similar manner and forming a polygonal pattern. Vertical propagation of cracks was observed to be simultaneous to lateral propagation. When the water content approached the shrinkage limit, cracks approached a steady state forming a complete crack network at the surface. Water content loss decreased at this stage. The final stages of drying were governed by vertical propagation of existing cracks and complete drying of the soil without any new crack formation.

Different plate geometries influenced the final cracking pattern, but not the cracking mechanisms. Desiccation rate, cracking cell shape, and cracking width were found to be different for three different soil thicknesses, but crack formation followed similar patterns in all plate depths and geometries. Crack propagation was limited to a short initial period of the desiccation process, beginning approximately 4 hours after the start of each test; 90% of crack development occurred during 20-30 hours of the drying period. Tests continued for 170-200 hours to ensure the crack network was fully-formed within the soil specimens. For the same drying area, cracking was found to be highly influenced by the soil layer thickness.

The presence of the smectite mineral montmorillonite in the Bengawan Solo clay seemed to be responsible for higher tensile strength values for reconstituted specimens when compared to compacted specimens. Linear shrinkage and volumetric shrinkage of the soil were found to be moderate to high. The significant

amount of smectite minerals (montmorillonites) influenced the plasticity and strength property of soil. The ratio of the liquid limit to shrinkage limit (LL/SL) was found to be low, which indicated that the Bengawan Solo soil did not exhibit undesirable volume change due to shrinkage during seasonal moisture change, but the soil did exhibit a high potential for desiccation and cracking. The results showed that the material exhibits cracking at highly-saturated conditions, close to its liquid limit of 55%. These observations have important implications for field performance of the embankment. Significant variations between the wet and dry seasons lead to long periods of drying where the embankment soil is vulnerable to cracking.

7.2 RECOMMENDED FURTHER WORK

The 2D/3D laser scanning methodology was used to study the behavior of drying soils in this work. This methodology provided significant advances over previous image methods that were limited to surface analysis and allowed for the 3D reconstruction of soil samples. This method has a wide range of further applicability in the study of soil behaviour and other engineering applications.

The 3D information generated by the scanning system can be used to model soil behavior; for example, changes in porosity of the intact soil can be used to estimate the changes in its permeability. Changes in crack geometry can be tracked and then used to develop models accounting for the effect of cracks on flow and evaporation.

The laser used in present work offered a small scanning area, and hence the present test set-up would be an obstacle in investigating the desiccation of larger specimens. Development of a larger-scale scanning system would be beneficial. One of the challenges in this work was the influence of lower boundaries on crack propagation. A larger-scale system would allow for the examination of larger specimens and is highly recommended for future work.

Study of crack morphology can be helpful in determining the origin of the cracks in geological time. Better understanding of the mechanisms involved in the formation

of crack patterns may lead to advances in characterisation and dating of cracking at the field scale, allowing for the identification of important morphological features. The tests performed were small in scale but informative and this data may be useful for morphological investigations in the future.

The variables that are important for tensile failure including pore water pressure, pore air pressure, and moisture condition are strongly interrelated in other aspects of the mechanical behaviour of unsaturated soils. The comparison of tensile strength between reconstituted and compacted states can be studied across a wide range of moisture content and dry density values as well as the tensile strength of soil-cement mixes given that are used routinely in a variety of construction projects.

Conceptual modelling by previous researchers is complex and specific to particular geotechnical applications. For example, models applied to desiccation of clay liners, compacted soils, mine tailings, and soft soils are highly specific. There are some general models but their applicability is limited to certain types of soils, and the complexity of using more than one concept to explain the whole mechanism is apparent. The initial step in modelling is to develop theoretical formulations based on experimental observations by applying basic concepts of fundamental principles. The present work is an experimental investigation and the test data could be used for further theoretical formulations. The data available from this work provide a good starting point for future mechanistic exploration of cracking behaviour in drying soils.

REFERENCE

- ABEDINE, Z. E., ROBINSON, G. H. & COMMISSA, A. 1971. Approximate Age of Vertisols of Gezira, Central Clay Plain, Sudan. *Soil Science*, 111.
- ABU-HEJLEH, A. N. & ZNIDARCIC, D. 1995. Desiccation Theory for Soft Cohesive Soils. *Journal of Geotechnical Engineering-Asce*, 121, 493-502.
- ADAMCEWICZ, A. S., MUHUNTHAN, B. & MASAD, E. 1997. Soil fabric changes during consolidation. *Geotechnical Testing Journal*, 20, 347-356.
- AGUS, S. S. & SCHANZ, T. 2005. Comparison of four methods for measuring total suction. *Vadose Zone Journal*, 4, 1087-1095.
- AGUS, S. S. & SCHANZ, T. 2007. *Errors in total suction measurements. Experimental Unsaturated Soil Mechanics*, pp. 59–70.
- AHMED, S., LOVELL, C., W. J., & DIAMOND, S. 1974. Pore size and strength of compacted clay. *Journal of the Geotechnical Engineering Division, ASCE*, 100(4), 407-425.
- AIRÒ FARULLA, C., FERRARI, A. & ROMERO, E. 2010. Volume Change Behaviour of a Compacted Scaly Clay During Cyclic Suction Changes. *Canadian Geotechnical Journal*, 47, 688–703, doi:10.1139/T09-138.
- AITCHINSON, G. D. & HOLMES, J. W. 1953. Aspects of swelling in the soil profile. *Aust. J. Appl. Sci.*, 4, 244–259,.
- AJAZ, A. & PARRY, R. H. G. 1975. Stress-Strain Behavior of 2 Compacted Clays in Tension and Compression. *Geotechnique*, 25, 495-512.

- AKROYD, T. N. W. 1964. *Laboratory Testing in Soil Engineering*, Soil Mechanics Limited, 65 OLD CHURCH STREET, LONDON, S.W.3.
- AL-ALSHAYEA, N. 2001. The combined effects of clay and moisture content on the behavior of remolded unsaturated soil. *Engineering Geology*, 62:319–342.
- AL-HUSSAINI, M. 1981. *Tensile Properties of Compacted Soils, Laboratory Shear Strength of Soil*, R. N. Young and F. C. Townsend, Eds., ASTM International, pp. 207–225.
- ALBRECHT, B. A. & BENSON, C. H. 2001. Effect of desiccation on compacted natural clays. *Journal of Geotechnical and Geoenvironmental Engineering*, vol. 127, pp. 67-75.
- ALONSO, E., OLIVELLA, S. & ARNEDO, D. 2006. Mechanisms of gas transport in clay barriers. *Journal of Iberian Geology*, 32, 175-196.
- ALONSO, E. E., GENS, A. & HIGHT, D. W. Groundwater effects in geotechnical engineering. Proceedings of the 9th European Conference on Soil Mechanics and Foundation Engineering, 1987 Dublin, Ireland. A. A. Balkema / Rotterdam / Brookfield.: E. T. Hanrahan, T. . L. L. Orr, and T. F. Widdis, eds.
- ALONSO, E. E., GENS, A. & JOSA, A. 1990. A Constitutive Model for Partially Saturated Soils. *Geotechnique*, 40, 405-430.
- ALONSO, E. E. & LLORET, A. Settlement of a 12 storey building due to desiccation induced by trees. a case study. 1st Intl. Conf. on Unsaturated Soils, 1995 Paris, France.
- ALSHIBLI, K. A. & AL-HAMDAN, M. Z. 2001. *Estimating Volume Change of Triaxial Soil Specimens from Planar Images* [Online]. *Comput. Aided Civ. Infrastruct. Eng.*, Vol. 16, No. 6, pp. 415–421.

- ALSHIBLI, K. A. & STURE, S. 2000. "Shear Band Formation in Plane Strain Experiments of Sand". *ASCE, Journal of Geotechnical & Geoenvironmental Engineering*, , Vol.126, No. 6, pp. 495-503.
- ALTHER, G., EVANS, J. C., FANG, H. Y. & WITMER, K. 1985. Influence of inorganic parameants upon the permeability of Bentonite, *Hydraulic Barriers in Soil and Rock. ASTM Special Technical Publication (STP)*, pp 64-73.
- ANDREWS, R. E., GAWARKIEWICZ, J. J. & WINTERKORN, H. F. 1967. Comparison of the interction of the three clay minerels with water, dimethyl sulfoxide and dimethyl formamide. Highway Research Reord No. 209,pp. 66-78.
- ATIQUE, A. & SANCHEZ, M. Investigation of crack desiccation in soil from a flood protection embankment. Proceedings of 4th Asia-Pacific Conference on Unsaturated Soils, 23-25 November 2009 2009 Newcastle, Australia. 413-418.
- AVERSA, S. & NICOTERA, M. V. 2002. A triaxial and oedometer apparatus for testing unsaturated soils. *Geotechnical Testing Journal*, 25, 3-15.
- BABU, G. L. S. & GARTUNG, E. 2001. Methodology for predection of desiccation of clay liners. *Clay science for Engineering, Adachi and Fukue eds*, 187-190.
- BAGGE, G. Tension cracks in saturated clay cuttings. 11th Int. Conf. on Soil Mechanics and Foundation Engineering, 1985 San Fransisco. 393-395.
- BAKER, R. 1981. Tensile strength,tension cracks and stability of slopes. *Soils and Foundations*, 21, 1-17.
- BARBOUR, S. L. 1998. Nineteenth Canadian Geotechnical Colloquium: The soil-water characteristic curve: a historical perspective. *Canadian Geotechnical Journal*, 35, 873-894.

- BARDEN, L., MCGOWN, A. & COLLINS, K. 1973a. Collapse Mechanism in Partly Saturated Soil. *Engineering Geology*, 7, 49-60.
- BARDEN, L., MCGOWN, A. & COLLINS, K. 1973b. The collapse mechanism in partly saturated soil. *Eng Geol*, 7, 49-60.
- BARDEN, L. & SIDES, G. R. 1970. Engineering behaviour of structured compacted clay. *J Soil Mech Found Div ASCE*, 96 SM4, , 1171-1201.
- BASNETT, C. & BRUNGARD, M. 1992. The Clay Desiccation of a Landfill Composite Lining System. Geotechnical Fabrics Report, Industrial Fabrics Association International.
- BAUMGARTL, T., WINKELMAN, P., GRAESLE, W., RICHARDS, B. G. & HORN, R. Measurement of the interaction of soil mechanical properties and hydraulic processes with modified triaxial test. Proc. 1st Int. Conf on Unsaturated Soils UNSAT'95 2, pp-433-438,, 1995. Paris, Balkema, Rotterdam.
- BIDDLE, P. G. 1983. Patterns of Soil Drying and Moisture Deficit in the Vicinity of Trees on Clay Soils. *Geotechnique*, 33, 107-126.
- BISHOP, A. W. & DONALD, I. B. The experimental study of party saturated soil in the triaxial apparatus. Proc. 5th Conf. On Soil Mechanics and Found Eng. 1, 13-21., 1961.
- BISHOP, A. W. & GARGA, V. K. 1969. Drained Tension Tests on London Clay. *Géotechnique*, Vol. 19, pp. 309–313.
- BLIGHT, G. E. & 1997. *Origin and formation of residual soils. Mechanics of Residual Soils*, Balkema, Rotterdam.
- BOIVIN, P., GARNIER, P. & TESSIER, D. 2004. Relationship between clay content, clay type, and shrinkage properties of soil samples. *Soil Science Society of America Journal* 68, 1145–1153.

- BOSO, M. 2005. *Shear strength behaviour of reconstituted partially saturated clayey silt. PhD dissertation.* Universita degli Studi di Trento, Italy.
- BRIAUD, J. L., ZHANG, X. & MOON, S. 2003. Shrink test-water content method for shrink and swell predictions. *Journal of Geotechnical and Geoenvironmental Engineering*, 129 (7), 590–600 ASCE.
- BRONSWIJK, J. J. B. 1990. Shrinkage Geometry of a Heavy Clay Soil at Various Stresses. *Soil Science Society of America Journal*, 54, 1500-1502.
- BRONSWIJK, J. J. B. 1991a. Drying, Cracking, and Subsidence of a Clay Soil in a Lysimeter. *Soil Science*, 152, 92-99.
- BRONSWIJK, J. J. B. 1991b. Relation between Vertical Soil Movements and Water-Content Changes in Cracking Clays. *Soil Science Society of America Journal*, 55, 1220-1226.
- BROSSARD, C., MONNIER, J.-C., BARRICAU, P., VANDERNOOT, F.-X., LE SANT, Y., F., C. & LE BESNERAIS, G. 2009. Principles and Applications of Particle Image Velocimetry. *Aerospace Lab Journal*, No. 1.
- BS1377-2:1990 1990. *Methods of test for soils for civil engineering purposes - part 2: Classification tests.*
- BS2742C:1957 1957. ingelmann chart.
- BULUT, R., LYTTON, R. L. & WRAY, W. K. Soil suction measurement by filter paper. *In: 115*), E. C. S. A. V. I. O. S. F. G., ed. *Proceedings of the Geo-Institute Shallow Foundation and soil Properties*, 2001. 243-261.
- BURLAND, J. B. 1990. 30th Rankine Lecture - on the Compressibility and Shear-Strength of Natural Clays. *Geotechnique*, 40, 329-378.

- CARTER, M. 1990. Relationship of strength properties to bulk density and macroporosity in cultivated loamy and to loam soils. . *Soil and Tillage Research* . 15:257–268.
- CHANDLER, R. J. & GUTIERREZ, C. I. 1986. The filter-paper method of suction measurement. *Geotechnique*, 36, 265-268.
- CHANDLER, R. J., HARWOOD, A. H. & SKINNER, P. J. 1992. Sample disturbance in london clay. *Geotechnique*, 42, 577-585.
- CLAYTON, C. R. I. & KHATRUSH, S. A. 1986. A New Device for Measuring Local Axial Strains on Triaxial Specimens. *Geotechnique*, 36, 593-597.
- COLE, D. M. 1978. Technique for Measuring Radial Deformation During Repeated Load Triaxial Testing. *Canadian Geotechnical Journal*, 15, 426-429.
- COLINA, H. & RONUX, S. 2000. Experimental model of cracking induced by drying shrinkage. *The European Physical J. E*, 1: 189-194.
- COLINA, H. & ROUX, S. 2000. Experimental model of cracking induced by drying shrinkage. *European Physical Journal E*, 1, 189-194.
- COLLINS, K. & MCGOWN, A. 1974a. Form and Function of Microfabric Features in a Variety of Natural Soils. *Geotechnique*, 24, 223-254.
- COLLINS, K. & MCGOWN, A. 1974b. The form and function of microfabric features in a variety of natural soils. *Géotechnique*, 24(2), 223-254.
- COOLING, L. F. & MARSLAND, A. Soil Mechanics of Failures in the sea Defence Banks of Essex and Kent. ICE Conference on the North Sea Floods of 31 January/ 1 February, 1953.
- CORTE, A. & HIGASHI, A. 1960. Experimental research on desiccation cracks in soil. *U.S Army Snow Ice and Permafrost Research Establishment*. Report No,66:Corps of Engineers Wilmette Illinois U.S.A.

- COSTA, S. & KODIKARA, J. Investigation of Desiccation Cracking Using Automated Digital Photography. 10th ANZ Conference on Geomechanics, 2007. pp. 338–343.
- CUI, Y. J. & DELAGE, P. 1996. Yielding and plastic behaviour of an unsaturated compacted silt. *Geotechnique*, 46, 291-311.
- DAS, B. M. 2009. *Soil Mechanics Laboratory Manual*, New York Oxford, OXFORD UNIVERSITY PRESS.
- DASOG, G. S., ACTON, D. F., MERMUT, A. R. & DE JONG, E. 1988. Shrink-swell potential and cracking in clay soils of Saskatchewan. . *Can. J. of Soil Sci.*, 68: 251-260.
- DE JONG, E. & WARKETIN, B. P. 1965. Shrinkage of soil samples with varying clay concentration. *Canadian Geotechnical Journal*, vol.11,n.1, pp.16-22.
- DELAGE, P. & GRAHAM, J. Understanding the Behavior of Unsaturated Soils Requires Reliable Conceptual Model, State of the Art Report. Proceedings, 1st International Conference on Unsaturated Soils, 1995 Paris, France, 1995. pp. 1223–1256.
- DELAGE, P. & LEFEBVRE, G. 1984a. Study of the Structure of a Sensitive Champlain Clay and of Its Evolution During Consolidation. *Canadian Geotechnical Journal*, 21, 21-35.
- DELAGE, P. & LEFEBVRE, G. 1984b. Study of the structure of a sensitive champlain clay and of its evolution during consolidation. *Can Geotech J*, 21, 21-35.
- DELAGE, P., MARCIAL, D., CUI, Y. J. & RUIZ, X. 2006. Ageing effects in a compacted bentonite: a microstructure approach. *Geotechnique*, 56, 291-304.
- DELAGE, P., TESSIER, D. & MARCEL-AUDIGUIER, M. 1982. "Use of the cryoscan apparatus for observation of freeze-fractured planes of a sensitive quebec

- clay in scanning electron microscopy." *Can Geotech J*, 21, 21-35., 19(1), 11-114.
- DEXTER, A. R. & KROESBERGEN, B. 1985. Methodology for Determination of Tensile-Strength of Soil Aggregates. *Journal of Agricultural Engineering Research*, 31, 139-147.
- DIAMOND, S. 1970. Pore size distribution in clays. *Clays Clay Miner*, 18, 7-23.
- DRISCOLL, R. 1983. The Influence of Vegetation on the Swelling and Shrinking of Clay Soils in Britain. *Geotechnique*, 33, 93-105.
- EL MOUNTASSIR, G. 2011. *Behaviour of a collapsible, structured,unsaturated fill material*. PhD A Thesis presented for the Degree of Doctor of Philosophy, University of Strathclyde.
- FANG, H. Y. 1997a. *Introduction to Environmental Geotechnology*, CRC press.
- FANG, H. Y. 1997b. *Introduction to Environmental Geotechnology*, CRC Press,Boca Raton. FL.
- FANG, H. Y. & DANIELS, J. L. 2006. *Introductory Geotechnical Engineering: An Environmental Perspective* Taylor & Francis, LONDON AND NEW YORK.
- FANG, H. Y. & HIRST, T. J. 1973. A Method for Determining the Strength Parameters of Soils. *Highway Research Record*, Vol. 463, pp. 45–50., Vol. 463, pp. 45–50.
- FLEUREAU, J. M., KHEIRBEKSAOUD, S., SOEMITRO, R. & TAIBI, S. 1993. Behavior of Clayey Soils on Drying Wetting Paths. *Canadian Geotechnical Journal*, 30, 287-296.
- FOOKES, P. G. & DENNESS, B. 1969. Observational studys of fissure patterns in cretaceous of south-east England. *Geotechnique*, 19:453-477.

- FRYDMAN, S. 1964. The Applicability of the Brazilian (Indirect Tension) Test to Soils. *Australian Journal of Applied Science*, Vol. 15, pp. 335–343.
- GACHET, P., GEISER, F., LALOUI, L. & VULLIET, L. 2006. Automated Digital Image Processing for Volume Change Measurement in Triaxial Cells. *Geotechnical Testing Journal*, Vol. 30, No. 2.
- GEISER, F., LALOUI, L. & VULLIET, L. On the volume measurement in unsaturated triaxial test. Proc. Conf. Unsaturated Soils for Asia, Unsat-Asia 2000, pp-669-674,, 2000 Balkema, Rotterdam.
- GENS, A., ALONSO, E. E., SURIOL, J. & LLORET, A. Effect of structure on the volumetric behaviour of a compacted soil. Proc. 1st Int. Conf. on Unsaturated Soils, volume-1, pp-83-88, 1995 Paris. 83-88.
- GOMEZ, R., ROMERO, E., LLORET, A. & SURIOL, J. Characterising the collapsible response of an in-situ compacted silt. pp371-376. Proc. of 4th Asia Pacific Conference on Unsaturated Soils, 2009. CRC Press.
- GRIFFITHS, D. V. & LU, N. 2005. Unsaturated slope stability analysis with steady infiltration or evaporation using elasto-plastic finite elements. *Int. J. Numer. Analyt. Meth. Geomech.*, 29, 249–267.
- GRIFFITHS, F. J. & JOSHI, R. C. 1989a. Change in Pore-Size Distribution Due to Consolidation of Clays. *Geotechnique*, 39, 159-167.
- GRIFFITHS, F. J. & JOSHI, R. C. 1989b. Changes in pore size distribution due to consolidation of clays. *Géotechnique* 1, 159-167.
- GRIFFITHS, F. J. & JOSHI, R. C. 1989. Changes in pore size distribution due to consolidation of clays. *Géotechnique*, 1, 159-167.
- GROISMAN, A. & KAPLAN, E. 1994. An experimental study of cracking induced by desiccation. *EUROPHYSICS LETTERS*, 25, pg. 415-420.

- GUÉRIF, J. 1990. Factors influencing compaction-induced increases in soil strength. .
Soil and Tillage Research . 16:167–178.
- GUIDI, G., PAGLIAI, M. & PETRUZZELLI., G. 1978. Quantitative size evaluation of cracks and clods in artificially dried soil sam-ples. *Geoderma* 19, 105–113
- GULER, M., EDIL, T. B. & BOSSCHER, P. J. 1999. Measurement of particle movement in granular soils using image analysis. *Journal of Computing in Civil Engineering*, 13, 116-122.
- HAINES, W. B. 1923a. The volume-changes associated with variations of water content in soil. *Journal of Agricultural Science*, 13, 296-310.
- HAINES, W. B. 1923b. The volume changes associated with variations of water content in soil. *Journal of agricultural science*, v.13, p.296.
- HALLET, P. D. & NEWSON, T. A. 2005. Describing Soil Crack Formation Using Elastic-Plastic Fracture Mechanics. *European Journal of Soil Science.*, Vol. 56 pp.31-38.
- HANNANT, D. J., BRANCH, J. & MULHERON, M. 1999. Equipment for Tensile Testing of Fresh Concrete. *Magazine of Concrete Research*, Vol. 51, No. 4.
- HARISON, J. A., HARDIN, B. O. & MAHBOUB, K. 1994. Fracture toughness of compacted cohesive soils using ring test. *Journal of Geotechnical Engineering* 120 5:872-891.
- HARRISON, B., SUDICKY, E. A. & CHERRY, J. A. 1992. Numerical analysis of solute migration through fractured clay deposits into underlying aquifers. *Water Resources Research*, 28(2), 515-526.
- HEAD, K. H. 1989. *Soil Technicians' Handbook*, PENTECH PRESS, Publishers.London, Halasted Press: a division of JOHN WILEY & SONS, New york. Toronto.

- HEAD, K. H. 1992. *Manual of Soil Laboratory Testing, Volume 1: Soil Classification and Compaction Tests (2nd Edition)*. , Pentech Press, London, 2nd edition.
- HEAD, K. H. 1998 *Manual of Soil Laboratory Testing, Volume 3: Effective Stress Tests*. , John Wiley & Sons, 2nd edition.
- HEATH, A. C., PESTANA, J. M., HARVEY, J. T. & BEJERANO, M. O. 2004. Normalizing behavior of unsaturated granular pavement materials. *J. Geotech. Geoenviron. Eng.*, 130(9), 896-904.
- HIDAYAT, F., SUNGGUH, H. M. & HARIANTO 2008. Impact of climate change on floods in bengawan solo and brantas river basins, indonesia. *11th International Riversymposium in Brisbane, Australia, 1 - 4 September 2008, published online at www.riversymposium.com*.
- HOGENTOGLER, C. A. 1937. *Engineering Properties of Soil*, McGraw-Hill Book Co. New York.
- HOLTZ, W. G. 1983. The Influence of Vegetation on the Swelling and Shrinking of Clays in the United-States-of-America. *Geotechnique*, 33, 159-163.
- HONG, E. S., LEE, I. M. & LEE, J. S. 2006. Measurement of rock joint roughness by 3D scanner. *Geotechnical Testing Journal*,, 29, 482-489.
- INDRAWAN, I. G. B., RAHARDJO, H. & LEONG, E. C. 2006. Effects of coarse-grained materials on properties of residual soil. *Engineering Geology*, 82, 154–164.
- ISRM 1978. International Society for Rock Mechanics, Commission on Standardization of Laboratory and Field Tests. Suggested methods for the quantitative description of discontinuities in rock masses. *Int. J. Rock Mech. Min. Sci. and Geomech.*, 15: 319-368.

- JAMEI, M., GUIRAS, H., BEN HAMOUDA, K., HATIRA, M., OLIVELLA, S. & 2008. A study of the slope stability in unsaturated marly clay soil. . *Studia Geotechnica et Mechanica* 2008; XXX(1–2).
- JANSEN, R. B. 1988. *Advanced dam engineering for design, construction, and rehabilitation*, pp 784-787.
- JARDINE, R. J., SYMES, M. J. & BURLAND, J. B. 1984. The Measurement of Soil Stiffness in the Triaxial Apparatus. *Geotechnique*, 34, 323-340.
- JOMMI, C. & SCIOTTI, A. 2003. A study of the microstructure to assess the reliability of laboratory compacted soils as reference material for earth constructions. *System-based vision for strategic and creative design*, , F. Botempi, ed., Vol. 3. A.A. Balkema, Lisse, pp 2409-2415.
- JOSA, A., ALONSO, E. E., GENS, A. & LLORET, A. Stress-strain behaviour of partially saturated soils. Proc. 9th Eur. Conf. Soil Mech. and Found. Eng., 2, 561-564., 1987.
- JOTISANKASA, A. 2005. *Collapse behaviour of a compacted silty clay. PhD thesis.* Imperial College London, UK.
- JP. 2009. Bojonegoro levee section collapses, affected residents flee. *The jakarta Post*, Saturday 28th February 2009, 9:31am.
- JUANG, C. H. & HOLTZ, R. D. 1986a. Fabric, Pore-Size Distribution, and Permeability of Sandy Soils. *Journal of Geotechnical Engineering-Asce*, 112, 855-868.
- JUANG, C. H. & HOLTZ, R. D. 1986b. Fabric, pore size distribution and permeability of sandy soils. *J Geotech Eng ASCE*, 112, No. 9, 855-868.
- KEMENY, J. & POST, R. 2003. Estimating three-dimensional rock discontinuity orientation from digital images of fracture traces. *Computer & Geosciences.*, 29(1): 65-77.

- KHAN, A. H. & HOAG, D. L. 1979. A non contacting transducer for measurement of lateral strains. *Canadian Geotechnical Journal* 16 : 409-411.
- KLEPPE, J. H. & OLSON, R. E. 1985. Desiccation cracking of soil barriers. *Hydraulic Barriers in Soil and Rock ASTM.*, 263–275 ASTM.
- KODIKARA, J., BARBOUR, S., FREDLUND, D. & 2000a. Desiccation cracking of soil layers. The Asian Conference in Unsaturated Soils, UNSAT ASIA, Singapore, may 18–19, Balkema, 2000; 693–698.
- KODIKARA, J. K., BARBOUR, S. L. & FREDLUND, D. G. 2000b. Desiccation cracking of soil layers. *Unsaturated Soils for Asia*, 693-698.
- KODIKARA, J. K. & CHOI, X. A simplified analytical model for desiccation cracking of clay layers in laboratory tests. . Proceedings of the Fourth International Conference on Unsaturated Soils, 2006 Carefree, Arizona, USA. 2558-2569.
- KOLIJ, A. 2008. *Mechanical behaviour of unsaturated aggregated soils. PhD thesis, No. 4011.* Ecole Polytechnique Federale de Lausanne, Switzerland.
- KOLIJ, A., LALOU, L., CUSINIER, O. & VULLIET, L. 2006. Suction induced effects on the fabric of a structured soil. *Transport in Porous Media*, 64, 261-278.
- KOLIJ, A., VULLIET, L. & LALOU, L. 2010. Structural characterization of unsaturated aggregated soil. *Canadian Geotechnical Journal*, 47, 297-311.
- KOLYMBAS, D. & WU, W. 1989. A device for lateral strain measurements in triaxial tests with unsaturated specimens. *Geotechnical Testing Journal*, 12(3), 227-229.
- KONG, L. W., GUO, A. G., ZHAO, Y. W. & LIU, Y. Y. Influence of moisture content on porosity features of Red clay. Proceedings International Symposium on Advanced Experimental Unsaturated Soil Mechanics, pp 419–424, 2005 Trento, Italy, 27–29 June 2005. . Taylor, Francis Group, London,, pp 419–424.

- KONRAD, J. M. & AYAD, R. 1997a. Desiccation of a sensitive clay: field experimental observations. *Canadian Geotechnical Journal*, 34, 929-942.
- KONRAD, J. M. & AYAD, R. 1997b. An idealized framework for the analysis of cohesive soils undergoing desiccation. *Canadian Geotechnical Journal*, 34, 477-488.
- KRISDANI, H., RAHARDJO, H. & LEONG, E. C. 2008. Effects of different drying rates on shrinkage characteristics of a residual soil and soil mixtures. *Engineering Geology*, 102, 31-37.
- KRISHNAYYA, A. V. G., EISENSTEIN, Z. & MORGENSTERN, N. R. 1974a. Behaviour of Compacted Soil in Tension. *Journal of the Geotechnical Engineering Division, Proceedings of the American Society of Civil Engineers*, 1051–1061., Vol. 100, No. GT9.
- KRISHNAYYA, A. V. G., EISENSTEIN, Z. & MORGENSTERN, N. R. 1974b. Behaviour of Compacted Soil in Tension. *Journal of the Geotechnical Engineering Division, Proceedings of the American Society of Civil Engineers*, 1051–1061., Vol. 100, No. GT9, pp. 1051–1061.
- LACHENBRUCH, A. H. 1961. Depth and spacing of tension cracks. *Journal of Geophysical Research*, 66 12:4273-4292.
- LAKSHMIKANTHA, M. R. 2009. *Experimental and Theoretical Analysis of Cracking in Drying Soils*. Ph.D. Thesis, Dept. of Geotechnical Engineering and Geosciences, Technical University of Catalonia.
- LAKSHMIKANTHA, M. R., PRAT, P. C. & LEDESMA, A. 2006. An Experimental Study of Cracking Mechanisms in Drying Soils. *Environmental Geotechnics*, V, H. R.Thomas ed., Thomas Telford, pp. 533-540.

- LAKSHMIKANTHA, M. R., PRAT, P. C. & LEDESMA, A. 2009. Image Analysis for the Quantification of a Developing Crack Network on a Drying Soil. *Geotechnical Testing Journal*, 32, 505-515.
- LAKSHMIKANTHA, M. R., PRAT, P. C. & LEDESMA, A. 2012. Experimental evidence of size effect in soil cracking. *Canadian Geotechnical Journal*, 49, 264-284.
- LAURITZEN, C. W. & STEWART, J. A. Soil-volume changes and accompanying moisture and pore-space relationships. Soil Science Society of America Proceedings, vol.6, pp.13-116, 1941. 113-116.
- LAWRENCE, G. P. 1878. Stability of soil pores during mercury intrusion porosimetry. *J Soil Sci*, 29, pp 299-304.
- LEAVELL, D. A. & PETERS, J. F. 1987. Uniaxial Tensile Test for Soil. *Department of the Army Technical Report GL-87-10*. Waterways Experiment Station, Vicksburg, MS.
- LEONG, E. C., TRIPATHY, S. & RAHARDJO, H. 2003. Total suction measurement of unsaturated soils with a device using the chilled-mirror dew-point technique. *Geotechnique*, 53, 173-182.
- LEONG, E. C., WIDIASTUTI, S. & LEE, C. C. 2007. Accuracy of suction measurement. technical note. *Geotechnique*, 57, 547-556.
- LIMA, L. A. & GRISMER, M. E. 1992. Soil Crack Morphology and Soil-Salinity. *Soil Science*, 153, 149-153.
- LLORET, A., LEDESMA, A., RODRÍGUEZ, R. L., S´ANCHEZ, M. J., OLIVELLA, S. & SURIOL, J. Crack initiation in drying soils. n 2nd Int. Conference on Unsaturated Soils, pages 497–502, Beijing China, 1998., 1998.

- LLORET, A., VILLAR, M. V., SANCHEZ, M., GENS, A., PINTADO, X. & ALONSO, E. E. 2003. Mechanical behaviour of heavily compacted bentonite under high suction changes. *Geotechnique*, 53, 27-40.
- LO PRESTI, D. C. F., PALLARA, O. & PUCI, I. 1995. A modified commercial triaxial testing system for small strain measurements : preliminary results on Pisa clay. *Geotechnical Testing Journal* 18(1), 15-31.
- LOGSDON, S. D., ALLMARAS, R., WU, L., SWAN, J. B. & RANDALL, G. W. 1990. Macroporosity and its relation to saturated hydraulic conductivity under different till age practices. *Soil Sci. Soc. Am. J.*, 54, 1096–1101.
- LU, N. & LIKOS, W. J. 2004. *Unsaturated soil mechanics*, Wiley, New York.
- LU, N., WU, B. L. & TAN, C. P. 2007. Tensile strength characteristics of unsaturated sands. *Journal of Geotechnical and Geoenvironmental Engineering*, 133, 144-154.
- MAÂTOUK, A., LEROUÉIL, S. & LA ROCHELLE, P. 1995. Yielding and critical state of a collapsible unsaturated silty soil. *Géotechnique*, 45 (3), pp 465-477.
- MACARI, E. J., PARKER, J. K. & COSTES, N. C. 1997a. Measurement of volume changes in triaxial tests using digital imaging techniques. *Geotechnical Testing Journal*, 20, 103-109.
- MACARI, E. J., PARKER, J. K. & COSTES, N. C. 1997b. Measurement of Volume Changes in Triaxial Tests Using Digital Imaging Techniques. *ASTM, Geotechnical Testing Journal*, Vol. 20, No. 1, pp. 103-109.
- MARINHO, F. A. M. 1994. *Shrinkage behaviour of some plastic soils. PhD thesis.* University of London (Imperial College), London, UK.
- MICROEPSILON-WEBSITE 2011. Micro Epsilon Website <http://www.micro-epsilon.co.uk/glossar/iconnect.html> 11 Dec 2011.

- MIKULITSCH, W. A. & GUDEHUS, G. Uniaxial tension, biaxial loading and wetting tests on loess. Proceedings of the first international conference on unsaturated soils, 6-8 September 1995 Paris/France p. 145-50.
- MILLER, C. J., MI, H. & YESILLER, N. 1998a. Experimental analysis of desiccation crack propagation in clay liners. *Journal of the American Water Resources Association*, 34, pp. 677-686.
- MILLER, C. J., MI, H. & YESILLER, N. 1998b. Experimental analysis of desiccation crack propagation in clay liners. *Journal of the American Water Resources Association AWRA*, 34 (3), 677–686.
- MILLER, C. J. & MISHRA, M. 1989. Modeling of Leakage Through Cracked Clay Liners- I: State of the Art. *Water Resources Bulletin* 25(3):551-555.
- MITCHELL, J. K. 1993a. *Fundamental of soil behaviour*, Wiley, New York.
- MITCHELL, J. K. 1993b. *Fundamental of soil behaviour*. New York: Wiley.
- MIZUGUCHI, T., NISHIMOTO, A., KITSUNEZAKI, S., YAMAZAKI, Y. & AOKI, I. 2005. Directional crack propagation of granular water systems. *Physical Review E*, 71(5): 056122.
- MOE, H., FITYUS, S. & SMITH, D. W. Study of cracking network in residual expansive clay. In: *Unsaturated Soils-Geotechnical and Geoenvironmental Issues*. Proc. 2nd Asian Conf. on Unsaturated Soils, 2003 Osaka, Japan., pp.149-154.
- MONROY, R. 2006. *The influence of load and suction changes on the volumetric behaviour of compacted London Clay*. Imperial College, London, UK.
- MONROY, R., ZDRAVKOVIC, L. & RIDLEY, A. Evolution of microstructure in compacted London Clay during wetting and loading. *Geotechnique*, 60, 105-119.

- MONTGOMERY, R. J. & PARSONS, L. J. 1989. The Omega Hills Final Cap Test Plot Study: Three Year Data Summary. Presented at the 1989 Annual Meeting of the National Solid Waste Management Association, Washington D.C.
- MORRIS, P. H., GRAHAM, J. & WILLIAMS, D. J. 1992a. Cracking in Drying Soils. *Canadian Geotechnical Journal*, 29, 263-277.
- MORRIS, P. H., GRAHAM, J. & WILLIAMS, D. J. 1992b. Cracking in drying soils. *Canadian Geotechnical Journal* 29, 263-277.
- MORRIS, P. H., GRAHAM, J. & WILLIAMS, D. J. 1994. Crack depths in drying clays using fracture mechanics. *Fracture Mechanics Applied to Geotechnical Engineering ASCE Geotechnical special Publication*, 40-53.
- MUNKHOLM, L. J., SCHJONNING, P. & KAY, B. D. 2002. Tensile strength of soil cores in relation to aggregate strength, soil fragmentation and pore characteristics. *Soil & Tillage Research*, 64, 125-135.
- MUNKHOLMA, L., SCHJØNNINGA, P. & KAY, B. 2002. Tensile strength of soil cores in relation to aggregate strength, soil fragmentation and pore characteristics. *Soil and Tillage Research* . 64:125–135.
- NAHLAWI, H., CHAKRABARTI, S. & KODIKARA, J. 2004. A direct tensile strength testing method for unsaturated geomaterials. *Geotechnical Testing Journal*, 27, 356-361.
- NAHLAWI, H. & KODIKARA, J. K. 2006. Laboratory experiments on desiccation cracking of thin soil layers. *Geotechnical and Geological Engineering*, vol.24, 1641–1664.
- NAM, S., GUTIERREZ, M., DIPLAS, P., PETRIE, J., WAYLLACE, A., LU, N. & MUNOZ, J. J. 2010. Comparison of testing techniques and models for establishing the SWCC of riverbank soils. *Engineering Geology*, 110, 1-10.

- NATIONAL RESEARCH COUNCIL 1996. Rock fractures and fluid flow: contemporary understanding and applications. Washington, D.C.
- NG, C. W. W., ZHAN, L. T. & CUI, Y. J. 2002. A new simple system for measuring volume changes in unsaturated soils. *Canadian Geotechnical Journal*, 39, 757-764.
- NINJGARAV, E., CHUNG, S.-G., JANG, W.-Y. & RYU, C.-K. 2007. Pore size distribution of Pusan Clay measured by mercury intrusion porosimetry. *KSCE Journal of Civil Engineering*, 11 (3), 133-139.
- NISHIMOTO, A., MIZUGUCHI, T. & KITSUNEZAKI, S. 2007. Numerical study of drying process and columnar fracture process in granule-water mixtures. *Physical Review E*, 76: 016102.
- NUTH, M. & LALOUI, L. 2008. Advances in modelling hysteretic water retention curve in deformable soils. *Computers and Geotechnics*, 35, 835-844.
- OBIDAT, M. T. & ATTOM, M. F. 1998. Computer Vision-Based Technique to Measure Displacement in Selected Soil Tests. *ASTM, Geotechnical Testing Journal*,.
- OKABE, A., BOOTS, B., SUGIHARA, K., CHIU, S. N. & KENDALL, D. G. 2008. "Spatial Tessellations: Concepts And Applications Of Voronoi Diagrams," John Wiley And Sons, New York.
- OMIDI, G. H., THOMAS, J. C. & BROWN, K. W. 1996. Effect of desiccation cracking on the hydraulic conductivity of a compacted clay liner. *Water Air and Soil Pollution*, 89, 91-103.
- ÖREN, A. H., ÖNAL, O., ÖZDEN, G. & KAYA, A. 2006. "Nondestructive Evaluation of Volumetric Shrinkage of Compacted Mixtures Using Digital Image Analysis,". *Engineering Geology*, Vol. 85, pp. 239-250.

- PERON, H., HU, L. B., LALOUI, L. & HUECKEL, I. 2007a. Mechanisms of desiccation cracking of soil: Validation. *Numerical Models in Geomechanics: Numog X*.
- PERON, H., HUECKEL, T. & LALOUI, L. 2007b. An improved volume measurement for determining soil water retention curves. *Geotechnical Testing Journal*, 30, 1-8.
- PERON, H., HUECKEL, T., LALOUI, L. & HU, L. B. 2009. Fundamentals of desiccation cracking of fine-grained soils: experimental characterisation and mechanisms identification. *Canadian Geotechnical Journal*, 46, 1177-1201.
- PÉRON, H., LALOUI, L., HUECKEL, T. & HU, L. 2006. Experimental study of desiccation of soil. UNSAT 2006. In: Miller, et al. (Ed.). *ASCE Geotechnical Special Publication*, 147, 1073-1084.
- PETERS, J. F. & LEAVELL, D. A. 1987. Relationship Between Tensile and Compressive Strengths of Compacted Soils. *Advanced Triaxial Testing of Soil and Rock*, ASTM STP 977, R. T. Donaghe, R. C. Chaney, and M. L. Silver, Eds., ASTM International, 1988,, pp. 169–188.
- POULOVAS, A. 1970. Effect of Entrapped Air on Hysteresis Curves of a Porous Body and on Its Hydraulic Conductivity. *Soil Science*, 109, 154-&.
- PRAPAHARAN, S., WHITE, D. M. & ALTSCHAEF, A. G. 1991. Fabric of field- and laboratory compacted clay. *J Geotech Eng ASCE*, 117(12), 1934-1940.
- PRAT, P. C., LEDESMA, A. & LAKSHMIKANTHA, M. R. Size effect in the cracking of drying soil. Proceedings of the 16th European Conference of Fracture, 2006 Alexandroupolis, Greece. pp.1373-1374.
- PRAT, P. C., LEDSMA, A. & CABEZA, L. Drying and cracking of soils: numerical modelling. 8th Int. Conference on Numerical Models in Geomechanics NUMOG VIII, 2002 Rome, Italy. pp. 705-711.

- PRIEST, S. D. 1993. *Discontinuity analysis for rock engineering.*, Chapman & Hall.
- PRIEST, S. D. & HUDSON, J. A. 1981. Estimation of discontinuity spacing and trace length using scanline surveys. *Int. J. Rock Mech. Min. Sci. and Geomech.*, 18: 183–197.
- RAMPINO, C., MANCUSO, C. & VINALE, F. 1999. Laboratory testing on an unsaturated soil: equipment, procedures, and first experimental results. *Canadian Geotechnical Journal*, 36, 1-12.
- RAVINA, I. 1983. The Influence of Vegetation on Moisture and Volume Changes. *Geotechnique*, 33, 151-157.
- REED, M. A., LOVELL, C. W., ALTSCHAEFFL, A. G. & WOOD, L. E. 1980. Reply: Frost heaving rate predicted from pore size distribution. *Can Geotech J*, 21, 21-35., 17, 639-640.
- RICHARDS, B. G., PETER, P. & EMERSON, W. W. 1983. The Effects of Vegetation on the Swelling and Shrinking of Soils in Australia. *Geotechnique*, 33, 127-139.
- RIDLEY, A. M. & WRAY, W. K. Suction measurement: a review of current theory and practices. Proceedings of the First International Conference on Unsaturated Soils, 1995 Balkema, Paris, France. pp. 1293–1322.
- RODRIGUEZ, R. 2006. Hydrogeotechnical characterization of a metallurgical waste. *Canadian Geotechnical Journal*, 43, 1042-1060.
- RODRÍGUEZ, R. 2002. *Experimental de flujoy transporte de cromo, níquel y manganeso en residuos de la zona minera de Moa (Cuba): Influencia del comportamiento hidromecánico (In Spanish)*. Technical University of Catalonia, Barcelona, Spain, 2002.

- RODRIGUEZ, R., SANCHEZ, M., LEDESMA, A. & LLORET. 2007. Experimental and numerical analysis of desiccation of a mining waste. *Can. Geotech. J.*, 44 (doi: 10.1139/T07-016), 644-658.
- ROMERO, E. 1999. *Characterisation and thermo-hydro-mechanical behaviour of unsaturated boom-clay: An experimental study*, PhD thesis. Universitat Politècnica de Catalunya, Barcelona, Spain.
- ROMERO, E., FACIO, J. J. A., LLORET, A., GENS, A. & ALONSO, E. E. A new suction and temperature controlled triaxial apparatus. Proc 14th Int Conf Soil Mech Found Eng., 1997 Hamburg, Germany,.
- ROMERO, E., GENS, A. & LLORET, A. 1999. Water permeability, water retention and microstructure of unsaturated compacted Boom clay. *Engineering Geology*, 54, 117-127.
- ROMERO, E. & SIMMS, P. 2008a. Microstructure investigation in unsaturated soils: A review with special attention to contribution of mercury intrusion porosimetry and environmental scanning electron microscopy. *Geotech Geol Eng*, 26, 705-727.
- ROMERO, E. & SIMMS, P. 2008b. Microstructure investigation in unsaturated soils: A review with special attention to contribution of mercury intrusion porosimetry and environmental scanning electron microscopy. *Geotech Geol Eng*, 26, 705-727.
- SHERARD, J. L. 1973. *Embankment dam Cracking*, New York, John Wiley & Sons.
- SHIN, H. & SANTAMARINA, J. C. 2011. Desiccation cracks in saturated fine-grained soils: particle-level phenomena and effective-stress analysis. *Geotechnique*, 61, 961-972.

- SHORLIN, K. A., DE BRUYN, J. R., GRAHAM, M. & MORRIS, S. W. 2000. Development and geometry of isotropic and directional shrinkage-crack patterns. *Physical Review E*, 61(6): 6950-6957.
- SIMMS, P. H. & YANFUL, E. K. 2001. Measurement and estimation of pore shrinkage and pore distribution in a clayey till during soil-water characteristic curve tests. *Canadian Geotechnical Journal*, 38, 741-754.
- SNYDER, V. A. & MILLER, R. D. 1985. Tensile-Strength of Unsaturated Soils. *Soil Science Society of America Journal*, 49, 58-65.
- SOEMITRO, R. A. A. 2005. Performance and reliability evaluation research, case study :River solo (indonesian). Report no., Report to East Java, Ministry of Public Works, Institut Teknologi Sepuluh Nopember.
- SRIDHARAN, A. & PRAKASH, K. 2000. Shrinkage limit of soil mixtures. *Geotechnical Testing Journal*, 23, 3-8.
- STIRK, G. B. 1954. Some Aspects of Soil Shrinkage and the Effect of Cracking Upon Water Entry into the Soil. *Australian Journal of Agricultural Research*, 5, 279-290.
- SUDARSONO 2009. The bengawan solo water council - providing insight and directions. Report no., CRBOM Small Publications Series No. 5, Centre for River Basin Organizations and Management, Solo, Central Java, Indonesia, Available at: <http://crbom.org/SPS/Docs/SPS05-TKPSDA-0.pdf>.
- TAKEUCHI, K., JAYAWARDENA, A. W. & TAKAHASI, Y. 1995. Catalogue of rivers for southeast asia and the pacific - volume 1. Report no., UNESCO-IHP Regional Steering Committee for Southeast Asia and the Pacific.
- TAMRAKAR, S. B., TOYOSAWA, Y., MITACH, T. & ITOH, K. 2005. Tensile strength of compacted and saturated soils using newly developed tensile strength measuring apparatus. *Soils and Foundations*, 45, 103-110.

- TANG, A. M. & CUI, Y. J. 2005. Controlling suction by the vapour equilibrium technique at different temperatures and its application in determining the water retention properties of mx80 clay. *Can Geotech J*, 42, 287-296.
- TANG, C., CUI, Y., SHI, B., TANG, A. & LIU, C. 2011. Desiccation and Cracking Behaviour of Clay Layer from Slurry State Under Wetting-Drying Cycles. *Geoderma*, Vol. 166, No. 1, pp. 111-118.
- TANG, C., SHI, B., LIU, C., ZHAO, L. & WANG, B. 2008a. Influencing factors of geometrical structure of surface shrinkage cracks in clayey soils. *Engineering Geology*, 101, 204-217.
- TANG, C., SHI, B., LIU, C., ZHAO, L. & WANG, B. 2008b. Influencing factors of geometrical structure of surface shrinkage cracks in clayey soils. *Engineering Geology*, 101, 204-217.
- TANG, G. X. & GRAHAM, J. 2000. A method for testing tensile strength in unsaturated soils. *Geotechnical Testing Journal*, 23, 377-382.
- TANG, G. X., GRAHAM, J., BLATZ, J., GRAY, M. & RAJAPAKSE, R. 2002. Suctions, stresses and strengths in unsaturated sand-bentonite. *Engineering Geology*, 64, 147-156.
- TARANTINO, A. 2009. A water retention model for deformable soils. *Geotechnique*, 59, 751-762.
- TARANTINO, A. Unsaturated soils: compacted versus reconstituted states. 5th International Conference on Unsaturated Soil, 2010. pp. 113-136
- TARANTINO, A. & TOMBOLATO, S. 2005. Coupling of hydraulic and mechanical behaviour in unsaturated compacted clay. *Geotechnique*, 55, 307-317.
- TEMPANY, T. A. 1917. The shrinkage of soils. *Journal of Agricultural Science*, 8, 312-330.

- TERZAGHI, K. V. 1925. Principles of soil mechanics: I - phenomena of cohesion of clay. *Engineering News - Recrd*, Vol.95 n.19, pp.742-746.
- TOWNER, G. D. 1987a. The mechanics of cracking of drying clay. *Journal of Agricultural Engineering Research*, 36:115-124.
- TOWNER, G. D. 1987b. The Mechanics of Cracking of Drying Clay. *Journal of Agricultural Engineering Research*, 36, 115-124.
- TRABELSI, H., JAMEI, M., GUIRAS, H., HATEM, H., ROMERO, E. & OLIVELLA, S. 2010. Some Investigations about the Tensile Strength and the Desiccation Process of Unsaturated Clay. *European Physical Journal Web of Conferences* 6, , 12005, 1-8.
- TRABELSI, H., JAMEI, M., ZENZRI, H. & OLIVELLA, S. 2011. "Crack Patterns in Clayey Soils: Experiments and Modeling". [Online]. *International Journal for Numerical and Analytical Methods in Geomechanics*, Article published online, DOI:10.1002/nag.1060.
- UN 2004. Indonesia factfile. United Nations Public Administration Network.
- USBR 1974. *Earth Manual, 2nd edn*, US Bureau of Recamation, CO.
- VALLEJO, L. E. 1988. The brittle and ductile behavior of clay samples containing a crack under. *Theoretical and Applied Fracture Mechanics*, 10(1), 73-78.
- VALLEJO, L. E. & LIANG, R. Y. 1994. Application of Fracture Mechanics to Soils: An Overview. *Fracture Mechanics Applied to Geotechnical Engineering*, ASCE, GSPNo. 43, pp. 1-20.
- VANAPALLI, S. K., FREDLUND, D. G. & PUFAHL, D. E. 1999. The influence of soil structure and stress history on the soil-water characteristics of a compacted till. *Geotechnique*, 49, 143-159.

- VELDE, B. 1999. Structure of Surface Cracks in Soil and Muds. *Geoderma*, Vol. 93, No. 1-2, pp. 101-1.
- VOGEL, H. J., HOFFMANN, H., LEOPOLD, A. & ROTH, K. 2005a. Studies of crack dynamics in clay soil - II. A physically based model for crack formation. *Geoderma*, 125, 213-223.
- VOGEL, H. J., HOFFMANN, H. & ROTH, K. 2005b. Studies of crack dynamics in clay soil - I. Experimental methods, results, and morphological quantification. *Geoderma*, 125, 203-211.
- WALLACE, K. 1998. "The Tensile Response of an Unbound Granular Pavement," *Road and Transport Research Journal, ARRB*, Vol. 7, No. 3, pp. 36-47.
- WASHBURN, E. W. Note on a method of determining the distribution of pore sizes in a porous material. *Proceedings of the National Academy of Sciences*, 7, 115-116., 1921.
- WEINBERGER, R. 1999. Initiation and growth of cracks during desiccation of stratified muddy sediments. *Journal of Structural Geology*, 21, 379-386.
- WELLS, R. R., DICARLO, D. A., STEENHUIS, T. S., PARLANGE, J. Y., ROMKENS, M. J. M. & PRASAD, S. N. 2003. Infiltration and surface geometry features of a swelling soil following successive simulated rainstorms. *Soil Science Society of America Journal*, 67, 1344-1351.
- WELLS, R. R., PRASAD, S. N. & ROMKENS, M. J. M. 2001. Cracking modes of an expansive Mississippi delta soil. Technical report, TEKTRAN, USA, The Agricultural research service of the U.S Department of Agriculture. 2.5.2.
- WHEELER, S. J. 1988. The Undrained Shear-Strength of Soils Containing Large Gas-Bubbles. *Geotechnique*, 38, 399-413.

- WHITE, D. J., TAKE, W. A., BOLTON, M. D. & MUNACHEN, S. E. A Deformation Measurement System for Geotechnical Testing Based on Digital Imaging, Close-Range Photogrammetry, and PIV Image Analysis. 15th International Conference of Soil Mechanics and Geotechnical Engineering, 2001 Istanbul, Turkey, pp. 539-542.
- WHITLOW, R. 1983. *Basic Soil Mechanics*.
- WHITLOW, R. 1995. *Basic Soil Mechanics*, Addison Wesley Longman Limited, Edinburg Gate, Harlow, England.
- YAN, A., WU, K. & ZHANG, X. 2002. A quantitative study on the surface crack pattern of concrete with high content of steel fiber. *Cem. Concr. Res.* 32: 1371-1375.
- YESILLER, N., MILLER, C. J., INCI, G. & YALDO, K. 2000. Desiccation and cracking behavior of three compacted landfill liner soils. *Engineering Geology*, 57, 105-121.
- ZHANG, G., GERMAINE, J. T. & WHITTLE, A. J. Drying induced alteration to the microstructure of a tropical soil. In: A. TARANTINO, E. R., AND Y. J. CUI, EDS, ed. Proceedings of International Symposium on advanced experimental unsaturated soil mechanics., 2005 Trento, Italy. Taylor & Francis Group, London, 443-449.
- ZHANG, X. & MORRIS, J. 2005. *Communication and Information Technology Research Technical Report 170, Volume Measurement Using a Laser Scanner* [Online]. <http://citr.auckland.ac.nz/techreports/2005/CITR-TR-170.pdf>.